MECHANICAL CHARACTERISATION OF PROTECTIVE COATINGS FOR OFFSHORE WIND TURBINE TOWERS AND TRANSITION PIECES

ISBELIS C. LOPEZ R.

PhD

2018

MECHANICAL CHARACTERISATION OF PROTECTIVE COATINGS FOR OFFSHORE WIND TURBINE TOWERS AND TRANSITION PIECES

ISBELIS C. LOPEZ R.

A thesis submitted in partial fulfilment of the requirements of the University of Northumbria at Newcastle for the degree of Doctor of Philosophy

Research undertaken in the Faculty of Engineering and Environment and in collaboration with Safinah Ltd and Hempel A/S

October 2018

ABSTRACT

The wind energy industry is increasingly moving to offshore areas and increasing the wind turbines' size and number. These are unmanned structures with limited access, costs of repairs are significantly higher than for their onshore counterparts, and higher reliability of the corrosion protection system is required. In recent years research has directed interest towards developing robust coating materials capable of tolerating hostile marine climates with minimum maintenance. When epoxy-based solvent-borne paints are applied onto metallic substrates and cured, intrinsic residual stresses originate within the coating due to film formation processes (cross-linking and solvent loss processes) and adhesion to the substrate. Excessive tensile residual stresses have an adverse effect on adhesion and may compromise the integrity of a complex system constituted by a substrate and coating scheme. Additionally, they reduce the coating's capacity to undergo further tensile stresses during service.

In this study, three epoxy-based paint systems, used on turbine towers and transition pieces, were airless-sprayed onto thin steel substrate and cured to produce bi-layer samples. Additionally, free films were produced. Mechanical tests on supported and unsupported coatings were performed using dynamic mechanical analysis. A mathematical model based on composite beam stress analysis was applied to determine the Young's modulus and residual stresses of the coatings. The mechanical and physical properties of the marine coatings were found to be dependent on coating thickness. The Young's modulus of the coatings decreases with an increase in coating thickness. This was found to be due to increasing solvent retention, porosity and stiffness associated with an increase in coating thickness. Retained solvent acts as a plasticiser reducing the tensile strength of the material and the glass transition temperature. The rate of evaporation of the solvent also has a relevant effect on the mechanical response of the material; fast solvent loss rates were found to be associated with lower internal stress development. In the present study, it has been found that it is possible to design more reliable and predictable coating systems by a judicious manipulation of the paint formulation, and control of the dry film thickness and post-cure schedule. A proper understanding of the stress development of organic coatings and the influencing factors is invaluable for not only offshore wind farms but also any structure where long-term corrosion protection (over 25 years) is required with minimal maintenance.

TABLE OF CONTENT

LIST OF FIGURES

LIST OF TABLES

LIST OF SYMBOLS

Chapter 1

PVC	pigment volume concentration

Chapter 2

η_T	viscosity of the polymer
T	temperature
T_g	glass transition temperature
T_{gM}	glass transition temperatures of the mixture
α_{tp}	linear coefficient of thermal expansion of the polymer
α_{ts}	linear coefficient of thermal expansion of the solvent
T_{gp}	glass transition temperatures of the polymer
T_{gs}	lass transition temperatures of the solvent
φ_p	volume fraction of polymer in the mixture
φ_f	volume fraction of the filler,
α_c	coefficient for the composite,
α_p	coefficient for the polymer, and
α_f	coefficient for the filler
PVC	pigment volume concentration
$CPVC$	critical pigment volume concentration
$\overline{OA}$	oil absorption value of the pigments in linseed oil
ρ	density of the pigments
DFT	dry film thickness
NDFT	nominal dry film thickness

Chapter 3

E'	storage modulus
E''	loss Modulus

$tan\delta$	tan delta, damping parameter
γ_c	critical surface tension
γ	surface tension
ε	strain
σ, S	stress
E	elastic modulus
ν	Poisson's ratio
T	temperature
T_g	glass transition temperature
t	time
ε^c	strain in the film
V_s	volume of solvent in the film
V_t	volume of the dry film at a time, t, after solidification
V_f	volume of the dry film
σ^c	stress due to film formation
ε^T	thermal strain
α_c^T	thermal expansion coefficient of the coating
α_S^T	thermal expansion coefficient of the substrate
ΔT	variation in temperature
σ^T	thermal stress
α, CTE	thermal expansion coefficient
ε^H	hygroscopic strain,
α_F^H	hygroscopic expansion coefficient = s of the coating, and
α_S^H	hygroscopic expansion coefficients of the substrate.
σ^H	hygroscopic stress
H	enthalpy

S'	entropy
S	tensile strength of the coating
S_∞	tensile strength at infinite molecular weight
B	constant characteristic of the material
M	molecular weight
E	effective Young's modulus of porous materials,
E_0	Young's modulus of the pore-free solid,
V	pore volume fraction, and
b	empirical constant.
P	porosity,
P_{crit}	porosity at which the effective Young's modulus becomes zero, and
f	material constant dependent on the grain morphology and pore geometry of the porous material.
s	radial flaw size
R_{pore}	pore radius

Chapter 4

E_s	Young's modulus of the substrate,
t_s	thickness of the substrate,
R	radius of curvature, and
t_c	thickness of the coating.
E_c	Young's modulus of the coating, and
ε_m	misfit strain.
α	ratio between the Young's modulus of the coatings and the substrate, and
β	ratio between the thickness of the coating and the substrate.
ν_s	Poisson's ratio of the substrate
d	maximum deflection of the beam, and
L	Length of the beam.

ν_c	Poisson's ratios of the coating.
y	distance from the beam's neutral axis,
M	bending moment,
I	second moment of area,
k	curvature for the beam.
σ_{xc}	stress in the coating,
σ_{xs}	stress in the substrate,
A	cross-sectional area.
I_c	the moment of inertia of the coating, and
I_s	the moment of inertia of the substrate.
b	width of the beam.
h_c	distance from the neutral axis to the top of the beam (coating's free surface)
h_s	distance from the neutral axis to the bottom of the beam (substrate's free surface)
y_c	neutral axis of the coating to the neutral axis of the sample
y_s	neutral axis of the substrate to the neutral axis of the sample
I_{cy}	moment of inertia of the coating with respect to the neutral axis
I_{sy}	moment of inertia of the substrate with respect to the neutral axis

Chapter 5

E^*	dynamic complex modulus
σ_o	dynamic stress, and
ε_o	dynamic strain.
K_s	stiffness,
F	drive force, and
x	displacement produced by the force
α	average of the coefficient of thermal expansion (CTE) for the temperature interval,

$\Delta l/\Delta T$ the slope of the displacement versus temperature curve, and

l_o= original length of the samples which is dictated by the distance between the clamps (free length)

F applied force,

h thickness of the specimen.

ε_f flexural strain

s deflection,

s_i deflections (s_1 or s_2), and

ε_{fi} flexural strain, with values of $\varepsilon_{f1} = 0.0005$ and $\varepsilon_{f2} = 0.0025$.

E_f flexural modulus

σ_{f1} flexural stress measured at deflection s_1, and

σ_{f2} flexural stress measured at deflection s_2.

s_C conventional deflection equal to 1.5 times the thickness of the specimen

σ_{fB} flexural stress at break,

σ_{fM} maximum flexural stress,

σ_{fC} flexural stress at conventional deflection,

ε_{fB} flexural strain at break,

ε_{fM} maximum flexural strain, and

ε_{fC} flexural strain at conventional deflection,

ACKNOWLEDGEMENTS

I would like to express my gratitude towards my supervision team. My academic supervisors Dr. P.S Leung and Dr. Fawad Inam, and my industrial supervisor Dr. Clare Till. Their advice and contrasting backgrounds provided me with an enriched experience as a PhD student and the capacity to pursue my research with an open mind.

I would like to thank my sponsoring companies Safinah Ltd, Hempel A/S, and Northumbria University for placing their trust in me. Specially Raouf Kattan and Andreas Paulsen for their constant support. I feel very lucky to have been selected to develop this research project and will always be extremely grateful. During these past three years with Safinah, Hempel, and Northumbria University I have gained immense technical knowledge and seen exceptional work ethics.

I would like to also thank my family, which grew during my studies. My parents for teaching me the importance of education and self-improvement. I grew up seeing how much they were able to overcome in Venezuela, all the effort they put into raising four successful daughters despite the adversities, and the help they gave us to pursue a better life somewhere safe. They are my main drive for success. My sisters for always taking care of me. My father in-law for his unconditional support. My sisters in-law for making me feel part of the family. My late mother in-law for the lovely three years I got to know her. And most importantly, my wonderful husband Alex Carter for absolutely everything he does.

Finally, I would like to thank my colleagues and members of staff at Northumbria University for the years we worked together as friends.

DECLARATION

I declare that the work contained in this thesis has not been submitted for any other award and that it is all my own work. I also confirm that this work fully acknowledges opinions, ideas and contributions from the work of others. The work was done in collaboration with Safinah Ltd. and Hempel A/S.

Any ethical clearance for the research presented in this thesis has been approved. Approval has been sought and granted by the Faculty Ethics Committee on 13th of October 2015

I declare that the Word Count of this Thesis is 37,966 words

Name: Isbelis Coromoto Lopez Rodriguez

Signature:

Date: 03/10/2018

1 INTRODUCTION

1.1 Context and purpose

Since the 2008 financial crisis, the coating industry has seen pressure from stakeholders, which has led to formulation changes that have resulted in higher internal stresses in coatings. Hempel S/A. has identified the following as possible causes for mechanical failure due to internal stresses in protective coatings:

- higher productivity has led to faster curing products,
- focus on flame point of liquid paint has led to use of slower evaporating solvents,
- lower costs have led to higher pigment volume concentration (PVC) and the use of sub-optimal pigment types, and
- lower applicator skills have led to products with a very high sag resistance that can result in over-application.

Three solvent-borne 2-pack paint systems, denominated A, B, and C and described in section 5.1.1, were supplied by Hempel S/A for mechanical characterisation. The paint systems had different compositions and were composed of different epoxy-based binders, hardeners, solvents, pigments and extenders. In service, the paint films show different behaviours. When applied to the specified dry film thickness (DFT) the paints do not show premature failure. However, coating C and, to some extent coating A, may experience mechanical failure, by cracking or flaking, when applied to excessive DFTs. On the other hand, coating B can be applied in much higher DFTs than specified, and cracking or flaking delamination is very seldom seen for this product.

This suggests that the mechanical performance of the coatings may be dependent on the applied film thickness. A study of the effect of the DFT on the properties of the film would give an indication of the effect of workmanship on the finished product. A better understanding of the mechanical properties would enable more appropriate testing protocols to be devised. Finally, this will lead to more robust paint formulations

that do not crack or detach, and consequently fewer failures of wind turbine coatings and less financial risk.

1.2 Statement of aims and objectives

1.2.1 Aims

- To understand the mechanical behaviour of modern coating systems on steel and develop a test methodology to characterise and compare them.
- To propose a mathematical model for the determination of the Young's modulus and residual stresses of supported coatings.

1.2.2 Objectives

- To determine the effect of dry film thickness and cure schedule on the mechanical properties, reliability of coatings, and their potential to perform under marine conditions.
- To contribute to the improvement in corrosion protection of offshore wind turbines by contributing to the mechanical characterisation of protective coatings.
- To determine the Young's modulus of supported and unsupported coatings.
- To examine the effect of internal stresses produced during curing on the mechanical properties of the cured films.
- To examine the effect of dry film thickness on internal residual stresses experienced by supported coatings.
- To establish the effect of coating/substrate interactions on the mechanical properties of supported coatings.
- To improve the fundamental understanding of the mechanical behaviour of the coatings to improve their reliability in service.

1.3 Contribution to knowledge

The present study has evaluated the effect of application-related factors on the mechanical properties of supported epoxy-based coatings. The analysis has provided an effective methodology for the mechanical characterisation of protective coatings used on offshore wind turbine towers and transition pieces. Due to the viscoelastic nature of the coatings, dynamic mechanical analysis DMA has been proposed as the

preferred test method for the mechanical characterisation of the protective coatings. The analysis indicates that the mechanical properties of the coatings are dependent on a wide variety of factors associated with coating formulation, application and progressive curing. The dry film thickness of the coatings is an important aspect of the application process and will affect coating reliability in service. Ultimately, it has been established that the increase in coating stiffness, solvent retention, and pore density associated with the increase in coating thickness will affect the glass transition temperature and effective Young's modulus of the coatings, and consequently the residual stress development within the supported film.

2 PROTECTIVE COATINGS FOR OFFSHORE WIND TURBINE TOWERS AND TRANSITION PIECES

2.1 Introduction

This chapter describes the basic principles of protective coatings and current practices for corrosion protection of offshore wind turbines by protective coatings. Oil and gas exploration and extraction platforms have been established in offshore areas for decades. One of the main sources of protection for metallic substrates in corrosive marine environments is the use of protective coatings. The coating industry has developed special coating systems designed to protect offshore structures from corrosion. A simple approach to protect offshore wind energy devices is to adapt coating systems intended for offshore oil platforms to wind towers[1]. It is believed that the real growth in the offshore oil and gas industry was related to the improvements achieved in corrosion protection by the development of modern high-performance coatings such as polyurethanes and epoxy-based paints. Modern coatings possess an inherently better long term stability than traditional ones such as alkyd paints [1, 2].

According to ISO 4618, a paint is defined as a pigmented coating material in liquid, paste or powder form which when applied to a substrate forms an opaque film having protective, decorative or specific technical properties [3]. Coatings are used to attribute specific engineering properties to a material by changing the surface properties by adding a thin layer to the substrate surface. Improvements in corrosion prevention and wear resistance are the two main driving forces for coatings used in the marine and offshore industry. In recent years, the coating industry has concentrated on enhancing reliability and performance of coatings [4, 5]. Organic coatings have long been the most convenient and commonly used method on metals for barrier protection against corrosion. However, corrosion is one of the hardest properties to predict since it depends strongly on when and how the coating fails [4-7]. The present study

[1] According to NACE this approach would also allow for the use of standard assessment schemes developed by the industry and regulatory bodies

concentrates on the mechanical aspect of coating failure. In general, coatings may provide protection to metallic structures through the following mechanisms:

- inhibition of the steel surface,
- cathodic protection, and
- barrier coatings.

The paint samples tested in this thesis all operate as anti-corrosive protective coatings by providing a physical barrier between the substrate and the environment. When used as a barrier coating, the following mechanisms apply:

- physical barrier against corroding species (i.e. H_2O, O_2, and Cl^-),
- the induction of a high electrical resistance into the circuit of the corrosion cell, and
- the suppression of anodic and/or cathodic reactions.

Nonetheless, protective coatings are not completely impermeable, and the initiation of a defect may result in the contact of aggressive species with the metallic surface and local corrosion [7, 9]. The development of minor cracks in a protective coating usually allows corrosion of the steel at the interface, subsequent loss of adhesion, and delamination of the coating [10].

Good adhesion to the substrate, specific mechanical and physical properties and good appearance are all properties which are also usually expected from coatings used to provide corrosion protection. The terms paint and surface coating are often used interchangeably. The term ‘paint’ is frequently used to differentiate a paint film from various other forms of surface coatings and treatments, such as electroplating, anodizing, and the lamination of polymer films onto surfaces [11]. To understand the behaviour of coating systems applied onto metallic substrates it is important to understand the role of the components of paints as well as the function of the different layers that constitute a coating scheme.

2.2 Coating schemes

Modern paint schemes are often a composite system composed of several discrete layers of paint some, or all, of which may be filled and pigmented. The number of layers in the scheme will depend primarily on the environmental conditions in which

the coating will be used in, but will also depend on the type of substrate, and the purpose of the coating. A typical paint system may consist of a primer, undercoat (or midcoat) and a topcoat. Each paint layer in the scheme has a given purpose, and consequently their mechanical and physical properties may differ from each other. The primer seals the substrate and allows good adhesion between the substrate and undercoat. Additionally, it contributes to opacity. The purpose of the undercoat is twofold; along with the primer it will contribute both to hiding the substrate and to smoothing the surface upon which the topcoat will be applied. Finally, the topcoat provides the appropriate aesthetic effect. All layers must have good adhesion to the surfaces below them [11].

Apart from promoting adhesion, the primer must accommodate the stresses developed by the differential movement of the substrate. It may also help relieve residual stresses within the coating system produced by ageing processes of the topcoat and the midcoat. Ageing may produce hardening and ultimately embrittlement of coatings. The undercoat is usually formulated in a colour similar to that of the topcoat, and a given undercoat may be used for several similar topcoat colours. Undercoats, unlike topcoats, are highly pigmented. High levels of fillers usually result in a semi matt or matt surface [11]

2.3 The components of paint

A wet paint, as opposed to a powder coating, is commonly composed of a binder (continuous phase), pigments and extenders (discontinuous phase), and solvent or water. The binder is the film former, and the solvent (in the case of solvent-borne coatings) aids the formation of a uniform and homogenous film. The term vehicle is often used to refer to the binder and solvent. Film formers (or binders) are largely responsible for the mechanical properties of the coating. Pigments are fine solid particles that do not dissolve in the binder and provide specific properties, e.g. colour and hiding power or opacity. Extenders, however, are much cheaper components that do not contribute to the colour of the film but may possess useful properties such as increasing paint viscosity and film strength [11-14]. The components of paint and their function are indicated in **Table 2.1**. Not all paints have every component. For instance, gloss paints are unlikely to contain extenders.

Table 2.1 Composition of paints [11].

	Components	Typical function
Vehicle (continuous phase)	Polymer or resin (Binder)	Provides the basis of continuous film, sealing or otherwise protecting the surface to which the paint is applied The chemical composition varies depending on the application
	Solvent/water	Aids the mixture and application of the paint Not used in compositions such as powder coatings and 100% solvent free systems
Pigments (discontinuous phase)	Additives	Minor components, wide in variety and effect, e.g. catalyst, driers, flow agents and rheological control agents.
	Primary pigment (fine particle organic or inorganic)	Provides opacity, colour, and other optical or visual effects Most frequently used for aesthetic reasons i.e. colour. In primers, anti-corrosive pigment may be included
	Extender (filler) (coarse particle inorganic matter)	Used for wide range of purposes including opacity/obliteration (as an adjunct to primary pigment), to facilitate sanding, e.g. in primer surfacers. Also used to make the formulation cheaper.

2.3.1 Binders

Binders are regarded as the most important constituent of a paint, and as a result, paints are generally named after their binder component (e.g. epoxy paints, chlorinated

rubber, etc.). The binder largely controls many fundamental physical and chemical properties of the coating [14, 15].

There are two main types of binder systems, non-convertible and convertible. A non-convertible binder consists of higher molecular weight polymers which form films solely through loss of solvent or water. No chemical reaction takes place, so a non-convertible binder can be redissolved in the original solvent or water after film formation has taken place. Convertible binders consist of lower molecular weight pre-polymers which form a cross-linked film by reaction with a curing agent. The curing agent may be oxygen or water from the environment or may be a material which needs to be mixed with the pre-polymer immediately prior to application. Once the film has been formed, it cannot be redissolved. When cure is achieved by chemical reaction between the binder and an added curing agent, the paints are commonly commercialised as "two pack systems". **Table 2.2** lists typical low molecular weight film formers [11].

Table 2.2 Typical low molecular weight film formers [11].

Low molecular weight film formers
Oleoresinous binders
Alkyds
Amino resins
Phenolic resins
Epoxide resins
Unsaturated polyesters
Polyurethanes

2.3.1.1 Epoxy resins

The systems under study in the current research are all based on epoxy resin chemistry. Epoxy resins are available in a range of molecular weights, from low molecular weight

liquids to higher molecular weight solids. The lower molecular weight resins are typically used in wet paint where use of the higher molecular weight counterparts would cause a problem with viscosity. The higher molecular weight resins are typically used in powder coatings where components of the formulation need to be solid. Epoxy resins are thermoset polymers that can be cured, or cross-linked, at room temperature by reaction of the terminal epoxy- or epoxide - group with amines or material with amine functionality. Curing can be achieved by polyaminoamines (polyamines), polyaminoamides (polyamides) or adducts[2] of these. Both the structure of the epoxy resin and the type and concentration of the curing agent affects the properties of the cured film during the curing process, long macromolecules cross-link with each other. Consequently, due to the formation of these networks the coating is stiff and brittle, and incapable of flowing when exposed to heat. [4, 11-13, 15-18].

The films obtained by reacting epoxies with polyamines or polyamides have exceptional chemical resistance, abrasion resistance, adhesion, and hardness. Primary or secondary amines such as triethylenetetramine may also be used. However, in order to avoid the toxic hazards associated with handling amines, amine adducts with low molecular weight solid epoxy resins are now also used as hardeners. These adducts are prepared by the reaction of excess of an amine such as diethylene triamine with an epoxy resin to produce fully amine-terminated adduct. Other adducting agents may also be used. [19].

Epoxy resin modification with a silicone resin is manufactured to enhance water resistance; epoxy/silicone combinations are used in blends with other polymers using the cure mechanisms mentioned above [19]. Generally, the curing process of epoxy resins may be accelerated by an increase in cure temperature or slowed-down by lowering the cure temperature. Two-pack systems usually cure at room or low-bake temperatures [20].

Epoxy-based coatings have applications as protective coatings, adhesives for joining various engineering elements and as matrices for composite materials [21, 22]. Almost 50% of the epoxy resins produced are destined to be used in the coatings and adhesive

[2] An “adduct” results from the direct addition of two or more distinct molecules, resulting in a single reaction product.

industry [12]. Epoxy-based coatings are widely used in the protection of metallic materials in marine and offshore environments due to their excellent performance when immersed in sea water. [9]. Epoxy-based coatings generally outperform other classes of coatings due to their versatility, good wetting ability, superior adhesive strength, good abrasion resistance, chemical resistance and convenient physical properties (i.e. low thermal expansion and good chemical and electrical resistance) [22].

The highly cross-linked network structure of an epoxy coating is responsible for its excellent performance in corrosion protection. A three-dimensional network is formed at gel point, which is marked by an irreversible and sudden change from a viscous liquid to an elastic gel, due to the chemical reaction between base (resin) and hardener (curing agent). However, the high degree of crosslinking makes epoxy-based products brittle materials, with weak peeling and impact strength; and they may exhibit low UV resistance. The combination of these factors limits their applications [22-25]. When the aesthetic appearance of the coating is important, the epoxy coating requires a top coat to prevent chalking due to sunlight exposure, such as an aliphatic polyurethane, waterborne coating or a physical drying coating [15]. Thermosets generally have higher dimensional stability and resistance to abrasion than thermoplastic polymers. On the other hand, thermoplastics have better flexural and impact properties [26].

Epoxy resins generally contain a maximum of two epoxide rings at each end of the molecule and may contain a number of hydroxyl groups, along the chain. The presence of the latter makes the resin polar and ensures good adhesion to other polar groups or metallic surfaces. In addition, the polymer chain comprises only carbon-carbon and ether linkages, which are very stable. Very severe conditions are required to break the ether linkage and both linkages are stronger than ester linkages. Therefore, epoxy resins have good chemical resistance [11, 13]. Epoxies consist of a linear chain molecule with a reactive epoxy group at each end. Different types of epoxies differ both in the length of the molecular chain between the epoxy groups and their detailed structure [14]. The epoxide group is specially reactive with active hydrogen atoms such as those present in alcohols, acids, amines and amides [20]. **Figure 2.1** shows the structure of the epoxide group.

Figure 2.1 Epoxide group [19].

The preparation of epoxy resins usually involves epichlorhydrin and a dihydroxy compound. The dihydroxy in question is usually a bisphenol such as bisphenol A though dihydric alcohol is also used. More than 80% of the epoxy resins currently produced are based on the product of the reaction between bisphenol A and epichlorohydrin in an alkaline medium. The variation of the percentages of each reactant will change the properties of the final product [19, 20, 27]. Two reactions of the phenolic hydroxyl produce the polymerization:

- Condensation with chlorine to eliminate HCl, and
- Addition to epoxide, opening the ring to produce one hydroxyl group [11, 13].

Figure 2.2 shows the reaction of bisphenol A and epichlorhydrin in an alkaline medium. **Table 2.3** presents the typical grades of bisphenol epoxide resins and their properties. The epoxide equivalent provided corresponds to the weight of the resin in grams that contains one 'gram-equivalent of epoxy [28]. When 'n' approaches zero, the resin approximates to the diglycidyl ether of bisphenol A, and the product is a liquid. An increase in the number of repeat units, 'n', results in an increase in density and melting points; the products are in solid form [19].

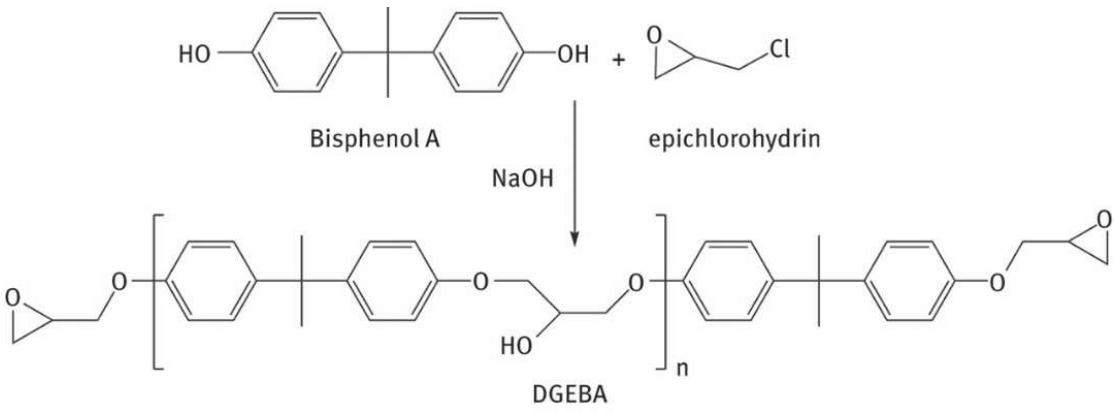

Figure 2.2 Reaction of Bisphenol A and epichlorohydrin in alkaline medium [29]

Table 2.3 Typical grades of bisphenol epoxide resins and properties [19].

Number of repeat units (n)	Melting point (°C)	Epoxide equivalent
0.5	Viscous liquid	225-290
2	64-76	450-525
4	95-105	850-950
9	125-132	1650-2050
12	140-155	2400-4000

Figure 2.3 presents the typical reactions of the epoxide or oxirane group, particularly the ones involving carboxyl, hydroxyl, phenol and amine [19]. The hydroxyl group (-OH) obtained from the reaction may produce further cross-linking under suitable conditions [20].

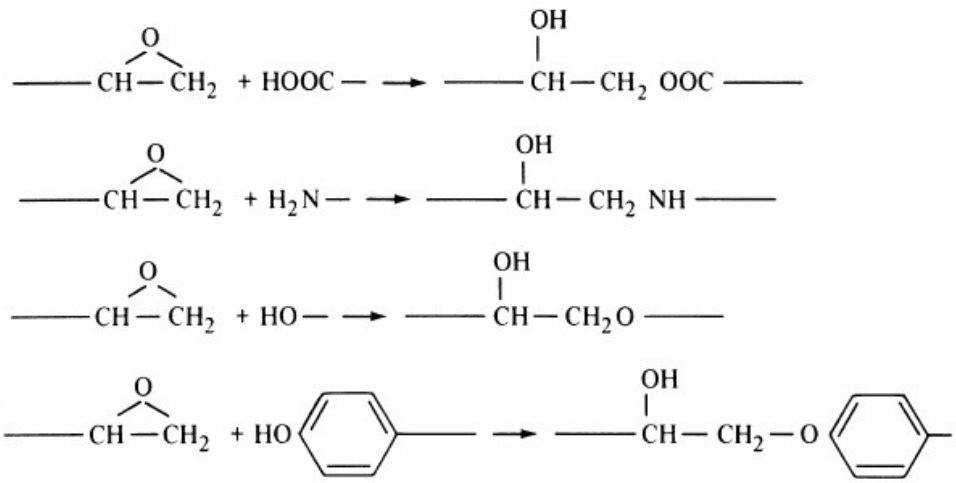

Figure 2.3 Typical reactions of the epoxide group [19].

2.3.2 Solvents

The solvent is the component of the paint that allows the paint components to be dispersed and produces a solution. The function of the solvent is twofold; firstly, it dissolves the resin or binder and other organic components so aiding in the production of a mixed and dispersed system. Secondly, it produces a paint of useful viscosity which assists in achieving an acceptable paint application consistency. In the case of water-based paints, the water acts as a diluent. The low viscosity of paint allows the

material to penetrate crevices in the substrate [11, 13, 14, 30]. Research has concentrated on the selection of suitable solvents for paint formulations. Often, more than one solvent are considered appropriate and a mixture of these is used. Very rarely is only one solvent suitable for a paint system. The selection criteria for solvents involves consideration of a wide range of factors, not only solvency properties. In general, the most important factors are evaporation rate, odour, toxicity, flammability, and cost. The degree of importance of these factors will depend on the paint application. All solvent vapours, excluding water, are considered toxic to some degree [11, 14].

When the paint is first applied, and it begins to dry or cure, the coating is capable of flowing out and accommodating volume changes during the initial stages of solvent evaporation. After the coating has achieved sufficient stiffness, however, further solvent evaporation may produce further coating thickness contraction [31]. The reduction of coating thickness by the combined effect of solvent retention and chemical reaction, termed shrinkage, produces internal stresses within the coating. The glass transition temperature and mechanical strength of the coating are decreased in the presence of residual solvent [25].

2.3.3 Pigments and extenders

Primary pigments contribute to both decorative and protective properties. If a paint formulation does not include pigments, the paint is a varnish. In general, the formulation can have primary pigments, supplementary pigments, extender, and fillers. Pigments and extenders are fine solid particles dispersed in the binder but not dissolved in it, nor are they significantly affected chemically or physically. Secondary pigments, extenders and fillers have a more minor role, but still important, on the overall properties of the paint. These are added to the formulation for other reasons, such as to reduce costs, enhance opacity, control sheen and ease sanding [11, 13, 30, 32]. An improvement in the physical and mechanical properties is not usually achieved by the use of a single type of filler. The final properties usually require the use of a group of fillers of different types and sizes (wide size distribution) in which every filler has an specific function [33].

2.3.3.1 Primary pigments

One of the main uses of primary pigments in paints is to provide colour when dispersed in organic coatings, as the solid pigment particles will absorb and scatter light. Colouring pigments can be either natural or manufactured and are classified as either inorganic or organic types [13, 14, 30]. Due to changes in legislation regarding the use of toxic materials, many of the inorganic pigments historically used by the paint industry have been replaced by less toxic organic materials [11]. The main properties of pigments are mass tone colour; undertone colour; gloss; strength; hiding; particle morphology; particle size distribution; dispersability, effect on viscosity; and stability to light, heat, chemicals, weathering [34].

Pigments impart properties to the coatings such as colour, opacity, mechanical properties, durability, barrier properties, anti-corrosive properties, biocidal properties, chemical resistance, fire resistance, and rheological modification [30].

Lamellar pigments such as mica, aluminium flake, and micaceous iron oxide contribute to the barrier properties, improving the water resistance of the paint films by increasing the distance water molecules must travel to effectively penetrate the film. These pigments are especially useful in coatings with application in the protection of substrates immersed in water or subjected to extreme climates [30].

Inhibitive pigments provide anticorrosive properties to the films by acting as sacrificial anode in the corrosion reaction and consequently preventing electrochemical dissolution. Zinc-rich primers are formulated with a high percentage of zinc metal or alloys which acts as sacrificial anodes. It has been found, however, that an increase in zinc oxide in the binder increases the internal stresses and decreases the adhesive strength of the cured coating [30, 35]. Well known inhibitive pigments for ferrous materials include oxides, chromates, phosphates, and molybdates; of which zinc phosphate, $Zn_3(PO)_4 \cdot 2H_2O$, is the most useful and manageable pigment. The latter is a lamellar pigment with low toxicity, low relative density and is white [30]. Zinc phosphate provides protection by barrier and inhibitive effects [36].

Certain pigments have a profound effect on the rheological properties of the paint by modifying its viscosity. The use of pigments may ease application, reducing sagging, running and excessive flow [30]. The refractive index of white pigments has a

profound effect on the hiding properties. White pigments with a refractive index of 1.7 or higher are classified as hiding pigments. However, white pigments with an index below 1.7 are classified as extenders [37]. In recent years, lighter colours have gained greater acceptance than stronger colours and constitute the largest percentage of pigments in the market. Titanium dioxide (TiO_2) is a highly developed pigment and the most popular, commonly used to provide white to pastel shades [11, 13, 37].

2.3.3.2 Extenders, fillers, and supplementary pigments

In the past, pigments first used in paint were minerals extracted from natural deposits and were refined to varying extents to improve their properties according to the application of the paint. Nowadays, the vast majority of such pigments are known as extenders or fillers [30].

Extenders, or fillers, and supplementary pigments, constitute a wide range of solid materials which are dispersed into the binder. Fillers, or extenders, are primarily used to bulk out the product and cheapen the formulation. Supplementary extenders can be used to improve various characteristics of the paint, such as application and good storage stability; and coating characteristics like water resistance and durability [30]. These materials are dispersed into the binder in the form of insoluble 'powders'. Some, such as talc, have laminar form and are incorporated specifically to improve barrier properties by slowing down the rate of water transmission through to the substrate. Fillers, or extenders, are relatively cheap and are used in conjunction with primary pigments to achieve specific paint formulation at a reduced cost, i.e. $CaCO_3$ cannot completely substitute TiO_2 but is used in conjunction with TiO_2 to contribute to whiteness and opacity and reduce cost. For many formulations, TiO_2 is the most expensive and indispensable component due to its high refractive index and inertness. Calcite ($CaCO_3$), is a significantly cheaper material and its production process is simpler than titanium dioxide's. Thus, any possible substitution of TiO_2 by $CaCO_3$ would be beneficial both financially and environmentally. However, $CaCO_3$ has a slight water solubility and its applications in marine environments are limited [38]. Furthermore, the addition of extenders contributes to adjusting the total volume of pigments to the required pigment volume concentration (PVC) of the formulation without the use of expensive primary pigments (see section 2.5.3) [36].

All extenders are inorganic materials and chemically inert. Many extenders are naturally occurring materials, which are refined to varying extents according to the application of the paint. The paint formulation requires homogeneity and consistency from batch to batch. However, extenders or fillers, particularly mined materials, tend to be more variable in composition and show higher size distribution and diversity of shapes than primary pigments. **Table 2.4** presents the typical extenders [11, 13, 14, 39].

Table 2.4 Typical extenders [11].

Chemical nature	Name
Barium Sulphate	Barites
	Blanc fixe
Calcium carbonate	Chalk
	Calcite
	Precipitated chalk
Calcuim sulphate	Gypsum
	Anhydrite
	Precipitated calcium sulphate
Silicate	Silica
	Diatomaceous silica
	Clay
	Talc
	Mica

Adding nanofillers to organic coatings has been found to reinforce the barrier properties and improve the mechanical properties of the cured film. The benefits of nanoparticles lie in their small size and large specific surface area. The most commonly used nanoparticles are SiO_2, TiO_2, ZnO, Al_2O_3, and Fe_2O_3 [40, 41]. However, there is evidence that nanoparticles can present serious health risks if human exposure occurs during manufacture, so the use of nanoparticles has to be carefully balanced between the improved properties of the coating and an increased risk associated with using these materials.

2.3.4 Additives

To produce a robust protective film, paint formulations require additives. The effect of additives can be dramatic, the addition of small quantities of additives attributes special qualities to the paint or cured film [30]. Typical additives are anti-floating agents, dispersion agents, stabilisers, viscosity controllers, adhesion promoters, antifouling agents, plasticisers and corrosion inhibitors [13, 14]. Plasticisers make a polymer more pliable by lowering its glass transition temperature and elastic modulus. The depression in the glass transition is proportional to the quantities of plasticisers added to the formulation. Plasticisers are particularly useful for paints which are based on binders that tend to be brittle by improving film flexibility [26, 42]. Plasticisers aid the improvement of adhesive strength. The addition of appropriate reactive rubbers is one of the most effective ways to produce high-performance films with optimal chemical, thermal, and mechanical properties [24].

2.4 The curing process of paint

Film formation is one of the most important processes for coatings. Film formation is the process of conversion from liquid to a solid film after application. The rate and extent of film formation are very important aspects of the process and will affect the final properties of the coating. In terms of the manufacturing process, aspects relating to the film formation such as how long it takes for the coating to be dry to touch, over-coated, or stored, and coating performance, are of great importance and closely assessed by both the supplier and the user [43]. The film formation process is often understood in terms of the glass transition temperature (T_g, see section 2.5.1) and its relationship to the coating's viscosity (η) provided by Williams-Landel-Ferry (WLF equation):

$$ln\,\eta_T = 27.6 - \frac{40.2(T - T_g)}{51.6 + (T - T_g)} \qquad \textbf{Equation 2.1}$$

Where:

η_T = viscosity of the polymer,

T = Temperature, and

T_g = glass transition temperature [43].

The viscosity of a polymer glass is assumed to be 10^{12} Pa s ($\ln 10^{12}=27.6$). The required glass transition temperature (T_g,) of the coating, relative to the test temperature, can be calculated by assuming the values of viscosity of a coating that is "dry to touch" [43].

In general, there are two different mechanisms of film formation. One involves curing; which involves chemical reaction whilst the other does not. The 'drying' of paint is accomplished by both solvent evaporation and chemical reactions, in the case of convertible coatings; or by simple solvent evaporation for non-convertible coatings. The latter correspond to simple solutions of fully formed polymers in suitable solvents. The drying process occurs exclusively by evaporation of liquids; the polymer is fully formed and when the solvent evaporates, it hardens over the substrate. The drying process does not produce any changes in the chemistry of the coating. These are known as one pack products and result in low performance systems which are used in low maintenance applications [13, 14].

Cross-linked polymers are insoluble; hence they cannot be re-dissolved in solvents. However, it is possible to carry out cross-linking chemical reaction after application of the paint by having linear polymers or lightly branched polymers in the can. Either of the two following processes can achieve this: drying by chemical reaction between paint and air (oxygen and water vapour are the reactive chemical ingredients in air), and drying, or curing, by chemical reaction between components in the mixed paint (base and curing agent). The products form high performance heavy-duty protective coatings (e.g. epoxy-based coatings) [13, 14].

To ensure that the base and curing agent do not react with each other before application, they are separated into two or more containers and thoroughly mixed before application. These paint systems are called "two-pack systems", accurate measuring of the correct amount of each component is required before mixing and the product, after application, is a cross-linked polymer film [13]. The paint must remain stable in the can for long periods of time, which means that the ingredients must not react with each other, and the pigment/filler has to remain in dispersed form, while being stored. Nonetheless, the paint must dry or cure when applied onto the substrate [13, 14]. A mixture of the two components, base and curing agent, results in a material

which has a limited pot life. Typically, the applied convertible paint cures by chemical reaction between base and curing agent, and evaporation of solvents if present [15]. Generally, the term 'drying' is used to refer to film formation of non-convertible coatings, and 'curing' for convertible coating.

The film formation process of both solvent-borne non-convertible and convertible paints is presented schematically in **Figure 2.4**. Film formation is strongly dependent on the solvent evaporation rate, solvent diffusion through the solvated film, and the rate of chemical reaction (for a convertible coating). The solvent evaporation rate decreases both as a function of solvent type – in general, aromatic solvents tend to have higher boiling points than aliphatic solvents - and with an increase in polymer concentration, whilst diffusion through the film is highly dependent on the size of the solvent molecules, solvent vapour pressure and the weight of residual solvent in the film [12].

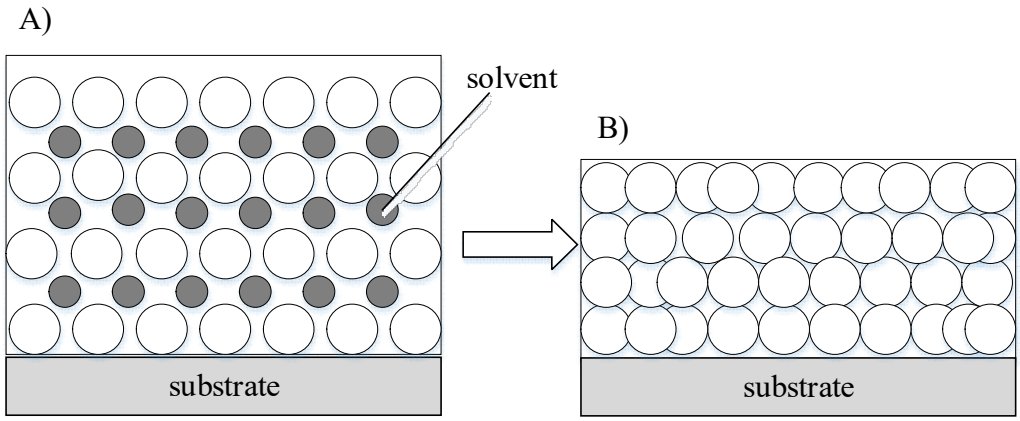

Figure 2.4 Representation of A) wet paint with solvent spread throughout and B) dry/cured coating without solvent.

The changes experienced by the paint during film formation can be explained through the concept of "free-volume". The volume-temperature relationship for polymers is presented in **Figure 2.5**. At temperatures below the glass transition (T_g) the polymer chain mobility is restricted, and the polymer behaves like a solid material. An increase in temperature above the glass transition temperature increases the chain mobility due to an increase in free volume. Therefore, in order to achieve the conversion of a paint into a solid film, the glass transition of the coating must increase during the film

formation process. An increase in T_g is achieved by solvent evaporation and the progressive increase in the cross-linking density by chemical reaction [22, 44].

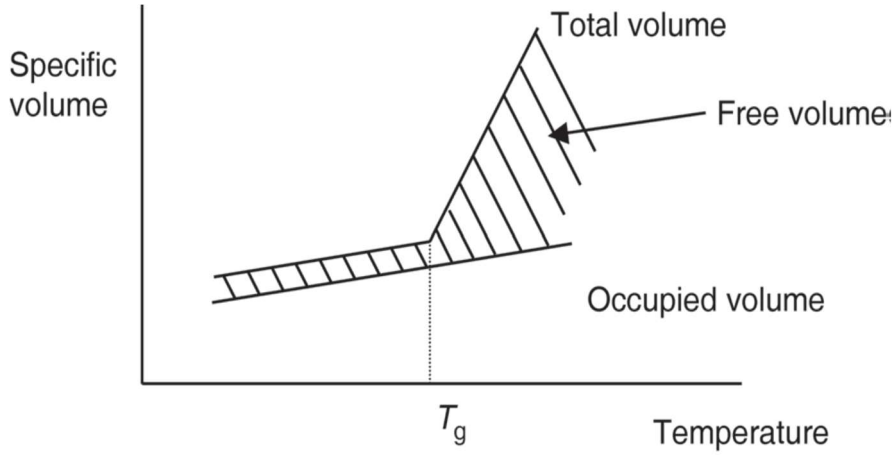

Figure 2.5 Free volume (empty space) variation with temperature in polymers [44].

The control and optimization of the curing process of paints is a crucial factor in the production of high-quality protective coatings. Drying of solvent-borne convertible coatings involves exothermic reactions, the development of stresses due to cross-linking and solvent evaporation, and the development of properties highly dependent on the curing schedule. Therefore, attention must be paid to the cure of paints expected to perform as protective coatings since the efficiency of the coating is highly dependent on its integrity [45].

Surface preparation and application are also crucial: the barrier properties of the coating may be lost if the coating is too thin or may crack if the coating is too thick. Also, the coating must be applied to a well-prepared surface, clean and with the recommended profile to provide adhesion and physical anchoring in the roughness profile. It is important to ensure application is even and paint does not contain defects. Also, that the two components are mixed together in the recommended proportions – excess of one component will mean that the coating cannot cure properly and therefore will not have the expected profile.

2.5 General properties of polymeric materials

2.5.1 Glass transition temperature (T_g)

The glass transition temperature (T_g) is one of the most important thermal properties of organic coatings. The T_g marks the temperature region in which the material transitions from a hard, glassy material to a soft, rubbery material. The temperature rise produces vibrational motion supplemented by rotational motion [46]. This increase in chain mobility produces a dramatic change in the physical and mechanical properties. Thus, it has an important bearing on the potential applications of a polymer.

The glass transition is not a discrete thermodynamic transition but a temperature range, and it is often identified by a temperature, T_g. The temperature range at which the glass transition is experienced depends on the chemical nature of the polymer chains. The changes experienced during the glass transition are reversible. The polymer behaves like a stiff spring below the glass transition temperature, due to the lack of chain mobility. With an increase in temperature, an increase in thermal energy allows the polymer segments to move. The change from glass state to rubbery state is achieved by the introduction of sufficient thermal energy into the system [16, 18, 26].

Epoxy-based coatings, as with most other two-pack systems, are thermosetting polymers. However, in the glass transition region they soften. Moreover, cross-linked polymer chains have multiple degrees of freedom and modes of polymer chain movement when exposed to temperature changes. The glass transition temperature is highly dependent on the degree of cure, as shown in **Figure 2.6**, and the reported T_g is usually represented by the T_g associated with 100% conversion (T_g^{∞}). The glass transition temperature increases with an increase in crosslinking density, a higher crosslinking density causes larger polymer segments. The glass transition temperature is also dependent on temperature of cure, and on whether a post-cure schedule is applied. If a coating is cured at low temperatures, such as room temperature, the resulting T_g of the material will be the lowest for that composition. Conversely, if the same coating is post-cured at a higher temperature the resulting T_g will be higher. By subjecting the coating to heat after the initial application (known as post-cure), it both accelerates the cross linking process and produces a greater degree of cross linking than would be achieved if the coat was left to cure at room temperature [16, 18, 26].

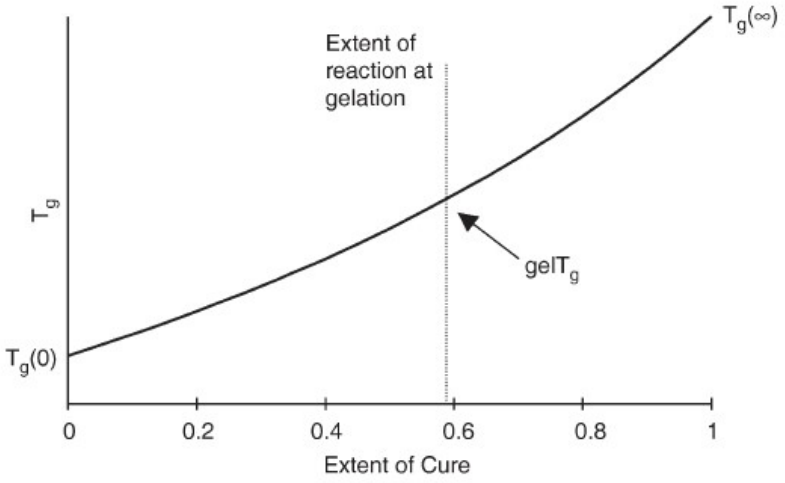

Figure 2.6 Typical dependence of the glass transition temperature on the extent of cure [44].

Secondary forces also affect the glass transition temperature; e.g. retained solvent can lower the glass transition temperature. The rule of mixtures can estimate the resultant glass transition temperature of the mixture coating/solvent:

$$T_{gM} = \frac{\varphi_p \alpha_{tp} T_{gp} - (1 - \varphi_p) T_{gs}}{\alpha_{tp} \varphi_p + (1 - \varphi_p) \alpha_{ts}} \qquad \textbf{Equation 2.2}$$

where:

T_{gM} = the glass transition temperatures of the mixture,
α_{tp} = the linear coefficient of thermal expansion of the polymer,
α_{ts} = the linear coefficient of thermal expansion of the solvent,
T_{gp} = the glass transition temperatures of the polymer,
T_{gs} = the glass transition temperatures of the solvent, and
φ_p = volume fraction of polymer in the mixture [18].

In general, the glass transition temperature is a useful parameter for characterisation of materials in terms of their processing and application conditions, thermal history, stability, degree of cure, mechanical and electrical behaviour [47].

2.5.2 Linear coefficient of thermal expansion

The linear coefficient of thermal expansion provides a measurement of the volume changes that occur in the polymer due to temperature variations. It indicates the changes in size per degree of temperature change at a constant pressure. The linear coefficient of thermal expansion varies with temperature. However, it is common practice to consider it constant within typical design and processing conditions. When polymers are filled with small particles or short fibres, the linear coefficient of thermal expansion can be determined by the rule of mixtures as follows:

$$\alpha_c = \alpha_p(1 - \varphi_f) + \alpha_f \varphi_f \qquad \textbf{Equation 2.3}$$

where:

α_c = coefficient for the composite,

α_p = coefficient for the polymer,

α_f = coefficient for the filler, and

φ_f = is the volume fraction of the filler [18].

The thermal expansion coefficient of coatings is related to the different binding forces in the film. A direct relationship between cross-linking density and stiffness exists for protective coatings: an increase in crosslinking density produces an increase in the stiffness of the polymer chains [48]. For polymeric materials, the thermal expansion coefficient (CTE) experiences an inflection point at the glass transition due to structural changes the materials experience during the change from glassy to rubbery state. Changes in the interstitial free volume and hole free volume experienced with an increase in temperature (**Figure 2.7**) are dependent on the crosslinking density and influence the CTE in the rubbery region. CTE is not constant below Tg [49]. Inorganic fillers are added to epoxy-based paints to produce organic-inorganic composites with improved thermal stability, glass transition temperature, and dimensional stability [50].

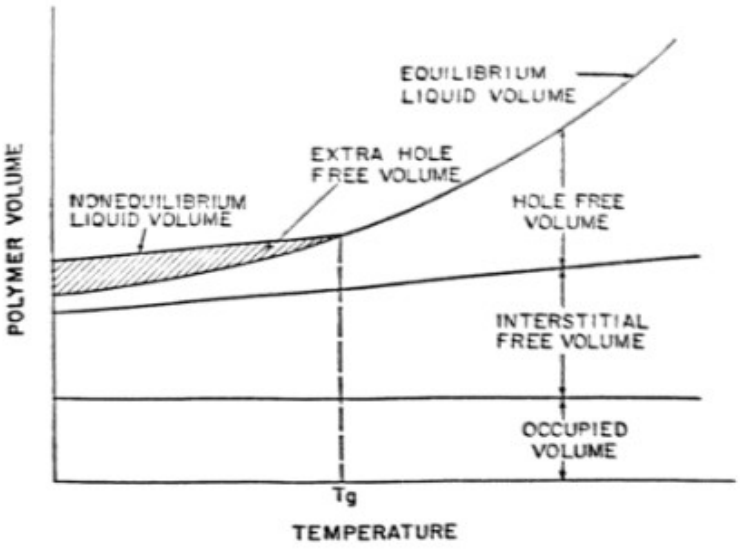

Figure 2.7 Characteristics of a polymer above and below the glass transition temperature [51].

2.5.3 Pigment volume concentration (PVC)

The presence and concentration of pigments and fillers has an important bearing on aesthetic and physical properties, as well as on the internal stresses in the cured film [39]. The pigment-volume concentration (PVC) represents the fractional volume of pigments in the total volume solids of the paint. The critical pigment-volume concentration (CPVC) characterises the optimum PVC and dramatic changes are observed above CPVC values. Low PVC values tend to produce glossiness and resistance to moisture permeation; properties which are lost above CPVC [12]. The ratio of the pigment volume concentration to the critical pigment volume concentration is known as one of the most important parameters of paints, and variations on this ratio can have a significant effect on its properties [52]. CPVC can be determined by the following equation:

$$CPVC = \frac{1}{1 + \overline{OA}\rho / 93.5} \qquad \textbf{Equation 2.4}$$

where $\overline{OA}$ is the oil absorption value of the pigments in linseed oil and ρ is the density of the pigments [12]. **Figure 2.8** shows the effect of PVC on some paint properties and

performance (rusting and blistering are both performance issues). Generally, permeability is the property which leads to rusting.

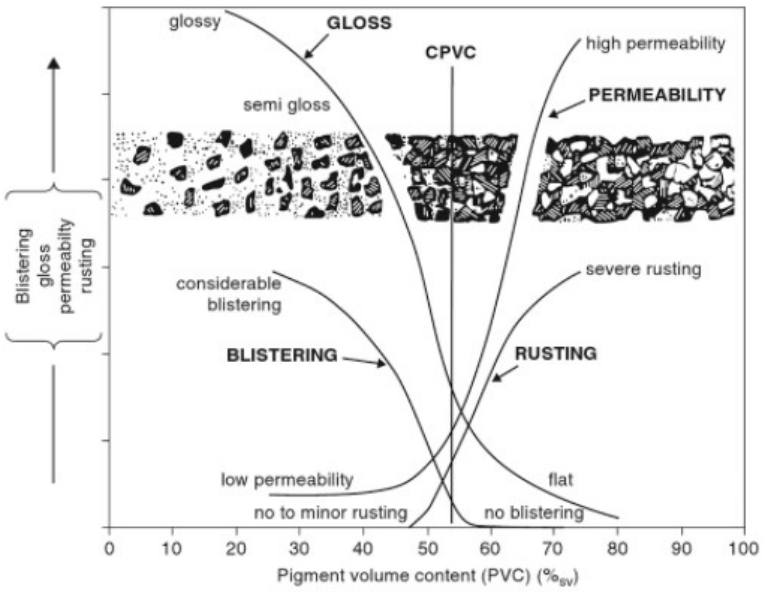

Figure 2.8 Effect of varying PVC on paint properties (Meyer et. al. 1997) [39].

2.6 Protective coatings for offshore wind turbines

Correct specification and application of a protective system in a marine environment is especially important due to the severity of exposure to corrosive elements. Painting is the last step during the production process, and any delays in production may compromise the quality of the paint application. The cost of coating repairs onshore are approximately 5 to 10 times more expensive than the original application costs in the paint shop. If the coating system fails prematurely on site, repairs must be performed offshore and these can cost more than 100 times the original application costs [53]. The following standards control corrosion protection of offshore structures in Europe:

- DIN EN ISO 12944-5: 2007 “Paints and varnishes – Corrosion protection of steel structures by protective paint systems – Part 5: Protective paint systems” [15]
- NORSOK Standard M-501 (2004) “Surface preparation and protective coating” [54]

- ISO 20340:2009 “Paints and varnishes – Performance requirements for protective paint systems for offshore and related structures” [55]

The effectiveness of a two-pack paint system not only depends on the formulation of the paint but also on the proportions of the two components which produces the product that provides corrosion protection. Many factors such as mixing ratios, curing temperature, and substrate’s surface preparation affect the quality of the finished product. About 50% of all premature failures of corrosion protection systems are due to application related problems [53]. According to EN ISO 12944, the most important factors affecting the durability of the coating system are:

- Design of the structure, access possibilities;
- Design of edges weld seams;
- Workmanship of the application;
- Conditions of the steel before surface preparation; and
- Exposure of the paint system immediately after completing application [15, 53].

An offshore wind energy device is composed of a foundation, a transition piece, a tower and turbine. Additional information regarding the offshore wind turbine industry is presented in Appendix A. In deep waters, monopiles are the most commonly used support sub-structure, representing 80.8% of installed substructures in Europe [56]. A monopile support structure is a steel cylindrical tube that is attached to the seabed, with or without excavation. **Figure 2.9** shows a typical arrangement of monopile, transition piece and tower for an offshore wind turbine [57, 58].

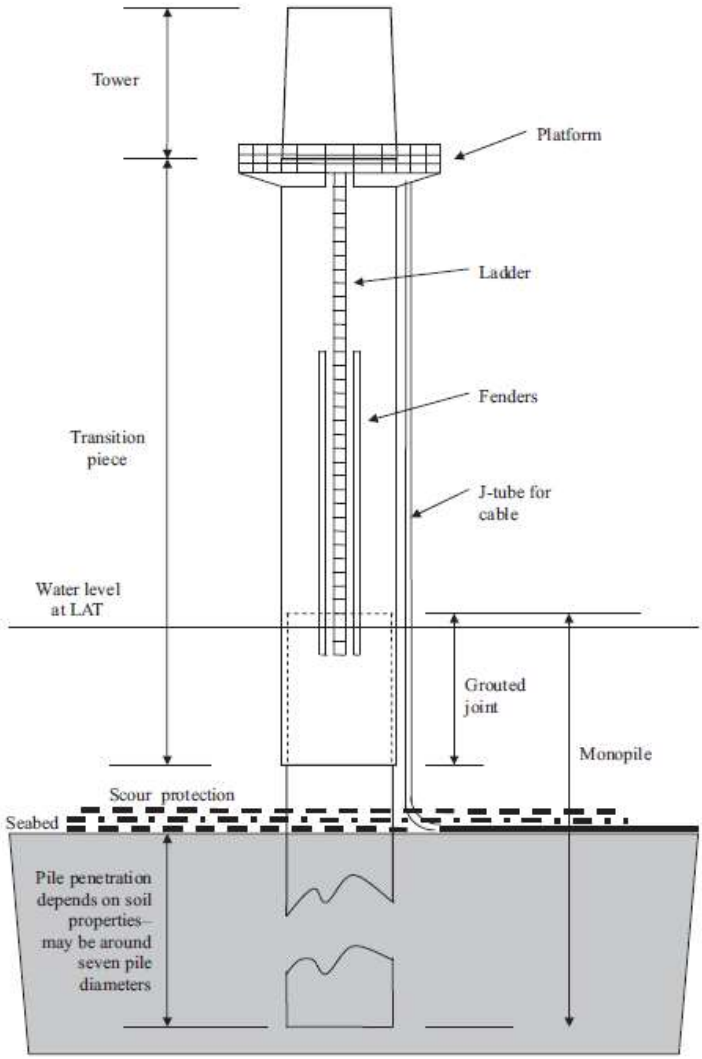

Figure 2.9 Typical arrangement of monopile and transition piece [1].

The diameter of the monopile in water depths of up to 10m at lowest astronomic tide (LAT) can range from 1.5 to 5m. The sizing requirements of the monopile is aimed at achieving resistance to extreme loads, resistance to fatigue loads, and the dynamics of the support structure's natural frequency (to avoid excitation by cyclic loading). Fixed bed offshore wind turbine foundations such as monopile offer the possibility of installing wind turbines further into the sea. Monopiles of 6m in diameter are required in deep waters. It is common practice to incorporate a "transition piece" in large monopiles to aid in maintaining the monopile vertical during operations[3]. The transition piece is tapered above the grouted joint in order to reduce the exposure to

[3] Exceptionally, at Scroby Sands wind farms, driving conditions were considered sufficiently favourable for the towers to be bolted directly to integral flanges at the top of the monopiles.

wave loading. As the name shows, it is a transition between the monopile and the tower. Transition pieces over 25m long, and consequently 200 tonnes in weight, may be required for installations in UK waters. 'Scour protection' in the form of rock armour is placed around the foundation to prevent erosion in the seabed (if its formed by sand and other granular materials) due to currents and water motion [57, 58].

The protective coating schemes currently used vary depending on the corrosive environment in which they are to work in. The exterior of the wind tower which is exposed to seawater/salt spray and an atmospheric corrosive environment must be protected with a high quality, multi-layer surface coating [57, 59]. Monopile towers are metallised and painted on the outside. On the inside, however, the steel is only metallised on the lower part (in some cases) and a paint system is considered enough for the upper sections [53].

All offshore wind towers are fully metallised unlike onshore counterparts, which are only metallised on the edges of the tower sections. Typical nominal dry film thickness of metallization coats is between 60 and 100µm. In the manufacturing of towers and transition pieces, reliability, quality and speed of production are crucial factors. Optimization of the production process results in increased production. One way to accelerate production is to optimise, or decrease the time required for, the paint process. This could include shorter application times, the ability to apply an over coat after a shorter period of time, which is linked to faster curing systems, and/or application of a post cure process to speed up elimination of solvent and reduce curing time. It is important for the coating on the towers to be dry enough, so they can be moved out of the production line to storage (for both automatic and manual processes). **Table 2.5** presents recommended paint systems for thermally sprayed (metallised) metal surfaces for C5-M environments (very high corrosivity marine environment) as suggested by DIN EN ISO 12944. Nowadays, regardless of the benefits of metallisation, the need for cost reduction, less application time, and experience in the field are pushing the industry towards reducing, and or removing the metallizing process from wind turbine tower construction and moving towards the use of single layer coating schemes (epoxy-based) rather than 2- or 3-layer schemes. According to DIN EN ISO 12944, for un-metallised steel structures in environments classified as C5-M, use of the following paint systems, as detailed in **Table 2.6** are suggested[15].

Table 2.5 Paint systems for thermally sprayed metal surfaces for corrosivity categories C5-M [14].

Substrate: thermally sprayed metal (zinc, zinc/aluminium alloys and aluminium)
Surface preparation: See ISO12944-4:1998, Clause 13
It is recommended that sealing or application of the first coat of the paint system be carried out within 4h
If used, sealers should be compatible with the subsequent paint system

Sealer coat			**Subsequent coat(s)**		**Paint system**
Binder	**No. coats**	**NDFT[b] in µm**	**Type of binder**	**No. coats**	**NDFT[b] in µm**
EP, PUR	1	NA[h]	EP, PUR	2	160
EP, PUR	1	NA[h]	EP, PUR	3	240
EP	1	NA[h]		3	450
EP, PUR	1	NA[h]	EP, PUR	3	320

Type of binder	**No. of components**	**Water-borne possible**	**Binder for subsequent coat(s)**	**No. of components**	**Water-borne possible**
EP = Epoxy	2-pack	√	EP = Epoxy	2-pack	X
EPC = Epoxy combination	2-pack		EPC = Epoxy combination	2-pack	
PUR = Polyurethane, aromatic or aliphatic	1 or 2-pack	√	PUR = Polyurethane, aromatic or aliphatic	1 or 2-pack	X

[b] NDFT = nominal dry film thickness

[f] Water-borne products are in general not suitable for immersion

[g] The durability is in this case related to the adhesion of the paint system to the thermally sprayed substrate

[h] NA= not applicable. The dry film thickness of the sealer coat will not significantly contribute to the total dry film thickness of the system

Table 2.6 Paint systems for low-alloy carbon steel for corrosivity categories C5-M [15].

Priming coat (s)				Subsequent coat(s)	Paint system	
Binder	**Type of primer[a]**	**No. coats**	**NDFT[b] in µm**	**Type of binder**	**No. coats**	**NDFT[b] in µm**
EP, PUR	Misc.	1	150	EP, PUR	2	300
EP, PUR	Misc.	1	80	EP, PUR	3-4	320
EP, PUR	Misc.	1	400		1	400
EP, PUR	Misc.	1	250	EP, PUR	2	500
EP, PUR	Zn (R)	1	60[e]	EP, PUR	4	240
EP, PUR, ESI[d]	Zn (R)	1	60[e]	EP, PUR	4-5	320
EP, PUR, ESI[d]	Zn (R)	1	60[e]	EPC	3-4	400
EPC	Misc.	1	100	EPC	3	300

EP= Epoxy

EPC= Epoxy combination

ESI= Ethyl silicate

PUR= Polyurethane, aromatic or aliphatic

a Zn (R) = zinc-rich primer

b NDFT = nominal dry film thickness

Manual airless spray application produces variations in dry film thickness (DFT) across the tower, which can result in thicknesses up to 3 times the nominal DFT (NDFT). This wide variation in thickness, due to overlapping of application passes is less likely when using automatic application processes. The magnitude of the internal stresses within the coating is thought to be dependent on the thickness of the coating, and unevenness of the thickness profile. Complicated sections such as brackets, and weld seams are especially sensitive to failure, both areas where high coating thickness are more likely.

2.7 Summary

The wind energy industry is increasingly moving to offshore areas and increasing both the size and number of wind turbines. Since these are unmanned structures with limited access, costs of repairs are significantly higher than for onshore repairs and higher reliability of the corrosion protection system is expected. The corrosion protection of steel in seawater is achieved by active (cathodic) and passive (coatings) protection. There are environmental issues associated with the use of sacrificial anodes and the use of coatings reduces the need for these. In recent years, research has directed interest towards developing coating materials capable of tolerating hostile marine climates with temperatures ranging from -25°C to +25°C with minimum maintenance [11, 57, 58, 60]. Protective coatings act as a physical barrier by tightly adhering to the metal and protecting it against corroding agents. However, organic coatings are not perfectly impermeable, and the presence of a defect can allow the corrosive agent to attack the surface and initiate corrosion [6, 7, 14, 61, 62]. The market for corrosion protection of steel wind turbine towers and transition pieces is marked by a strong competition [53].

In the corrosion protection of metallic structures with coating systems, the nature of the surface and roughness of the substrate play a crucial role. The adhesion performance of the paint will be affected by the nature and cleanliness of the surface. Moreover, chemical degradation of the paint can produce changes in the mechanical properties and subsequent deterioration of the system. In many cases, deterioration of paints is due to changes in the chemical nature of the film former (chemical degradation) rather than the pigments. The development of new and improved pigments may contribute to the durability of the coating. However, in most cases the weakest link is the film former. It is crucial to produce paint systems capable of

accommodating high levels of contamination and variability of surfaces. A paint system is termed “robust” when a desired level of tolerance can be achieved [11].

An increasing number of studies of the stress phenomena experienced by organic coating films provides strong evidence linking stress to coating degradation. Modern coating systems such as two-pack epoxides are more susceptible to high stresses than traditional coatings such as alkyd paints [63]. It is imperative to understand the underlying physics of the curing film, the effects of mechanical stress on the film, and the manner in which the film responds; in order to fully comprehend coating failure and therefore, avoid it and ensure good coating performance during the components lifetime [64].

3 MECHANICAL BEHAVIOUR OF PROTECTIVE COATINGS

3.1 Viscoelastic behaviour of organic coatings

The present chapter gathers the key aspects affecting the barrier properties and mechanical properties of paints for marine environments. Organic coatings respond in a non-linear manner to mechanical stress and strain. The mechanical behaviour of the coatings will run from that of ideal elastic solids to Newtonian liquids. The characteristic properties of elastic solids and Newtonian liquids are Hookean elasticity and viscosity, respectively [46, 65-69]. In an ideal elastic solid, strain is stored as potential energy within the molecular arrangement. The molecules adapt to the higher level of energy and resume their original levels once the stress is removed. Conversely, in a Newtonian liquid the energy causing the strain is dissipated as the liquid flows to relieve the stress in the form of kinetic energy. The coexistence of both behaviours is known as viscoelasticity [46].

The modulus of elasticity is one of the most important properties for understanding the strength and performance of a coating and the functionality of the coating/substrate system. Understanding the mechanical properties of protective coatings is crucial for the adequate selection, application and maintenance of coatings [22, 65-67, 69].

Hardness is frequently related to brittleness in films, and flexibility is often related to ductility. Increase of hardness can be experienced by the coatings due to rapid temperature changes and often leads to coating failure due to flaking. Flexibility, on the other hand, is introduced into cross-linked films by increasing the space between cross-links. Polymer-based coatings are made more flexible by the introduction of plasticisers to separate the large polymer chains and reduce the attractive forces between them [13].

The mechanical properties of paint films evolve with time as they cure progressively during their lifetime. This includes the ultimate mechanical properties such as tensile strength, elastic modulus and fracture strength. This progressive evolution influences the durability of the coating as an effective protective system [69].

3.2 Dynamic mechanical analysis of coatings

As viscoelastic materials, the mechanical behaviour of organic coatings consists of an elastic component and a viscous component. Dynamic mechanical analysis (DMA) allows the characterisation of coatings by isolating the two components from the overall mechanical response. The elastic component is represented by the storage modulus (E') whilst the viscous component is represented by the loss modulus (E''). DMA studies the evolution of the viscoelastic properties as a function of time, temperatures and frequency. In the study of coatings, DMA is considered a far more valuable technique than simple static stress-strain analysis [47, 64, 69]. **Figure 3.1** shows an example of a thermogram of an organic coating showing the storage modulus, loss modulus and tan δ (E''/E'). At temperatures below the glass transition, the material is in the glassy state and the storage modulus is nearly constant: the material behaves as an elastic solid. During the glass transition, the configurational changes developing in the material cause a drastic decrease of the storage modulus. In the rubbery state the storage modulus stays relatively constant with the increase in temperature: the material behaves as a viscous liquid. At high temperature, viscous flow dominates the material's response and the loss modulus and tan delta experiences a peak during the glass transition [68, 69].

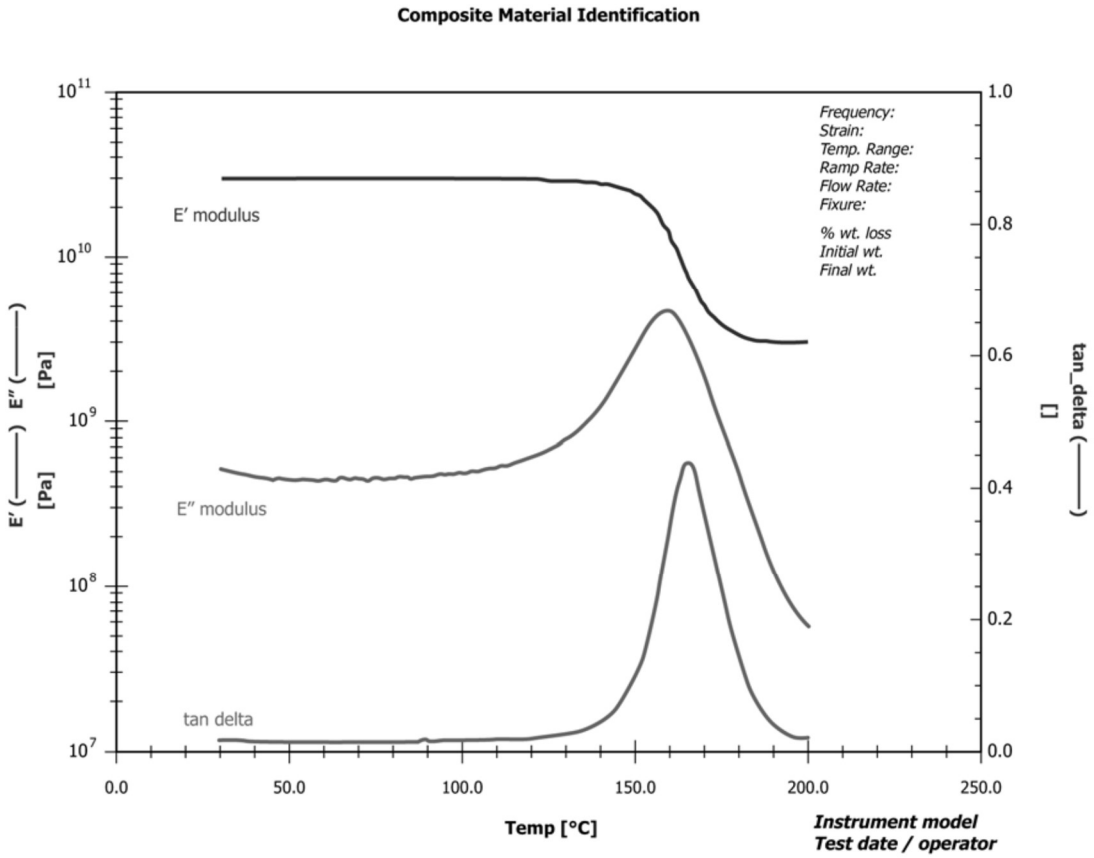

Figure 3.1 An example of an ideal DMA thermogram showing storage modulus, loss modulus, and tan delta [70].

3.3 Adhesion

During cure, the paint will change from a liquid to a solid and mechanically lock onto the surface of the substrate; the adhesion of the coating will also depend on the strength of the coating/substrate molecular attractions. These attractions can be significantly improved with the addition of chemical groups in the binder that promote adhesion to metals, (e.g. carboxyl groups) [13].

Inter-molecular attractions operate over short distances (less than 10nm), the strength of the attraction is reduced with an increase in distance between the atoms. For a paint to effectively adhere to a substrate, it must wet the surface, dispersing air and other adsorbed materials. In general, it needs to have good adhesion to it, be flexible enough to completely cover the surface, and must be able to maintain protective properties for long periods of time. The critical surface tension (γ_c) is a measure of the material's ease or difficulty to be wet by another material. The wet paint must have a surface tension (γ) equal or lower to that of the substrate. Contaminants on the surface of the

metal drastically affect its surface tension. If the paint is applied onto a contaminated substrate surface, it will adhere to the contaminants and not the substrate. It might also not wet the surface properly if the paint is repelled by the contaminant as happens with cases caused by the presence of silicone. Substrate cleanliness is crucial for good adhesion [13]. Additionally, the roughness of the surface also contributes to adhesion by providing a physical key for the coating to lock into i.e. adhesion is achieved by a mixture of both physical and chemical contributions.

3.4 Stresses development in organic coatings

According to Hooke's Law, an increment in the induced strain (ε) will produce a proportional increase in the stress produced (σ). The stress in the coating is shown by the following equation:

$$\sigma = \frac{E\varepsilon}{1-\nu} \qquad \textbf{Equation 3.1}$$

where:

σ = stress,

E = elastic modulus,

ε = strain, and

ν = Poisson's ratio.

The Poisson's ratio is a dimensionless ratio and it defines the relation of the lateral strain to the axial strain. **Equation 3.1** represents the stress for a biaxial deformation, taking into consideration the Poisson's ratio of the material [71].

Stresses are developed in all stages of the coating's life. Stresses may be due to internal or external factors, and tensile or compressive in nature. Internal stresses may be experienced due to film formation, thermal history, presence of pigments, aging, and film thickness. External stresses may be due to bending and forming, abrasion, impact, electrical stress, and substrate effect. The latter will largely depend on the environmental conditions experienced by the coatings [65]. Tensile stresses typically

result from the coating's contraction due to film formation and exposure to low temperatures; whereas compressive stresses result from coating expansion due to increase of temperature (reducing the 'T-T_g gap'), decrease of the elastic modulus, and increase of flexibility of the film. Compressive stresses are more likely to dissipate than tensile stresses, and are considered less damaging [72]. **Figure 3.2** schematically represents examples of the different causes of contractive and expansive stresses in a coating. Film formation and the extraction of soluble film constituents cause contraction of the film. Swelling by water intake causes expansive internal stresses. The internal stresses experienced by the film will be the sum of all the different stress components [73].

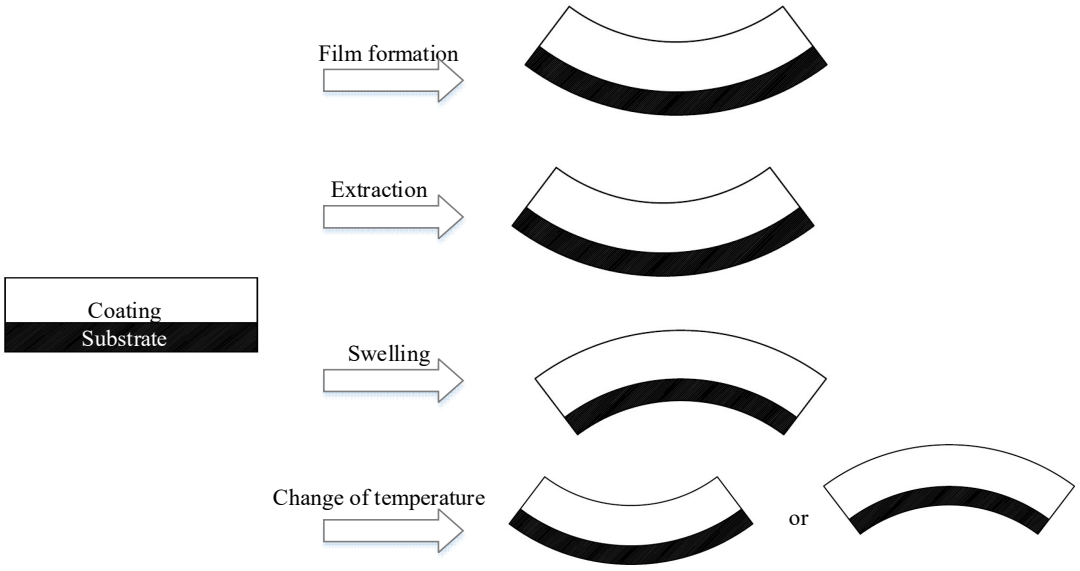

Figure 3.2 Residual stresses in organic coatings [73].

Compressive and tensile stresses will act against adhesion and cohesion, the total stresses experienced by the coating is cumulative. If the tensile and compressive stresses experienced are large enough, cohesive or adhesive failure may occur (i.e. cracking or peeling, respectively) [63, 72, 74]. Failure can also occur at low stress levels if there are heterogeneities in the coating that could act as stress concentrators. These heterogeneities may be uneven dispersion of pigments, presence of impurities, holes, and variations in film thickness [63]. In general, the complex system of stresses (internal and external) experienced by the coatings is influenced by the following factors:

- coating's chemistry,

- composition,
- curing mechanism,
- thickness,
- age,
- conditions under which film formation took place, and
- the service condition in which the film operates.

The three main sources of internal stresses in the coatings are as follows:

- film formation,
- variation in temperature, and
- variation in relative humidity (RH).

The stresses listed above are generally known as: curing, thermal, and hygroscopic stresses respectively. Hygrothermal stresses refers to a combination of thermal and hygroscopic stresses [35, 63]. Curing stresses are also known in the literature as shrinkage, internal, or drying stresses.

Residual stresses always exist within a coating to some extent. Their presence will generally affect the mechanical properties of the coating and consequently, their performance. This will influence the decision of whether to test a coating as a free film or supported to determine their mechanical properties. Stresses due to film formation will act against adhesion. Only when high compressive stresses from environmental factors or service conditions act upon the coating, will tensile stresses act in favour of adhesion and cohesion. In most robust coatings, internal stresses are smaller than cohesive and adhesive forces keeping the coating/substrate system together. Generally, these stresses will be stored within the film reducing its capacity to accommodate any additional tensile stresses from external factors during service [72]. Additionally, any polymer which has been stressed for a long time will be weaker than one stressed for a short time [75].

3.4.1 Effect of film formation on stress development

The film formation of solvent-borne convertible coatings involves a reduction in volume due to the combined effect of solvent evaporation, chemical reaction between binder and hardener, and the cooling process from curing temperature to room

temperature (for systems cured at high temperatures). When a coating is applied to a rigid substrate and cured, it is restrained by its adhesion to the surface area that the wet paint was applied to. Therefore, any reduction in volume will be reflected in the thickness of the coating. After the film cures, the resistance of the coating to accommodate a change in volume produces residual stresses parallel to the plane of the coating, which cannot flow to accommodate the changes [31, 35, 63, 72, 76].

Figure 3.3 presents the stages of stress development for convertible solvent based supported coatings. At the initial stage (stage 0) most of the reduction in thickness will occur while the mixture is in liquid state, and therefore will not produce residual stresses [31]. Solvent evaporation is controlled by volatility and occurs without difficulty. In stage 1, the film starts to reduce its viscosity, volume contraction is restricted, and stress develops within the film. From this stage, the controlling mechanism in the solvent loss process is diffusion-controlled. In stage 2 different behaviours may be observed depending on the coating's composition. The stress development will be the result of two opposing processes acting simultaneously: the progressively increasing curing stresses and stress relaxation. Stress relaxation becomes evident in stage 2. The stress relaxation process will be affected by the presence of any defects, cracks, micro-cracks, or loss of adhesion in the film [63].

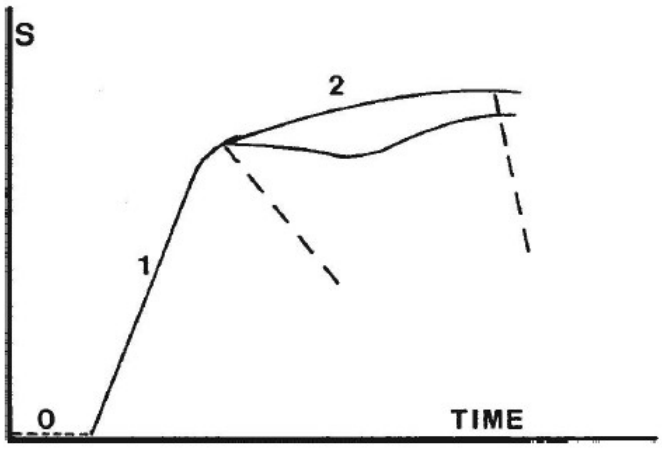

Figure 3.3 Schematic description of stress (S) dependence on time [63].

The strain developed on film formation can be expressed in terms of the volume changes experienced by the coating due to cross-linking and solvent loss. The strain can be expressed as:

$$\varepsilon^c = \frac{V_s - V_t}{3V_s} = \frac{\Delta V}{3V_s} \qquad \textbf{Equation 3.2}$$

Where:

ε^c = strain in the film,

V_s = volume of solvent in the film,

V_t = volume of the dry film at a time, t, after solidification, and

The stress due to film formation, σ^c, can now be determined by combining **Equation 3.2** and **Equation 3.1** to produce Equation 2.3:

$$\sigma^c = \int_{V_t}^{V_s} \frac{E}{1-\nu} \frac{1}{3V_s} dV \qquad \textbf{Equation 3.3}$$

Figure 3.4 shows the dependence of the solvent volume fraction (V_s/V_f) and stress ($S \; or \; \sigma$) with time for solvent-borne coatings. Stresses develop in the film when the glass transition temperature is at least equal to the experimental temperature, and the diffusion process begins (stage II). In stage II the liquid paint forms a solid coating, and the volume fraction $\left[V_s/V_f\right]_s$ corresponds to the volume fraction necessary to increase T_g over the experimental temperature [63, 72].

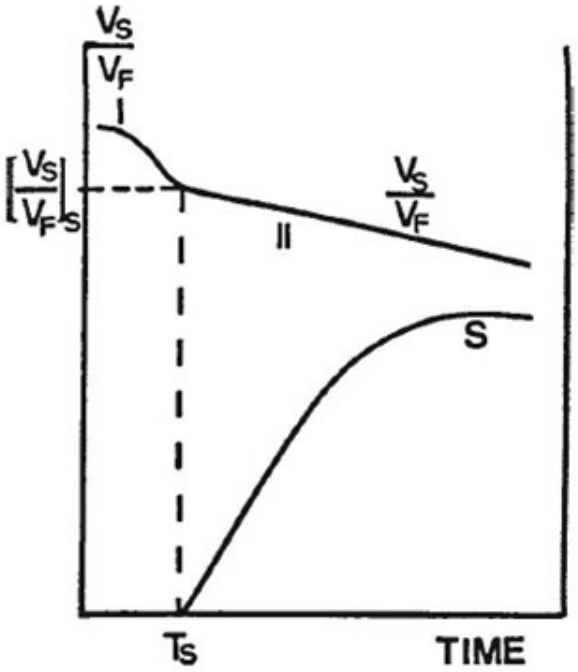

Figure 3.4 Schematic representation of the dependence of Vs/Vf and stress (S or σ) on time, Vs=volume of solvent present in the film; Vf= volume of the dry film [63].

The main factors influencing the magnitude of curing stresses are the elastic or Young's modulus, T_g of the coating, plasticising effect of residual solvent, pigmentation, and crosslinking [35]. If the application processes involves elevated temperatures, thermal stresses will also be produced [31]. Curing stresses are also affected by factors at the molecular level, configuration and conformation affect molecular movement. The mobility of the macromolecular segments affects the ease with which the coating reacts to the changes. Inter-chain cross-links, bulky side groups, hydrogen bonds, and chain entanglements can all contribute to stress development, as they obstruct film compaction [72].

Conformational and configurational changes in molecular structure due to curing and polymerization do not stop after film formation. Slow release of retained solvent and the last stages of polymerization continue to develop for months after application. These progressive changes result in internal stresses; the extend of the stresses will depend on the components in the formulation and the environment [77].

Due to irregular stress distribution, curing stresses increase at the vicinity of the free ends of the coating, by about 30% [35]. Moreover, modern thermoset coatings such as

epoxy-based coatings, are more susceptible to high internal stresses than traditional coatings such as alkyd paints [63, 74].

3.4.2 Effect of temperature on stress development

When a coated metallic substrate is exposed to temperature variations, dimensional changes are induced into the system. Since the thermal expansion coefficient (CTE or α) of polymeric materials is generally higher than that of metals, there will be a strain mismatch in the system and a thermal stress (σ^T) will be developed [63]. **Equation 3.4** shows the thermal strain, ε^{T}, produced by temperature changes in a substrate/coating system:

$$\varepsilon^{\mathrm{T}} = (\alpha_{\mathrm{c}}^{\mathrm{T}} - \alpha_{\mathrm{S}}^{\mathrm{T}})\Delta\mathrm{T} \qquad \textbf{Equation 3.4}$$

Where:

$\alpha_{\mathrm{c}}^{\mathrm{T}}$ = thermal expansion coefficient of the coating, and

$\alpha_{\mathrm{S}}^{\mathrm{T}}$ = thermal expansion coefficient of the substrate.

The combination of **Equation 3.1** and **Equation 3.4** provides **Equation 3.5**, which shows the thermal stress, σ^{T}, experienced by the system [63]:

$$\sigma^{\mathrm{T}} = \int_{\mathrm{T_2}}^{\mathrm{T_1}} \frac{\mathrm{E}}{1-\nu}\left(\alpha_{\mathrm{c}}^{\mathrm{T}} - \alpha_{\mathrm{S}}^{\mathrm{T}}\right)\mathrm{dT} \qquad \textbf{Equation 3.5}$$

Figure 3.5 presents the effect of temperature on the stress (S or σ), elastic modulus (E), Poisson's ratio (ν), and thermal expansion coefficient (α or CTE). A drastic change in these parameters is experienced at $\mathrm{T_g}$. In the glassy region, stress show a linear dependence with temperature due to the independence of E, ν, and α with temperature in this region. In the rubbery region, the stress is very low and constant [63].

In solvent-borne thermoset coatings subjected to post-curing schedules, an increase in the modulus is observed. The coating contracts due to evaporation of residual solvent

and other low molecular weight volatiles. As a result, the internal stresses increase and reaches a stress equilibrium. In service, if the application temperature is different from the service temperature, further thermal stresses will be developed due to thermal expansion mismatch between the coating and the substrate. If the service temperature is lower than the application temperature, there will be an increase in residual tensile stresses during service. Additionally, the volume shrinkage reduces the intermolecular distance and improves the cohesion of the film [35, 78].

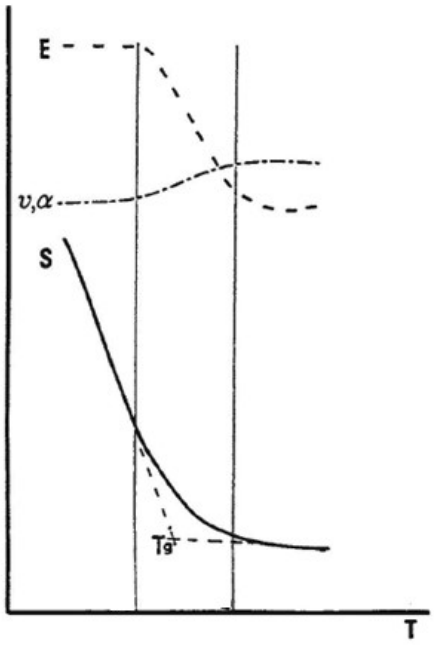

Figure 3.5 Schematic of the representation of dependence of stress (S), elastic modulus (E), thermal expansion (α), and Poisson's ratio (ν) on the temperature (T) [63].

3.4.3 Effect of relative humidity changes on stress development

Hygroscopic stresses are experienced due to dimensional changes related to changes in the relative humidity (absorption and desorption of water). A mismatch in the expansion coefficient of the coating and substrate will produce hygroscopic strain, ε^{H}, as shown in **Equation 3.6**:

$$\varepsilon^{H} = (\alpha_c^{H} - \alpha_S^{H})\Delta H \qquad \textbf{Equation 3.6}$$

Where:

α_F^H = hygroscopic expansion coefficient = s of the coating, and

α_S^H = hygroscopic expansion coefficients of the substrate.

Combining **Equation 3.1** and **Equation 3.6**, the hygroscopic stress, σ^H, is determined by:

$$\sigma^H = \int_{RH_2}^{RH_1} \frac{E}{1-\nu}\left(\alpha_c^H - \alpha_S^H\right)dH \qquad \textbf{Equation 3.7}$$

Figure 3.6 presents the variation of σ^H (S^H in the diagram) with relative humidity for four different coating materials [63]. At a given temperature and humidity, the coating is in equilibrium with the moisture in the air. When the relative humidity changes, the internal stresses vary. The changes in internal stresses with relative humidity changes are similar to those associated with immersion in water [35].

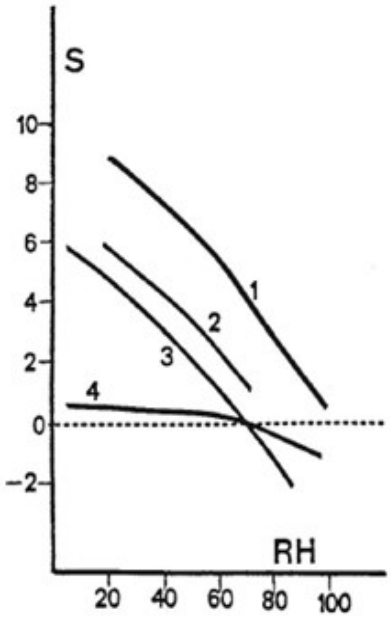

Figure 3.6 Stress (S or σ) dependence on relative humidity (RH) for (1) a polyester powder coating; (2) an epoxy; (3) a polyurethane; and (4) a latex coating [63].

Internal stresses generally decrease with an increase in moisture absorption and increase with desorption. Absorption of water causes the coating to swell, causing compressive stresses. The coating, which had originally contracted during film formation, experiences expansion by moisture absorption. The internal stresses are consequently reduced. The intake of water has a plasticizing effect, causing molecular relaxation and reduction of the glass transition temperature. Water desorption causes recovery of some, but not all, of the tensile shrinkage stresses [35, 73, 79].

Exposure to wet dry cycles in which the coating is exposed to air and water condensation on the surface may lead to leaching of low molecular weight species, such as solvent or plasticisers that would otherwise soften the coating. Long term exposure to these cycles may increase the coating's brittleness and reduce its capacity to accommodate service stresses [80].

Epoxy-based coatings are hydrophilic in nature and can absorb water from their surroundings. The presence of pores in the coatings can contribute to the migration of absorbed water and other species into the film. Water migration may lead to coating delamination, compromising its capacity to protect the substrate from corrosion [4, 35, 81].

3.5 Ageing

Ageing is a degradation process that affects coatings in the glassy state. Since most organic coatings are formulated to be in the glassy state under normal service conditions, ageing is an inevitable factor. The ageing of organic coatings is generally associated with an increase in stresses due to the influence of environmental factors. These factors, such as water, UV, or temperature, may cause increase of porosity, loss of adhesion, blistering and/or debonding [82-84].

When a coating is heated above the T_g and then cooled to the temperature below it; volume, enthalpy and entropy are brought to a non-equilibrium state above the equilibrium state, as illustrated in **Figure 3.7**. In equilibrium, these properties have a lower magnitude; the mechanical, thermal, and electric properties of the coating change [82, 85]. With time, the thermodynamic values will continuously decrease until they reach the equilibrium state. The rate at which the coating recovers will depend on magnitude of the temperature with respect to the T_g [63].

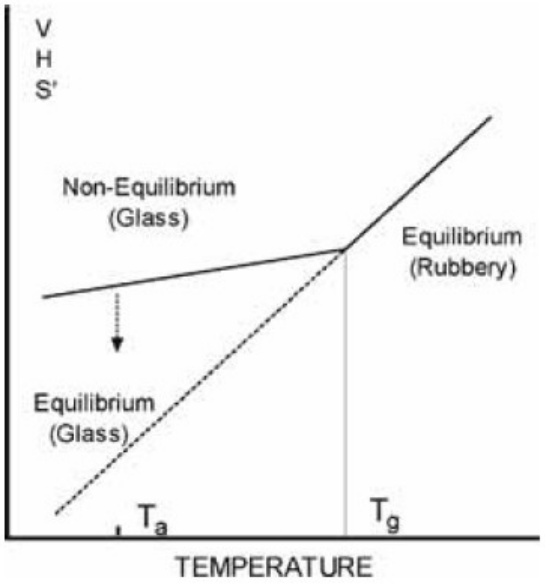

Figure 3.7 Schematic description of the dependence of volume (V), enthalpy (H), and entropy (S') on temperature (Ta=physically aging temperature) [85].

Figure 3.8 shows the variation of the storage modulus (E') with temperature for a coating post-cured at 50°C for different times (0h, 24h, and 89h). The storage modulus was obtained by DMA under dynamic conditions in dual cantilever mode, frequency 1Hz, and heating rate of 2K/min. The storage modulus increases with an increase in time of exposure to aging conditions (temperature) due to coating densification; the stress relaxation rate is also reduced and consequently, the coating becomes more brittle. Ultimately, physical ageing may influence the long-term reliability of the coating [82, 85, 86].

The performance of organic coatings in marine corrosion protection is often studied through laboratory tests, which produce accelerated degradation with controlled environmental factors. Many researchers have established that generally there is not a good correlation between the results obtained through accelerated aging tests and real environmental degradation. It has been argued by Fredj et al. (2012) that the disparity between experimental and natural ageing is due to the oversimplification of laboratory tests, which only take into account a small number of environmental factors [87].

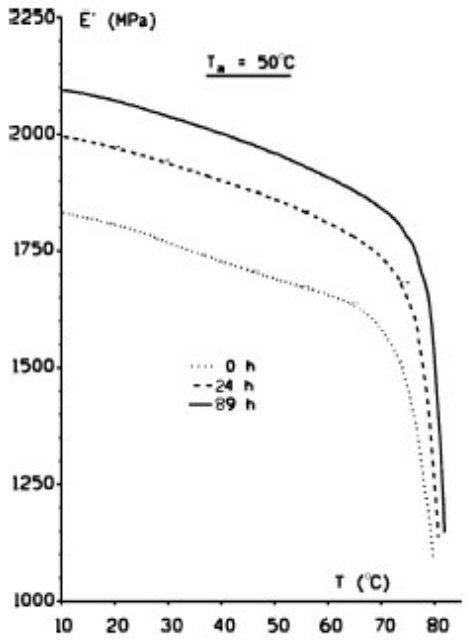

Figure 3.8 Storage elastic modulus (E') as a function of temperature (T) for a non-pigmeted powder coating physically aged at 50°C for different times (0, 24, and 89h). Frequency 1Hz rate: 2K/min [85].

Physical ageing effects on the elastic properties of the coating may be reversed by increasing the temperature to a temperature above the glass transition temperature for sufficient time. Chemical ageing, however, is an irreversible phenomenon induced in a material by UV radiation, moisture, etc. Chemical ageing is particularly damaging when it directly affects the coating/substrate interface [82, 88].

3.6 The influence of composition on the mechanical properties of coatings

The paint components in a formulation have an important bearing in the mechanical properties of a coating. The mechanical properties of the polymer matrix are modified by the incorporation of additional components. Moreover, most coating schemes are multi-layered. Although the polymer matrix may be constant within each layer, the pigment nature and concentration may vary between layers. Additionally, solvent loss and non-uniform cross-linking may also lead to gradients or heterogeneities in mechanical properties [69].

The binder is largely responsible for the mechanical properties of the cured film and it's a key aspect in stress development [63]. The modification of the binder's

composition by copolymerization, blending of polymers, and addition of plasticisers, are the main means of influencing the properties of the films. To produce a hard film, the vehicle coating should have a glass transition above room temperature. Conversely, if an application requires a soft coating, a binder is chosen whose film glass transition is below room temperature. If a tough coating is desired, the glass transition should be near service temperature. Copolymerisation and plasticising have a similar effect on the T_g [89].

The glass transition temperature can also influence the magnitude of the residual stresses developed in the coating. Coatings with a T_g below or close to the service temperature will develop low to negligible internal stress. The mobility of the binder molecule segments is high when the T_g is low, and the stresses due to film formation can partially or completely be dissipated. Conversely, a coating with a T_g higher than the service temperature will develop significant stresses [63].

In general, changes in the molecular structure of the binder may produce changes in E, ε, and ν, and T_g. The stress magnitude is directly proportional to these parameters. The cross-linking density is directly proportional to the modulus and T_g, and therefore the internal stresses. In brief, the smaller the values of E, ε, and ν, and T_g; the smaller the resulting stress [35, 63]. The tensile strength of the coating, S, increases as the molecular weight is increased, as shown in the following equation:

$$S = S_\infty - \frac{B}{M} \qquad \textbf{Equation 3.8}$$

Where:

S_∞ = tensile strength at infinite molecular weight,

B = constant characteristic of the material, and

M = molecular weight [89].

The molecular weight of the polymer binder is chosen to suit the desired application characteristics and dry film properties. Low molecular weight polymers with low viscosity can be used to produce coatings with high solid content. Low molecular

weight polymers also facilitate application. However, high molecular weight polymers provide better film properties. In order to have good application characteristics without compromising the film properties, low molecular weight pre-polymers are cross-linked to form high molecular weight coatings (i.e. two pack urethane and epoxy systems) [89].

The stress development of a coating is affected by the pigment volume concentration (PVC) and the type and morphology of the pigments and fillers. The addition of pigments increases the elastic modulus and internal stresses of the film. Some pigments induce higher stresses than others due to filler/binder interactions (e.g. TiO2 contributes to higher stresses than CaCO3) [35, 63].

Fillers may have a reinforcing effect on coatings depending on their nature, morphology and surface area. Flake-like particles such as alumina and talc arrange themselves parallel to the surface of the coating, restricting the volume shrinkage in the plane parallel to the surface, increasing the elastic modulus, but not the internal stresses [35, 63]. Moreover, the pigment and filler interactions with the binders, or absorption of driers and catalysts by the pigments affect the mechanical properties of the film [89]. When PVC is above CPVC holes appear in the cured film. These act as stress concentrators and decrease the tensile strength and elastic modulus of the film [75].

It has been previously established that solvent evaporation is closely related to the development of internal stresses (**Figure 3.4**). The rate of evaporation of the solvent also affects the rate of stress development. For convertible solvent-borne coatings, fast evaporating solvents may develop lower stress levels. According to **Equation 3.2**, coatings based on solvents with slow evaporation rates would have a higher volume of retained solvent at a given point of the cross-linking process (after most of the cross-links have been formed or made); the strain in the film (ε^c) will increase the slower the solvent evaporates out of the film. If stress relaxation is negligible, small internal stresses are associated with faster solvent evaporation.

Ultimately, the relative rate of solvent loss and polymerisation will determine the stress magnitude. As solvent evaporates from the coating, holes are left in the matrix in which polymer molecules should ideally migrate into. The adjacent cross-links and secondary

bonds, however, may restrict the ability of the polymer segments to migrate into the holes left by the solvent [63, 72]. Plasticisers, like retained solvent, increase coating flexibility and decrease the glass transition temperature, reducing the internal stresses. The extent of the effect will depend on the type of plasticiser. Finally, coating thickness is also relevant in stress development of convertible coatings. Internal stresses increase with increasing coating thickness. However, when the internal stresses exceed the tensile strength or adhesive strength of the coating, the stresses will decrease due to cracking or peeling of the coating [35].

3.7 Effect of porosity in the elastic modulus of solids

The presence of pores has a strong effect on the physical and mechanical properties of solid materials. Several theories regarding the effect of porosity (number, size and volume fraction) on the elastic modulus of the material have been established [90]. Initial attempts to characterise the elastic response of a porous solid were based on semi-empirical equations of the form:

$$E = E_0 e^{-bV} \qquad \textbf{Equation 3.9}$$

where:

E = Effective Young's modulus of porous materials,

E_0 = Young's modulus of the pore-free solid,

V = pore volume fraction, and

b = empirical constant.

This simple approach does not satisfy the boundary condition: $V = 1 \rightarrow E = 0$. However, the equation agrees with experimental results for low levels of V, presenting great deviations for $V \geq 0.2$ [91].

Phani and Niyogi (1987) studied the effect of porosity on the elastic modulus of porous materials, especially those obtained from powders with wide size distributions and morphology [91]. The researchers developed the following power-law empirical relationship:

$$E = E_0 \left(1 - \frac{P}{P_{crit}}\right)^f \qquad \textbf{Equation 3.10}$$

where:

P = porosity,

P_{crit} = porosity at which the effective Young's modulus becomes zero, and

f = material constant dependent on the grain morphology and pore geometry of the porous material.

The approach has been proved effective for uniform spherical particles arranged in cubic, orthorhombic and rhombohedral configurations [91]. A different approach to characterize the elastic behaviour of a porous solid is to consider the pores as nearly flat oblate spheroids and treat them as crack-like defects. Krstic and Erickson (1985) produced a model based on crack opening displacement and stress concentration. The model considers that the opening of cracks associated with pores produces an additional elastic strain in the material [90]. The dependency of the Young's modulus on the porosity based on this approach is calculated by the following equation:

$$\frac{E}{E_0} = (1 - V)\left\{1 + \frac{12V(1-\nu)^2}{\pi}\left[(1 + s/R)^3 + \frac{9}{2(7-5\nu)(1+s/R)^2} + \frac{4-5\nu}{2(7-5\nu)}\right]\right\} \qquad \textbf{Equation 3.11}$$

where:

E_0 = Young's modulus of a cavity free solid,

E = Effective Young's modulus of porous materials,

ν = Poisson's ratio,

s = radial flaw size, and

R_{pore} = pore radius.

These models, applied to ceramic materials formed from sintered powders allows the calculation of the porosity dependent Young's modulus (E_0), which is shown to decrease with an increase in porosity, as presented in **Figure 3.9** (Phani and Niyogi) and **Figure 3.10** (Krstic and Erickson) [90, 92].

In general, the presence of pores produces a reduction of Young's modulus and an increase of elastic strain for a given stress level The response of the material to stress will be affected by the number, volume fraction, and size of the pores [90]. The effect of pores in the mechanical properties of paint films has not been extensively studied. Porosity is also relevant in paints due to its direct relation to water vapour adsorption and permeability [93, 94].

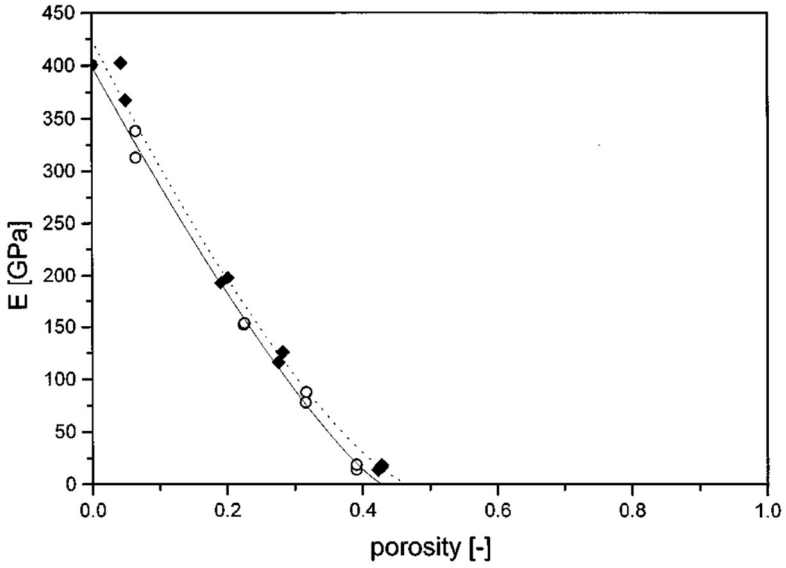

Figure 3.9 Young's modulus porosity dependence for α-Al_2O_3 trigonal corundum, bending measurements: (-o-) spherical powder; (♦) egg-shaped powder [92].

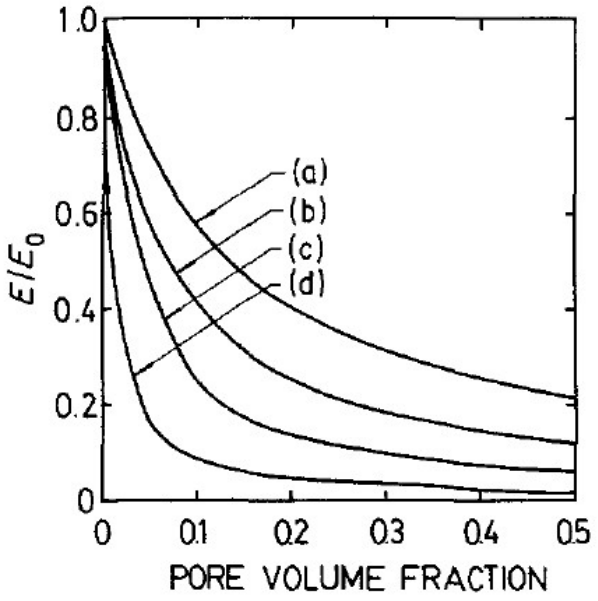

Figure 3.10 Predicted change of Young's modulus with porosity for given s/R values and ν=0.2. s/R= (a) 0.001, (b) 0.5, (c) 1, and (d) 2 [90].

3.8 Mechanical testing of coating films

Determination of the mechanical properties of supported coatings provides basic understanding of the relationship between coating composition and performance. Generally, standard mechanical tests require coatings as free films or as thick rectangular samples [95]. The production of flat, uniform free films is time consuming and, due to their brittleness, produces films difficult to handle without premature breakage. In many applications, coatings are applied as thin layers, if these were to be tested as free films they would be too brittle to perform mechanical tests on as they would not self-support. Additionally, testing a coating applied on its substrate takes into account the effect of coating/substrate interactions on the mechanical properties [65]. The elastic properties of the coatings are always coupled with their adhesion to the substrate [22]. There is a need for test methods which allow the determination of both mechanical response of the coatings applied onto a substrate and also the mechanical properties of the coatings [68].

A group of studies on the mechanical properties of supported epoxy-diamine based coatings have been performed by Roche and Bouchet. The research analysed the effect of coating thickness, substrate surface treatment and extent of reaction on the mechanical properties of the films. The mechanical response of the coating was

determined by static 3 point bending flexural tests of the supported coatings. Through composite beam stress analysis, the Young's moduli of the coatings were determined. Subsequently, the residual stresses were determined by the application of one-dimensional thin plate theory to the system. The Young's moduli and residual stresses of the coatings were found to be dependent on coating thickness, extent of curing reaction and substrate material characteristics. The researchers concluded that the phenomenon is due to the formation of an interphase between the coating and the substrate. The thickness of the interphase was hypothesised to be around 200 and 250 μm. Therefore, the bi-layered system was later assumed to be a tri-layer system; and the 'bulk' coating layer was assumed to have properties independent of coating thickness. **Figure 3.11** shows the interpretation of the variation of the Young's modulus through the tri-layer system [96-98].

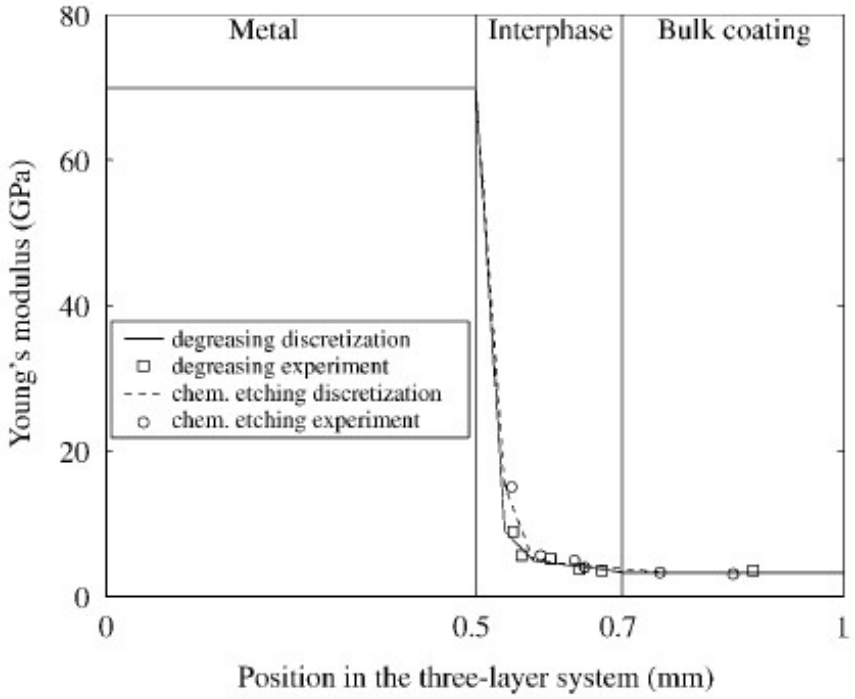

Figure 3.11 Variation of the Young's modulus as a function of the position in the three-layer system [98].

These studies used static mechanical tests to obtain the mechanical properties of the coatings at room temperature. DMA is a far more valuable technique for the mechanical characterisation of coatings, as it accounts for the complex modulus (consisting of both elastic and viscous components), and the glass transition temperature of the films. DMA may be used to correlate composition, glass transition

temperature, curing conditions of polymeric coatings and the mechanical properties of coating materials.

Fawcett (1998) used composite beam stress analysis to determine the elastic modulus of thin (~35 μm) organic coatings applied onto ceramic beams (~65 μm). The data regarding force and deflection obtained by DMA in 3 point bending mode was used to determine the elastic modulus and had an associated error of 5% [99]. The use of a double coated substrate (**Figure 3.12**) simplified the calculation of the neutral axis of the sample. Fawcett's method may be applicable to any coated beam within the linear-elastic region. Spinks et al. (2004) applied a similar mechanical model to polymer/steel composite beams with coating thicknesses from 20 to 50 μm. The elastic moduli of the coatings were found to be very sensitive to the geometry of the beams (especially the thickness of the substrate and the coating), and the properties of the substrate material [100].

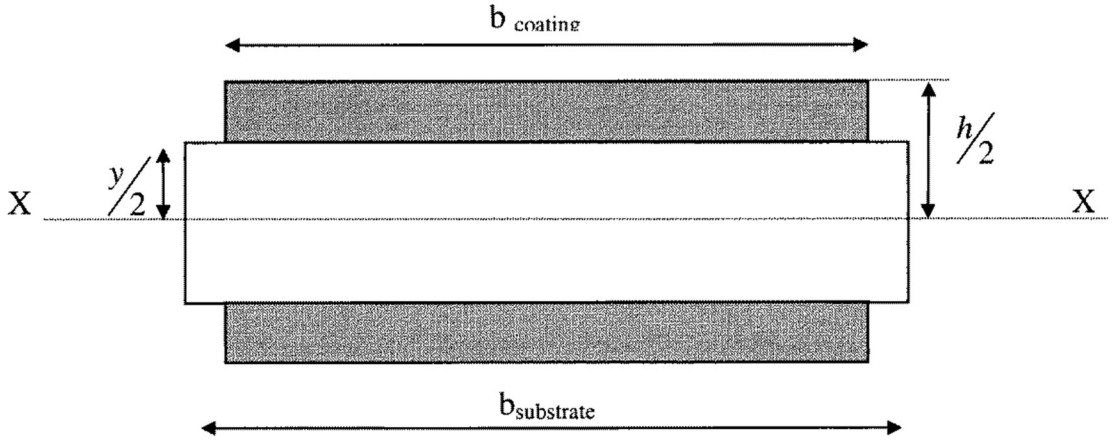

Figure 3.12 Transverse sections of double coated ceramic beams used by Fawcett [99].

The theory that the formation of the interphase is responsible for the variation of mechanical properties with coating thickness was later investigated further by the researchers [101-103]. The existence of an interphase has since been refuted/countered by Goyanes et al. (2005) using the same substrate and coating materials. However, these researchers performed DMA flexural tests rather than static flexural tests as Rochet and co-workers did [104].

The researchers deposited un-filled epoxy-diamine (Diglycidyl ether of bisphenol A (DGEBA)/Isophoronediamine (IPDA)) coatings on aluminium alloy substrates. The coatings were detached from the substrate and the 'interphase' was removed from the coating/substrate interface by polishing. The results showed that the physical and mechanical properties of the coating depend on coating thickness. However, the properties do not change by the removal of the 'interphase, suggesting that for a given thickness the properties are homogeneous within the coating. This is presented in **Figure 3.13**. Nevertheless, it is important to consider the possible hardening effect that the material removal method would have on the coating.

Ultimately, Goyanes et al. agree with Roche and co-workers in that when prepolymer DGEBA-IPDA is applied onto aluminium alloy substrates and cured, the cured film has chemical, physical, and mechanical properties that are dependent on coating thickness (**Figure 3.14**). However, this is not thought to be a consequence of the formation of an interphase [104]. The notion that coatings exhibit properties different to that of the bulk, and that these properties varied with coating thickness has been the subject of several studies and has been observed for different materials [67]. The wide variety of parameters influencing the performance of solvent-borne pigmented commercial paints suggests that there are many factors that can possibly affect the mechanical properties of these materials.

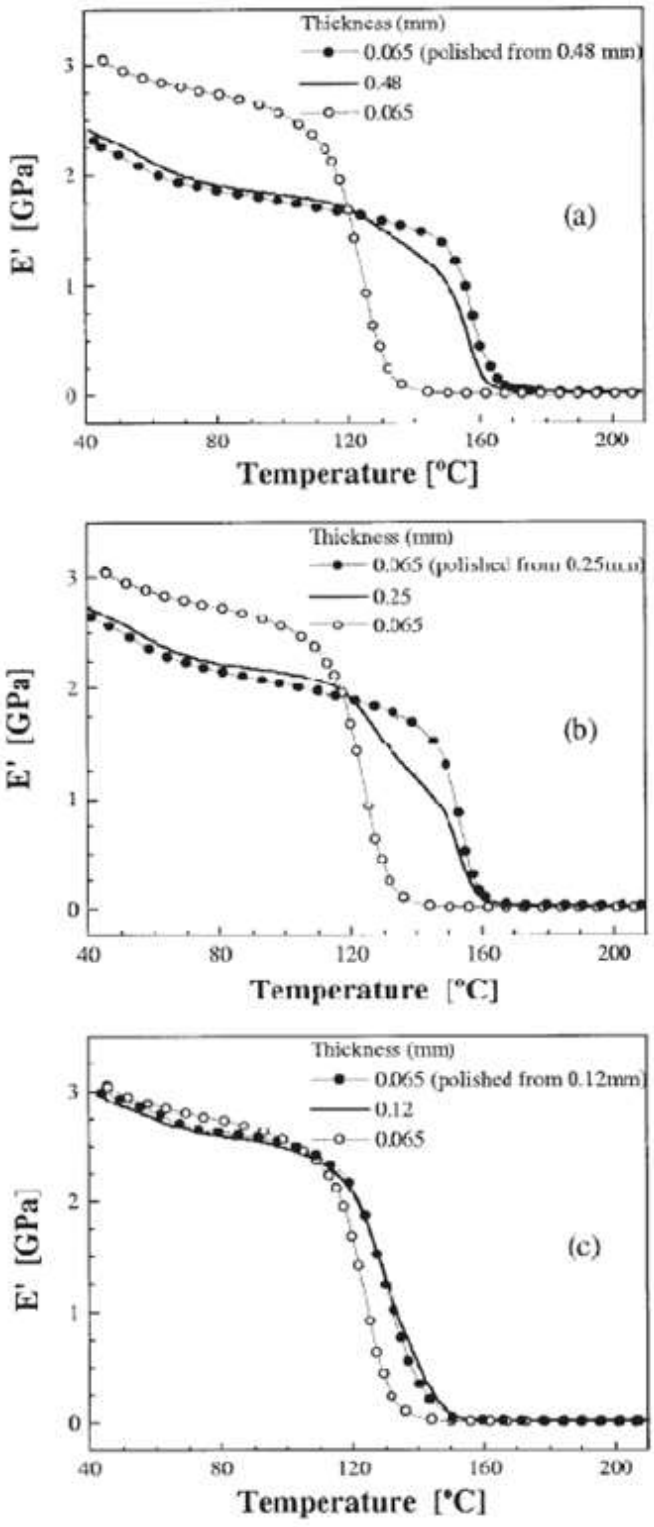

Figure 3.13 Dynamic mechanical properties of detached coating before and after interphase removal [104].

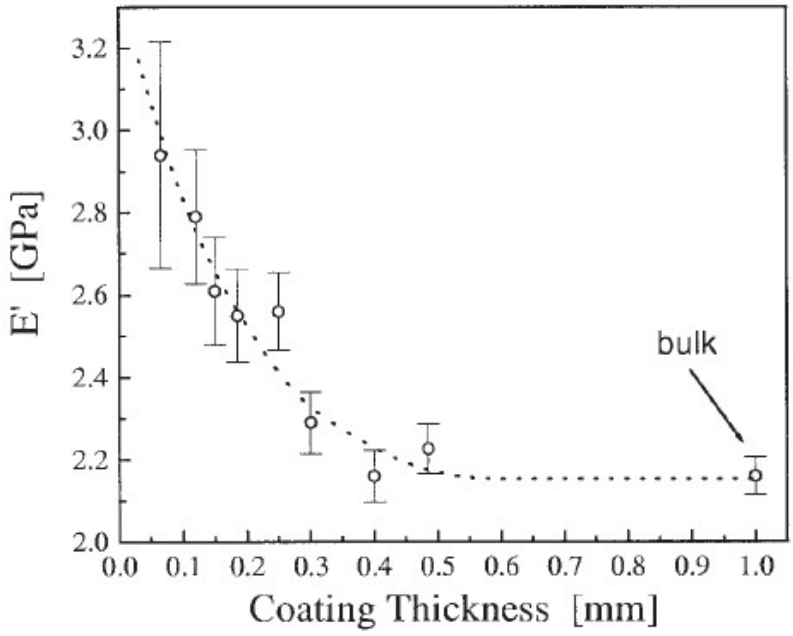

Figure 3.14 The storage modulus (E') of the coating, measured at 53˚C, as a function of coating thickness [104].

3.9 Summary

Several studies have been performed on the barrier properties and mechanical properties of paint for marine environments. The mechanical behaviour and stress development of paint depends on a series of interacting factors such as type of binder, coating/substrate interactions, application conditions, service conditions, pigmentation, additives, among others [105].

When epoxy-based paints are applied onto metallic substrates and cured, residual stresses due to film formation develop in the coating and strain the substrate. Stresses due to film formation act against adhesion and excessive stresses may cause coating failure and degradation. In harsh marine environments, coating failure may lead to corrosion and thus compromise the integrity of the substrate being protected. Knowledge of the elastic modulus and residual stresses of supported coatings is crucial for the understanding and modelling of the mechanical behaviour of protective coatings. Both will influence the mechanical behaviour of the complex system consisting of a substrate and an applied coating scheme [71].

The mechanical characterisation of protective coatings faces many challenges due to the brittle nature of the coatings and general ‘voids/lacunae’ of knowledge in the field. The difficulties encountered in the calculation of mechanical properties of paint films are thought to be part of the reason for the lack of information in the field [100]. Pass/fail tests do not provide a property or parameter that can be related to well-known mechanical properties or be used to model the behaviour of the films.

In the past, research has been directed towards relating specialised coating test methods to mechanical parameters [89]. Efforts must be made to propose test methods for the determination of the mechanical properties of supported coatings and evaluate the different factors affecting the mechanical performance of coating. In the present study it is proposed that due to the viscoelastic nature of coatings, any improvements or contributions in the field of coating’s mechanical properties will involve dynamic mechanical analysis (DMA).

4 MATHEMATICAL MODEL: COMPOSITE BEAM STRESS ANALYSIS

4.1 Introduction

The Young's modulus is a crucial property for the proper understanding of the mechanical behaviour and stress development of a coating applied onto a substrate. Several methods have been developed to determine the Young's modulus of films. Generally, properties such as Young's modulus, are available in the literature for materials in their bulk form. However, when the same material is bonded to a substrate as thin layers (coating), its Young's modulus is different from that of the bulk [106].

Several studies have been developed to determine the mechanical properties of thin and thick films applied to metallic substrates. The application of a coating onto a thin and flexible metallic substrate causes the coating/substrate system to bend due to the residual stresses within the coating; the severity of the curvature is proportional to the magnitude of the residual stresses. Therefore, direct measurement of the curvature in the beam when it is subjected to bending is a commonly used technique [76, 107]. Bending-beam and bending-plate techniques are frequently used methods to calculate the stresses within the films. Thin flexible substrates are used since these can be deformed by the stresses in the coating. From the deformation produced, the stresses can be estimated [108].

In the past decades, equations for the calculation of the stresses from the deformation have been presented. Generally, a number of assumptions and limitations were associated to the methods, such as isotropic and/or homogenous stresses, equal Young's moduli for the coating and substrate, and equal Poisson's ratio for the coating and substrate [108].

Stoney (1909) introduced the concern for the development of tensile internal stresses of thin films and consequent failure by delamination. The researcher, who considered stresses experienced in thin metallic films deposited by electrolysis, was interested in determining the stresses that caused peeling of these films when deposited under

tension. The stress analysis produced an expression for the stresses in a bi-layer beam with the coating thickness being infinitesimal compared to the substrate, and the neutral axis of the beam located in the geometrical neutral axis. Therefore, this approach assumed that the Young's modulus of the coating is equal to the Young's modulus of the substrate [109]. **Figure 4.1** presents a curved coated beam due to shrinkage stresses. Stoney's residual stresses, σ, are presented in the following equation:

$$\sigma = -\frac{E_s t_s^2}{6Rt_c} \qquad \textbf{Equation 4.1}$$

where:

E_s= Young's modulus of the substrate,

t_s = thickness of the substrate,

R = radius of curvature (see **Figure 4.1**), and

t_c = thickness of the coating.

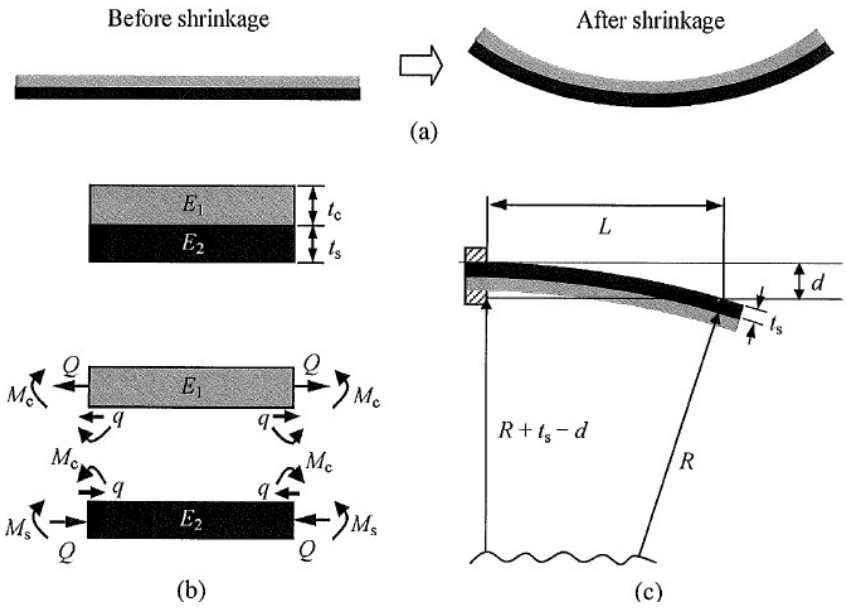

Figure 4.1 Representation of a curved beam due to shrinkage stresses [10]

Whether beam or plate theory is considered, elastic theory is the fundament behind calculating the film's stress as a function of the deflection produced. It assumes that the film strains the substrate, and the latter bends until it reaches equilibrium. This requires the coating/substrate bond to be strong in order to avoid debonding of the layers. Early approaches on the stress analysis consider that since the deflection in the substrate is studied, the film's properties need not be considered. Stoney's stress convention considers that if the beam/plate bends decreasing the film length, the residual stresses are tensile. On the other hand, if the length of the coatings increases, the residual stresses are compressive [110].

Timoshenko (1925), contributed to the development of classical beam theory in an analysis oriented towards bimetallic strip thermostats. The study considered the large deflections produced by a bending moment applied to two opposite edges of the plate [111]. Timoshenko's classical formula for curvature of a beam, κ, is given below:

$$\kappa = -\frac{6E_c t_c \varepsilon_m}{RE_s t_s^2}\gamma \qquad \textbf{Equation 4.2}$$

where:

E_c = Young's modulus of the coating, and

ε_m = misfit strain.

with:

$$\gamma = \frac{(1+\beta)^3}{1 + 4\alpha\beta + 6\alpha\beta^2 + 4\alpha\beta^3 + \alpha^2\beta^4} \qquad \textbf{Equation 4.3}$$

and:

$$\alpha = E_c/E_s \qquad \textbf{Equation 4.4}$$

$$\beta = t_c/t_s. \qquad \textbf{Equation 4.5}$$

where:

α = ratio between the Young's modulus of the coatings and the substrate, and

β = ratio between the thickness of the coating and the substrate.

Beam theory has since grown to suit the stress analysis of different materials and applications, such as thin and thick protective coatings, thin film resistors, etc. [112]. Hoffman (1966) reviewed Stoney's limitations and evaluated its validity in thin condensed films. In a comparative study regarding the effect of the substrate thickness, Hoffman concluded that the sensitivity of the beam's deflection measurements may be increased by the use of thinner substrates. However, thin substrates could also introduce limitations in the validity of the stress analysis equations for plates. Moreover, a significant improvement to Stoney's equation was achieved by considering the bending of the substrate as the bending of a thick plate. Plate theory introduces the notion of an isotropic stress in equilibrium with the resultant strain, and the consideration of the Poisson's ratio, ν_s, of the substrate [110]. **Equation 4.6** presents the stress with considerations of the ratio of the transverse strain to the axial strain in the substrate:

$$\sigma = -\frac{E_s t_s^2}{6R(1-\nu_s)t_c} \qquad \textbf{Equation 4.6}$$

The consideration of plate theory increases the estimated stress by approximately 1.5 times due to the introduction of the Poisson's effect. Previous work had concentrated on the determination of stresses in metallic and ceramic coatings applied by vacuum deposition or electroplating, and not organic coatings. The previously mentioned deposition methods consist of layering infinitesimally thin increments of coating.

In organic coatings, the need for the determination of the elastic modulus of the material becomes complicated due to the nature of the materials. Some film formers produce brittle films that are difficult to handle and test when produced as free films. As a solution, thicker films may be produced. However, the film thickness is a determining factor in the mechanical behaviour of the films and it would not produce a good approximation. Additionally, a coating applied to a rigid substrate may undergo

stress relaxation, the extent of which depends on the rheological properties of the coating and substrate characteristics [113].

Corcoran (1969) developed an analysis based on beam/plate theory for the determining of stresses in organic coatings. In the case of organic coatings applied onto metallic substrates, the coating does not behave as expressed in classical beam theory, as it is in tension in all directions. Hence, a coating adhered to a flexible substrate will bend the substrate in two directions and not only in the direction of the length as dictated by beam theory. Therefore, the flexible substrate supporting an organic coating will behave as a plate [113].

Corcoran's analysis considered an organic coating supported on a metallic substrate and fixed at one end (cantilever beam). A deflection (d) is produced due to the compressive forces exerted at the beam-coating interface due to the internal stresses related to film formation and solvent release. The author approximated the neutral axis of the beam as the neutral axis of the substrate. **Equation 4.7** indicates an approximation of the residual stresses that may be produced when $E_s \gg E_c$ and $t_s \gg t_c$. **Equation 4.8** shows the residual stresses of the coating's considering the Young's modulus and thickness of the coating [113].

$$\sigma = \frac{dE_s t_s^2}{3t_c L^2(1-\nu_s)(t_c+t_s)} \qquad \textbf{Equation 4.7}$$

where:

d = maximum deflection of the beam, and

L = Length of the beam.

$$\sigma = \frac{dE_s t_s^2}{3t_c L^2(1-\nu_s)(t_c+t_s)} + \frac{dE_c(t_c+t_s)}{L^2(1-\nu_c)} \qquad \textbf{Equation 4.8}$$

where:

E_c = Young's modulus of the coating, and

ν_c = Poisson's ratios of the coating.

Equation 4.7 and **Equation 4.8** are designed for the experimental case of a bi-layered beam clamped by one end which deflects due to the residual stresses experienced by the coating, as presented in **Figure 4.2**, in where $h = d$ [114].

Figure 4.2 Diagram of the cantilever method for measurement of internal stresses in organic coatings: a) original position, b) free end deflected from original position [114].

Corcoran's equations have since been published by ASTM in D6991 -05 (2010) Standard test method for measurement of internal stresses in organic coatings by cantilever (beam) method. According to the standard, the first term in **Equation 4.8** refers to the stresses that remain in the coating after it bends the substrate, whilst the second term indicates the stresses 'removed' due to the bending of the substrate. The latter is identified as an indicator of stress relaxation. In real applications, when coatings are applied to thick steel substrates ($t_s \approx 8mm$), where $E_s \gg E_c$ and $t_s \gg t_c$, the second term of the coating may be neglected [114].

Röll (1976) deduced an equation for the residual stresses which considered an inhomogeneous and anisotropic plane stress distribution in the coating, and different elastic constants for the coating and the substrate ($E_c \neq E_s$ and $t_c \neq t_s$). The expression is applicable to bi-layered beams with a very thin coating layer ($t_s \gg t_c$). Röll used a linear approximation by omitting second and higher order terms in β [$\beta^n = \left(\frac{t_c}{t_s}\right)^n \cong 0 \; for \; n \geq 2$] [108].

$$\sigma = -\frac{E_s t_s^2}{6 t_c R}[1 + (4\alpha - 1)\beta] \qquad \textbf{Equation 4.9}$$

Benabdi and Roche (1999) determined the effect of Young's modulus and residual stresses of supported films with thickness, applying both beam and plate theory [106, 115]. The deduced equation for the residual stresses in the coating is presented in **Equation 4.10**.

$$\sigma = -\frac{E_s t_s^2}{6 t_c (1 - \upsilon_s) R}\left[1 + \beta(4\alpha^* - 1) + \beta\left[\alpha^{*2}(\beta - 1) + 4\alpha^* + \frac{(1 + \alpha^*)^2}{1 + \beta}\right]\right] \qquad \textbf{Equation 4.10}$$

with:

$$\alpha^* = \frac{E_c(1 - \upsilon_s)}{E_s(1 - \upsilon_c)} \qquad \textbf{Equation 4.11}$$

Ohtsuki (2011) applied the 'compression column method' based on nonlinear large deformation theory to determine the Young's modulus of multi-layered materials. The method considers the vertical displacement and the deflection angle of beams compressed between freely pivoted ends. The test subjects were coated plates and the method is said to be applicable for a wide variety of coatings, including paints [116]. Several other studies have been performed on ceramic coatings based on Hoffman's equations [117, 118].

4.2 Coating-substrate bi-layer beams

The neutral axis, y, is the axis formed by the intersection of the neutral plane and the transverse section of the bi-layer material. There is no strain in the neutral plane, but it may deform by bending, maintaining its original length constant. An additional stress state, assumed also to be in a plane stress state, arises owing to this deformation [108]. The longitudinal fibre is defined as any segment of the bi-layer system parallel to the

neutral axis [115]. **Figure 4.3** presents the cross-sectional area of the bi-layer beams constituted by the coating and the substrate. In the present simplified model, it is assumed that the internal stresses within the coating due to film formation are negligible. The neutral axis of the sample is taken as a reference plane. On the other hand, **Figure 4.4** shows the schematic representation of a bi-layer system owing to tensile stresses in the coating layer (xy plane).

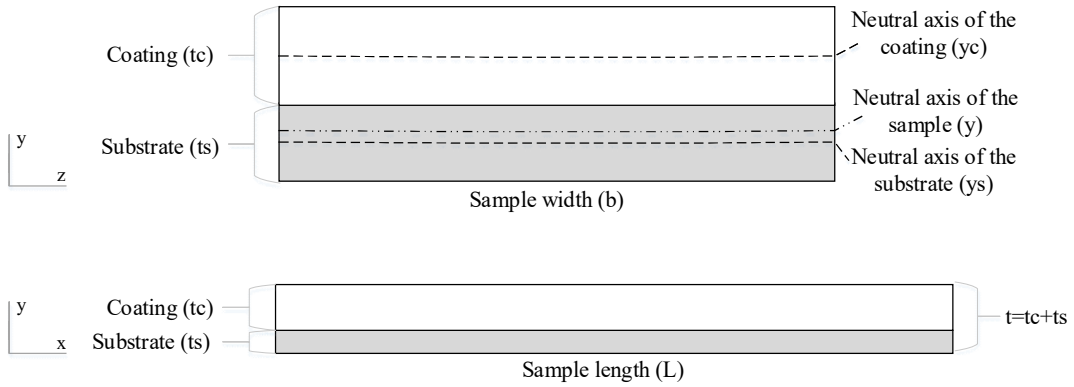

Figure 4.3 Schematic demonstration of the bi-layer beams without residual stresses within the coating (cross-sectional and side views).

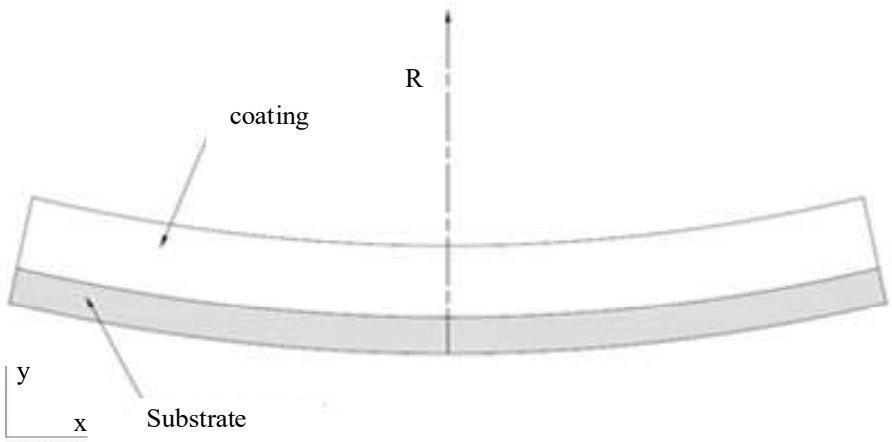

Figure 4.4 Schematic representation of the coating/substrate system resulting from tensile stresses in the coating layer due to film formation.

Basic beam theory corresponds to a one-dimensional approach without lateral stresses. The beams are subjected to bending with no in plane deformation and consideration of the Poisson's effect. Transverse sections of the beam are planar before, during, and after bending. Therefore, the effect of transverse shear is neglected $\tau_{xz} = 0$, following the Navier-Bernoulli hypothesis [119].

The materials forming the bi-layer systems are assumed to be homogeneous, isotropic, and elastic. The materials behave in a linear-elastic manner and there is a linear variation of normal strain, which consequently results in a linear variation in normal stress. The Young's moduli of the coating and the substrate each have the same values on both tension and compression (flexural modulus).The stress and the normal strain will variate from zero at the member's neutral axis to a maximum value, σ_{max}, at a distance h_c farthest from the neutral axis [115, 120].

The radius of curvature is large compared with the transverse dimensions, $R \gg b, t$. This suggests that it can be assumed that the stress distribution during bending is linear throughout the beam, as it would be for a flat beam. Conversely, assuming that the thickness of the beam is of the same order of magnitude as the radius of curvature, could imply a non-linear stress distribution [106, 115].

Beam theory provides small deflection elasticity relations that apply to the bending of beams, at any location along the beam [121]. For a beam subjected to bending, the following equation applies:

$$\frac{\sigma}{y} = \frac{M}{I} = \frac{E}{R} \qquad \textbf{Equation 4.12}$$

where:

σ = is the tensile or compressive stress,

y = distance from the beam's neutral axis,

M = bending moment,

I = second moment of area,

E = Young's modulus, and

R = radius of curvature of the beam.

So, by rearrangement of **Equation 4.12**, the tensile or compressive stress can be expressed as:

$$\sigma = \frac{Ey}{R}$$ **Equation 4.13**

The strains in composite beams are determined in the same manner as for the strains in homogenous beams; the cross sections are considered to remain plane during bending. This is valid for beams subjected to pure bending and any solid regardless of their nature [122]. The longitudinal strains, ε_x, will vary linearly from the top to the bottom of the composite beam, as shown in **Equation 4.14**:

$$\varepsilon_x = -\frac{y}{R} = -ky$$ **Equation 4.14**

Where:

k = curvature for the beam.

The stress distribution for a composite beam can now be determined. Considering a beam constituted by a coating and a substrate firmly bonded, the two layers act as a single solid, as presented in **Figure 4.3**. As the beam is made of two different materials, the neutral axis does not pass through the centroid of the cross-sectional area (yz plane). The xz plane is the neutral plane of the beam, and the xy plane is taken as the plane of symmetry. The normal stress can be determined using the stress-strain relationships for the two materials, as presented in **Equation 4.13**, and assuming that both materials are linearly elastic and, therefore, satisfy Hooke's Law [122]. As composite beam, the layers will have different Young's moduli, and the normal stress in each of the layers (coating and substrate) are defined as follows:

$$\sigma_{xc} = -E_c ky = \frac{-E_c y}{R}$$

$$\sigma_{xs} = -E_s ky = \frac{-E_s y}{R}$$ **Equation 4.15**

where:

σ_{xc}= the stress in the coating,

σ_{xs}= the stress in the substrate,

E_c = Young's modulus of the coating, and

E_s = Young's modulus of the substrate.

Figure 4.4 presents the case of a coating with residual stresses inducing a curvature into the substrate. In the interface between the materials, the stresses are different due to the fact that the Young's moduli of the materials are different. Considering that the resultant axial force acting on the cross section of the composite beam is zero, as presented in **Equation 4.16**, the position of the neutral axis can be determined [122].

$$\int_c \sigma_{xc} dA + \int_s \sigma_{xs} dA = 0 \qquad \textbf{Equation 4.16}$$

$$dA = bdy$$

Where:

A = Cross-sectional area.

Substituting σ_{xc} and σ_{xs} in the previous equation by their expressions from **Equation 4.15**:

$$-\int_c \frac{E_c y}{R} dA - \int_s \frac{E_s y}{R} dA = 0 \qquad \textbf{Equation 4.17}$$

The radius of curvature, R, of the beam is constant across the cross section, and can be removed from the equation:

$$-E_c \int_c ydA - E_s \int_s ydA = 0 \qquad \textbf{Equation 4.18}$$

The integrals in **Equation 4.18** correspond to the first moment of the coating and substrate with respect to the neutral axis [122]. The moment resultant of a bending stress is equal to the bending moment acting at the cross section:

$$M = -\int_A \sigma_x ydA = -\int_c \sigma_{xc} ydA - \int_s \sigma_{xs} ydA = \frac{E_c}{R}\int_c y^2 dA + \frac{E_s}{R}\int_s y^2 dA \qquad \textbf{Equation 4.19}$$

Equation 4.20 is obtained by simplifying the previous equation:

$$M = \frac{E_c I_c + E_s I_s}{R} \qquad \textbf{Equation 4.20}$$

where:

M = bending moment,

I_c = the moment of inertia of the coating, and

I_s = the moment of inertia of the substrate.

The moment of inertia, I, of the composite beam composed the coating and the substrate can be expressed as:

$$I = I_c + I_s \qquad \textbf{Equation 4.21}$$

An expression for the curvature is obtained based on **Equation 4.20**:

$$k = \frac{1}{R} = \frac{M}{E_c I_c + E_s I_s} \qquad \textbf{Equation 4.22}$$

Equation 4.22 is the known as the moment-curvature equation of a bi-layered composite beam. The denominator in the right-hand side is the flexural rigidity of the beam. Substitution of **Equation 4.22** in **Equation 4.15** provides the bending stresses, or normal stresses, in the beam [122]. The equations are known as the flexural formulas of the composite beam:

$$\sigma_{xc} = -\frac{M y E_c}{E_c I_c + E_s I_s}$$

$$\sigma_{xs} = -\frac{-M y E_s}{E_c I_c + E_s I_s} \qquad \textbf{Equation 4.23}$$

4.3 The neutral axis of a composite beam

The neutral axis is determined considering the equilibrium condition regarding the resultant axial force acting on the cross section presented in **Equation 4.18**. The origin of the coordinate system is placed in the neutral axis of the sample (**Figure 4.5***)*; and the distance from the neutral axis to the top of the beam (coating's free surface) is defined as h_c whilst the distance from the neutral axis to the bottom of the beam (substrate's free surface) is defined as h_s.

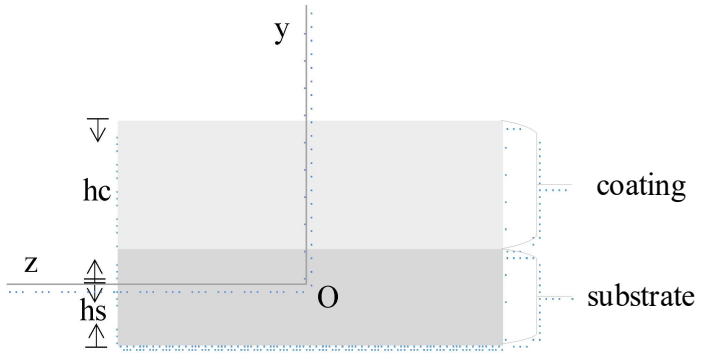

Figure 4.5 Cross section of a coated substrate (yz plane).

Equation 4.24 shows the equilibrium equation for a coated substrate, such as the ones subjected to this study:

$$-E_c \int_{(h_c - t_c)}^{h_c} ydA - E_s \int_{h_c - t_s - t_c}^{h_c - t_c} ydA = 0 \qquad \textbf{Equation 4.24}$$

$$dA = bdy$$

where:

b = width of the beam.

Solving the integral provides the position of the neutral axis for a bi-layered composite beam:

$$h_c = \frac{E_c t_c^2 + 2 t_c t_s E_s + E_s t_s^2}{2E_c t_c + 2E_s t_s} \qquad \textbf{Equation 4.25}$$

The neutral axis of the bi-layer beam from the coating/substrate interface (y_o) can be determined considering that $y_o = h_c - t_c$:

$$y_o = \frac{1}{2} \frac{E_s t_s^2 - E_c t_c^2}{E_c t_c + E_s t_s} \qquad \textbf{Equation 4.26}$$

The position of the neutral axis depends on the Young's modulus and thickness of both the coating and the substrate. In the case of an epoxy-based coating applied onto a steel substrate, the neutral axis of the sample will be within the substrate and very near to the neutral axis of the substrate since $E_s \gg E_c$. The neutral axis of the coating to the neutral axis of the sample (y_c) and the neutral axis of the substrate to the neutral axis of the sample (y_s) can be rewritten as:

$$y_c = \frac{E_s t_s (t_c + t_s)}{2(E_c t_c + E_s t_s)} \qquad \textbf{Equation 4.27}$$

$$y_s = \frac{E_c t_c (t_c + t_s)}{2(E_c t_c + E_s t_s)} \qquad \textbf{Equation 4.28}$$

With knowledge of y_c and y_s, the moment of inertia of the coating and the substrate with respect to the neutral axis, I_{cy} and I_{sy} respectively, can be determined by the following equations:

$$I_{cy} = \frac{b \cdot t_c^3}{12} + b \cdot t_c \cdot {y_c}^2 = I_c + b \cdot t_c \cdot \frac{E_s t_s (t_c + t_s)}{2(E_c t_c + E_s t_s)}^2 \qquad \textbf{Equation 4.29}$$

$$I_{sy} = \frac{b \cdot t_s^3}{12} + b \cdot t_s \cdot {y_s}^2 = I_s + b \cdot t_c \cdot \frac{E_c t_c (t_c + t_s)}{2(E_c t_c + E_s t_s)}^2 \qquad \textbf{Equation 4.30}$$

Where:

I_c= moment of inertia of the coating; and

I_s = moment of inertia of the substrate.

Therefore, the moment of inertia of the substrate (I_{sy}) and coating (I_{cy}) are:

$$I_{cy} = \frac{b t_c (E_c^2 t_c^4 + 2E_c E_s t_c^3 t_s + 4E_s^2 t_c^2 t_s^2 + 6E_s^2 t_c t_s^3 + 3E_s^2 t_s^4)}{12(E_c t_c + E_s t_s)^2} \qquad \textbf{Equation 4.31}$$

$$I_{sy} = \frac{b t_s (3E_c^2 t_c^4 + 6E_c^2 t_c^3 t_s + 4E_c^2 t_c^2 t_s^2 + 2E_c E_s t_c t_s^3 + E_s^2 t_s^4)}{12(E_c t_c + E_s t_s)^2} \qquad \textbf{Equation 4.32}$$

4.4 Beam curvature and maximum deflection

The measurement of coating shrinkage can be achieved by gravimetric and dilatometric methods, strain-gauge, bi-material strips, among others [123]. In the present study, the maximum deflection and radius of curvature of the bi-layered beams were determined by optical methods in order to calculate the residual stresses in the coatings. Assuming that the curvature of the beam, calculated from the interface, is

very large compared to the length and thickness of the beam, the curvature can be calculated by:

$$R = \frac{L^2}{8\delta_{max}} \qquad \textbf{Equation 4.33}$$

4.5 Flexural rigidity of a bi-layered composite beam

The flexural rigidity (EI) of the composite beam is a measure of the resistance of the beam to bending; and can be expressed as:

$$EI = E_s I_{sy} + E_c I_{cy} \qquad \textbf{Equation 4.34}$$

Incorporating **Equation 4.29** and **Equation 4.30** into the previous equation, gives:

$$EI = E_s(I_s + bt_s y_s^2) + E_c(I_c + bt_c y_c^2)$$

$$EI = E_s\left(I_s + bt_s\left(\frac{E_c t_c(t_c + t_s)}{2(E_c t_c + E_s t_s)}\right)^2\right) + E_c\left(I_c + bt_c\frac{E_s t_s(t_c + t_s)}{2(E_c t_c + E_s t_s)}^2\right)$$

Finally, an expression for the flexural rigidity of a bi-layer beam is obtained:

$$EI = E_s I_s + E_c I_c + \frac{E_s t_s E_c t_c(\frac{t_c}{2} + \frac{t_s}{2})^2}{E_c t_c + E_s t_s} \qquad \textbf{Equation 4.35}$$

The previous equation considers a beam in which the width of the coating (b_c) and the substrate (b_s) are the same ($b_c = b_s = b$). A more general case can be made for a beam which consists of two layers of different widths ($b_c \neq b_s$). The difference in widths would induce a curvature at the edges of the coating [106, 115, 122]. Development of the equation for the flexural rigidity considering dissimilar widths, and introducing the cross-sectional area of the coating ($A_c = b_c t_c$) and substrate ($A_s = b_s t_s$) as a parameter produce the more general expression:

$$EI = E_s I_s + E_c I_c + \frac{E_s A_s E_c A_c \left(\frac{t_c}{2} + \frac{t_s}{2}\right)^2}{E_c A_c + E_s A_s} \qquad \textbf{Equation 4.36}$$

The previous equation was presented by Roche et al (1991) [124]; the term EI is first introduced as the "bending stiffness of a coated substrate" (H_p) and later termed by Benabdi and Roche (1997) [106] as the "equivalent bending stiffness of the bi-layer system". **Equation 4.35** can be rearranged to produce the following equation for the determination of the Young's modulus of a coating applied onto a substrate of known mechanical properties:

$$E_c^2(I_c t_c) + E_c\left[E_s I_s t_s + E_s I_s t_c - EI t_c + E_s b t_c t_s \left(\frac{t_c}{2} + \frac{t_s}{2}\right)^2\right] + [E_s^2 I_s t_s - EI E_s t_s] = 0 \qquad \textbf{Equation 4.37}$$

The latter assumes that the beams are subjected to pure bending with no shear. The beams are simply supported, and loaded with a concentrated load, applied in the middle of the span. Flexural tests in a dynamic mechanical analyser, in 3-point bending mode, can be performed in a bi-layer beam composed of a coating (unknown mechanical properties) and a metallic substrate of know mechanical properties. Finally, the Young's modulus of the supported coatings may be determined. The mechanical response of the samples and the geometrical characteristics provide two solutions to the equation presented. One of the solution is negative and has no physical meaning; the remaining solution is considered the Young's modulus of the coating.

4.6 Internal stresses due to film formation affecting the bi-layer beams

4.6.1 Neglecting the effect of the Poisson's ratio

Now, it can be considered that the final stress in the x direction, in a bi-layer beam, is affected by the initial residual stresses within the coating. These residual stresses have been previously presented as the stresses produced during film formation (chemical curing and solvent evaporation). During the curing process, the free movement of the coating is limited by the substrate and the bi-layer beam bends producing a tensile stress within the coating. Therefore, in a bi-layered beam without any in-plane

deformation and neglecting the Poisson's ratio effect ($\varepsilon_x = \varepsilon_y$), it can be said that final stress state in the x direction is described by **Equation 4.38** [124]:

$$\sigma_{xc,s} = \sigma_{xc,s}^{i} + \sigma_{xc,s}^{a} = \sigma_{xc,s}^{i} + E_{c,s}\varepsilon_{xc,s} \qquad \textbf{Equation 4.38}$$

where:

$\sigma_{xc,s}$= the final uni-axial stress in the x direction of the system,

$\sigma_{xc,s}^{i}$= the initial residual stress within the coating (internal due to film formation),

$\sigma_{xc,s}^{a}$= additional residual stress in the coating or substrate (related to the response strain),

$E_{c,s}$= Young's modulus of the coating (c) or substrate (s), and

$\varepsilon_{xc,s}$= response strain of the coating (c) or substrate (s).

Assuming that there is no deformation (contraction or elongation) in the plane of the bi-layer system, the response strain $\varepsilon_{xc,s}$ can be described by the pure bending solution:

$$\varepsilon_{xc,s} = \frac{y_o - y}{R} \qquad \textbf{Equation 4.39}$$

where:

y_o= the position of the neutral axis; and

y= coordinate distance of any longitudinal fibre.

In **Figure 4.4**, y_o and y are determined from the coating/substrate interface. **Equation 4.38** can be re-written as:

$$\sigma_{xc,s} = \sigma_{xc,s}^{i} + E_{c,s}\frac{y_o - y}{R} \qquad \textbf{Equation 4.40}$$

In the coating, the coordinate of the longitudinal fibre (y) will be in the range ' $-t_c \leq y \leq 0$'; and the substrate '$0 \leq y \leq t_s$'. **Equation 4.40** shows that the final state of the stresses in the coating and the substrate depends on the initial stresses, Young's moduli, and the location of the neutral axis. Two equilibrium conditions regarding the force and the moment of the cross-sectional area (A) of the coating/substrate system must be met in order for the system to be in equilibrium:

$$\sum_n F_n = 0 \Rightarrow \int_A \sigma_{xc,s}\, dA \qquad \textbf{Equation 4.41}$$

$$\sum_n M_n = 0 \Rightarrow \int_A \sigma_{xc,s}\, y dA \qquad \textbf{Equation 4.42}$$

with $dA = bdy$. For the general case of a beam constituted by two layers of different widths, b_c and b_s for the coating and substrate, respectively. By applying **Equation 4.40** to **Equation 4.41** and **Equation 4.42**, respectively, the equilibrium conditions can be expressed as:

$$\int_{t_c}^{0} \sigma_{xc}^{i} b_c\, dy + \int_{t_c}^{0} b_c E_c \frac{y_o - y}{R} dy + \int_{0}^{t_s} b_s E_s \frac{y_o - y}{R} dy = 0 \qquad \textbf{Equation 4.43}$$

$$\int_{t_c}^{0} \sigma_{xc}^{i} b\, y dy + \int_{t_c}^{0} b_c E_c \frac{y_o - y}{R} y dy + \int_{0}^{t_s} b_s E_s \frac{y_o - y}{R} y dy = 0 \qquad \textbf{Equation 4.44}$$

The initial residual stresses, or internal stresses, are assumed constant across the thickness of the coating. Therefore, σ_{xc}^{i} is constant when evaluated across the y axis. Integration of **Equation 4.43** provides the location of the neutral axis:

$$y_o = -\frac{Rb_c t_c \sigma^i_{xc,s}}{E_c b_c t_c + E_s b_s t_s} + \frac{1}{2}\frac{E_s b_s t_s^2 - E_c b_c t_c^2}{E_c b_c t_c + E_s b_s t_s} \qquad \textbf{Equation 4.45}$$

Equation 4.45 provides the location of the neutral axis from the coating/substrate interface. This equation considers the effect of the curvature produced by the internal stresses within the coating. If the internal stresses are neglected, **Equation 4.26** is obtained. The previous equation can be re-written considering the cross-sectional areas of the coating, $A_c = b_c t_c$, and the substrate, $A_s = b_s t_s$:

$$y_o = -\frac{RA_c \sigma^i_{xc,s}}{E_c A_c + E_s A_s} + \frac{1}{2}\frac{E_s A_s t_s - E_c A_c t_c}{E_c A_c + E_s A_s} \qquad \textbf{Equation 4.46}$$

Relocating the origin of the coordinate system from the interface to the top surface of the coating and neglecting the effect of the residual stresses in the coating provides **Equation 4.25**; which also considers a flat beam with no in-plane deformation and neglecting the effect of the residual stresses within the coating layer. From now on, the calculations consider the general case of "$b_c \neq b_s$" from which the case "$b = b_c = b_s$" can be deduced straightforwardly.

With knowledge of the position of the neutral axis from the coating/substrate interface, **Equation 4.46** is solved and the expression for the residual stresses is obtained:

$$\sigma^i_{xc} = -\frac{A_c^2 E_c^2 t_c^2 + 2A_c A_s E_c E_s (2t_c^2 + 3t_c t_s + 2t_c^2) + A_s^2 E_s^2 t_s^2}{6R(t_c + t_s)(A_c A_s E_s)} \qquad \textbf{Equation 4.47}$$

For a bi-layer beam of width b ($b = b_c = b_s$), a simplified expression can be deduced. Beforehand, it is convenient to define the relationship between the thickness of the coating and the substrate, and the Young's modulus of the coating and the substrate. This approach simplifies the final expressions [106, 111, 115]. The constants α and β are introduced:

$$\alpha = \frac{E_c}{E_s}$$ **Equation 4.48**

$$\beta = \frac{t_c}{t_s}$$ **Equation 4.49**

Finally, **Equation 4.50** presents the internal stress in a bi-layer beam with no in-plane deformation or the effect of the Poisson's ratio.

$$\sigma_{xc}^{i} = -\frac{E_s t_s^2}{6Rt_c}\frac{1 + 2\alpha\beta(2 + 3\beta + 2\beta^2) + \alpha^2\beta^4}{1 + \beta}$$ **Equation 4.50**

As previously mentioned, Stoney's approach assumed the equality of Young's moduli ($E = E_c = E_s$), and that the thickness of the coating is negligible compared to the coating thickness. Applying those conditions to **Equation 4.50** allow the determination of Stoney's residual stress (termed "P" by the author) previously presented in **Equation 4.12**.

4.6.2 Considering the effect of the Poisson's ratio

Equation 4.50 was developed considering the elastic theory of simple beams. However, the bending of the substrate by the effect of the residual stresses in the beam should be treated as a plate rather than a thin beam. Plate theory provides the isotropic stress in equilibrium with the resultant strain, where the Poisson's ratio of the substrate and coating now have an important bearing in the determination of the residual stresses [110]. The coated substrate is considered as a plate, in which the stresses rises in the two in-plane directions. The analysis requires the incorporation of the bi-axial Young's modulus ($E_{c,s}{}^{*}$) into the analysis [115]:

$$E_{c,s}{}^{*} = \frac{E_{c,s}}{1 - \nu_{c,s}}$$ **Equation 4.51**

where:

$\nu_{c,s}$ = Poisson's ratio of the coating or substrate.

Substituting **Equation 4.51** into **Equation 4.38**, the final state of the stresses in the plate is obtained:

$$\sigma_{xc,s} = \sigma^{i}_{xc,s} + \sigma^{a}_{xc,s} = \sigma^{i}_{xc,s} + \frac{E_{c,s}}{1-\nu_{c,s}}\frac{y_o - y}{R} \qquad \textbf{Equation 4.52}$$

The equilibrium conditions for the force and the momentum of the cross-sectional area (A) of the coating/substrate system, **Equation 4.41** and **Equation 4.42**, respectively, with the consideration of the Poisson's ratio are developed:

$$\int_{t_c}^{0} \sigma^{i}_{xc} b_c \, dy + \int_{t_c}^{0} b_c \frac{E_c}{1-\nu_c}\frac{y_o - y}{R} dy + \int_{0}^{t_s} b_s \frac{E_s}{1-\nu_s}\frac{y_o - y}{R} dy = 0 \qquad \textbf{Equation 4.53}$$

$$\int_{t_c}^{0} \sigma^{i}_{xc} b \, y dy + \int_{t_c}^{0} b_c \frac{E_c}{1-\nu_c}\frac{y_o - y}{R} y dy + \int_{0}^{t_s} b_s \frac{E_s}{1-\nu_s}\frac{y_o - y}{R} y dy = 0 \qquad \textbf{Equation 4.54}$$

Execution of **Equation 4.53** provides the location of the neutral axis from the coating/substrate interface:

$$y_o = -\frac{RA_c(1-\nu_c)(1-\nu_s)\sigma^{i}_{xc,s}}{E_c A_c(1-\nu_c) + E_s A_s(1-\nu_s)} + \frac{1}{2}\frac{E_s A_s t_s(1-\nu_c) - E_c A_c t_c(1-\nu))_s)}{E_s A_s(1-\nu_c) + E_c A_c(1-\nu_s)} \qquad \textbf{Equation 4.55}$$

Translation of the neutral axis to the top (free) surface of the coating, neglecting the effect of the residual stresses, and equal widths ($b = b_c = b_s$):

$$y_c = \frac{1}{2}\frac{E_c t_c^2 + 2t_c t_s E_s + E_s t_s^2 - (E_c t_c^2 \nu_s + 2E_s t_c t_s \nu_c + E_s t_s^2 \nu_c)}{E_s t_s (1-\nu_c) + E_c t_c (1-\nu_s)} \qquad \textbf{Equation 4.56}$$

Development of **Equation 4.54** provides an expression for the residual stresses in the bi-layered plate:

$$\sigma_x^i = -\frac{E_s t_s^2}{6R t_c (1-\nu_s)} \frac{1 + 2\alpha'\beta(2 + 3\beta + 2\beta^2) + \alpha'^2\beta^4}{1+\beta} \qquad \textbf{Equation 4.57}$$

with:

$$\alpha' = \frac{E_c(1-\nu_s)}{E_s(1-\nu_c)} \qquad \textbf{Equation 4.58}$$

The two equations presented for the determination of the residual stresses within coatings (**Equation 4.50** and **Equation 4.57**) have been proposed by Benabdi and Roche (1997) [106, 115]. Similarly, Yun and White (1999), have proposed an expression in which $\alpha = t_s/t_c$ and $\beta = E_s(1-\nu_c)/E_c(1-\nu_s)$, presented in **Equation 4.59**.

$$\sigma_{xc}^i = -\frac{E_c \alpha}{6R(1-\nu_s)} \frac{1 + 4\alpha\beta + 6\alpha^2\beta + 4\alpha^3\beta + \beta^4\alpha^2}{(1+\alpha)(1+\alpha\beta)} \qquad \textbf{Equation 4.59}$$

The presented mathematical model provides a facile method for the determination of the Young's modulus (**Equation 4.37**) and residual stresses (**Equation 4.57**) of supported coatings. The model, based on plate theory, provides the isotropic stress in equilibrium with the resultant strain, where the Poisson's ratio of the substrate and the coating have a relevant bearing on the stresses. The consideration of the Poisson's ratio, and introduction of the factor '$1/1-\nu_{c,s}$', as shown in **Equation 4.31**, produces

residual stresses approximately 1.5[4] times greater than those calculated for uniaxial stresses (**Equation 4.50**).

The mathematical model provides results for the elastic modulus and residual stresses which take into consideration the following assumption:

- the materials forming the bi-layer system (coating and substrate) are homogeneous, isotropic and elastic;
- the Young's moduli of the coating and the substrate each have the same values on both tension and compression (flexural modulus);
- the residual stress are considered bi-axial and isotropic;
- the radius of curvature of the beam, R, is large compared to the width, b, and thickness, t, of the bi-layered plate;
- the internal residual stresses, σ_x^i, are homogeneous and have a linear distribution across the thickness of the coating.

4.7 Conclusions

Composite beam stress analysis provides a solution for the Young's modulus and residual stresses of supported coatings. The equation for the flexural rigidity of a beam subjected to pure bending with no shear provides the Young's modulus of a supported coating. The previously presented models for the determination of the elastic modulus of supported coatings have been applied to bi-layered samples subjected to 3-point bending tests on static mechanical testing equipment. In the present study this theory is applied to bi-layered samples analysed by DMA in 3-point bending mode. The determination of the mechanical response of the composite beam (coating/substrate) and the substrate, and the geometrical parameters of the beam provide a solution for the Young's modulus of the supported coatings.

The developments in beam/plate theory provides a solution for the internal residual stresses in the coating due to film formation. Several contributions have been made to the analysis since Stoney introduced the concern for tensile residual stresses in coatings and consequent coating failure [67, 108-113]. In the present analysis it was found that Benabdi and Roche's (1997) [106, 115] equation provides the residual

[4] Considering: $\nu_c = \nu_s = 0.35$

stresses for thick and thin supported coatings of known mechanical properties (**Equation 4.57**). As the analysis shows, the Young's modulus and thickness of both the coating and the substrate have a relevant effect on the stress development within the coating. This practise requires the use of very thin substrates in order to visually appreciate the deformation in the substrate produced by the coating's residual stresses.

The Young's modulus and the residual stresses are important parameters for understanding the mechanical behaviour of coatings in service. Excessive residual stresses may be detrimental for supported coatings in marine applications. Stresses due to film formation, generally tensile in nature, reduce the coating's capacity to stand additional tensile stresses in services. Tensile stresses act against adhesion to the substrate or previous coating layer in the coating scheme. By testing bi-layered beam with increasing film thickness, the effect of both Young's modulus and coating thickness on the residual stresses may be evaluated.

5 EXPERIMENTAL METHODS

5.1 Materials and specimen characterisation

5.1.1 Materials

In the present study, a series of coatings formulations were applied onto steel substrates with the objective of studying their mechanical properties as a system (coating/substrate). When experimentally practicable, a test on a coating applied to its normal substrate is always preferable to a free film or flexible substrates. However, some tests such as dynamic mechanical analysis, require the use of free films or flexible substrate to accommodate the equipment's limitations [125]. **Table 5.1** indicates the coating systems studied. These coatings have applications as transition piece and wind turbine tower coatings. Additionally, **Table 5.2** provides further physical properties for the coatings. The characterisation and detailed study of their mechanical properties is of great importance in the understanding of their reliability.

Table 5.1 Coating description from technical data sheet.

Name	Description	Application
Coating A	Two component polyamide adducts cured, high build epoxy paint which combines relatively high-volume solids with a short drying time	1) Intermediate coating (Zinc rich primer + coating A + PU overcoat) 2) Primer in mild to medium corrosive environments
Coating B	Two-component high build, epoxy polyamide/amine paint, which cures to an abrasion and corrosion resistant coating.	Severe corrosive environments where an abrasive resistant coating is needed. Splash and immersion zones
Coating C	Two-component, high build epoxy phenalkamine paint, which combines relatively high-volume solids content with a short drying time.	Primer in mild to medium corrosive environments

Table 5.2 Physical constants for the coatings.

Name	Maximum Service Temperature [˚C]	Volume solids, VS [%]	Specific gravity [kg/l]	Dry to touch [h, ˚C]	Fully cured [days, ˚C]
Coating A	dry conditions only 140 ˚C	70±1	1.5	2 (20 ˚C)	7 (20 ˚C)
Coating B	dry conditions only: 140 ˚C Wet: 50 ˚C	79±1	1.6	8-10 (10 ˚C)	14 (10 ˚C)
Coating C	dry exposure only: 140˚C	74±1	1.5	1.5 (20 ˚C)	7 (20 ˚C)

The term high-build indicates that the coatings are capable of producing a series of films thicker than those normally associated with paints. Coating A is a polyamide adduct epoxy, i.e. the amide curing agent used to cure the epoxy has been modified by adduction with another epoxy. Polyamide adduct epoxies do perform like other epoxies, but their overall physical properties are improved, and the curing time can be much faster than in regular epoxy systems. The improved properties include, but are not limited to, higher colour stability and the capability to cure at slightly lower temperature [42].

5.1.2 Specimens

5.1.2.1 Airless-sprayed samples

Airless spraying is the main method of paint application in the wind turbine industry. When using this application method, the viscosity holds the paint together and atomisation by the spray gun dissipates the paint to produce a mist of droplets instead of a continuous mass of fluid. Since airless spraying applies a very ‘wet’ coating, assuming that the surface is properly prepared, then good adhesion is achieved, and the coating is less likely to fail and more likely to keep its integrity. During application,

the spray gun moves in horizontal lines, rather than in an arch, perpendicularly to the substrate's surface.

Nowadays, the industry demand is for faster drying coatings, lower thicknesses and fewer coats in the scheme [53]. In this study, both supported coatings and free films were produced as single layer coatings, and the supported systems are considered as bilayer composites. Samples of the three different paint systems were airless-sprayed onto steel flexible substrates, thick steel plates, and silicone release paper (to produce free films). Five to six different film thicknesses (from 100 to 1200μm) were prepared on steel shim substrates, four film thicknesses on silicone release paper and three different thicknesses for the thick panels (from 350 to 750 μm) were prepared. The flexible substrates were roughened with abrasive paper and the thick panels were sandblasted to aid adhesion. **Table 5.3** shows the characteristic of all airless-sprayed samples.

Table 5.3 Characteristics of the supported coating samples.

Type of samples	**Coating DFT [μm]**	**Substrate**			
		Material	**Length [mm]**	**Width [mm]**	**Thickness [mm]**
Supported coatings	100 to 1200	Spring steel panels	50	8.5	0.23
	350 to 750	Mild steel panels	200	145	0.8
Free films	200 to 1100	Silicone release paper	50	8.5	-

All the samples were oven cured to the schedule presented **Table 5.4**. A post-cure process ensures that there is a stable baseline that can be reproduced, even though these are not the curing conditions that are commonly used in real life applications. The cure temperature is kept below the glass transition temperature (T_g) to avoid the relief of internal residual stresses. Traditionally, a post-cure process accelerates the curing process of a coating and improves the mechanical and thermal resistance of the

coatings by increasing the cross-linking density. However, an increase in cross-linking density may also increase the brittleness of the coatings.

Table 5.4 Oven curing process applied to coated steel samples.

Step	Temperature	Duration
1	Room Temperature	3 days
2	50˚C	4 days

5.1.2.2 Cast specimens

Thick unsupported films were produced in order to evaluate the solvent loss kinetics and its effect on the physical and mechanical properties of the coatings. The samples were produced by pouring paint onto silicone moulds and then cured in situ. The use of silicone moulds allows the production of thick free films of rectangular cross sections. To make the moulds, the positive of the specimens was 3D printed and placed in a box, the silicone and catalyst (Polycraft GP-3481-F general purpose RTV condensation mould making silicone rubber) were mixed in the proportions specified by the manufacturer and poured into the box. The silicone was left to cure for 24 hours. The configuration of the sample preparation is shown in **Figure 5.1**. The characteristics of the cast specimens are presented in **Table 5.5**.

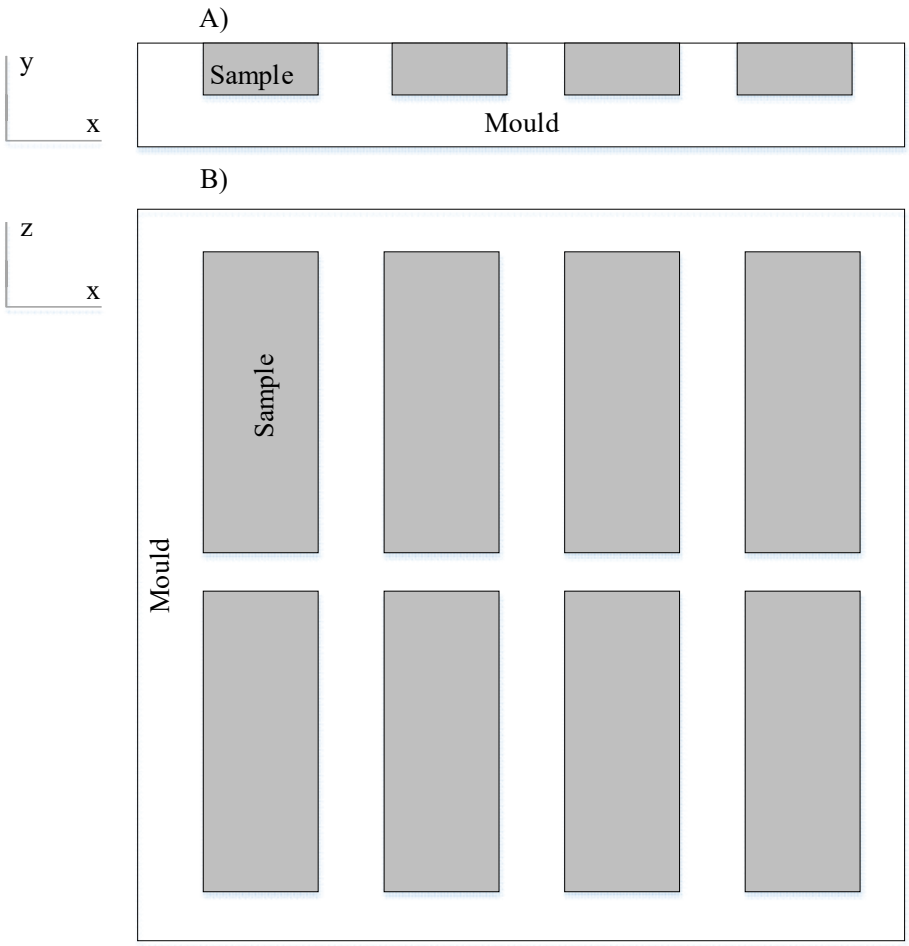

Figure 5.1 A) cross section and B) 'frontal' view of the silicone/sample system

Table 5.5 Characteristics of cast samples.

Sample type	Characteristics	Dimensions		
		Nominal thickness [mm]	Length [mm]	Width [mm]
Thin films	Cast onto silicone moulds	1.5-1.7	50	8.5
Thick films		3.5	80	10

5.1.2.3 Preparation of mounted cross sections

The cross sections of supported and unsupported coatings were prepared for analysis by scanning electron microscopy (SEM) and electron dispersive spectroscopy (EDS). Coatings supported by flexible substrates and free films were mounted in clear epoxy (West systems number 05) to facilitate handling, grinding and polishing. The cross sections were placed in mounting cups (FixiForm manufactured by Struers) and secured with fixation clips (Multiclips by Struers). The mounting cups were previously coated with silicone grease (manufactured by RS components Ltd) to facilitate the release of the epoxy. Finally, the samples were ground with SiC papers (400, 600, 1200, and then 4000) for 3 minutes with each grade. Final polishing was achieved with a SiO_2 suspension (Mastermet 2 0.02µm by Buehler) and polishing cloths (Chemomet 8" by Buehler). **Figure 5.2** shows a polished and mounted set of coating A samples for SEM and EDS analysis.

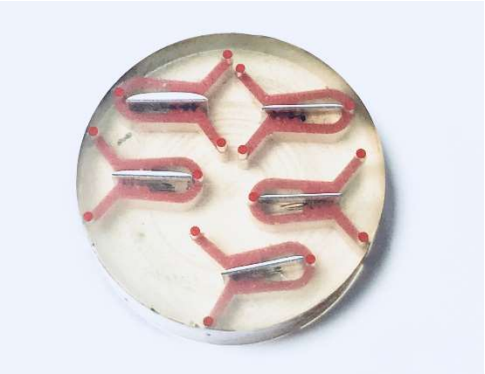

Figure 5.2 Polished and mounted representative samples of coating A.

5.2 Measurement of dry film thickness (DFT) of the coatings

The dry film thickness was measured in accordance with ASTM D1005 – 95 (2013) 'Standard test method for measurement of dry-film thickness of organic coatings using micrometers'; using a 456 coating thickness gauge manufactured by Elcometer. This test method is applicable to both free films and coatings supported on test panels. The accuracy and precision of the measurements may be affected by the deformability of the coatings and the homogeneity of the substrate's thickness when applied to panels. The micrometre was steadily held against the surface of the coating, and the thickness readily taken from the dial and recorded. A minimum of four measurements were performed of both the uncoated and coated panels. These were then used to provide an

average thickness. The thickness of the substrate used in the preparation of the mounted samples was then subtracted from the composite thickness to provide the coating film thickness [126].

5.3 Solvent loss kinetics calculation

The effect of solvent retention on the mechanical performance of the coatings was determined by analysing the solvent evaporation kinetics of the coatings through weight change measurements. The samples were prepared with the use of silicone moulds to the dimensions specified in **Table 5.5**. The samples were separated into three groups and each group was subjected to a different cure schedule, as shown in **Table 5.6**. The weight changes of the samples were monitored daily for over 31 days.

Table 5.6 Post cure schedule for the study of solvent retention.

Cure schedule	Description
Schedule 1	31 days at RT (50% RH)
Schedule 2	3 days at RT (50% RH) + 4 days at 50˚C + 24 days RT (50% RH)
Schedule 3	3 days at RT (50% RH) + 28 days at 50˚C

The post-cure schedule 3 is designed to determine if further weight loss can be achieved by prolonging the time at 50˚C. This approach was selected (instead of increasing the temperature) in order to maintain the temperature below the glass transition temperature and avoid any chemical changes in the coating by loss of low molecular weight components.

5.4 Surface metrology and form measurement

Surface profile and roughness measurement was performed with an Alicona Infinite Focus optical scanner. The surface of the coated flexible substrates was scanned along the length of the samples to evaluate the variation of roughness parameters with coating thickness. The roughness was determined in a scan area of 10mm in the centre of the samples as illustrated in **Figure 5.3.a**. The cross-sectional area of the samples was also examined in order to calculate variation in thickness of the samples with the

cross section assumed by the mathematical model presented in Chapter 4. Supported flexible films have a curvature due to internal stresses. Therefore, the scans are limited to the centre of the samples, as shown in **Figure 5.3.b**, where there is minimal bending. The analysis was performed with a magnification of 10X.

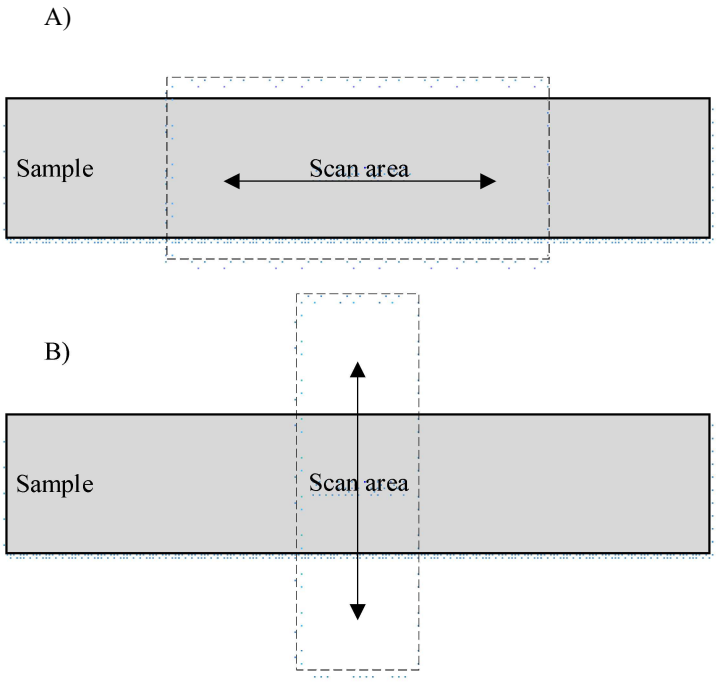

Figure 5.3 A) Area for the calculation of the roughness parameters and B) area for the calculation of the cross-sectional area.

5.5 Scanning electron microscopy (SEM) and electron dispersive spectroscopy (EDS)

The SEM used in the present study is a TESCAN MIRA 3 field emission scanning electron microscope. The scanning electron microscope (SEM) is the most widely used type of electron microscope. It examines the microscopic structure by scanning the surface of materials. A focused electron beam scans the surface area of the specimen and forms the image. Perhaps the most important feature of an SEM is the three-dimensional appearance of its images because of its large depth of field and very high magnification [127]. The SEM consists of three main groups of components; the electron-optical column with its accompanying electronics, the vacuum system and specimen chamber and stage, as well as the signal detection and display system[128].

Due to the insulating nature of organic coatings, all samples were coated with a 20nm layer of sputtered platinum. Sample examination was carried out under high vacuum and through the use of the backscatter detector. The backscatter detector allows the appreciation of the coating's topographical contrast profile and atomic number contrast. Backscattering increases with the atomic number of the elements detected, elements with higher atomic number are presented brighter than elements with lower numbers. This characteristic is particularly useful for the characterisation of paint/substrate cross-sections [129].

Finally, electron dispersive spectroscopy (EDS) analysis was performed using an Oxford Instruments X Max 150mm^2 with a silicone drift solid-state detector. After a suitable area of the specimen is selected for analysis, a high energy electron beam interacts with the sample and produces an X-ray with energies (wavelength) which is characteristic of the elements present in the sample [130]. The X-rays are generated not only from the surface of the specimen but also a few cubic microns into the material [131].

5.6 Adhesion test

The adhesion test was performed according to the standard method "Corrosion protection of steel structures by protective paint systems – Assessment of, and acceptance criteria for, the adhesion/cohesion (fracture strength of a coating – Part1: Pull-off testing (ISO BS EN 1626-1:2007)" [132] with a Positest AT-A, an automatic adhesion tester manufactured by DeFelsko.

The adhesion test measures the adhesive/cohesive bond strength of applied coatings. The equipment is based on the pull-off principle and the test introduces the concept of fracture strength, which involves both adhesion and cohesion. The surfaces of the coatings and dollies are slightly roughened with SiC abrasive paper (number 800). Then, the roughened dolly (a cylinder) is glued to the surface of the coating with a 2-pack epoxy adhesive, which is left to cure for 24 hours. A cylindrical cutter is then used to cut around the dolly through the coating down to the substrate prior to the test. The adhesion tester is placed over the dolly and the test is performed (**Figure 5.4**). The fracture strength is dependent on the rate at which the force is applied to remove the test dolly. The tensile stress is applied perpendicularly to the plane of the coated

substrate and increases at a constant rate. The rate is set to ensure its compliance with the standard. Moreover, this rate should not be greater than 1MPa/s and allow for the fracture to occur within 90s [132]. If more than 20% of the area of the end face of the dolly exhibits failure of the adhesive, the test is deemed not to be valid and should be repeated. Additional information on the adhesion test provided in the reference [133].**Table 5.7** presents the parameters of the adhesion test.

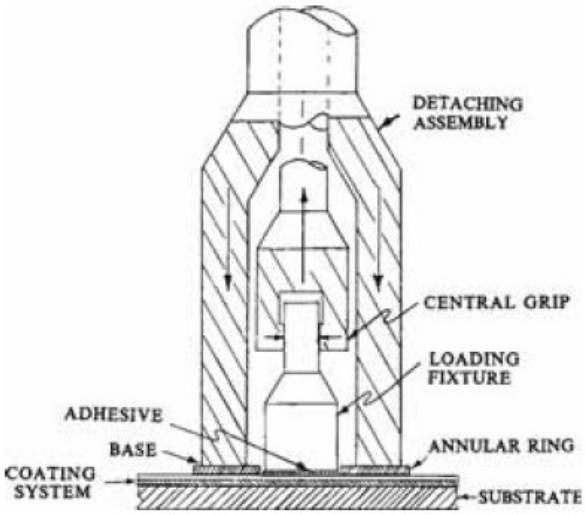

Figure 5.4 Portable adhesive tester [133].

Table 5.7 Adhesion test parameters.

Parameter	Value
Panel dimensions [mm]	200 x 150 x 80
Dolly's diameter [mm]	20
Force rate [MPa/s]	0.69
Dolly's per sample	4

Visual inspection of the fracture surfaces will be reported according to **Table 5.8**. The structure showing the interfaces of the samples between the dolly, coatings and substrate are presented in **Figure 5.5**. The diagram illustrates types of fracture for

multi-layer systems. However, the test samples consist of a substrate and a single layer coating. The topcoat, intermediate coat, and second coat must be ignored.

Table 5.8 Result criteria for visual inspection of adhesion test[5] [36].

Result	Description
A	Cohesive failure of substrate
A/B	Adhesive failure between substrate and 1st coat (primer)
B	Cohesive failure of 1st coat
B/C	Adhesive failure between 1st coat and 2nd coat
C	Cohesive failure of 2nd coat
C/m	Adhesive failure between 2nd coat and *m*th coat of a multicoat system
M	Cohesive failure of the *m*th coat of a multicoat system
m/n	Adhesive failure between *m*th coat and *n*th coat of a multicoat system
n/-	Adhesive failure between *n*th coat and topcoat of a multicoat system
-	Cohesive failure of topcoat
-/Y	Adhesive failure between topcoat and adhesive
Y	Cohesive failure of adhesive
Y/Z	Adhesive failure between adhesive and dolly

[5] Applicable to systems with "n" number of coats. In the current study, n=1.

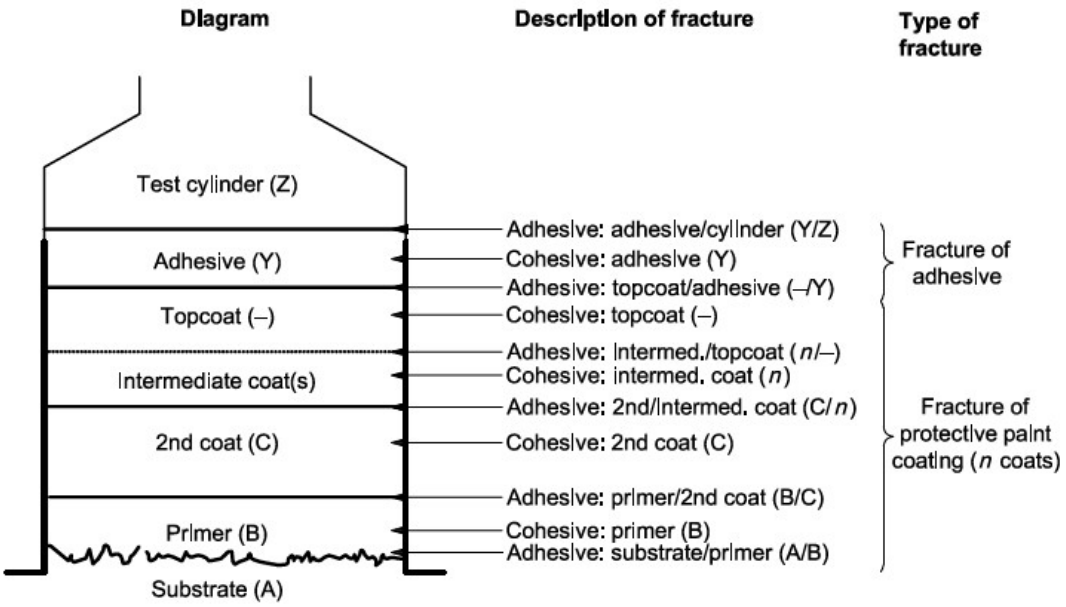

Figure 5.5 Description of types of fracture [132].

5.7 Dynamic mechanical analysis (DMA)

Dynamic mechanical analysis (DMA) was performed on supported and unsupported coatings with different loading fixtures. The DMA used in the present project is a DMA 8000 manufactured by PerkinElmer.

DMA is a versatile and widely used technique for the characterisation of materials in terms of time, temperature, frequency, stress, atmosphere or a combination of these [134]. The equipment allows the study of curing processes, the effect of frequency changes on materials, stress-strain curves, creep recovery, and stress relaxations using only small amounts of material. Changes in glass transition temperature are strongly related to the mechanical strength of epoxy-based coatings. Thus, the present study uses DMA to quantify this relationship [135, 136]. A force motor is used to generate a sinusoidal wave, which is transmitted to the sample via a drive shaft. **Figure 5.6** shows the schematics of the analytic train of the DMA 8000 [134].

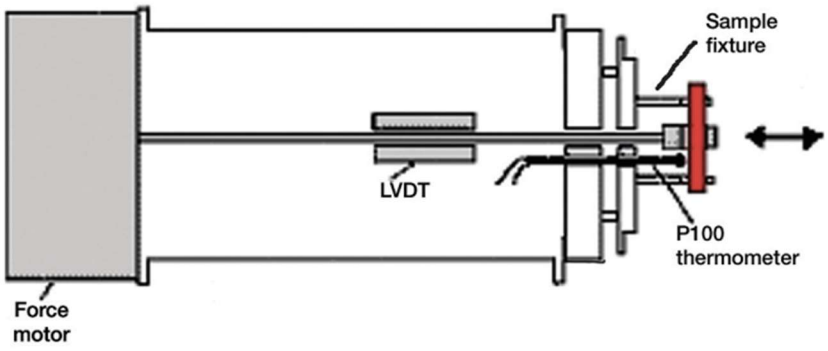

Figure 5.6 Schematic of the DMA 8000 analytic train[6] [134].

The dynamic complex modulus (E^*) is represented by:

$$E^* = E' + iE'' \qquad \textbf{Equation 5.1}$$

where:

E' = indicates the real component (in-phase with the applied strain), and

E'' = the imaginary component (90˚out of phase with the applied strain).

E' is the storage modulus which is proportional to the energy that is fully recovered per cycle of deformation; whereas E'' indicates the loss modulus which is proportional to the total energy dissipated per cycle of deformation in the form of heat [137, 138].

The dynamic storage modulus is given by the following equation:

$$E' = (\sigma_o/\varepsilon_o)\cos\delta \qquad \textbf{Equation 5.2}$$

Whilst the dynamic loss modulus is given by the equation:

$$E'' = (\sigma_o/\varepsilon_o)\sin\delta \qquad \textbf{Equation 5.3}$$

[6] LVDT stands for "Linear variable differential transformer"

where:

σ_o = dynamic stress, and

ε_o = dynamic strain.

The angle, δ, represents the phase angle; the tangent of the phase angle is represented by:

$$\tan\delta = \frac{E''}{E'} \qquad \textbf{Equation 5.4}$$

The instrument calculates E' from the following equation:

$$E' = K_s \frac{L^3}{6I}\left[1 + \frac{12}{5}(1+\nu)\left(\frac{t}{L}\right)^2\right] \qquad \textbf{Equation 5.5}$$

where:

K_s = stiffness,

L = the span length,

I = the sample moment of inertia,

ν = the Poisson's ratio, and

t = the sample thickness.

In thin plates, the shear effect can be ignored. However, the shear effect increases with an increase in the ratio (t/L) [137]. In a DMA, stiffness, K_s, (not E) is calculated with the drive force. This distinction is made to point out how K rather than E' can be dependent on the geometry [137, 138]. The stiffness, K, is represented in the following equation:

$$K_s = \frac{F}{x}$$ **Equation 5.6**

where:

F = the drive force, and

x = the displacement produced by the force [137].

The equipment provides the storage modulus (E'), loss modulus (E''), and damping (tan δ) by applying a sinusoidal deformation to the specimen, which can be achieved by applying either a controlled stress or strain. Depending on the loading mode and sample type (specially for low damping materials) the elastic modulus calculated may indicate the tensile, shear or flexural modulus [135].

The thermal dependence of the mechanical properties of the coatings will be determined in two different bending modes: dual cantilever (**Figure 5.7**) and 3-point bending mode (**Figure 5.8**). In three-point bending, the beam rests on two supports and is loaded through a nose midway between the supports. Whilst 3-point bending is useful to eliminate the effect of the clamps on the results, the supported coatings are curved due to internal stresses from film formation. When these coatings are tested in 3-point bending and the temperature approaches the glass transition, sample softening due to phase changes within the paint from glassy to rubbery relieve the internal stresses and consequently the sample curvature is lost. Therefore, the midspan loses the equilibrium position and the results are not reliable. The rectangular beams are placed in mechanical linear displacement at a fixed frequency with linear temperature variation [139].

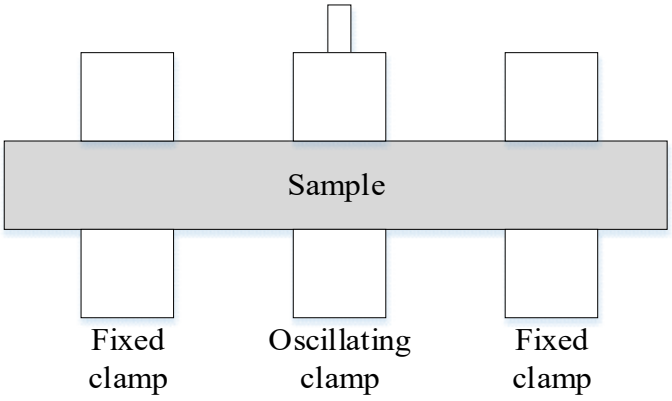

Figure 5.7 Configuration of dual cantilever bending mode (DMA).

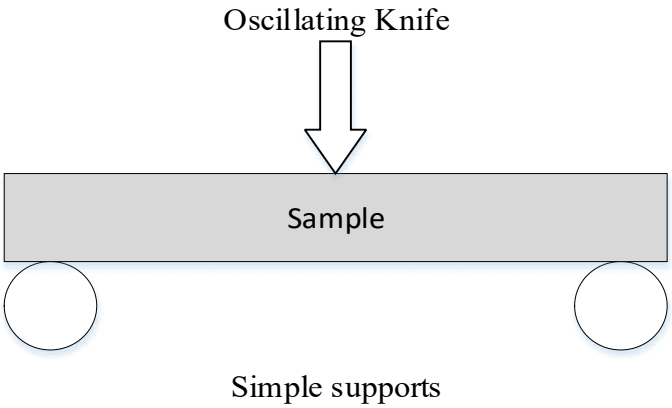

Figure 5.8 Configuration of 3-point bending mode (DMA).

The mechanical response of the materials is highly dependent on the test parameters. A slow speed test would allow the polymer chains to disentangle whilst a fast test speed would not give sufficient time for the polymer chains to disentangle. Therefore, in order to compare results, all test samples must be tested with the same test parameters [140].

DMA tests were performed on the coated shim samples with the parameters presented in **Table 5.9**, as recommended by PerkinElmer. Three coated beams per sample type were tested. A cross section representative of the samples is presented in **Figure 5.9**. All samples were 8.5 mm wide and the free length were 25 mm and 35 mm for dual cantilever and three-point bending mode respectively. To ensure that the samples are properly centred in the stage, the centreline is drawn on the surface of the samples.

Table 5.9 Parameters of the bending DMA tests.

Parameter	Value
Temperature range [°C]	25-140
Temperature rate [°C/min]	5
Frequency [Hz]	1
Static force [N]	2
Dynamic force [N]	1
Force multiplier	1.5
Load strain	0.01

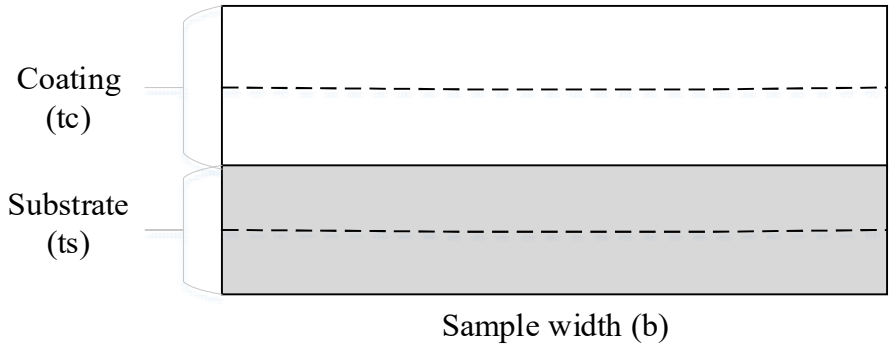

Figure 5.9 Cross section of coated beams for dynamic mechanical analysis.

5.7.1 Determination of the thermal expansion coefficient by thermal mechanical analysis

Determination of the thermal expansion and rate at which it changes for both substrate and coating allows to design around thermal strain mismatches that may cause failure in service. The thermal expansion coefficient (CTE) is determined from analysis of the results obtained by dynamic mechanical analysis. In the determination of the thermal properties of the epoxy coatings, the DMA is used in thermal mechanical analysis (TMA) mode and the DMA will act as a constant strain analyser (the oscillating force is turned off). To determine the thermal expansion of the specimens, the DMA acts as a micrometre and measures the changes in height of the sample

(reported as displacement) with an increase in temperature. For this, the samples are placed in tension mode (**Figure 5.10**).

The tensile test must be performed with the tension geometry that allows for longer samples to be tested (10mm free length) to maximise the signal of the sample and increase the accuracy of the test. Full temperature scans from 25 to 140 °C are performed on free films, however, only the results from 25°C to T_g are considered in the CTE calculations. And additional load of +0.1N is added once the experiment is started to ensure that the sample is in tension.

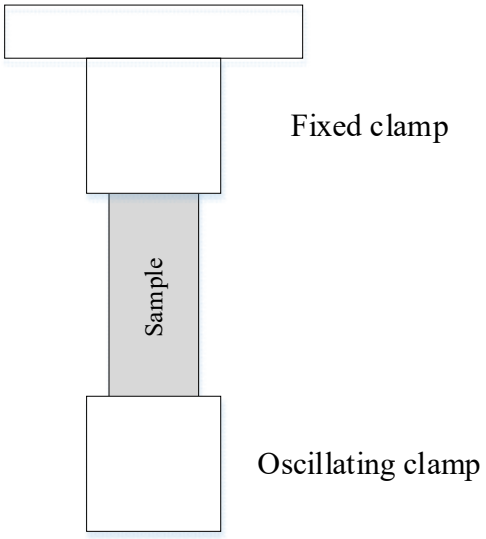

Figure 5.10 Configuration of the tension mode (DMA).

During glass transition the material undergoes configurational changes which interfere with the results. The evolution of the displacement [mm] versus temperature [°C] of the samples is considered for the calculations. Since the instrument's thermal expansion influences the results, a calibration test must be performed on a known material, such as aluminium. The graph of displacement versus temperature for aluminium is obtained, and the theoretical behaviour of aluminium is subtracted from it to obtain a curve that represents the equipment's effect on the results, this curve is used to calibrate the results.

The coefficient of thermal expansion is determined by the following equation:

$$\alpha = \frac{1}{l_o}\frac{\Delta l}{\Delta T} \qquad \textbf{Equation 5.7}$$

where:

α = average of the coefficient of thermal expansion (CTE) for the temperature interval,

$\Delta l/\Delta T$= the slope of the displacement versus temperature curve, and

l_o= original length of the samples which is dictated by the distance between the clamps (free length) [48].

5.8 3-point bending static mechanical tests

Flexural tests in 3-point bending mode on bulk coating (**Table 5.5**) samples were performed with an Instron 3382 static mechanical testing machine. The flexural tests on thick bulk samples were performed according to the standard method 'DIN EN ISO 178:2003 Plastics – Determination of the flexural properties' [95]. Static flexural tests are preferred over static tensile tests when the test materials are brittle, as is the case for epoxy-based coating. Moreover, the present method is ideal for determining the flexural properties of rigid and semi-rigid plastics under specified conditions.

Two lower cylindrical supports, each 6.35mm in diameter, are adjusted to produce a span of a minimum length of 34.25mm between them, the length of the span is adjusted to suit the length of the specimens. The top cylinder placed in the middle of the span (midspan) is a cylindrical support with a diameter of 10mm. The specimens were placed in the 3-point bending setting and deflected at a constant rate at the midspan until failure or the samples reached a predetermined value of deformation. If necessary, the samples must be pre-stressed in order to obtain correct alignment and avoid a curved region at the start of the stress/strain curves. The equipment produces load [kN] versus displacement [mm] curves. The slope of the curves in the elastic region produced the bending stiffness of the samples [95].

The present method for the measurement of flexural properties is designed for room temperature results. The test conditions were 23˚C and humidity of 50% as specified by the standard test method by 'ISO 291: Plastics - Standard atmosphere for

conditioning and testing (2008)' [141]. The samples were placed on the lower cylindrical supports for 3 minutes without producing deformation from the upper cylinder in order to minimise the effect of relaxation of the polymer [106]. **Table 5.10** shows the test parameters for the flexural test suggested by ISO 178.

Table 5.10 Flexural test parameters in accordance with ISO 178.

Parameter	Value
Sample length, l [mm]	80 ± 2 mm
Sample width, b [mm]	10 ± 0.2 mm
Sample thickness, t [mm]	3.5 ± 0.2 mm
Span, L [mm]	56 ± 4
Cross head speed [mm/min]	2
Max load [kN]	100

The results from specimens which fail outside the central third of their span length must be discarded and a new sample shall be tested. If any samples exceed the tolerance specified by the standard test method, ±2% of the mean value, they should also be discarded [95]. The flexural properties calculated for the material are calculated from the force and deflection data within the elastic region. The flexural stress (σ_f) is:

$$\sigma_f = \frac{3FL}{2bh^2} \qquad \textbf{Equation 5.8}$$

where:

F = the applied force,

L = the span,

b = the width of the specimen, and

h = the thickness of the specimen.

The flexural strain, ε_f, may be calculated as a dimensionless ratio (**Equation 5.9**) and as a percentage (**Equation 5.10**):

$$\varepsilon_f = \frac{6sh}{L^2} \qquad \textbf{Equation 5.9}$$

$$\varepsilon_f = \frac{600sh}{L^2}\% \qquad \textbf{Equation 5.10}$$

where:

s = the deflection,

h = the thickness of the specimen, and

L= the span.

For the calculation of the flexural modulus, two different deflections there are determined:

$$s_i = \frac{\varepsilon_{fi}L^2}{6h} \qquad (i = 1; 2) \qquad \textbf{Equation 5.11}$$

Where:

s_i = the deflections (s_1 or s_2), and

ε_{fi} = the corresponding flexural strain, with values of $\varepsilon_{f1} = 0.0005$ and $\varepsilon_{f2} = 0.0025$.

The flexural modulus, E_f, is then calculated through the following equation:

$$E_f = \frac{\sigma_{f2} - \sigma_{f1}}{\varepsilon_{f2} - \varepsilon_{f1}} \qquad \textbf{Equation 5.12}$$

where:

σ_{f1}=flexural stress measured at deflection s_1, and

σ_{f2} = flexural stress measured at deflection s_2.

The three typical curves that results from

Figure 5.11 presents the three typical curves of flexural stress versus flexural strain. [95].

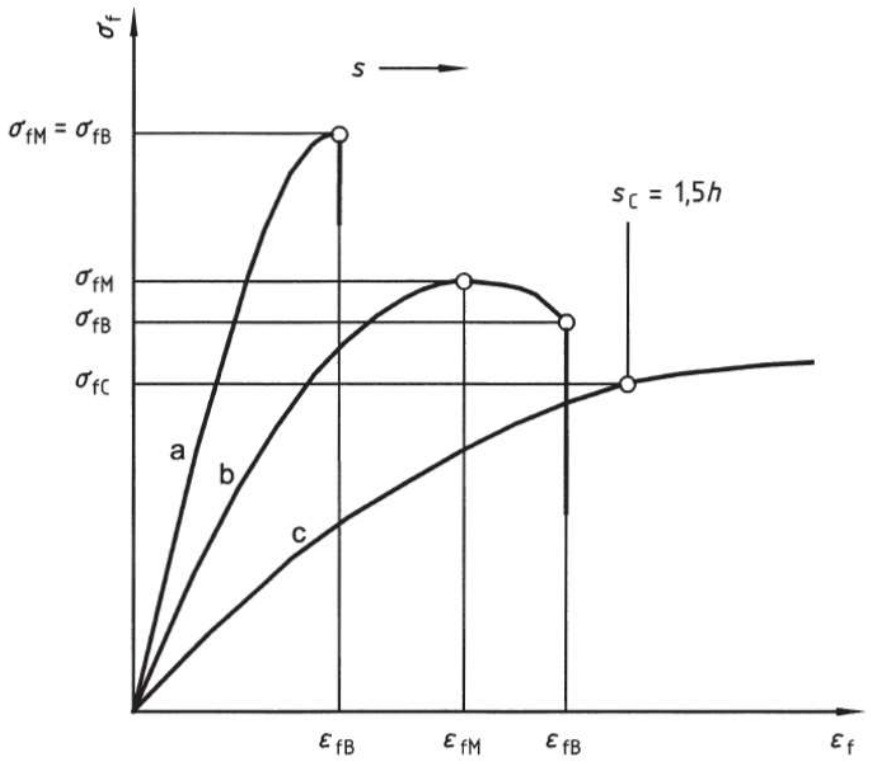

Figure 5.11 Typical curves of flexural stress versus flextural strain for specimens that: a)fail before yielding, b)gives a maximum and then breaks before s_C, and c)neither gives a maximum nor breaks before s_C [95]

where:

s_C = conventional deflection equal to 1.5 times the thickness of the specimen

σ_{fB} = flexural stress at break,

σ_{fM} = maximum flexural stress,

σ_{fC} = flexural stress at conventional deflection,

ε_{fB} = flexural strain at break,

ε_{fM} = maximum flexural strain, and

ε_{fC} = flexural strain at conventional deflection,

5.9 Summary

The methodology presented is intended to give an indication of the different factors affecting the mechanical properties of coatings, both supported and unsupported. Several methods have been selected for the mechanical characterisation of protective coatings used in offshore wind turbine towers and transition pieces. Microscopy methods provide results regarding the roughness parameters, sample morphology, microstructure and composition. Additionally, the study of solvent evaporation kinetics allows the evaluation of the effect of solvent on the physical and mechanical properties of the coatings. Finally, the mechanical properties of supported and unsupported coatings will be determined by dynamic mechanical analysis (DMA), static 3-point bending, and adhesion tests (pull off test). The use of a mathematical model is required in order to determine the Young's modulus and residual stresses in supported coatings.

6 CHARACTERISATION OF PROTECTIVE COATINGS

6.1 Introduction

In an automatic process such as the fabrication of wind turbine towers and transition pieces, production time is crucial and manufacturers are constantly trying to reduce this factor. In terms of paint application, this entails the pursuit of faster drying times and shorter over coating intervals. Therefore, more focus on the application and curing process of paint is required. Fast production processes require shorter overcoat intervals. Transition pieces are coated with total DFT of 700µm and higher. The use of sacrificial anodes is associated with environmental concerns, and its reduction is desired [142]. A typical scheme for exterior atmospheric corrosion protection is presented below:

- Metallization (e.g. Zn/Al, 85/15) 60-100µm
- Epoxy paint 2 coats 100-200µm (including flash coat), and
- Polyurethane paint 50-80µm [53].

However, in reality, the dry film thicknesses (DFT) tend to vary across the tower producing a profile of thicknesses. Due to the application method, there will be overlaps between each pass of the spray gun. The dry film thickness and quality of the coating will depend on the application conditions, workmanship, condition of substrate and environmental conditions. In the past, component failure has been associated with variations in coating thickness across the component, poor surface preparation of the substrate (hard steel) and changes in the cross sections of the substrates. These failures are typically observed around the weld seams where the profile of the substrate changes and are typically hard to paint [53, 143, 144].Good practice in welding involves rounding of the welds so the transition of the profile is smooth rather than sharp. According to NORSOK M-501, an offshore coating standard, a stripe coat should be applied to all welds, corners, behind angles, edges of beams, etc., as well as areas not fully reachable by spray in order to obtain the specified coverage and thickness [54]. The poor treatment of surfaces, changes in geometry and application of higher thicknesses than specified promote internal stresses in the coating that can

lead to failure. Thus, in the present study a group of coatings for offshore wind turbine towers and transition pieces were characterised.

6.2 Cross-sectional profile characterisation

In this section, the cross-sectional profile of the supported coatings and free films were analysed. In Chapter 4, the ideal rectangular cross section of a bi-layered beam was presented in **Figure 4.3**. However, the actual cross section of the samples differs from this ideal rectangular cross section. As the coatings cure on the substrate, the surface tension of the coatings affects the profile. In order to account for the possible variations in the sample's profile, the cross-sectional area of the cured samples was analysed through the 3D optical scanner, as shown in **Figure 5.3.b.** The cross-section's 3D maps were converted into data points and plotted to demonstrate profile changes with increasing coating thickness. **Figure 6.1**, **Figure 6.2**, **Figure 6.3** present the average cross-sectional area of coating A, B, and C respectively.

The dynamic mechanical analyser software performs the tests assuming that the samples are rectangular. Changes in the shape of the cross sections due to coating thickness may result in an increase in the associated error. Moreover, the force applied by the midspan in the 3-point bending tests and the clamps in the dual cantilever bending and tension tests will not be applied evenly on the free surface of the coatings. In 3-point bending DMA tests, the samples were tested with the substrate surface up and in contact with the midspan.

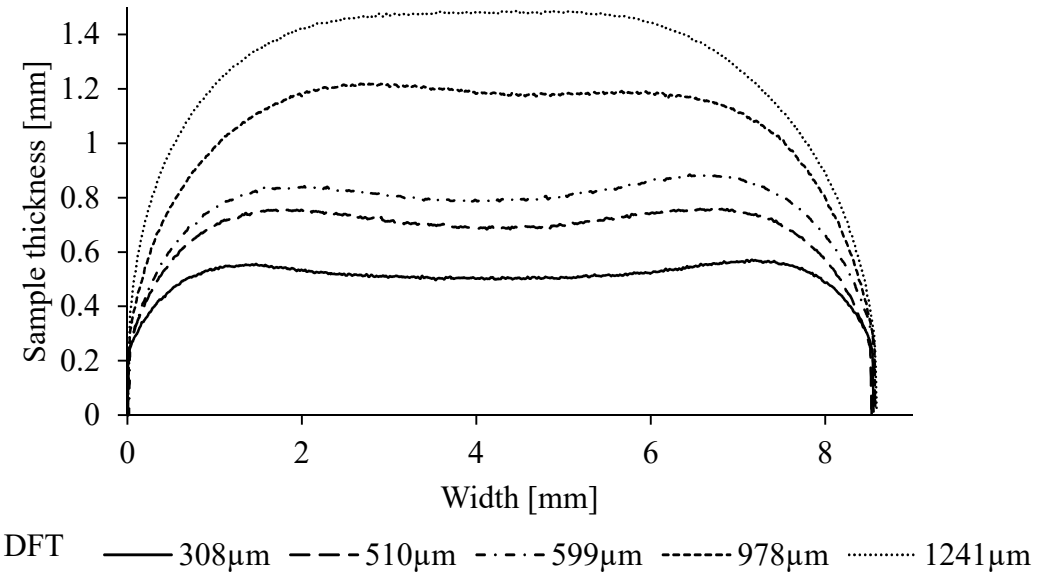

Figure 6.1 Profile of sample cross section with increasing coating thickness for Coating A.

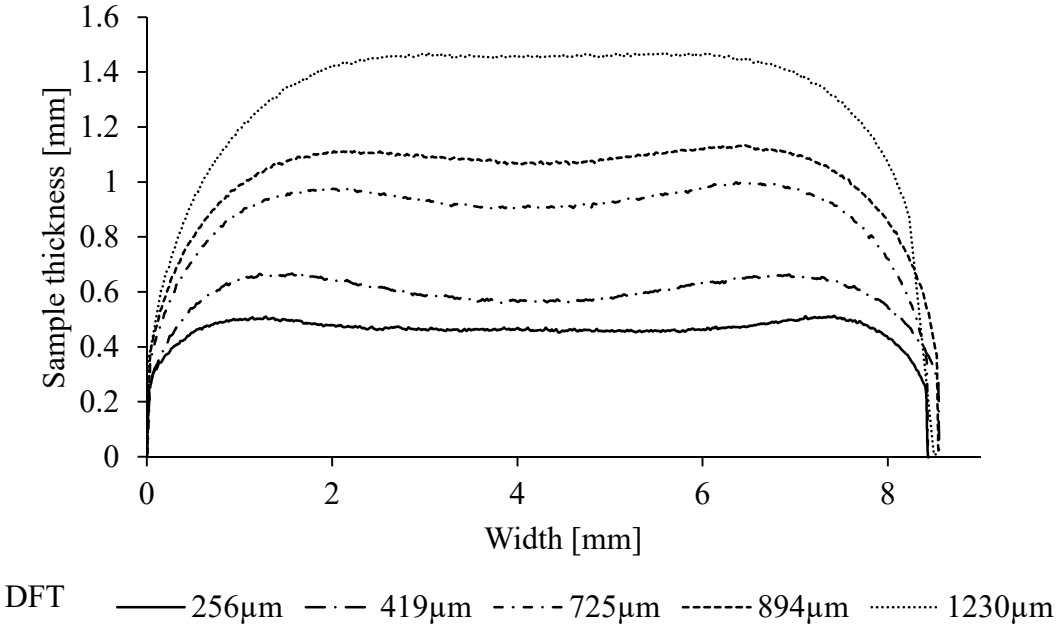

Figure 6.2 Profile of sample cross section with increasing coating thickness for Coating B.

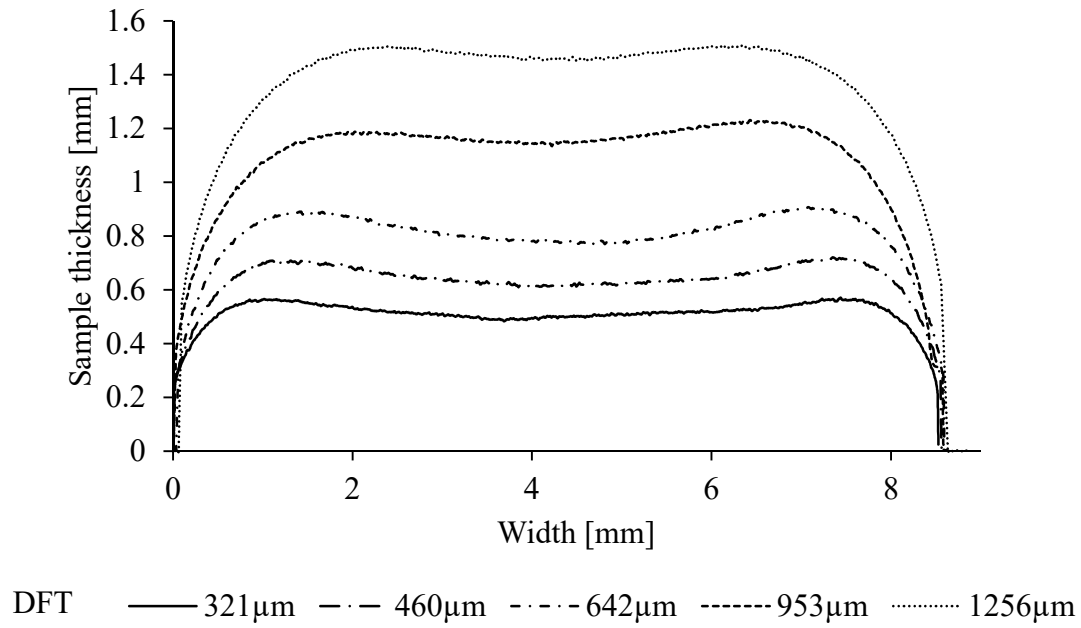

Figure 6.3 Profile of sample cross section with increasing coating thickness for Coating C.

A comparison between the model's cross-sectional areas and the actual ones are shown in **Table 6.1**. The samples vary from the mathematical model on average by 7 to 13%. In general terms, higher variations are observed for higher coating thicknesses. The morphology of the cross section depends on the coating's application method.

The roughness parameters, Ra and Rq, of the coatings were determined, as indicated in **Figure 5.3.a**. Ra represents the average roughness of the profile and Rq represents the root mean square roughness of the profile. For the study of the roughness parameters, three measurements were taken in different areas on each sample, and the results presented as an average with the associated error. **Figure 6.4** and **Figure 6.5** show the average roughness and root mean square roughness of the profiles for all coatings, respectively. The calculations follow the standards set by ISO 4287 and ISO 4288 [145, 146]. The results show that the roughness parameters are independent of coating thickness. The roughness of the coatings is dependent on the application method and workmanship.

Table 6.1 Cross sectional area of the coated substrates for DMA

Coating	DFT [µm]	Model's area [mm^2]	Actual area [mm^2]	Variation [%]
A	308	4.50	4.35	7
	510	6.18	5.81	9
	599	7.02	6.58	8
	978	9.77	9.06	12
	1241	12.20	9.06	13
B	256	4.48	3.89	8
	419	5.36	5.06	10
	724.7	7.62	7.43	9
	894	9.05	8.63	10
	1230	12.33	11.2	10
C	320.6	4.25	4.32	9
	460	5.54	5.47	8
	642	7.35	6.86	8
	953	9.28	9.32	8
	1256	12.59	11.6	9

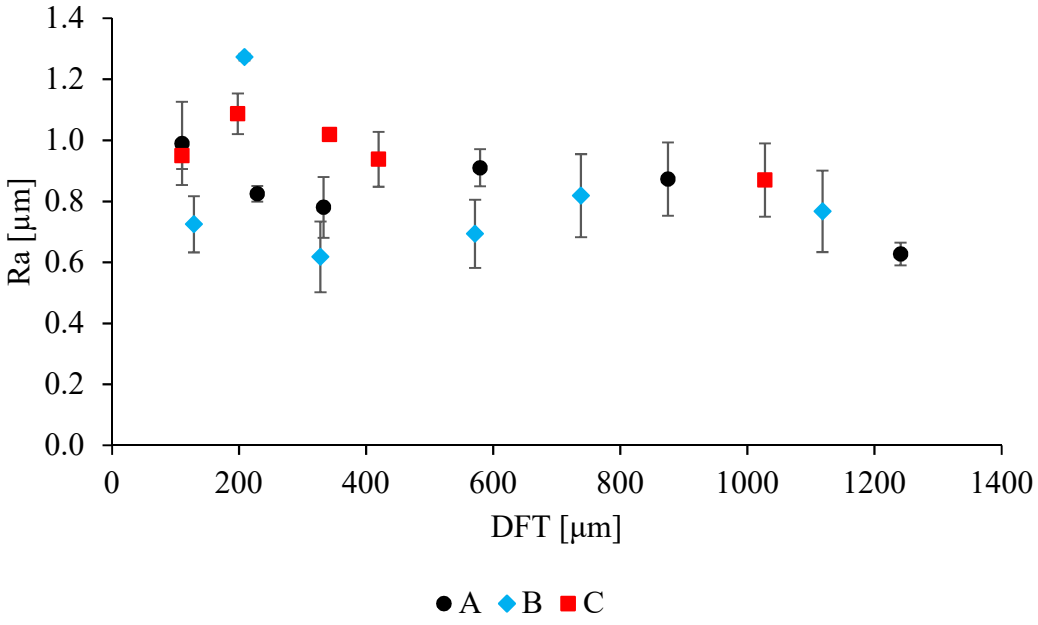

Figure 6.4 Average roughness of the profile (Ra).

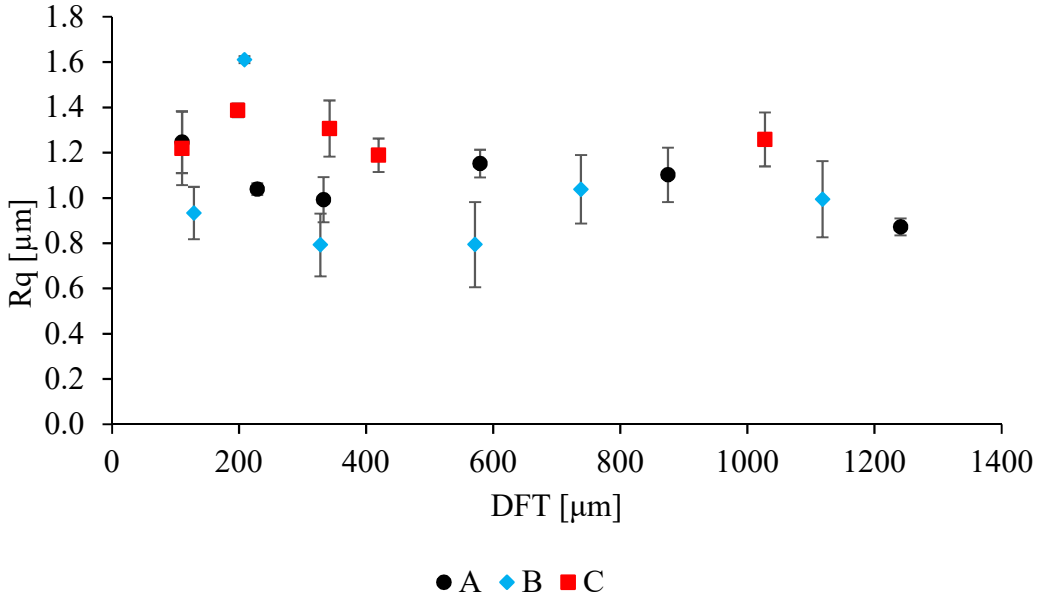

Figure 6.5 Root mean square roughness (Rq).

6.3 Microstructural characterisation

The samples were analysed through SEM and EDS. The SEM micrographs provided information regarding the surface and cross-sectional microstructure and EDS analysis produced quantitative data regarding the elements present in the coatings. The coating cross sections, for all thicknesses, were characterised by SEM using a backscatter detector. The contrasts in the resultant micrographs are due to differences in the atomic weight of the elements present. Bright areas in the micrograph indicate the presence of heavy elements, whilst dark areas indicate the presence of lighter elements, such as carbon and oxygen.

Figure 6.6 presents the cross sections of a representative area of each coating (A, B, C). Note that although the coatings are applied onto thin metal substrates, only the coatings are evident. **Figure 6.7** shows the interface between the coating and the substrate, where the substrate is represented by the 'white' area at the bottom of each micrograph. The heterogeneous nature of the coatings is consistent across the thickness of the coatings, and the distribution of the pigments does not show a gradient in pigment density across the coatings [129]. Several studies have proposed that the orientation of pigments and fillers changes across the coating thickness, producing a gradient of 'orientations' or a profile that is said to affect adhesion and mechanical performance of the material as a protective coating [71, 98, 101, 103, 147]. Commercial paints, unlike laboratory-made formulations, have additives such as anti-floating agents, dispersion agents, and stabilisers in their formulation in order to produce a cured film with homogeneous distribution of fillers in the epoxy-based matrix.

Pigments and fillers are three dimensional components, their orientation in the micrograph only indicates one arbitrary plane of their structure, i.e. a circular cross section may correspond to a lamellar, spherical, or amorphous filler. The presence, volume fraction, size, and morphology of fillers affects the physical properties such as opacity, gloss, colour, and viscosity [38].

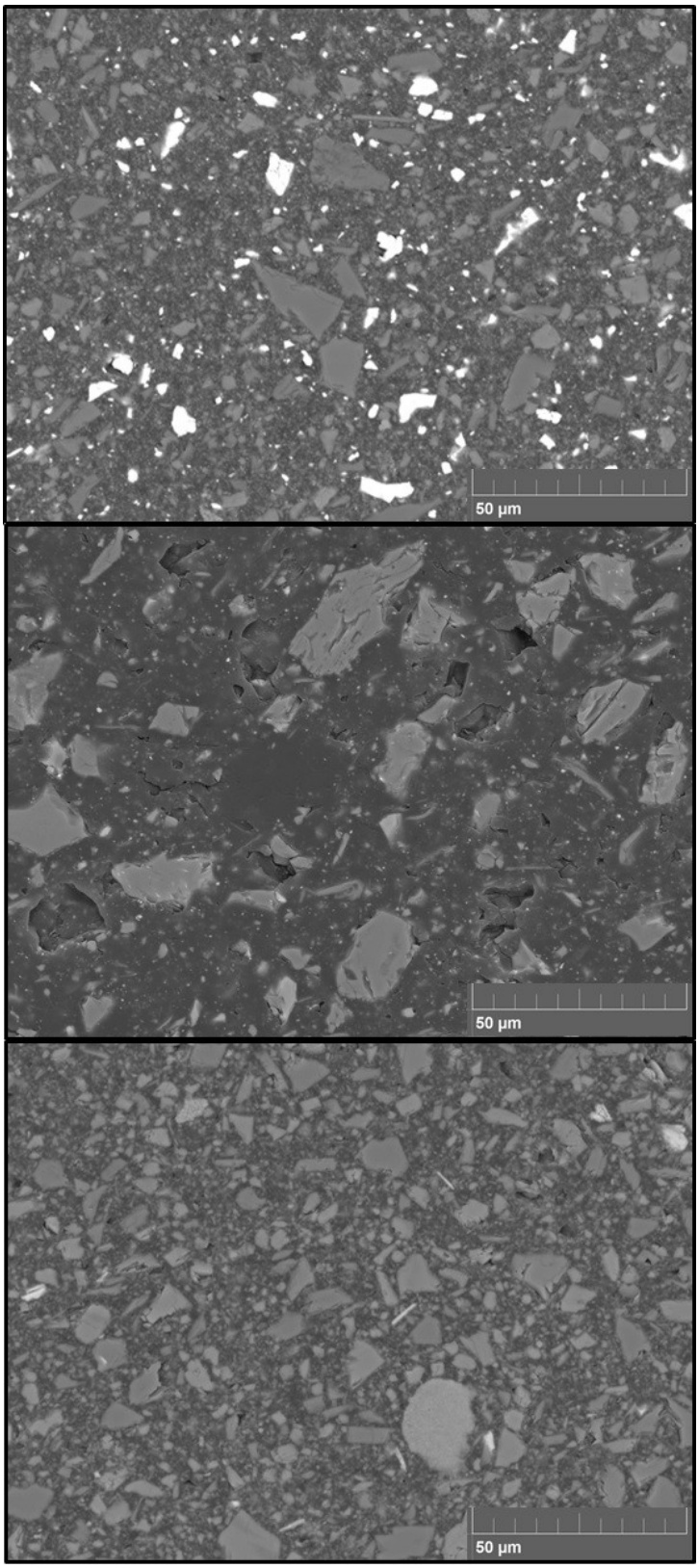

Figure 6.6 Micrographs of the cross-sectional areas of coatings A, B, and C (DFT~350µm) applied on steel substrate with a view field of 160µm, working distance of 15mm, and magnification of 2230X.

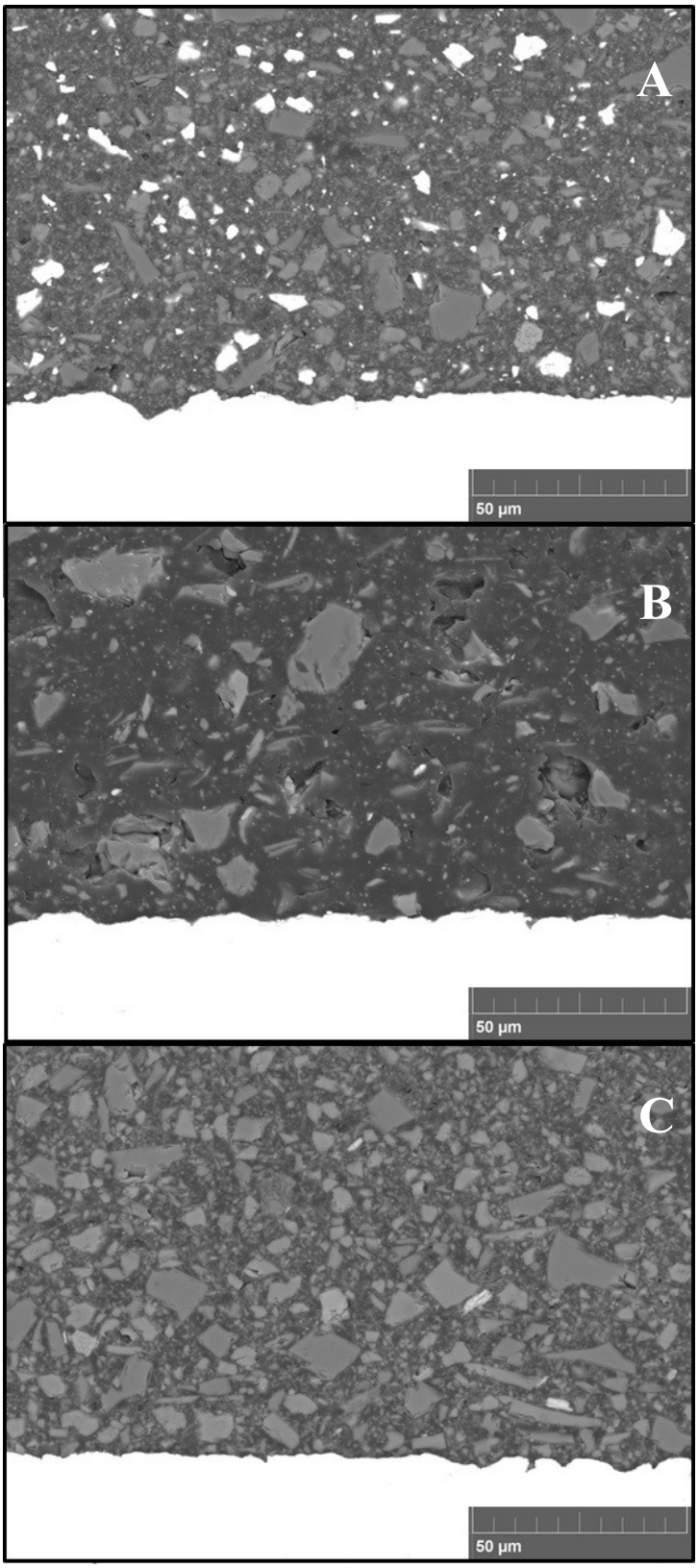

Figure 6.7 Micrographs of the coating/substrate interface of coatings A, B, and C (DFT~350µm) with a view field of 160µm, working distance of 15mm, and magnification of 2230X.

These micrographs all show that the coatings all have a heterogeneous structure consisting of pigments and fillers of different sizes dispersed in an organic matrix. In general, it was observed that coatings A and C show similar pigment and fillers morphology and size distribution. Coating B, on the other hand, shows generally bigger pigments and a lower concentration of these. The presence of bigger pigments may be associated to increased toughness in the coating, indicating that coating B may exhibit better performance compared to A and C.

The presence of pigments and fillers, and the bonds these form with the epoxy matrix, increase the stiffness of the coating. Additionally, as protective coatings form a barrier between the metal substrate and the marine environment, larger pigments present a greater obstacle for corrosion agents than smaller ones. And generally, the presence of larger pigments are associated with increase corrosion protection [33].

The presence of fillers in the coatings influences its mechanical properties, increasing the storage modulus of the coatings and providing increased thermal stability. The fillers can decrease the free space between the macromolecules, producing a decrease in the movement in the polymer chains and an increase in coating stiffness. Fillers tend to increase the heat resistance of epoxy-based coatings [50]. Additionally, fillers with low thermal expansion coefficient (CTE) reduce the shrinkage (volumetric contraction during film formation) and internal stresses in the coating [123]. The three coating systems studied are commercial products and consist of a mixture of fillers in a wide range of morphologies, as shown in **Figure 6.6**. The presence, size, and concentration of pigments (PVC) have an important bearing in the mechanical properties of the cured films. In general, the introduction of pigments into the formulation is associated with an increase of the Young's modulus [68].

The surface roughness of the substrate aids adhesion to the coating layer. The substrates were roughened before coating application with this purpose. In the interface, interlocking of the resin and the substrate is observed. (**Figure 6.7**).

The SEM samples correspond to the supported coatings prepared for dynamic mechanical analysis (**Figure 5.6**). The micro-cracks observed in the micrographs are most likely to have been induced during the grinding and polishing process, and therefore unlikely to be attributed to the coating's mechanical properties.

Figure 6.8, **Figure 6.9**, and **Figure 6.10** show the surface compositional analysis of representative samples from each coating thickness subjected to the study, of coatings A, B, and C, respectively. The compositional analysis was performed on random areas of the cross sections, such as the ones presented in **Figure 6.7**. The analysis was performed to confirm the consistency from sample to sample as well as to study the possible formation of an interphase between the substrate and coating. No significant compositional gradient was found for any of the coatings. The comparison of the results of the EDS analysis indicates that the elemental composition of the three different coatings are different.

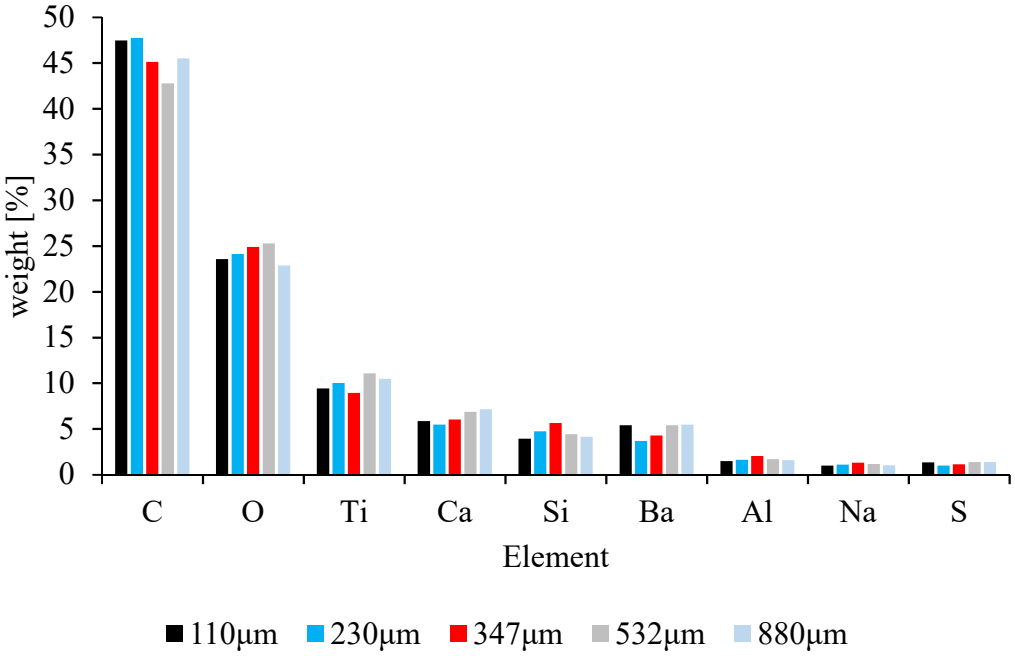

Figure 6.8 Elements detected by EDS on coating A samples.

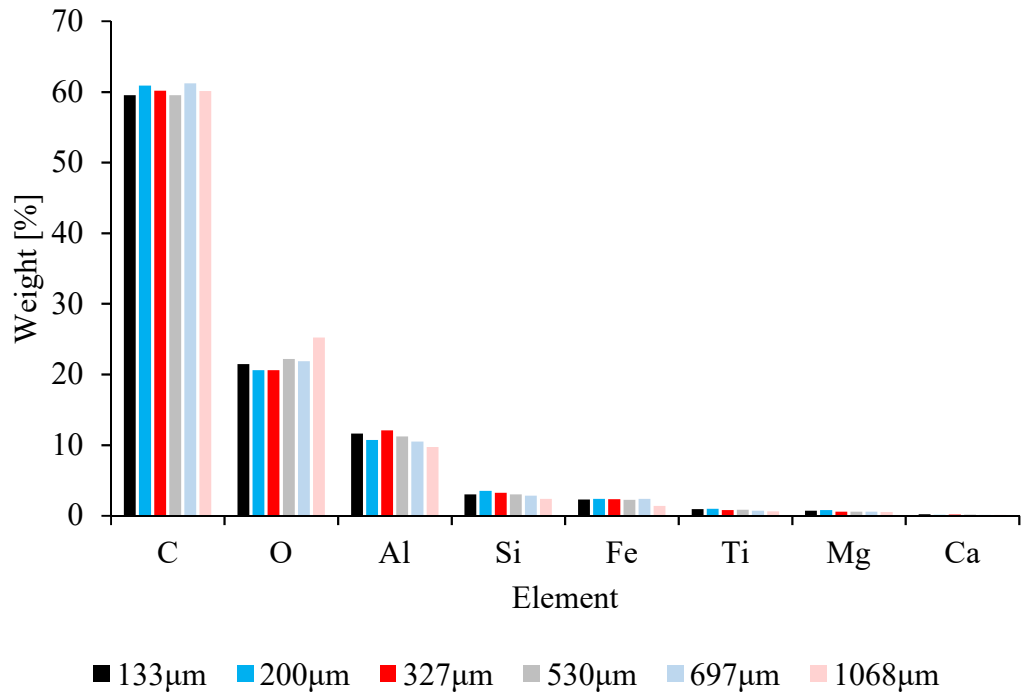

Figure 6.9 Elements detected by EDS on coating B samples.

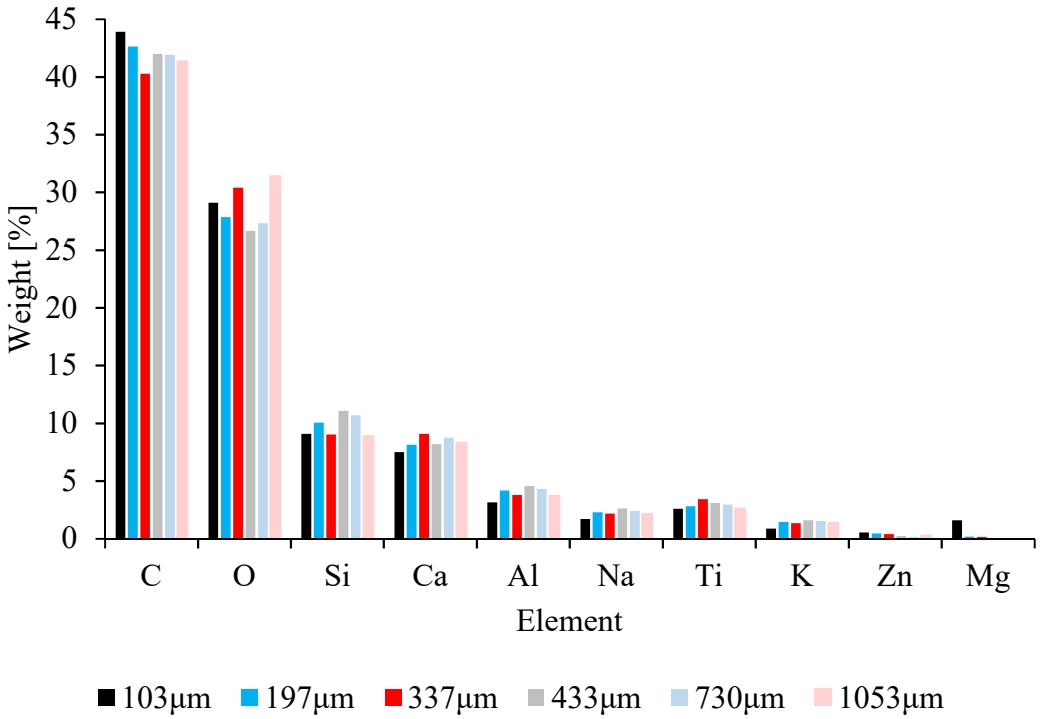

Figure 6.10 Elements detected by EDS on coating C samples.

Visual inspection of the cross-sectional micrographs in **Figure 6.11** of thick films of coatings A, B, and C show pores of varying sizes within the thickness of the coating. These pores may be related to trapped air during application. Qualitatively, the density and size of the holes appears to increase with an increase in coating thickness. No pores were detected in coatings of nominal DFT ~100μm. Defect dense areas are observed in coatings with DFT>500 μm, as shown in **Figure 6.12**.

According to BS EN ISO 29601:2011 "Paint and varnishes – corrosion protective paint systems – assessment of porosity in dry films"; porosity in paints is defined as the presence of one or more discontinuities in a coating. These discontinuities may be holes, pits, pinholes, voids, cracks, thin spots, inclusions, contamination or other flaws in the dry film that may lower the dielectric strength of the coating [148].

The density of pores within the coating cannot be quantified from SEM analysis as the cross sections are random and the analysis only detects the pores present in the particular cross section examined. Qualitatively, coatings A and B appear to show a higher pore density than coating C (**Figure 6.12**). Coating C shows resin-rich spherical areas, which appear to also have a small concentration of fillers. The change in composition, as the pores, act as stress concentrators and possible crack initiators.

The effect of porosity on the mechanical properties has been extensively studied for solid materials such as ceramics formed from sintered powders. Two models for the determination of the porosity dependent Young's modulus (E) have been studied. Phani and Niyogi (1987) [91] characterised the porosity in terms of a porosity factor P (**Figure 3.9**) and Krstic and Erickson (1985) [90] in terms of the pore volume factor V (**Figure 3.10**). Both models indicate that E decreases with an increase in porosity.

In general, the presence of pores produces a reduction in Young's modulus and an increase in elastic strain for a given stress level. The response of the material to stress will be affected by the number, volume fraction, and size of the pores [90]. The effect of pores in the mechanical properties of paint films has not been extensively studied. Porosity is also relevant in paints due to its direct relation to water vapour adsorption and permeability [93, 94].

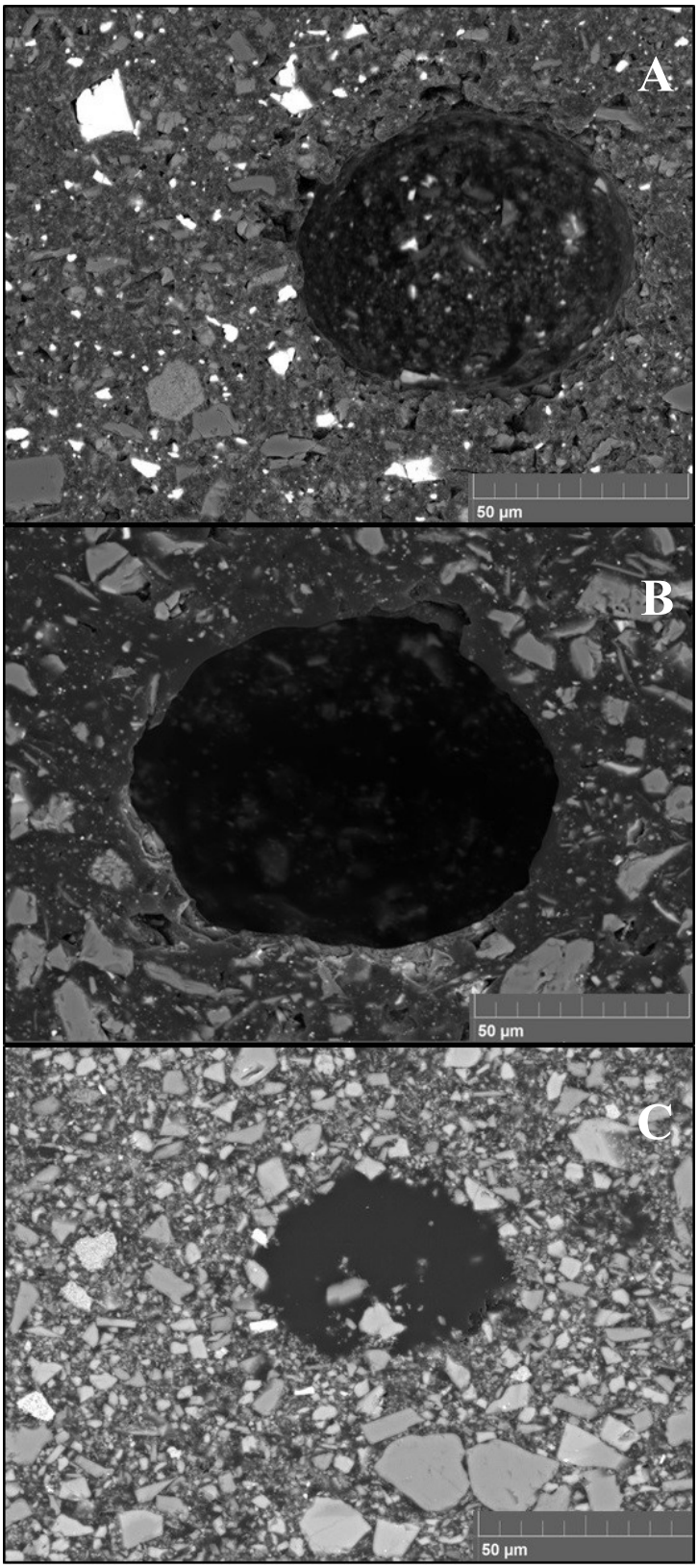

Figure 6.11 Cross sectional micrographs of pores observed in coatings A, B, and C (DFT>1000µm) with 160µm view field, working distance 15mm, and 2230X magnification

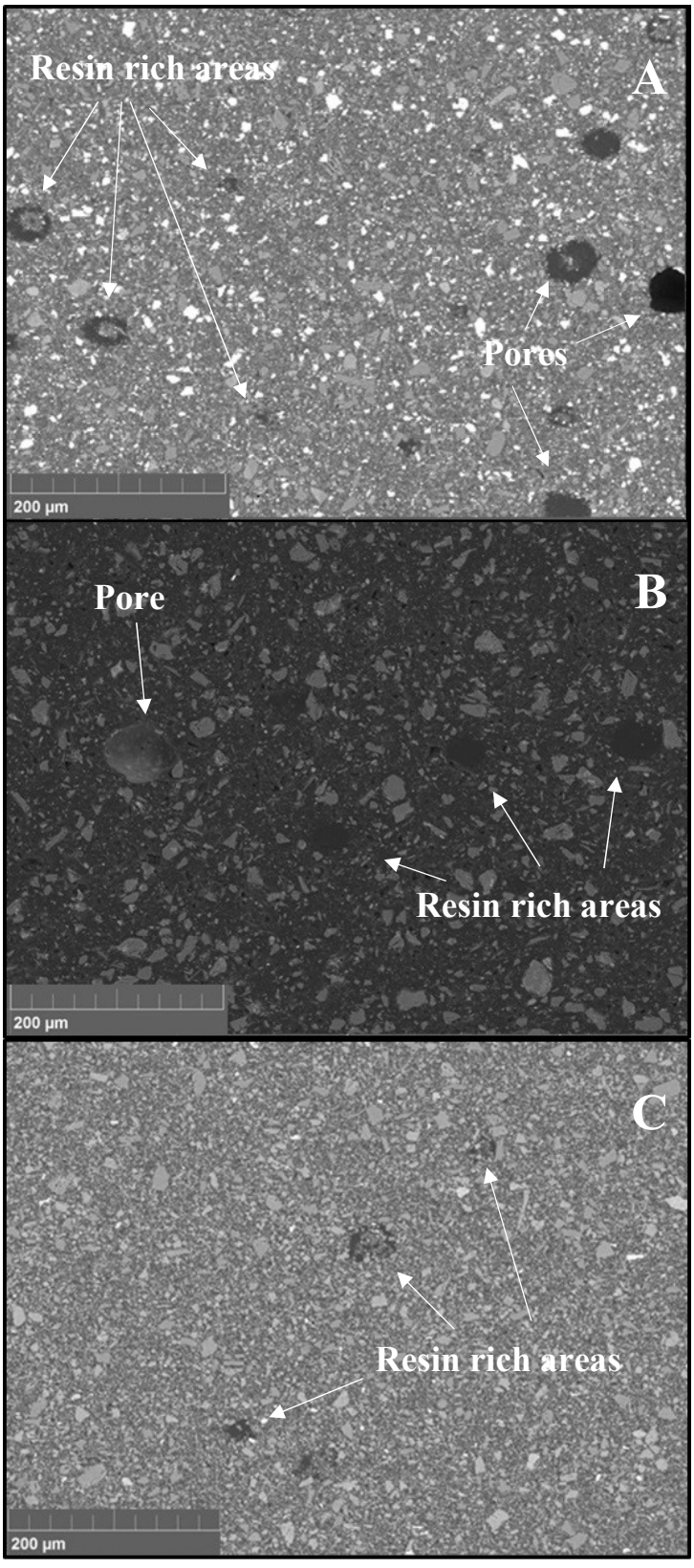

Figure 6.12 Cross sectional micrographs of pore/defect density in coatings with a view field of 640µm, working distance of 15mm, and magnification of 550X.

6.4 Solvent evaporation kinetics of solvent-borne coatings (coating A)

The solvent evaporation kinetics of solvent-borne coatings was evaluated for thick free films produced with silicone molds with dimensions presented in **Table 5.5**, and subjected to the three post cure schedules presented in **Table 5.6**. Weight loss was monitored from the first day of cure, when the samples were hard enough to handle and weigh. Between sample preparation and the first measurement, there will be solvent evaporation that is not accounted for. The cumulative weight loss experienced by the free films subjected to the different post-cure schedules was evaluated. **Figure 6.13**, **Figure 6.14**, and **Figure 6.15** present the measured total weight loss (to allow for solvent loss which is not accounted for) experienced by thick free films exposed to cure schedules 1, 2, and 3, respectively. All the weight loss may not be attributed to solvent evaporation as a small portion could be due to loss of lower molecular weight material.

Film formation is achieved by chemical reaction and solvent release; throughout the cure process the density of the samples increases whilst the volume is reduced due to the combined effect of these two processes. If the coating material is unsupported i.e. a free film, shrinkage will occur in all dimensions. On the other hand, if the material is applied onto a substrate as a coating, shrinkage will be restricted to its thickness. As the coatings cure, the density increases. The weight loss [%] was identified as an indicator of solvent loss [%].

The effect of the post-cure schedule on solvent release is evident. As **Figure 6.13** indicates, during room temperature cure of the coatings, weight loss occurs periodically until all the solvent that can be released is depleted, and the weight of the free films becomes stable. The use of a post-cure schedule of 3 days at RT and 4 days at 50°C, allows for further solvent evaporation, as it is shown in the growth of the total weight loss curve in **Figure 6.14**. This proves that when the coatings are post-cured at room temperature for 3 days at RT and then for 4 days at 50°C, further solvent loss is achieved. **Figure 6.15** demonstrates that further solvent loss can occur if the temperature is kept at 50°C for an extended period of time. Indicating that some solvent is retained within the coating when the coating is post-cured at RT for 3 days and 50°C for 4 days as used on the samples in this study. Therefore, the effect of the retained solvent in the physical and mechanical properties of the coating must be evaluated.

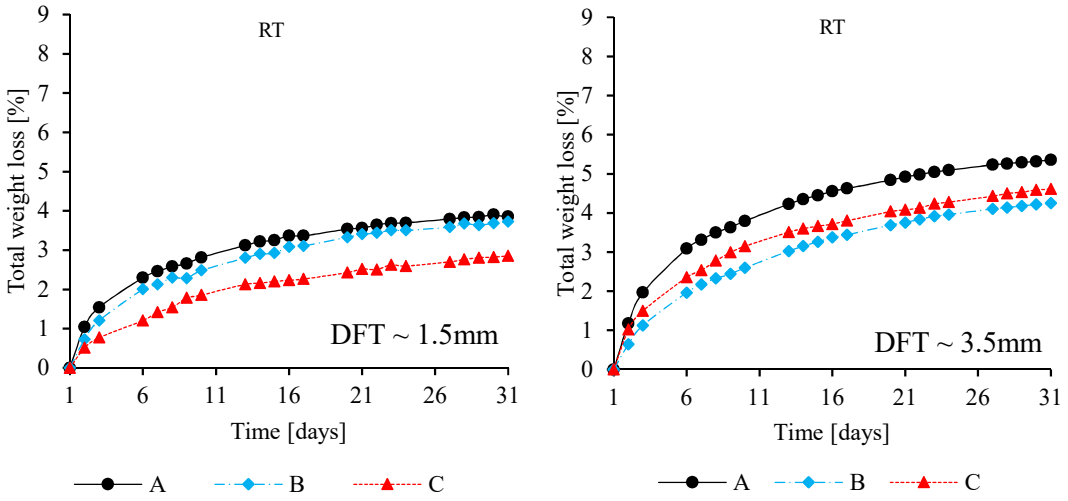

Figure 6.13 Cumulative weight loss of thick films subjected to cure schedule 1.

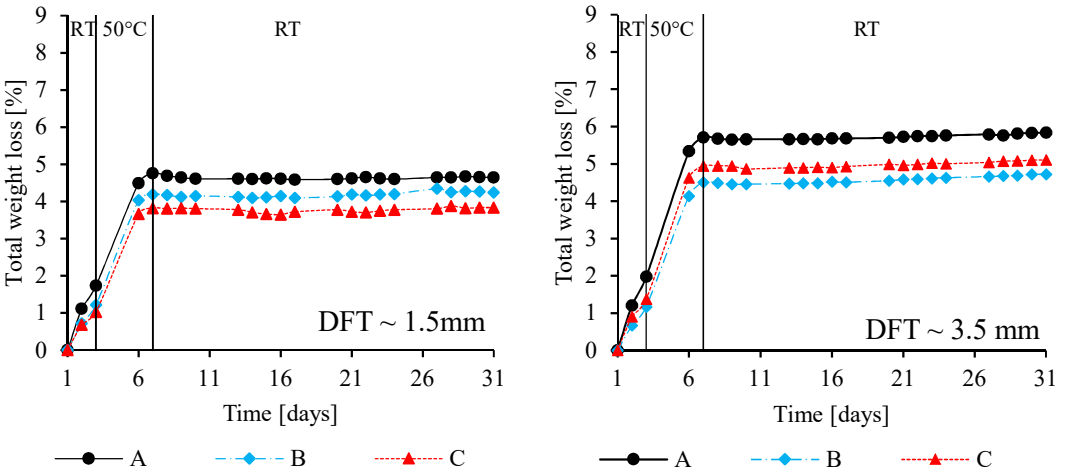

Figure 6.14 Cumulative weight loss of thick films subjected to cure schedule 2.

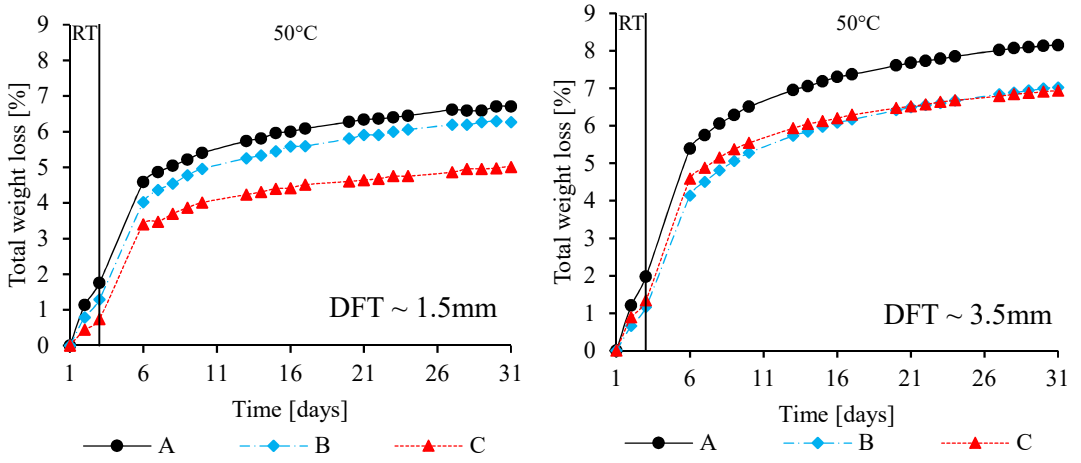

Figure 6.15 Cumulative weight loss of thick films subjected to cure schedule 3

The total weight loss experienced by the samples of all coatings is presented in **Table 6.2**. These results correspond to day 31 of the cure schedules. The weight loss is proportional to coating thickness, the thinner films produce lower solvent loss percentages than the thicker film samples. It is expected that in the first day of cure a considerable amount of solvent will evaporate, and thinner films will have a lower percentage of retained solvent to release in latter stages of curing.

Additionally, cure schedule 2 allows further solvent release and cross-linking without the need of prolonged heat treatments. The prolonged exposure to 50°C (schedule 3) produces additional solvent loss. However, this cure schedule may increase the brittleness of the materials and produce changes on their mechanical response to stress. Therefore, the mechanical response of the samples exposed to all schedules must be determined and compared.

Table 6.2 Total weigh shrinkage (%) of coatings of free films of A, B, and C after 5 weeks of cure.

Cure schedule	A		B		C	
	Thin	**Thick**	**Thin**	**Thick**	**Thin**	**Thick**
RT	3.9	5.4	3.7	4.3	2.9	4.2
RT + 4 days 50°C +RT	4.6	5.8	4.2	4.7	3.8	5.1
RT + 4 weeks 50°C	6.7	8.2	6.3	7.0	5.0	6.9

Figure 3.8 indicates that exposure to high temperatures contributes to physical ageing in the coating, which increase the elastic modulus of the coating. Physical ageing is a reversible process and the coating can relieve the stresses produced [82]. It may also reduce the coating's reliability and capacity to accommodate further hygrothermal stresses in service.

The solvent loss kinetics analysis provides an indication of the possible stress development during film formation, as coating shrinkage is proportional to internal stresses formed. As the cast free films have thicknesses above the actual application

thicknesses for offshore structures, it is expected that a much higher solvent retention [%] is experienced on the test samples compared to that experienced in real applications. The solvent evaporation rate also affects stress development in the coating, as shown in **Figure 3.4**. In convertible solvent-borne coatings, fast evaporation rates develop lower stress levels. This indicates that coating A should develop lower stresses than coating B and C.

Institutions such as ISO and ASTM have established standard tests for the performance of flexural tests in plastics. DIN EN ISO 178:2003 suggests the preferred dimensions of 3.5-4mm x 10mm x 80 mm. However, a thickness of 3.5-4mm will provide the bulk properties of the epoxy-based paint rather than the thin film properties, which have been reported as different to the bulk in several studies [67, 99, 106]. In solvent-borne coatings, it has been shown that thicker samples will show higher percentages of solvent retention. The study of the mechanical properties of the cast samples and the comparison with the properties of thin films may provide evidence of these differences.

6.5 Conclusions

Coating characteristics affect the ease of mechanical testing. An increase in coating thickness affects the thickness profile of the samples and consequently, the stress distribution during mechanical testing. Additionally, the real cross-sectional area of airless-sprayed samples differs from the one assumed by the mathematical model for the determination of the elastic modulus and residual stresses of supported coatings. Furthermore, coating thickness has no relevant effect on roughness parameters such as Ra and Rq.

SEM and EDS analysis show that the coatings have a heterogeneous composition. The coatings are composite materials composed of several types of pigments and fillers, of varying size and morphology, dispersed in an epoxy-based matrix. The analysis of the coating/substrate interface shows that there is no formation of an interphase that may affect the mechanical properties of the coatings.

Comparison of samples of different thicknesses show that the heterogeneous nature of the coating is consistent. However, an increase in coating thickness does appear to be associated with an increase in the porosity volume fraction. Studies on the effect of

porosity on the mechanical behaviour of coatings have shown that an increase in porosity produces a reduction in the elastic modulus of the coatings. The elastic modulus of materials with defects is denominated the “effective Young’s modulus”, in order to distinguish from the Young’s modulus, which is a material property independent of factors such as defects, thickness, etc. High porosity in paint is generally undesired, as it reduces the tensile strength of the coating and it may promote cracks and expose the substrate to corrosive agents.

The solvent loss kinetics results have shown that the use of a post-cure schedule allows the acceleration of the curing process (cross-linking and solvent release). Application of a post-cure has an effect on the solvent loss kinetics of the coating. Additionally, solvent loss will be dependent on coating thickness, and it is expected for the solvent retention to increase with coating thickness. Mechanical tests on thick samples subjected to the three post-cure schedules will indicate the effect of the post-cure temperature and duration on the mechanical properties of the films. Moreover, solvent evaporation rate is related to stress development. In solvent-borne convertible coatings, fast evaporating solvents are related to lower stress levels.

.

7 MECHANICAL CHARACTERISATION OF PROTECTIVE COATINGS

7.1 Introduction

In this chapter, the mechanical properties of the coatings are discussed. Epoxy-based coatings are viscoelastic materials and their behaviour ranges from an elastic solid to a viscous material, i.e. they are in glassy state below the glass transition and rubbery above it. The mechanical properties are temperature dependent and this is particularly relevant when they are placed in harsh marine environments. Therefore, the characterisation of these materials should include studies of both static and dynamic mechanical properties. In their working temperature range, epoxies are generally elastic with Young's moduli ranging from 1-3GPa, according to the literature, and brittle with breaking strains of just a few percent. Due to the versatility of these materials, and the large number of factors involved in application and curing, it is very difficult to provide typical values of properties for a given epoxy-based coating. Epoxy-based solvent-borne paints are two-component systems supplied separately, which are mixed together immediately prior to application. The ratio of the two components is crucial. Off-ratio mixing will affect the physical and mechanical properties of the final coating. Close attention was taken when mixing to avoid inconsistencies in results from batch to batch [65, 104, 149].

When convertible two-component systems are applied onto metallic substrates and cured, internal and thermal residual stresses originate within the entire organic layer. Tensile residual stresses reduce the practical adhesion and may induce cracks in the coating producing a drop in the overall performance of the paints and consequently, the corrosion protection offered by the paint to the structure it protects [98]. The stress phenomena experienced by coatings will be greatly dependent on the environment and operating conditions. In recently times, interest has been placed in changes in coating technology due to increasing concerns with energy considerations and pollution problems [65].

It is reasonable to perform mechanical tests in order to gain an understanding of the relationship between coating structure or composition and performance. To study the mechanical performance of systems consisting of a coating applied onto a metallic substrate, a bi-layer mathematical model can be assumed. The lack of extensive studies on the mechanical properties of epoxy-based paints with marine applications is considered to be associated to difficulties in the production of flat and uniform free films. Testing as supported coatings is more convenient than as free films as it facilitates production, handling, and testing (i.e. sample loading and stability during the test). Moreover, the performance of the coatings will be dependent on the interaction of the coating with the substrate. Therefore, it is considered that testing epoxy coatings applied on a substrate will produce more reliable results [65].

7.2 Adhesive strength of the coatings

The epoxy paints studied have commercial applications as anticorrosive protective coatings. Therefore, knowledge of the factors affecting the adhesion between epoxy paints and metal surfaces is of great importance [104, 140]. Good adhesion between the coating and substrate is crucial for the proper corrosion protection of metallic substrates. Epoxy coatings are known to provide excellent adhesive strength, which is said to be attributed to the formation of various bonds between the polymer groups within the paint and the steel oxide layer. Degradation of the adhesive bond may be followed by corrosion initiation and propagation [150].

The three coatings were airless sprayed onto thick mild steel plates to produce samples specified in **Table 5.3**. The substrates were degreased and blasted before paint application. In commercial applications, a metallisation layer (zinc or zinc alloy) is applied to wind turbine towers after blasting. The tests were performed at 19˚C and 49.6% relative humidity.

Adhesion of the coatings was studied in accordance with the standard method, ISO 1626-1:2007 ‘Corrosion protection of steel structures by protective paint systems – Assessment of, and acceptance criteria for, the adhesion/cohesion (fracture strength of a coating – Part1: Pull-off testing’[132]. **Figure 7.1**, **Figure 7.2**, and **Figure 7.3** provide photographic documentation of the fracture site and of the detached face of the test dollies. Four adhesion measurements were made on each sample and an

average of the results is presented in **Table 7.1**. Additionally, **Figure 7.4** shows the pull-off stress reported by the adhesion test for all coated panels.

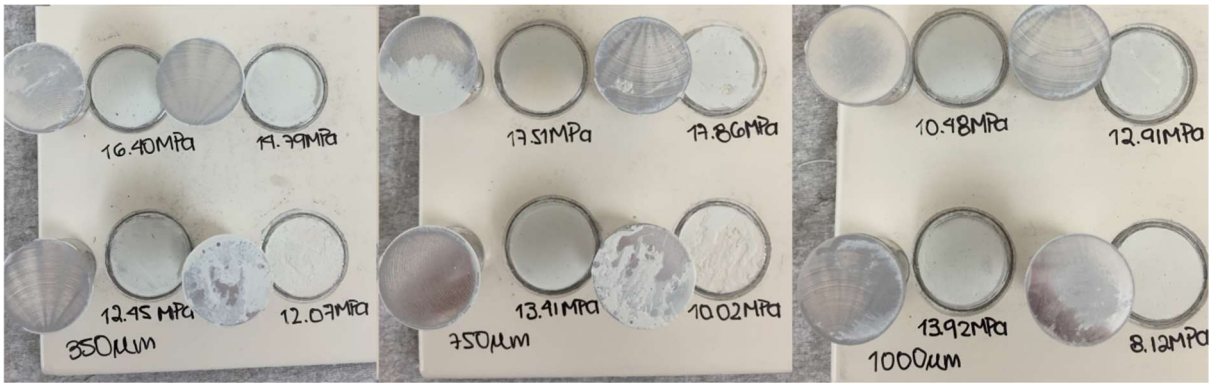

Figure 7.1 Adhesion test results on coating A

Figure 7.2 Adhesion test results on coating B

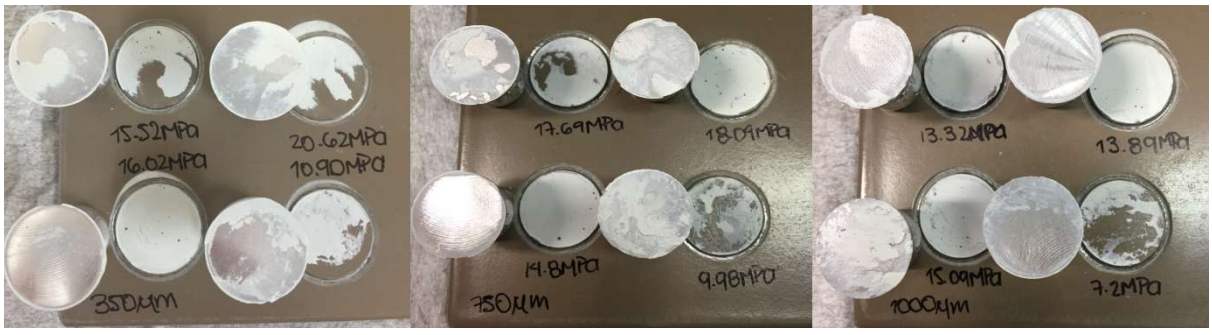

Figure 7.3 Adhesion test results on coating C

Table 7.1 Pull-off values of the coatings

Coating	DFT [µm]	Maximum stress [MPa]	Type of failure		
			Adhesive: adhesive/cylinder (Y/Z) [%]	Cohesive: adhesive (Y) [%]	Adhesive: Topcoat/adhesive (-/Y) [%]
A	365 ± 10	14 ± 2	75	25	-
	657 ± 11	15 ± 4	50	50	-
	1036 ± 54	11 ± 3	100	-	-
B	323 ± 5	13 ± 3	54	-	46
	769 ± 21	14 ± 1	32.5	22.5	45
	1099 ± 37	12 ± 1	22.5	22.5	55
C	372 ± 24	16 ± 4	56.25	16.25	27.5
	706 ± 26	15 ± 4	41.25	31.25	17.5
	983 ± 51	12 ± 4	47.5	37.5	15

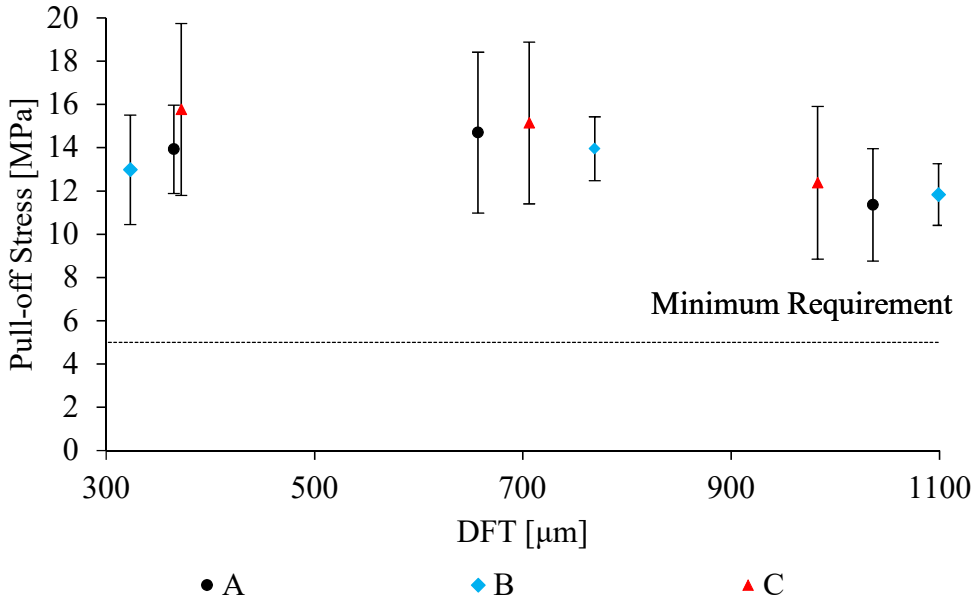

Figure 7.4 Pull-off stress reported by adhesion test for all coatings

According to the NORSOK Standard M-510 ‘Surface preparation and protective coatings’, the acceptance requirement of coating systems for the corrosion protection of offshore structures, such as transition pieces and towers, is that a minimum pull off stress of 5MPa should be achieved [54]. Therefore, the adhesion results in **Figure 7.4** show that all coatings meet the acceptance criteria and the values obtained are well above the minimum specified by the accepted industry standards. The relationship between internal stresses and tensile strength needs to be established. The influence of internal stresses is expected to be higher for thicker coating film thicknesses [150]. Commercial protective coatings are not expected to fail the pull-off tests since they generally have good adhesive properties even at high DFTs.

7.3 Dynamic mechanical properties of supported coatings

Dynamic mechanical analysis is a powerful method in the characterisation of viscoelastic coatings [151]. The storage modulus provided by the DMA is a measure of the elastic energy stored within a viscoelastic solid, which is determined by the application of an oscillatory stress and recording the strain [121]. The storage modulus may represent shear, tensile, or flexural modulus depending on the test mode selected. According to ASTM D4065 – 94 [152] and D5023 – 91 [139], the elastic modulus E’ provided by the DMA is mainly intended to be used for a comparative study since the measurements are influenced by experimental conditions and instrument compliance. Therefore, in order to account for all possible discrepancies, all experimental conditions must be reported in full [137].

Moreover, the storage or elastic modulus calculated by DMA is not precisely the same as the Young’s modulus of the classic stress-strain curve provided by static mechanical tests. In a static mechanical test, the Young’s modulus is the slope of a stress-strain curve in the elastic region. However, the modulus obtained by DMA can be approximated to Young’s modulus. There are several benefits of using a DMA over static mechanical tests, these include: the use of smaller samples (less material needed); the possibility of studying the variation of the mechanical properties with temperature without the need of an expensive temperature chamber and the execution of several tests at different temperatures, amongst others [138].

As the coatings were tested supported by a substrate, the neat substrates were also tested in order to account for their contribution to the mechanical response of the bi-layered samples. The substrates were subjected to full temperature scans in dual cantilever (DC) and 3 point (3-PT) bending modes. The thermogram of the uncoated steel substrate is presented in **Figure 7.5**. The general properties of the substrate are presented in **Table 7.2**, the elastic modulus determined by DMA was 210 ± 2GPa. The theoretical value for the elastic modulus is 210GPa (determined by universal tensile testing machine), which proves the dynamic mechanical analysis produces a result close to that obtained by static mechanical instruments [122].

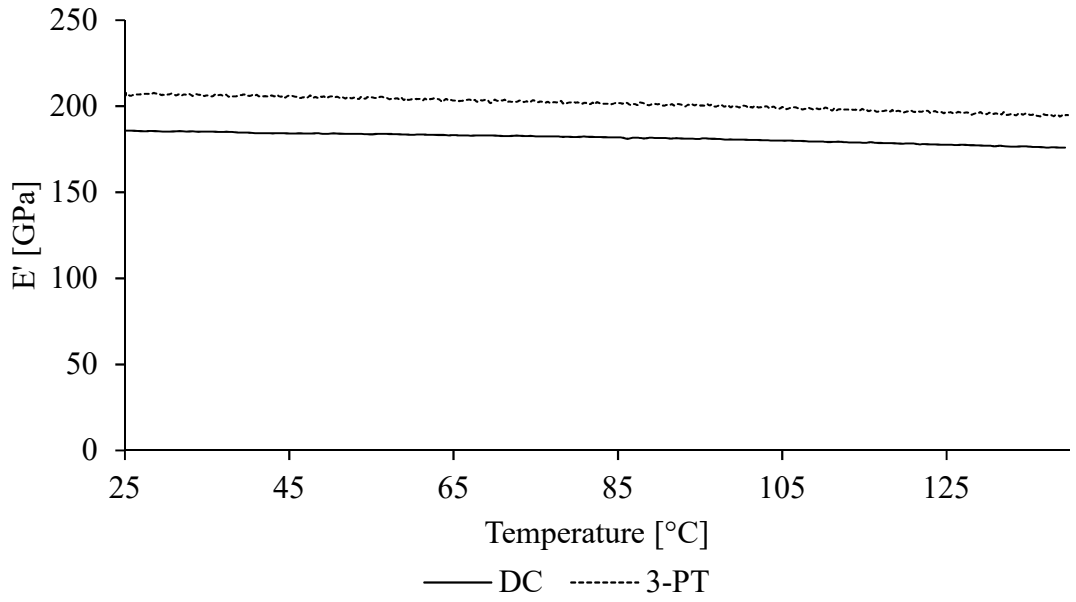

Figure 7.5 Variation of the storage modulus of the substrate with temperature

Table 7.2 Properties of the spring steel substrates determined by DMA in 3-point bending

Material	**Poisson's ratio** ν_s	E_s **[GPa]**	**Stiffness [kN/m]**
Spring steel	0.35	210 ± 2	2.03 ± 0.02

7.3.1 Temperature dependence of the mechanical properties of the coatings

In this study dynamic mechanical analysis was used to determine the mechanical behaviour of supported protective coatings and to evaluate the effect of temperature and coating thickness. To look at the temperature dependence of storage modulus, bending tests on the coated substrates were performed in dual cantilever mode. For temperature scans that extend over the glass transition region of the coatings, clamped modes are preferable over the 3-point bending mode, which is affected by sample softening during heating.

The use of dual cantilever (DC) mode, rather than single-cantilever mode, is beneficial when a comparison needs to be made to samples tested in 3-point bending mode, as the same sample size may be used. However, for very stiff and brittle samples, the single cantilever (SC) mode would be beneficial. The latter requires smaller samples (about half the size of the DC samples), and the sample curvature developed from shrinkage stresses are therefore smaller.

Figure 7.6, **Figure 7.7**, and **Figure 7.8** show the temperature dependence of the storage modulus (E') of the supported coatings, of various thicknesses, between 25 and 140˚C. Each thermogram shows the average obtained from at least three different samples. Considering that all coatings were applied on the same type of steel and that its storage modulus is relatively constant across the temperature range selected (**Figure 7.5**); any temperature related variations on the storage modulus may be attributed to the influence of the coating systems. The elastic modulus of the composite samples is relatively constant below the glass transition. In the glass transition phase, from the glassy state to the rubbery state, the molecules are excited due to an increase in temperature and the storage modulus decreases drastically. In general, the glass transition produces distinct changes in properties such as modulus, heat capacity, specific volume, among others [26]. In this region, the loss modulus and tan delta (damping parameter) exhibit a peak. After the glass transition region, the modulus decreases at a much slower rate and is stabilised. An increase in temperature should have an effect similar to a decrease in strain rate. If temperature increases, viscosity will decrease. Hence, at a fixed rate of strain, higher temperatures results in decreased stress [75].

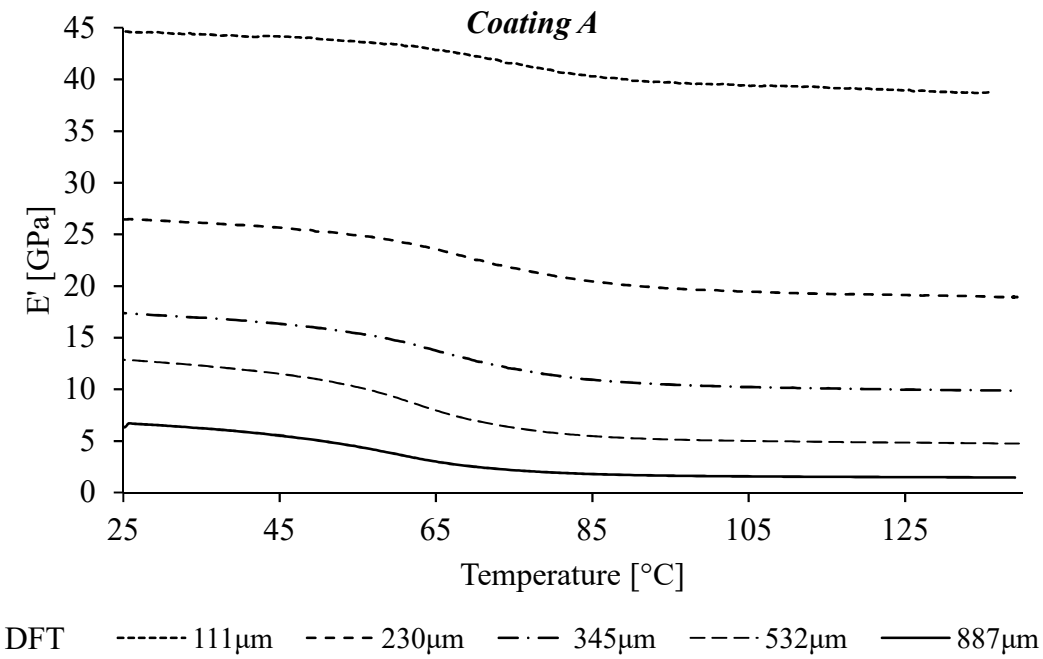

Figure 7.6 Coating A variation of the storage modulus with coating thickness

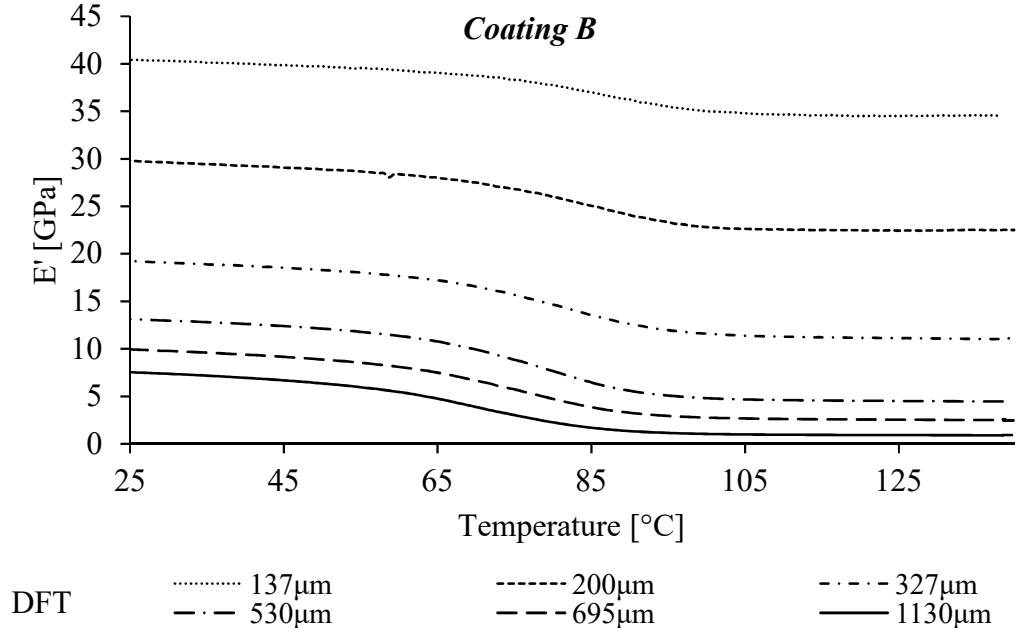

Figure 7.7 Coating B variation of the storage modulus with coating thickness

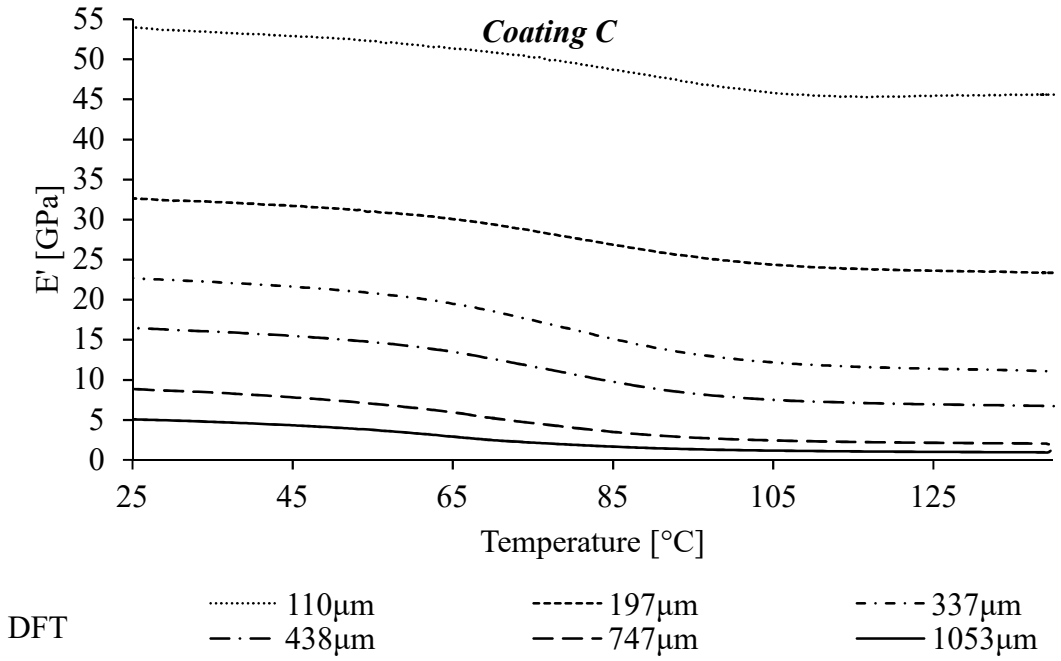

Figure 7.8 Coating C variation of the storage modulus with coating thickness

For all coatings, the composite (coating and substrate) elastic modulus decreases with an increase in coating thickness due to the increasing influence of the coating properties on the overall properties of the composite samples. In order to compare the storage modulus results of coatings A, B and C; and their dependency with coating thickness, the room temperature values (25˚C) for all coatings were plotted in terms of coating thickness and all presented in **Figure 7.9**. It shows that the storage modulus of the composite samples decreases with an increase in coating thickness. Moreover, in general terms, the storage modulus of coating C up to ~700µm is higher than the storage moduli of A and B.

Previous research has considered that the decrease in the composite modulus[7] with an increase in coating thickness as an artefact introduced by the assumption in the DMA software that the sample is homogeneous and not a composite structure. However, this behaviour has also been observed in tests performed by static mechanical tests in 3-point bending mode [100].

[7] Refers to the modulus of the composite which consists of a coating and a substrate

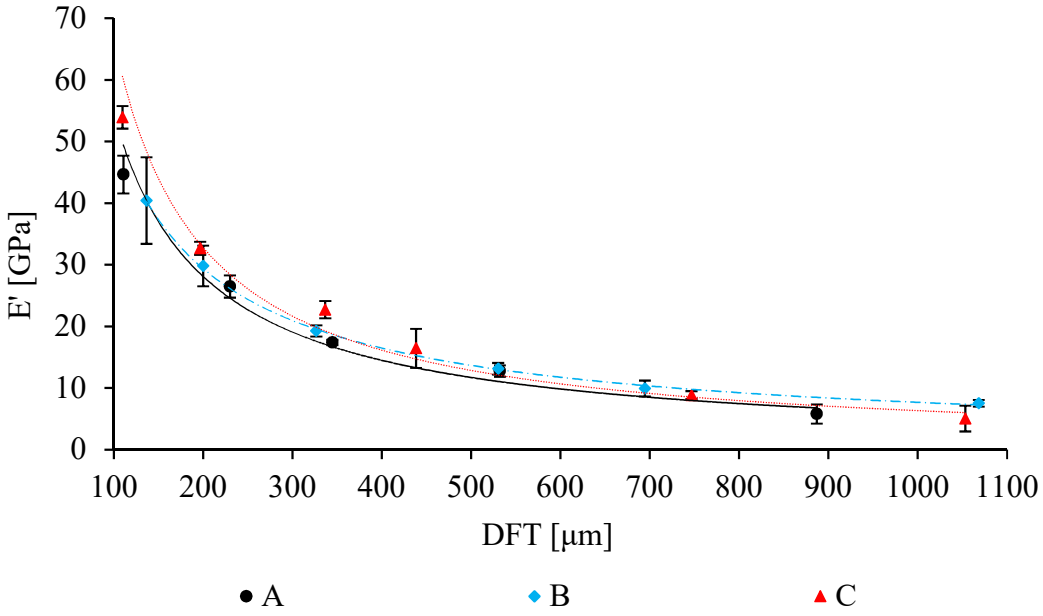

Figure 7.9 Variation of storage modulus (at RT) with coating thickness for all supported coatings

The variation of the stiffness at room temperature of the supported coatings with DFT is presented in **Figure 7.10**. The stiffness of all coatings increases with an increasing coating thickness. In the thermograms the bending stiffness decreases with increasing temperature and shows a rapid decrease in the glass transition region. For epoxy coatings, an increase in stiffness also means an increase in the brittleness of the coating and decrease in molecular mobility. As the coating is supported by a metallic substrate, the stiffness and brittleness are significantly increased by its adhesion to the substrate. This affects sample handling as the coating may flake off the substrate when an excessive DFT is applied ($DFT \geq 1100\mu m$).

The stiffness of the samples is a geometry-dependent parameter; the results obtained will depend on the sample geometry and the test mode used (i.e. dual cantilever, 3-point bending, and tension). Therefore, in order to compare the samples, they must be tested in the same mode [153].

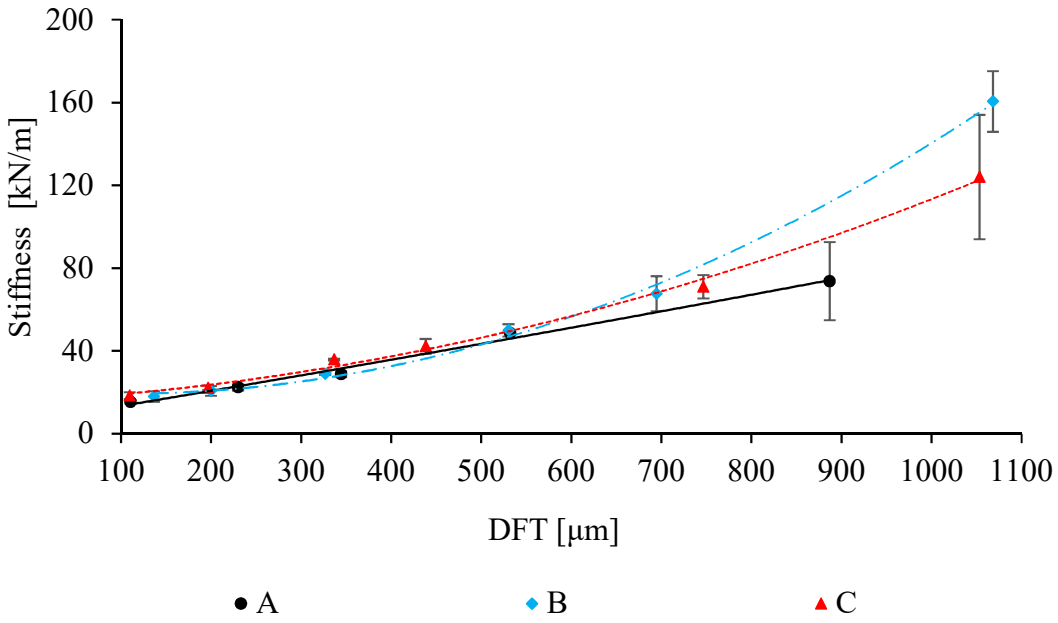

Figure 7.10 Variation of the stiffness S (at RT) with coating thickness for all supported coatings

The glass transition temperature is determined by locating the peak on the damping ($\tan \delta$) curve on the temperature scans. Alternatively, it may be determined by locating the peak of the loss modulus curve or by analysis of the storage modulus curve. After selecting a method for the determination of the T_g, it must be kept constant throughout the analysis. The values of T_g obtained by the $\tan \delta$ curves are generally larger than the ones obtained by the loss modulus and storage modulus curve. **Figure 7.11** presents the variation of the T_g with coating thickness for all coating types; it can be observed how an increase in coating thickness produces a decrease in glass transition temperature.

Given the wide variety of aspects affecting the mechanical and physical properties of coatings, the variation of T_g with coating thickness can be attributed to a combination of factors. The glass transition temperature range is related to the structure and mobility of the polymer macromolecules. The T_g of each coating will depend on the formulation of the coating and the post-cure schedule applied on the coating. As the coating cures, the glass transition temperature of the coatings increases with the degree of crosslinking and consequently, the reduction of chain mobility and increase of stiffness [68, 100].

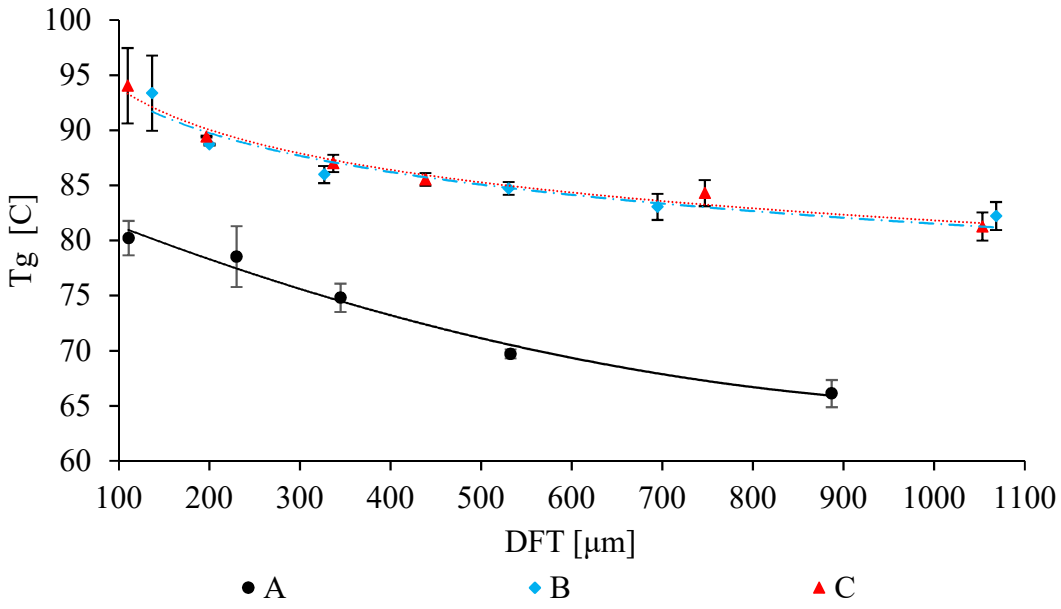

Figure 7.11 Glass transition temperature dependence on coating thickness for all supported coatings

An increase in coating thickness is also associated both with an increase in the level of retained solvent and porosity (size of pores and density). Both pores and solvent retention result in a decrease in the glass transition temperature and tensile strength of the coatings. Film formation of convertible solvent-borne coatings is achieved by chemical reaction and solvent release. Both these processes occur progressively throughout the coating's life. At any given time, the coating will have a given percentage of retained solvent within it. As indicated in **Table 6.2**, solvent retention increases with increasing coating thickness. The retained solvent acts as a plasticiser decreasing the tensile strength and glass transition temperature of the coatings. Similarly, moisture absorption also plasticises the coating, reducing the T_g and tensile strength. This is of particular importance for coatings used in marine corrosion protection [18].

For supported coatings, as the coatings are cured on metallic substrates, the solvent release is restricted to one surface. When compared to a free film, in which solvent release is achieved through two large surfaces, solvent evaporation may be reduced or slowed down and further affect the final properties of the film. Also, as the substrate limits the coating's movement during the glass transition, its presence may affect the results. A comparative analysis of free films and supported coatings based on the glass

transition temperature may provide further understanding with respect to solvent retention.

7.3.2 Flexural properties of supported coatings at room temperature

The mechanical response of the supported coatings in 3-point bending mode was calculated. The coated substrates are curved due to the internal stresses in the coating. In a temperature scan, the softening of the sample produces stress relaxation and the curvature is reduced (δ_{max} decreases and R increases, see section 4.4) during heating, consequently the mid-span of the stage (**Figure 5.8**) loses contact with the centre of the sample incapacitating the application of a force and ultimately rendering the results beyond T_g invalid. Additionally, the 3-point bending mode does not clamp the samples to restraint their motion when heated. In order to obtain results that would not be affected by sample softening, the temperature range used in the 3-point bending tests was restricted from RT to 45 ˚C; and only the room temperature results are considered. This indicates that the DMA results in 3-point bending have limitations in terms of sample thickness and stiffness.

The storage modulus at RT (25°C) of the supported coatings determined by DMA in 3-PT bending is presented in **Figure 7.12**. The elastic modulus of the composite samples decreases with increasing coating thickness. **Figure 7.13** shows the bending stiffness of the supported coatings and its variation with coating thickness.

With the exception of samples of DFT ~ 100µm, coating systems B and C generally show higher storage modulus and stiffness than coating A. Note that the stiffness of A increases less than for coating systems B and C. Yet storage modulus decrease is essentially the same/constant across A, B, and C at all DFTs. It is also evident in **Figure 7.11** that coating systems B and C show higher T_g than coating A for all DFTs. There is a clear relationship between the storage modulus, coating stiffness and glass transition temperature: coatings with higher storage modulus and stiffness also show higher T_g.

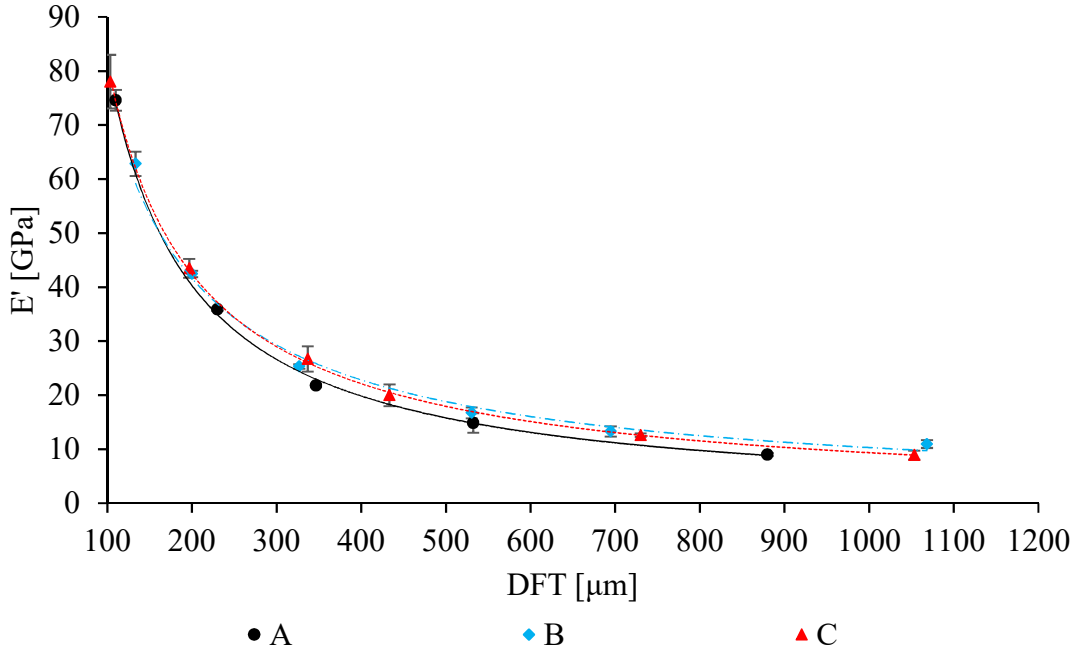

Figure 7.12 Variation of the storage modulus (at RT) in 3-point bending with coating thickness for all supported coatings

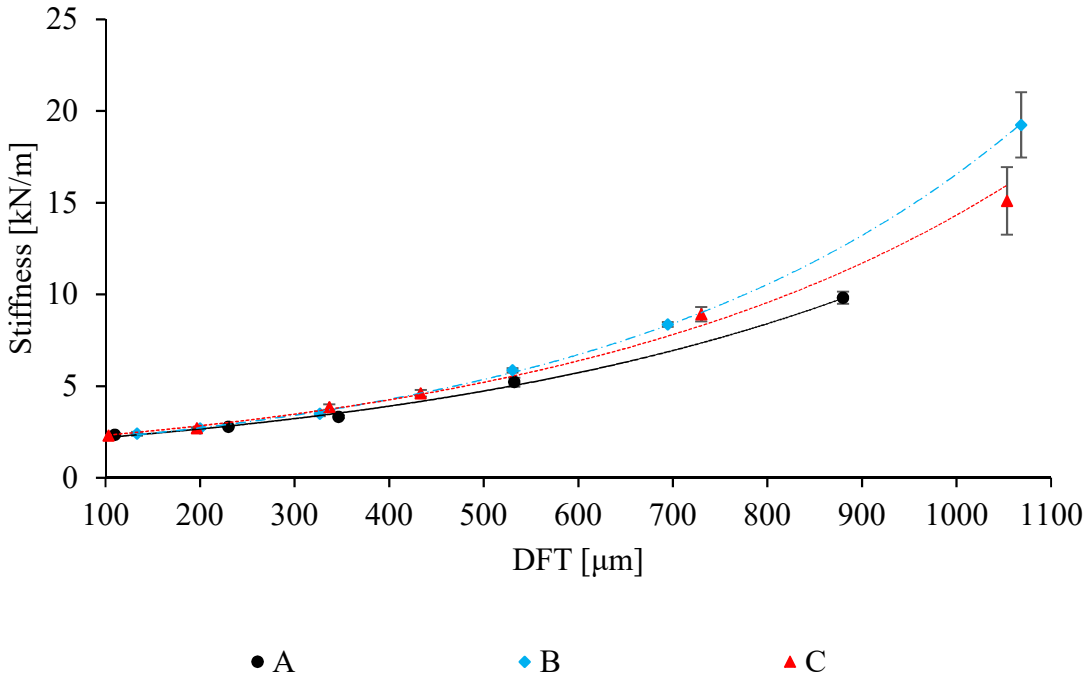

Figure 7.13 Variation of the stiffness S (at RT) in 3-point bending with coating thickness for all supported coatings

The elastic modulus results are consistent with those obtained by dual cantilever and presented in **Figure 7.9**. However, due to the clamping effect, dual cantilever produces lower modulus results than 3-point bending mode. Deng, Hou and Ye (2007) compared the clamping effect of single cantilever, dual cantilever, and 3-point bending mode and showed the discrepancies between the three modes. In this study it was established that the three modes produce notably different results, however the properties obtained from each mode varies with temperature in the same manner. It was also established that the T_g determined by each method is almost the same [135]. This premise may be used to produce a more complete dynamic mechanical analysis of the coatings. Thus, the storage modulus of the coatings may be determined at room temperature by 3-point bending and extrapolated to fit the behaviour of the same sample in dual cantilever mode over a wider range of temperatures.

The latter may be done by selecting a representative sample thickness and extrapolating the difference between the two moduli for all coating thicknesses. However, as the mechanical response of the material is strongly dependent on coating thickness, the difference between the modulus obtained by each mode was determined for all coating thicknesses. Given that the same sample is used to determine the storage modulus at room temperature in 3-point bending, and the temperature dependence of the storage modulus (25 to 140°C) in dual cantilever mode; the difference between both moduli may be determined for each coating thickness. In the present study, the following equation is suggested for the determination of the difference between the modulus obtained by the two bending modes:

$$\Delta E' = E'_{3PT} - E'_{DC} \qquad \textbf{Equation 7.1}$$

Where:

$\Delta E'$ = difference between the modulus obtained by 3-point bending and dual cantilever

E'_{3PT} = storage modulus determined by 3-point bending mode; and

E'_{DC} = storage modulus determined by dual cantilever mode.

Figure 7.14 presents $\Delta E'$ obtained from solving **Equation 7.1** with data obtained from the 3-point bending (**Figure 7.12**) and dual cantilever (**Figure 7.9**) tests. It can be observed that the effect of the clamps on the material is neither constant nor independent of coating thickness. The effect of the clamps on the results is especially relevant for low DFT samples (low stiffness samples). However, this effect is lower for high DFT samples (high stiffness samples). $\Delta E'$ decreases with an increase in DFT and for $DFT \geq 350\mu m$ the clamping effect is relatively constant. It is also evident that there is a higher calculated error associated with low DFT samples of coatings B and C.

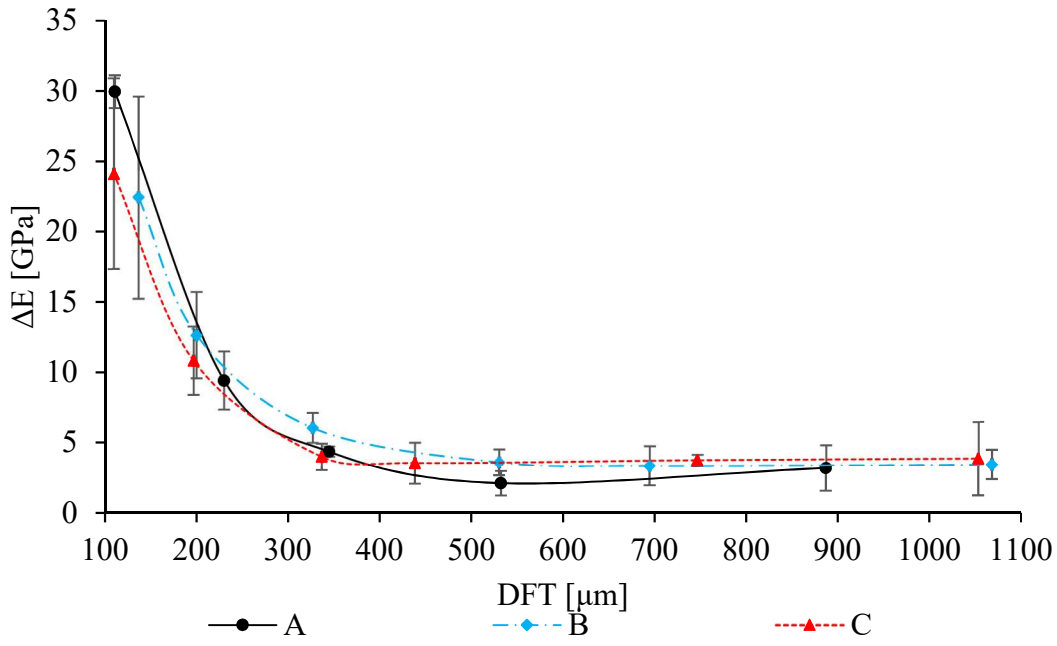

Figure 7.14 Difference between the moduli (at RT) obtained by 3-point bending and dual cantilever mode

The glass transition, storage modulus and stiffness are closely related; an increase in coating thickness produces a decrease in glass transition temperature, storage modulus and an increase in coating stiffness. **Table 7.3** summaries DFT, elastic modulus (E') and bending stiffness (BS) at room temperature, and the glass transition temperature of all supported coatings.

Table 7.3 Summary of dynamic mechanical properties of supported coatings.

Coating	DFT [µm]	T_g [°C]	DC		3-PT	
			E' [GPa]	S [kN/m]	E' [GPa]	S [kN/m]
A	111 ± 2	80 ± 2	45 ± 3	15.4 ± 0.8	75 ± 2	2.33 ± 0.06
	230	79 ± 3	26 ± 2	22 ± 2	35.9 ± 0.3	2.78 ± 0.02
	345 ± 7	75 ± 1	17.4 ± 0.4	29 ± 1	21.8 ± 0.3	3.32 ± 0.07
	532 ± 18	70 ± 0.4	12.8 ± 0.9	48.6 ± 0.4	15 ± 2	5.2 ± 0.2
	887 ± 6	66 ± 1	6 ± 2	74 ± 19	9.0 ± 0.3	9.8 ± 0.3
B	137 ± 6	93 ± 1	40 ± 7	18 ± 3	63 ± 2	2.4 ± 0.1
	200	89 ± 3	30 ±3	21 ± 2	42.4 ± 0.6	2.69 ± 0.04
	327 ± 6	86 ± 2	19.3 ±0.9	29.0 ± 0.5	25.3 ± 0.4	3.5 ± 0.1
	530 ± 11	84.7 ± 0.3	13.1 ± 0.9	50 ± 3	17 ± 1	5.9 ± 0.1
	695 ± 18	83 ± 1	10 ± 1	68 ± 8	13.3 ± 0.9	8.4 ± 0.1
	1068 ± 26	82 ± 1	7.5 ± 0.6	161 ± 15	11.0 ± 0.7	19 ± 2
C	110 ± 10	94 ± 3	54 ± 2	18 ± 2	78 ± 5	2.30 ± 0.04
	197 ± 6	89.42 ± 0.08	33 ± 1	22 ± 1	43 ± 2	2.70 ± 0.05
	337 ± 12	87.0 ± 0.8	23 ± 1	35.8 ±0.4	27 ± 2	3.9 ± 0.1
	438 ± 25	85.5 ± 0.6	16 ± 3	42 ± 4	20 ± 2	4.6 ± 0.2
	747 ± 9	84 ± 1	8.8 ± 0.7	71 ± 6	12.6 ± 0.3	8.9 ± 0.4
	1053 ± 35	81 ± 1	5 ± 2	124 ± 30	8.9 ± 0.8	15.1 ± 2

7.4 Young's modulus of supported coatings

Young's modulus, or modulus of elasticity, is considered one of the most important mechanical properties of a coating, it characterises the strength of the material and influences the functionality of the composite system constituted by paint and steel substrate [67]. The Young's modulus is an inherent material property and it is considered to be independent of geometrical factors such as thickness.

However, when a material, such as paint, which is composed of several components which progressively change with the degree of cure (binder and hardener) and the level of retained solvent over time, factors such as film thickness, cure schedule, solvent retention, porosity and defects all affect the final properties of the material. Therefore, the Young's modulus of the supported coatings determined by composite beam stresses analysis is denominated 'effective Young's modulus' to indicate that it's the modulus affected by a wide group of factors and their interactions with each other.

The effective Young's modulus of the supported coatings was determined with the equation for the flexural rigidity of bi-layered beams (**Equation 4.37**). The mathematical model assumes that the coating and the substrate exhibit the same deformation. The variation of the effective Young's modulus with coating thickness for all coatings (A, B, and C) is presented in **Figure 7.15**.

The effective Young's moduli of the coatings decrease with an increase in DFT and for higher DFTs, the modulus seems to be converging to a constant value. This behaviour has also been observed by Roche and Bouchet in a series of studies on thin solvent-free epoxy coatings applied onto aluminium substrates and post-cured above T_g. The researchers considered the organic layer in the vicinity of the substrate surface as an interphase with gradients of residual stresses and Young's modulus. This phenomenon has been attributed to structural rearrangement, intermolecular and inter-atomic interactions, and diffusion phenomena where some new chemical species and/or network may be formed. **Figure 7.16** shows the vicinity of the substrate's surface subjected to study by Bouchet, Roche, and Jacquelin. Bouchet proposed that organo-metallic crystal growth in the vicinity of the surface of the substrate is parallel to it, leading to a significant increase of the longitudinal Young's modulus determined by the mechanical tests [71]. The study proposes that the coating's Young's moduli

reach the 'bulk' properties for coatings at thicknesses higher than 200-250µm, suggesting that as the thickness of the interphase formed between the coating and the metal substrate [71, 96-98].

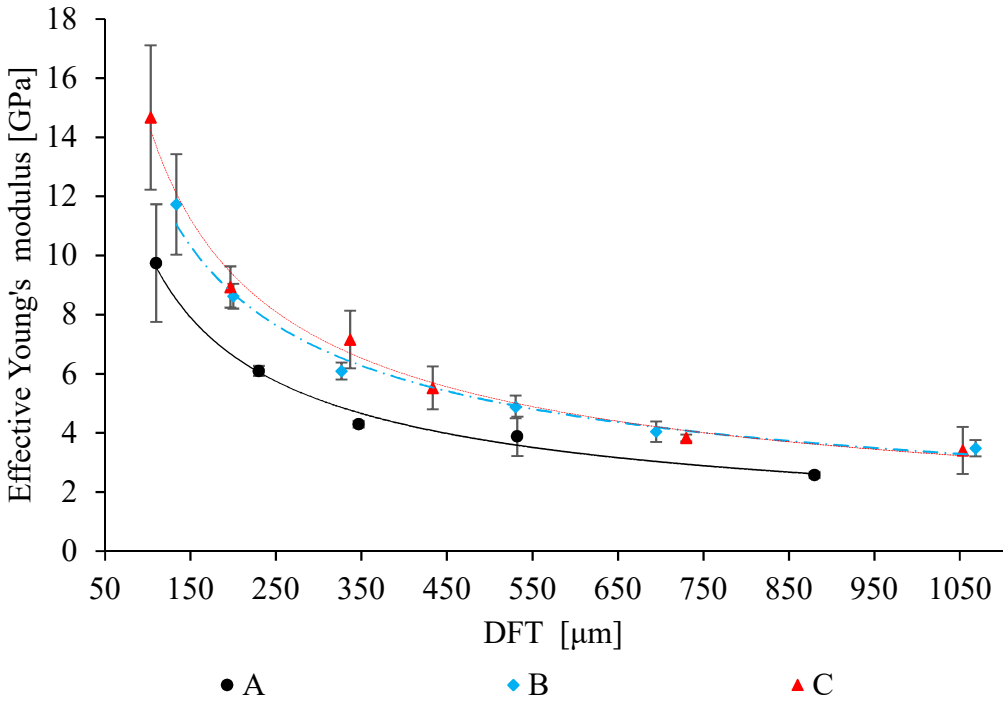

Figure 7.15 Variation of Young's modulus of the coatings with coating thickness at RT

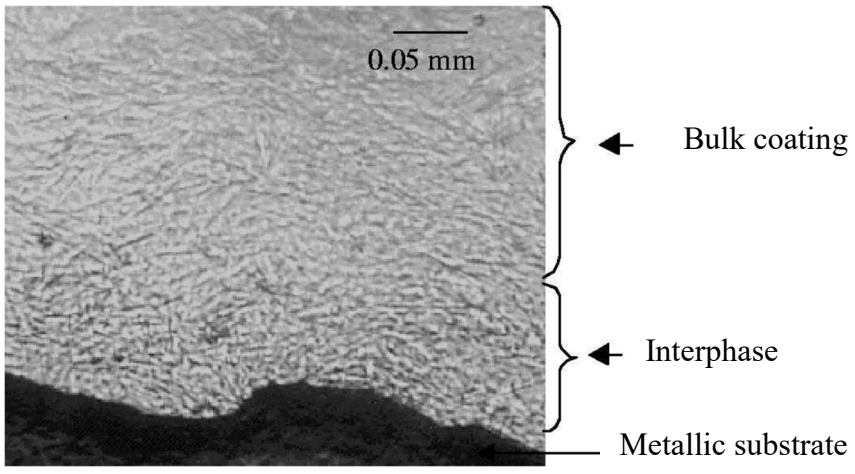

Figure 7.16 Optical microscopic observation of the interfacial region of a diamine-aluminum system [71]

Coatings A, B, and C are solvent-borne epoxy coatings, and post cured below the glass transition temperature. In coatings post-cured below T_g, a portion of the solvent may

be retained in the samples and the presence of trapped solvent plays an important role in the mechanical properties of the coatings. In chapter 6 the solvent evaporation kinetics was evaluated. It was established that exposure of the coatings to 50°C for 4 weeks produced additional solvent evaporation for all coatings, showing that the samples cured for 3 days at RT followed by 4 days at 50°C still have a percentage of retained solvent after 5 weeks of cure. Overall, solvent retention was found to increase with increasing coating thickness (**Table 6.2**). The previous statement indicates that very thin samples may have very low levels of retained solvent or even be solvent-free. Additionally, the retained solvent is not thought to be evenly distributed, and a profile is formed within the coating with a minimal concentration in the air-coating interface. Further work is needed to clarify this theory.

Solvents are added to paint to dissolve the resin component, reduce the viscosity of the paint and facilitate coating application. Solvents are volatile liquids and evaporate during the curing process. The evaporation of the solvent during and after curing contributes to the volumetric contraction (shrinkage) and consequently produces internal stresses in the films. Moreover, the solvent must have a the right evaporation rate and be capable of depositing a film with optimum characteristics [25, 42].

The retained solvent behaves as a plasticiser. The solvent acts as a lubricant easing the movement of the polymer chains and increasing the flexibility of the polymers. The presence of solvent flexible chains, which have high mobility even in the glassy state, increases the free volume in the film. Thus, the presence of retained solvent lowers the T_g, tensile strength and elastic modulus of the coatings [25, 26, 31, 42]. An equivalent effect is observed with porosity. An increase in porosity is associated with the reduction of the effective Young's modulus of the coating and an increase of the elastic strain for a given stress level, i.e. the tensile strength of the material is reduced [90]. Therefore, an increase in solvent retention and porosity associated with an increase in coating thickness also produces a reduction in the effective Young's modulus of the coating.

The thickness-dependent effective Young's modulus could also be attributed to structural changes of the cross-linked structure across the thickness of the coating. An important aspect of coatings is the effect that coating thickness has on coating stiffness.

As shown in **Figure 7.13**, sample stiffness increases with an increase of coating thickness.

An increase in pore density with an increase in coating thickness has been observed by Dolgov (2004) and linked to the decrease of the effective Young's modulus with an increase in coating thickness. Dolgov studied the elastic modulus of powder coatings, which are solvent-free, and concluded that a coating's elastic modulus is inherently different to that of the material in the bulk form. Therefore, the modulus must be determined for each thickness of interest. The author stated that a coating's elastic modulus generally depends on the application conditions, substrate characteristics and surface treatment, type of loading, composition and state of the paint, application method, and the substrate's surface treatments [67].

Dynamic mechanical analysis is useful for performing comparative studies; it is known that there are small discrepancies between the temperature-dependent elastic moduli measured by DMA and the ones measured with a static mechanical testing machine. From all the test modes used in DMA, 3-point bending mode is considered to be the most suitable for measuring the elastic modulus of supported materials. This bending mode eliminates the clamping effect, present on the single cantilever and dual cantilever modes, and serves as an analogous method to static mechanical 3-point bending tests [135].

The present analysis was developed considering room temperature properties. However, depending on the application, the mechanical response of the material at any other temperature can be used to determine the Young's modulus of the material at the given temperature, as long as the material is elastic at that temperature.

Static 3-point bending tests on coated substrates has long been performed in order to determine the mechanical properties of coatings [106, 107, 115, 124]. This approach has been found reliable to determine the Young's modulus; and the results have been used to determine the residual stresses of coatings. In many cases however, the variation of these properties with temperature cannot be readily determined. In static mechanical testing, the influence of the temperature can be obtained by the addition of an expensive temperature chamber, perform static tests at several temperatures, and finally the construction of a curve connecting the data points to predict the behaviour

of the mechanical properties with temperature. This lengthy and costly process entails long man-hours and the use of a large number of samples.

7.5 Internal stresses of supported coatings

The development of residual stresses in organic coatings cannot be overlooked. Coating reliability and performance can be directly affected by the accumulation of residual stresses; with delamination and cracking as possible outcomes. When the stresses exceed the cohesive and adhesive strength of the film, they may produce cohesive or adhesive failure. In a supported coating, such as the ones subjected to this study, the residual stresses are particularly detrimental at the edges of the samples, as they cannot cancel each other. Residual stresses are affected by coating characteristics (composition, elastic modulus), film formation processes (chemical reaction and solvent release), thermal history, pigment characteristics (type, concentration and morphology), DFT, defects, substrate characteristics (type, thickness, surface treatments), etc. [63, 72, 107, 154].

According to Lange, Toll, and Månson (1995), the build-up of stress over time is influenced greatly by the change of volume and the stiffness of both the coating and the substrate [76]. Solvent-borne epoxy-based coatings solidify through two mechanisms: (1) solvent evaporation and (2) chemical curing. The two mechanisms produce shrinkage or contraction of the films and build-up stiffness. Hence, the residual stresses produced within the coating are tensile in nature. Additionally, if the coating is cured at elevated temperatures then thermal stresses and/or stress relaxation will be experienced. Generally, tensile stresses are developed in films due to film formation or exposure to low temperature. Conversely, compressive stresses develop when a coating expands as a response to high humidity or elevated temperatures. The cumulative nature of stresses, however, indicate that compressive and tensile stresses may compensate each other, thus reducing the overall stress stored within the coating. Therefore, the application of a heat treatment (post-cure schedule) may result in stress relaxation and relieve residual stresses produced during film formation [72, 76, 155].

With knowledge of the Young's modulus of the coatings, and the associated maximum beam deflection (**Figure 7.17**) and radius of curvature (**Figure 7.18**) of the supported coatings, the residual stresses may be determined. The maximum deflection (δ_{max}) of

the curved beam increases with an increase in DFT. Similarly, the radius of curvature (R) decreases with an increase in DFT. R is inversely proportional to the residual internal stresses developed. The maximum beam deflection and radius of curvature are related to the ratio of the coating thickness to substrate thickness. When a coating is applied to one side of a thin substrate, the stresses in the coating due to film formation processes cause the coating/substrate system to bend to restore moment equilibrium. The magnitude of the curvature is directly related to the stress as indicated in **Equation 4.59** [78].

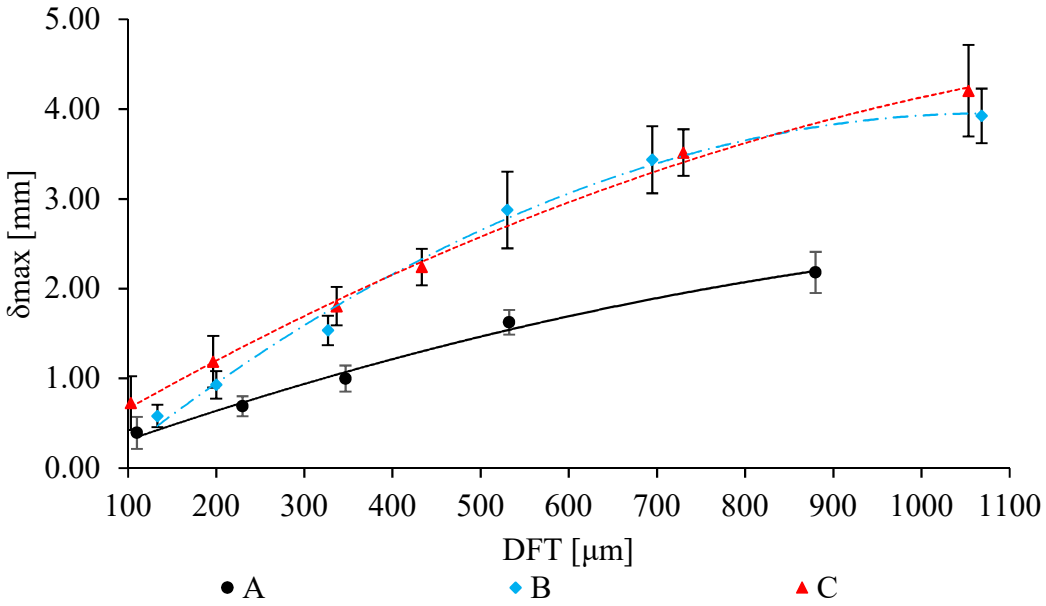

Figure 7.17 Maximum deflection of the bi-layer beams

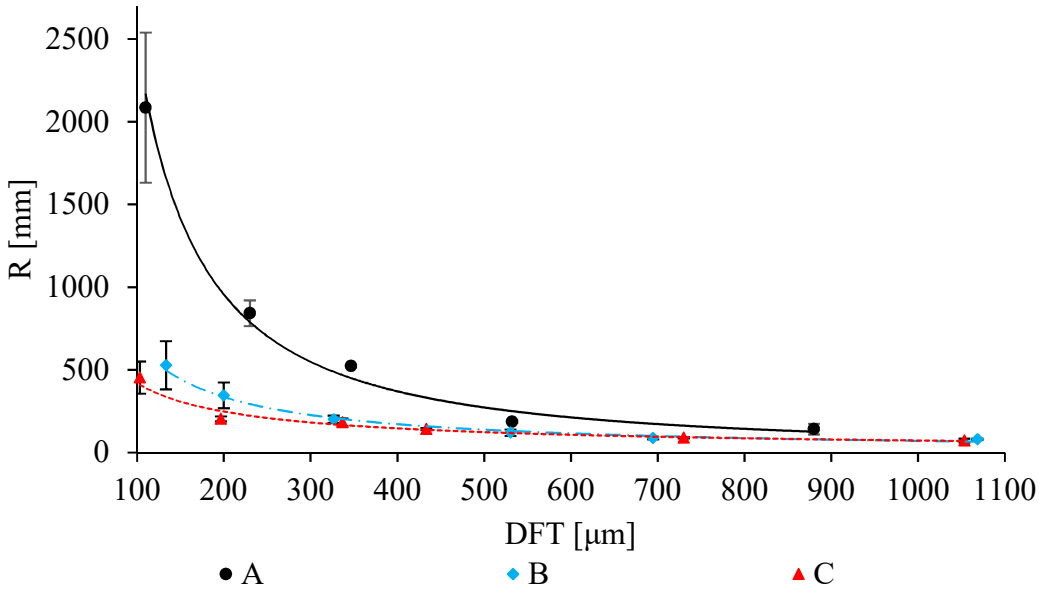

Figure 7.18 Radius of curvature of the bi-layer beams

Figure 7.19 presents the variation of the internal stresses with coating thickness for coating systems A, B, and C. The internal stresses shown are associated with the coated substrates used for the 3-point bending test (section 7.3.2). In general, tensile internal stresses increase with an increase in dry film thickness for all coatings. Coating systems A and B show an increase of σ_c with an increase of DFT. Coating C, however, shows relatively constant σ_c for DFT < 440µm and an increase with DFT for DFT > 440 µm.

Further, coating system A has markedly lower internal stresses at all thicknesses than either B or C. The residual stresses developed in the film are proportional to the Young's modulus, strain and T_g of the coating. In general, when applied to the same substrate, materials with lower Young's modulus and T_g will produce lower residual stresses than materials with higher Young's modulus and T_g, as observed in **Figure 7.19** [63].

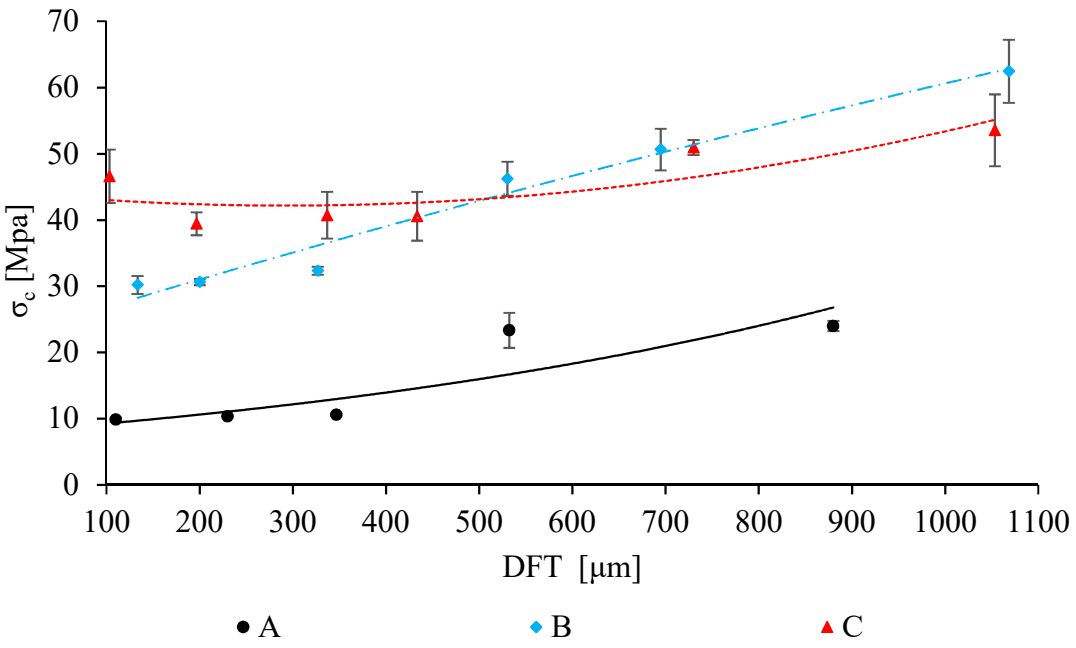

Figure 7.19 Variation of internal stresses with coating thickness for coatings A, B, and C

The stress relaxation rate and magnitude depend on the T_g of the coating. The latter depends on both the binder and curing agent, extent of cure, cure conditions. As the coatings cure progressively throughout their life, the magnitude and rate of change of the residual stress and relaxation will consequently change as well [156].

The solvent release kinetics also have a relevant bearing on the stress development in the coating. For solvent-borne convertible coatings, such as epoxy and polyurethane coatings, a given coating formulated with faster evaporating solvents can develop lower stress levels than a coating containing slow evaporating solvent. The volume of solvent (V_s) within the coating after most of the crosslinking has taken place affects the magnitude of the strain due to film formation, ε^c. This assumption is valid when stress relaxation is negligible [63]. Solvent retention has been observed to increase with an increase of DFT (**Table 6.2**). The prolonged release process experienced by thick films, compared to thin films, induces greater residual strain on the films [31, 155]. Coating A shows higher solvent evaporation rates than coating systems B and C and consequently lower tensile internal stresses.

In the corrosion protection of steel structures, paints are applied to large cross sections. The shrinkage in the plane of the coating due to the combined effect of chemical

reaction and solvent release is resisted by the substrate. Consequently, bi-axial tensile residual stresses are developed [63].

7.6 Dynamic mechanical properties of airless-sprayed free films

It has been established that for supported coatings both the composite modulus (coating/substrate bi-layer system) and effective Young's modulus decrease with an increase in coating thickness. In the following section, free films airless-sprayed in the same conditions as the supported coatings were studied by dynamic mechanical analysis in tension mode in order to compare the behaviour of supported coatings to free films to investigate the possible effect of coating/substrate interactions.

Testing coatings applied onto steel substrates provides the benefit of increasing the stiffness of the samples, making it possible to test thin coatings in DMA using either 3-point bending or dual cantilever modes. It is also beneficial for sample preservation and improves the reliability of the tests. 3-point bending produces results for storage or elastic modulus that are not affected by test clamping. However, this method requires the samples to be stiff and able to self-support during the tests. Unsupported low stiffness samples do not self-support and an increase in temperature produces significant softening, which is observed in the results as 'noise'.

Tension mode is a convenient method for the mechanical characterisation of free films; this mode requires a shorter span length[8] and records larger stiffness values. Therefore, the method can be used to characterise free films which would otherwise produce unreliable results in 3-point bending or dual cantilever mode. Moreover, placing the sample in tension reduces the risk of buckling.

Figure 7.20, **Figure 7.21**, and **Figure 7.22** show the storage modulus for free films of coating systems A, B and C respectively in tension mode. As observed for the supported coatings, the storage modulus decreases with an increase in temperature with a drastic drop being observed in the glass transition phase of the coating before

[8] Tension mode allows a maximum span length of 10mm, whilst dual cantilever and 3-point bending samples tested in the previous section have a span length of 25mm and 35mm respectively.

reaching a steady state. Additionally, the storage modulus not only decreases with sample DFT in the glassy region but also in the rubbery region [157].

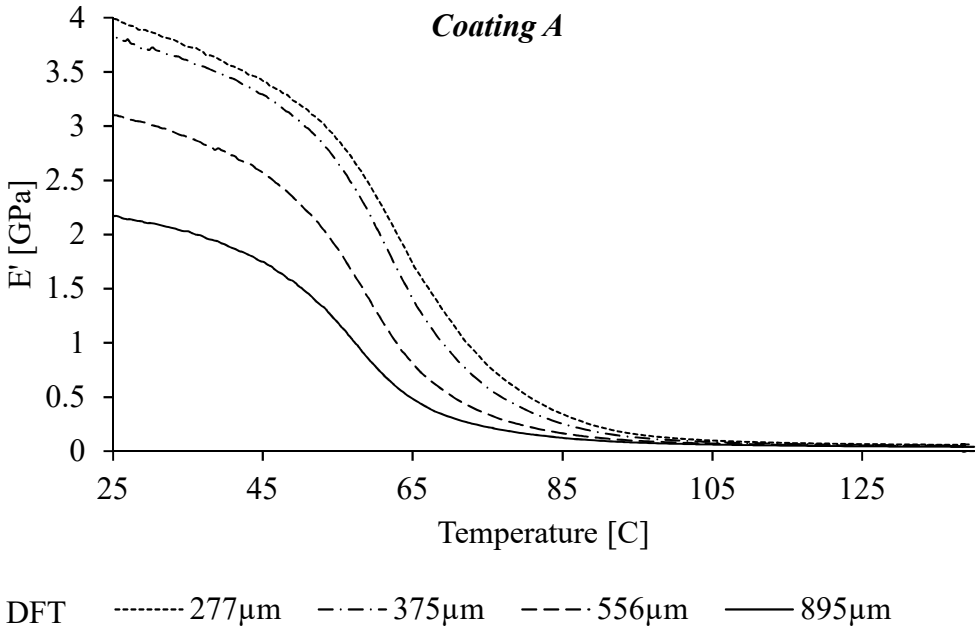

Figure 7.20 Coating A variation of the storage modulus with temperature in tension mode (free films)

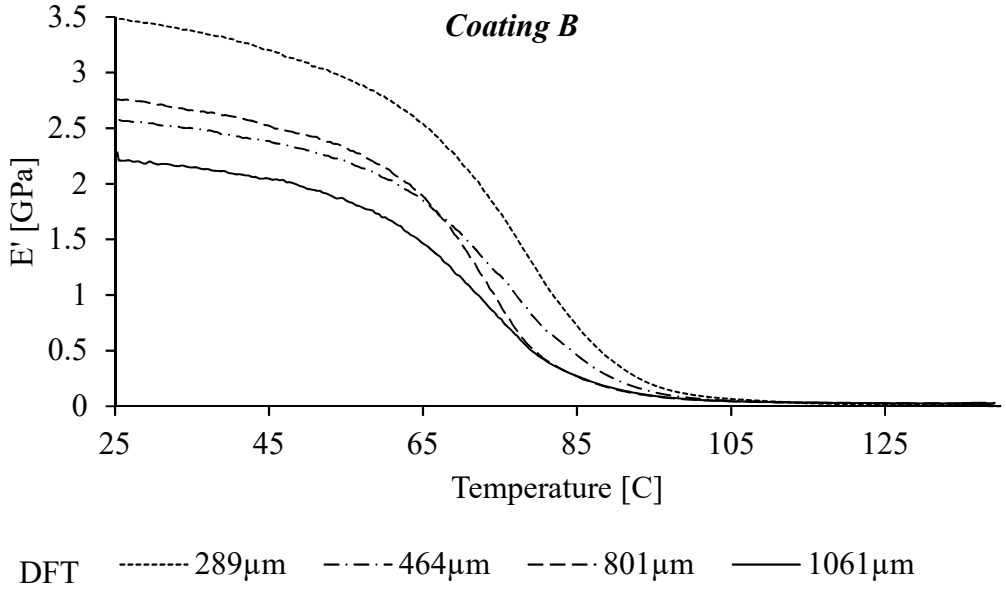

Figure 7.21 Coating B variation of the storage modulus with temperature in tension mode (free films)

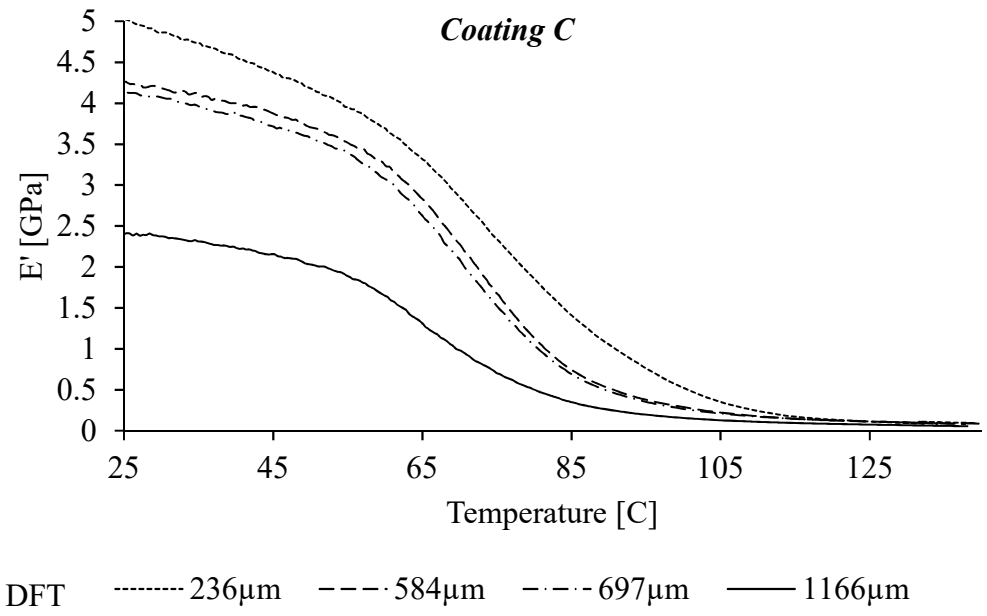

Figure 7.22 Coating C variation of the storage modulus with temperature in tension mode (free films)

The variation of the storage modulus at room temperature with coating thickness across the coating systems studied is presented in **Figure 7.23**. As observed for the supported coatings, the free film's elastic modulus is dependent on coating thickness. The three coating types show a reduction in the elastic modulus with an increase in coating thickness. Note that, the storage modulus results obtained for the free films may not be compared to the supported coating as they were calculated by different test modes. Similarly, the sample stiffness at room temperature increases with an increase in coating thickness as shown in **Figure 7.24**.

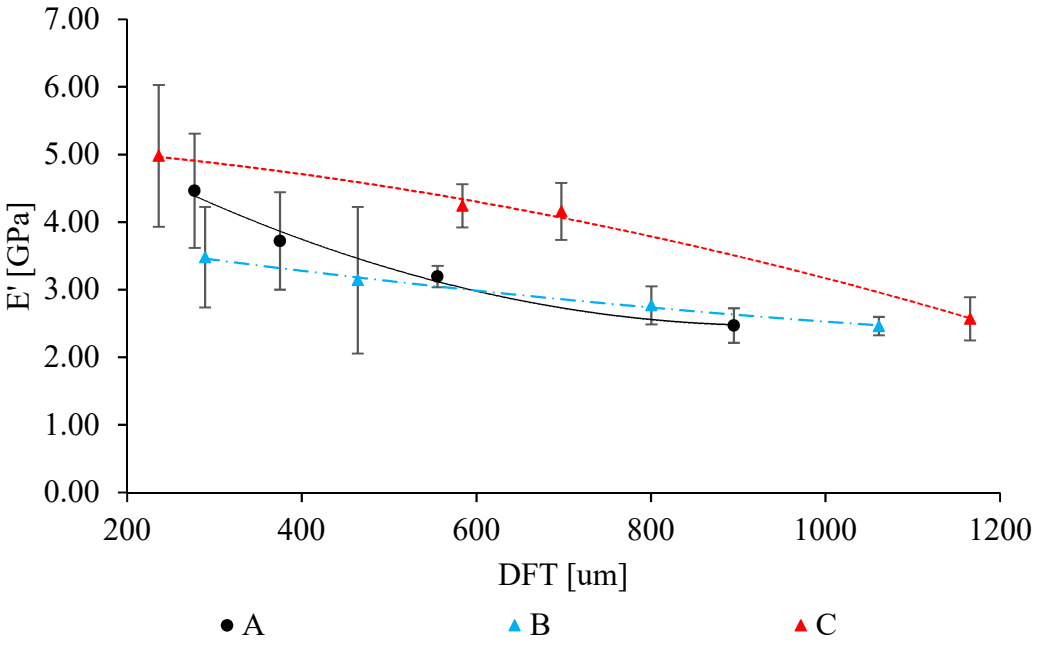

Figure 7.23 Variation of the storage modulus of all coatings with DFT

The glass transition of the free films was calculated from the maximum point in the tan δ curves and is presented in **Figure 7.25**. Comparison of the results to the T_g of supported coatings presented in **Figure 7.11** shows that free films have a higher glass transition temperature than restrained coatings. Previously, it was discussed that if coatings cure supported or unsupported, the presence or lack of a substrate, may influence the final physical and mechanical properties of the coatings due to solvent retention and/or coating/substrate interactions. Coatings applied onto steel substrates may retain additional solvent within them when compared to free films. The behaviour observed for supported coatings is also observed on free films. Coating C shows higher storage modulus, stiffness and T_g than coating systems A and B.

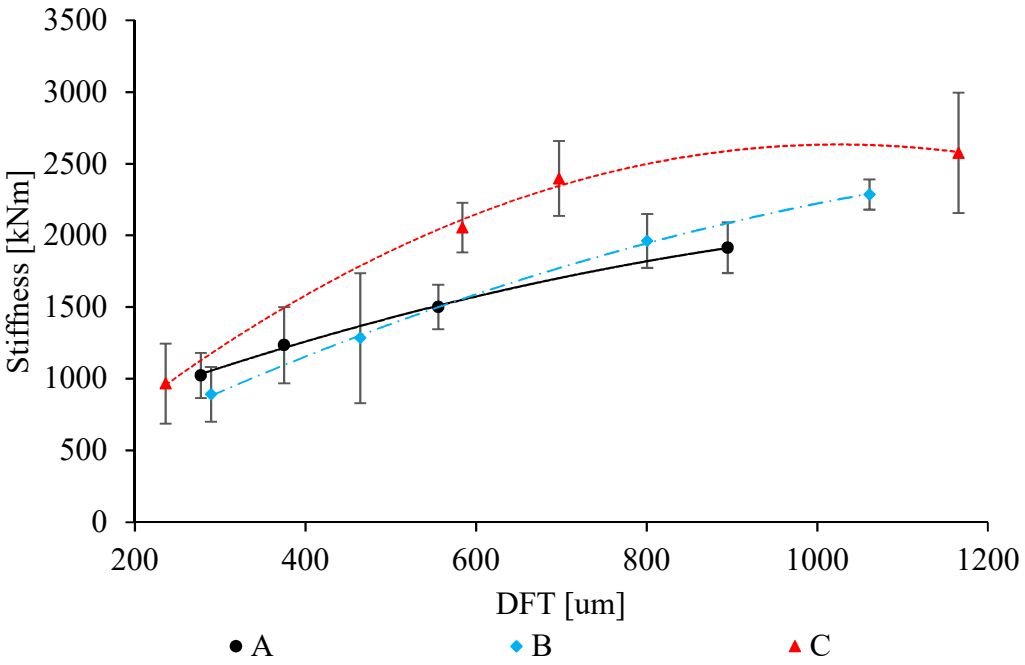

Figure 7.24 Variation of the stiffness of all coatings with DFT

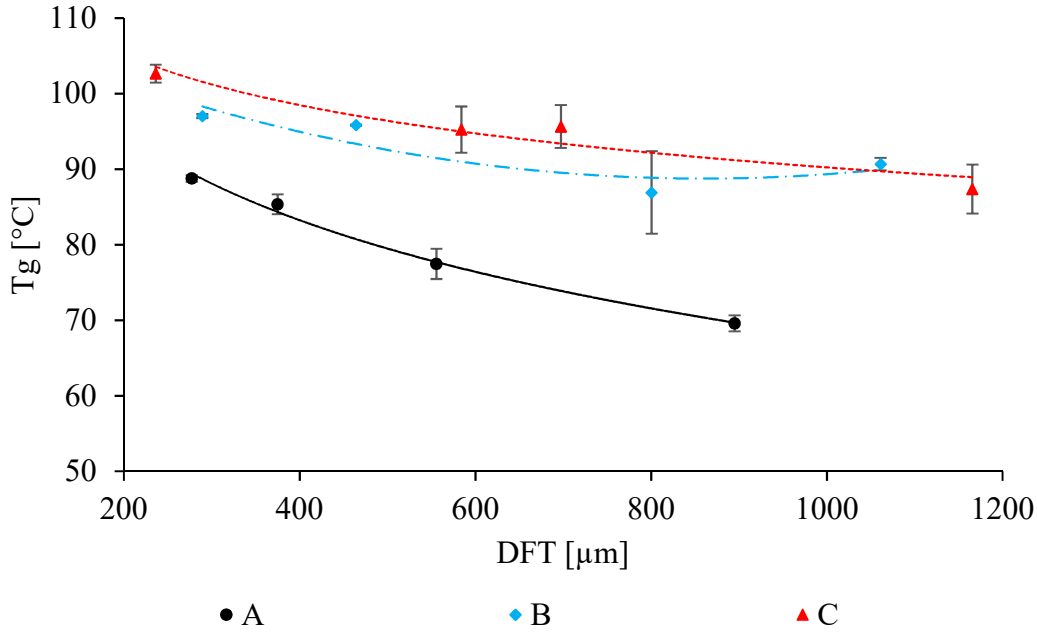

Figure 7.25 Variation of T_g with DFT for all coatings

7.6.1 Thermal expansion of coatings

In the glassy state, the static displacement experienced by the coatings increases with an increase in temperature due to thermal expansion. The rate at which these changes occur, however, is not constant due to differences in the configurational changes associated with molecule excitation with an increase in temperature. Thermosetting polymers experience distinct changes at the glass transition, these changes do not allow for the calculation of the thermal expansion coefficient during or beyond the T_g through DMA. The glass transition of the coatings corresponds to the range of the displacement curve where the free volume allows for greater chain mobility. In order to determine the coefficient of thermal expansion (CTE) of the coatings, linear sections of the curve must be considered. The temperature range of 25-45°C was selected to calculate CTE since all three coatings show linear behaviour (displacement versus temperature) in this range. Therefore, CTE is the average thermal expansion in that temperature region. **Figure 7.26** presents the variation of the thermal expansion coefficient with DFT for all coatings.

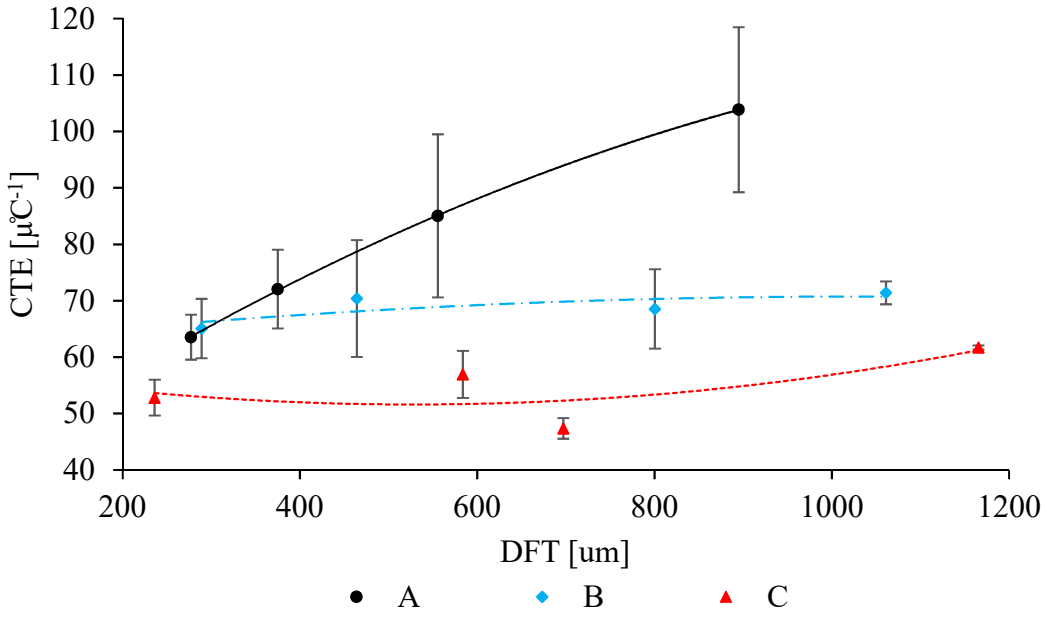

Figure 7.26 Variation of the average CTE with DFT

The thermal expansion is an appropriate parameter for the characterisation of different binding forces in coatings. A direct relationship between cross-linking density and stiffness exists in protective coatings; and depends on the interactions between

pigments and binders in these materials [48]. The presence of fillers in the coatings produced organic-inorganic composites with improved thermal stability, glass transition temperature, and dimensional stability [50].

The thermal expansion of polymers is associated with changes in the free volume. The free volume of a polymer is related to viscoelasticity, aging, and impact properties. Coating A shows higher values of thermal expansion coefficient than coatings B and C. The two latter coating systems also generally present higher values of glass transition temperatures at all thicknesses studied. The CTE depends on the T_g of the coatings, as the latter characterises transition from glassy to rubbery state and the molecular excitement associated with an increase in temperature.

Polymers have higher thermal expansion coefficients than the hard substrate (steel and metallisation layer). The coefficient of thermal expansion of hard steel, ranges from 10 to 16 $\mu℃^{-1}$, while that of the polymer system should range from 40 to 100 $\mu℃^{-1}$. In applications in which the service temperature changes drastically, such as marine environments, there will be further increment in the residual stresses due to the CTE mismatch [107].

The dynamic mechanical analysis showed that the T_g of the coatings decreases with an increase in coating thickness. Conversely, the thermal expansion coefficient increases with an increase in coating thickness (more drastically for coating A than coatings B and C). The decrease of the T_g is not desired as it is associated to a reduction of the thermo-resistance of the material [158]. The glass transition temperature is also associated with stress relaxation, a coating with a lower T_g is prone to experience more stress relaxation [156].

7.7 Dynamic mechanical analysis of cast samples

Dynamic mechanical analysis was performed on the cast free films subjected to three different cure schedules, as presented in Section 6.4. The curing schedule has an important role in the solidification process and stress development. An increase in temperature aids the curing reaction and solvent evaporation, as discussed in Chapter 6. An increase in temperature also produces stress relaxation. Residual stresses and stress relaxation are coupled phenomena and separating the contribution of each of these to the overall stresses is challenging [159].

Figure 7.27, **Figure 7.28**, and **Figure 7.29** show the temperature dependent storage modulus of coatings A, B, and C, respectively. The thermograms do not show a distinct change in the storage modulus with post-cure schedule and no clear relationship between storage modulus and cure temperature has been observed. However, the glass transition does show a distinct change with post-cure schedule. An increase in T_g with the exposure of the coating to 50°C is presented in **Figure 7.30**. The glass transition temperature depends on the cure schedule, and it progressively increases with time. In general, the higher the post-cure temperature, the higher the T_g for $T \leq T_g$[156]. Coatings subjected to cure schedule 2 (RT + 4 days 50°C + RT) show glass transition temperatures higher than coatings subjected to cure schedule 1 (RT). The exposure to the coating to cure schedule 3 (RT + 4 weeks 50°C) produces even higher glass transition temperatures. The summary of the properties of all coatings subjected to the three cure schedules is presented in **Table 7.4**.

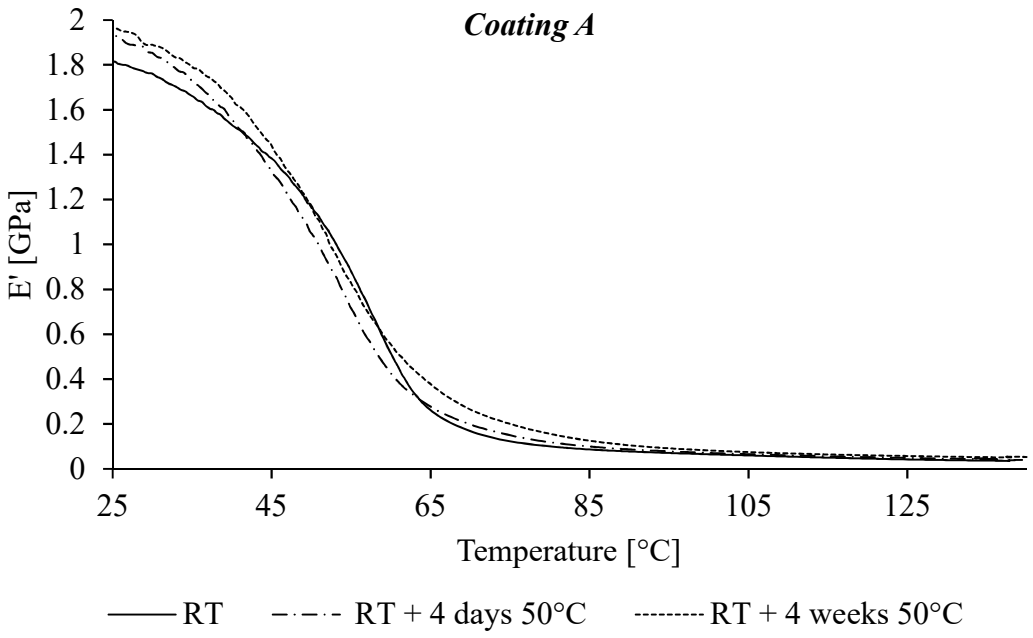

Figure 7.27 Coating A variation of storage modulus with temperature of cast samples subjected to different cure-schedules

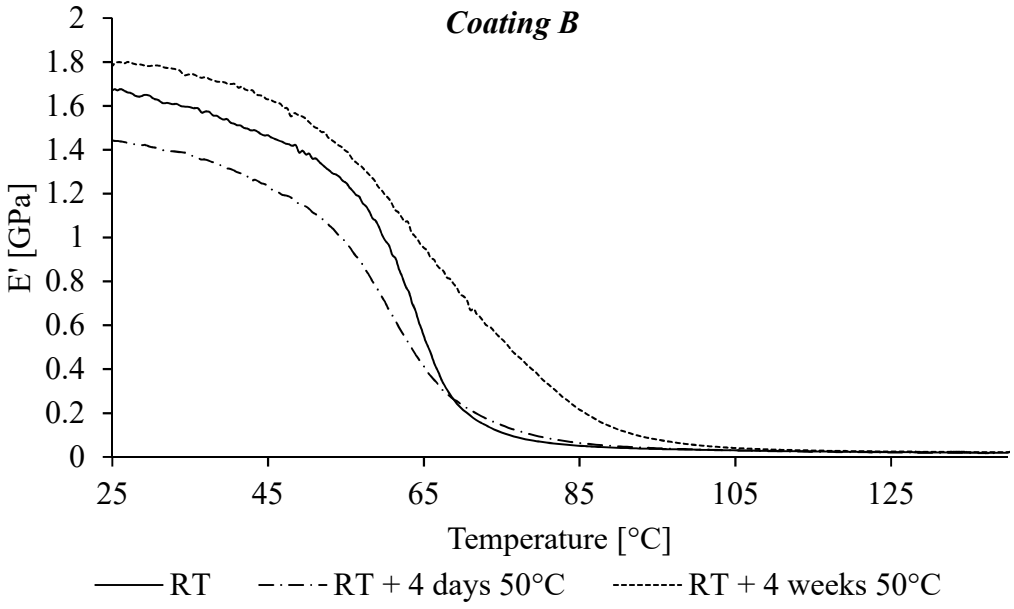

Figure 7.28 Coating B variation of storage modulus with temperature of cast samples subjected to different cure-schedules

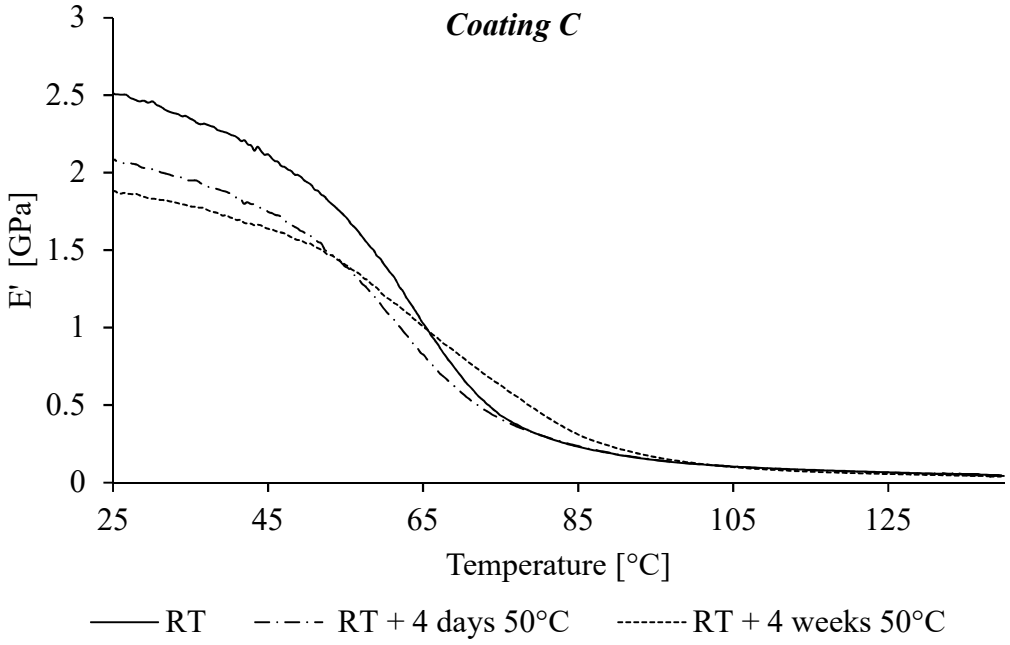

Figure 7.29 Coating C variation of storage modulus with temperature of cast samples subjected to different cure-schedules

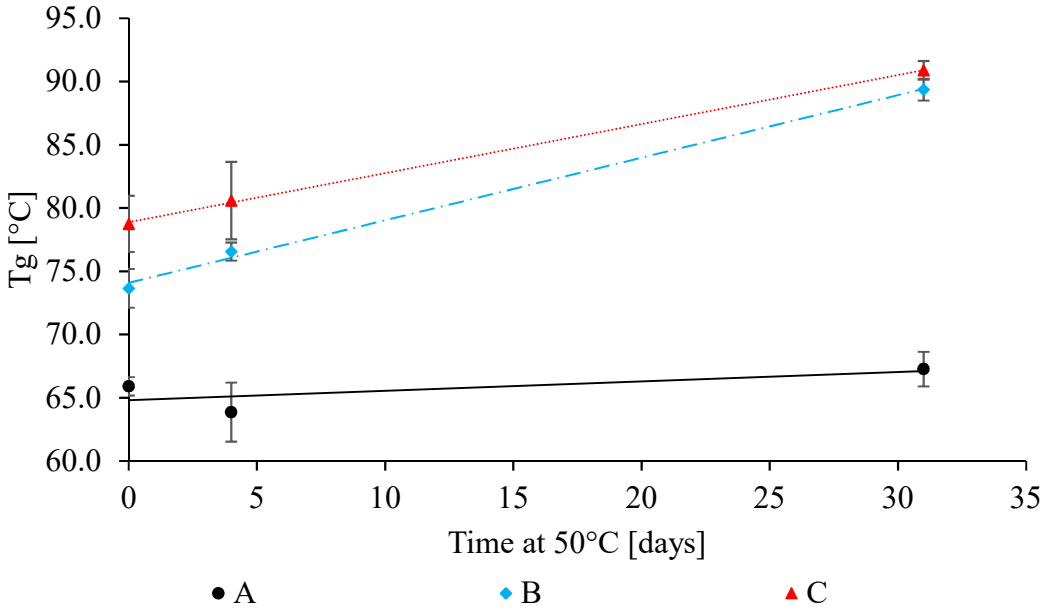

Figure 7.30 Effect of the curing time on the T_g of cast samples of coatings A, B, and C

Table 7.4 Summary of the properties of films exposed to three different cure schedules

Coating	Cure schedule	DFT ± ΔDFT [µm]	E ± ΔE [GPa]	S ± ΔS [KN/m]	$T_g \pm \Delta T_g$ [°C]
A	RT	1490 ± 109	1.9 ± 0.1	2248 ± 289	65.9 ± 0.7
	RT + 4 days 50°C + RT	1666 ± 209	1.9 ± 0.3	2214 ± 308	64 ± 2
	RT + 4 weeks 50°C	1670 ± 212	2.0 ± 0.2	2651 ± 184	67 ± 1
B	RT	1541 ± 14	1.6 ± 0.5	2118 ± 651	74 ± 2
	RT + 4 days 50°C + RT	1680 ± 92	1.4 ± 0.1	2005 ± 65	76.6 ± 0.7
	RT + 4 weeks 50°C	1475 ±150	1.8 ± 0.3	2154 ± 152	89.4 ± 0.9
C	RT	1395 ±75	2.5 ± 0.3	2858 ± 219	79 ± 2
	RT + 4 days 50°C+ RT	1447 ± 128	2.1 ± 0.5	2482 ± 636	81 ± 3
	RT + 4 weeks 50°C	1421 ± 28	1.9 ± 0.2	2192 ± 230	90.9 ± 0.7

7.8 Static mechanical properties of thick film samples

The flexural properties of bulk coating samples (DFT~ 3.5mm) were determined by 3-point bending on a static mechanical testing machine in accordance with ISO 187 (**Table 5.10**) [95]. **Figure 7.31**, **Figure 7.32**, and **Figure 7.33** show the flexural stress versus flexural strain plots for coatings A, B, and C, respectively. The stress-strain curves show that the materials exposed to schedule 1 (RT) have a viscoelastic response

to stress. The application of schedule 2 (RT + 4 days 50°C + RT) produces a curve very similar to that corresponding to schedule 1: the coating retains its viscoelastic behaviour as a response to mechanical stress. An increase in the time of exposure to the post-cure temperature, as in schedule 3 (RT + 4 weeks 50°C), produces a progressive change from a ductile to a brittle material. In the flexural stress-strain plots, the curves corresponding to the samples subjected to schedule 3 presents an increased slope in the elastic region, i.e. a higher flexural modulus of elasticity. The prolonged exposure to 50°C produces an increase in the flexural stress experienced for a given value of flexural strain. Due to the considerably larger thickness of the thick cast samples it is expected that a higher percentage of solvent is retained in the samples, compared to the supported samples and free films tested by DMA.

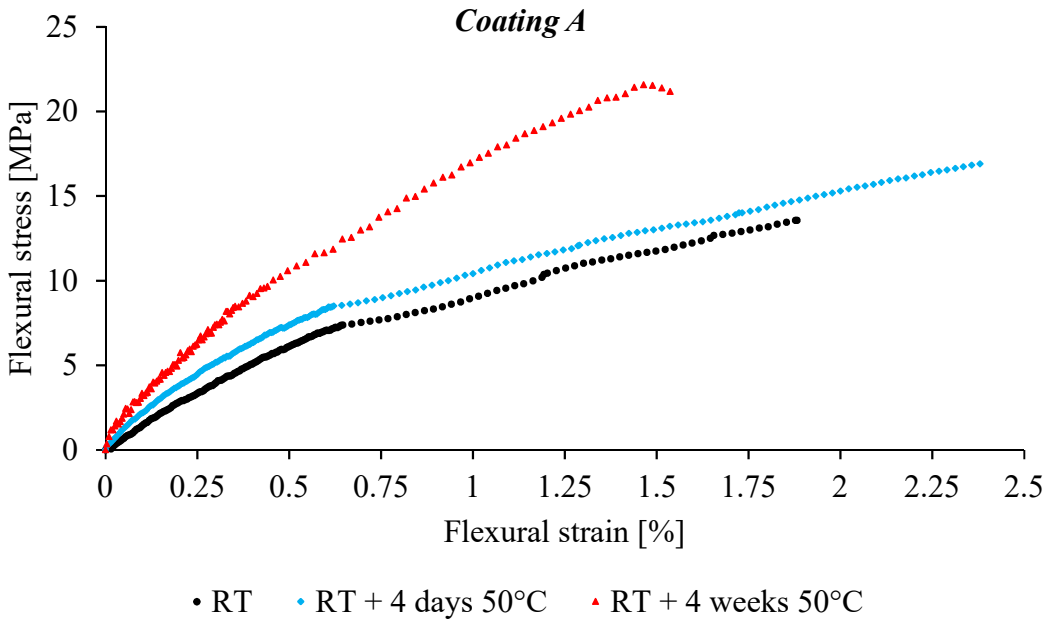

Figure 7.31 Flexural stress versus flexural strain for coating A subjected to different post-cure schedules

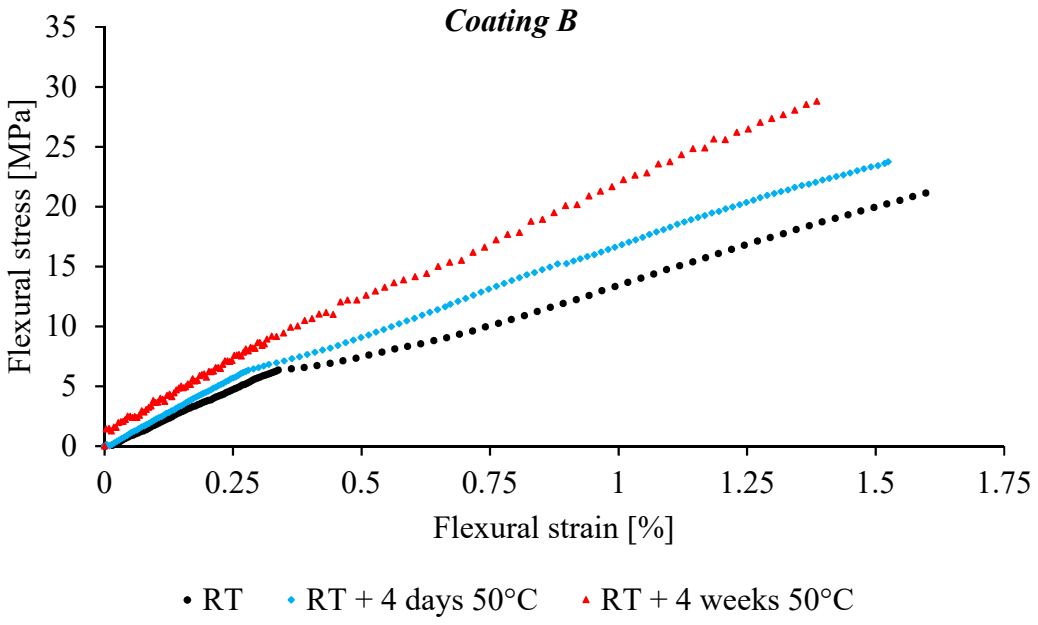

Figure 7.32 Flexural stress versus flexural strain fot coating B subjected to different post-cure schedules

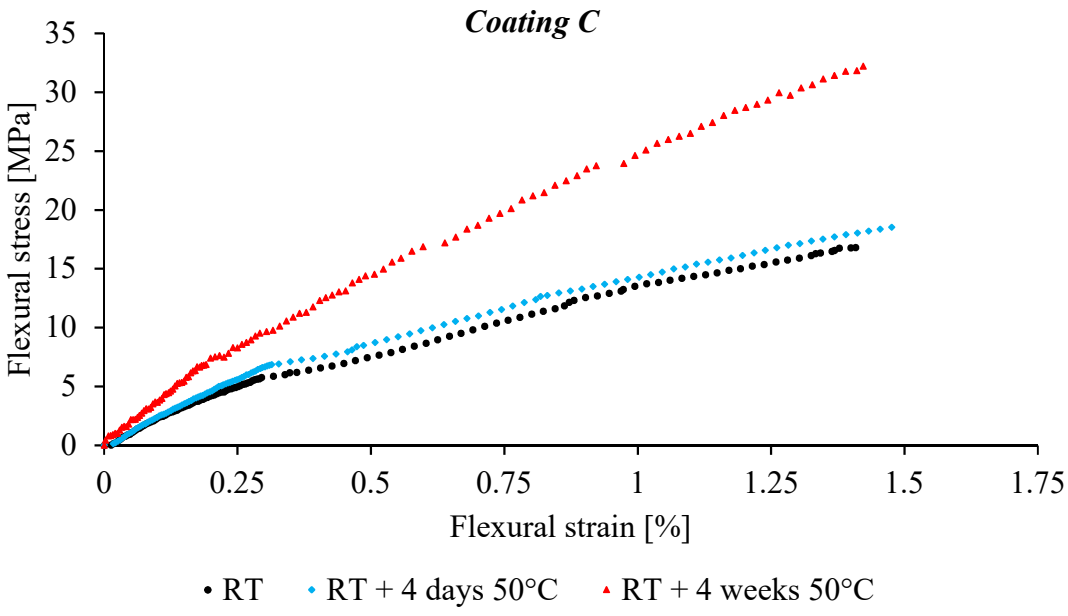

Figure 7.33 Flexural stress versus flexural strain for coating B subjected to different post-cure schedules

The calculated weight loss of the cast samples is presented in Section 6.4 (DFT ~3.5 mm in **Figure 6.13**, **Figure 6.14**, and **Figure 6.15**). In order to compare the behaviour of the three coatings, the modulus of elasticity in flexure (E_f), flexural stress at break

(σ_{fB}), and flexural strain at break (ε_{fB}) are presented in **Table 7.5**. Due to the viscoelastic nature of the epoxy-based coatings and the effect of the clamps, the elastic modulus of the epoxy-based coatings measured by DMA is different to that measured by static experiments [17].

Table 7.5 Flexural modulus of bulk coatings determined by 3-point bending

Coating	Cure schedule	E ± ΔE [GPa]	σfb ± Δ σfb [MPa]	εfb ±Δ [%]
A	RT	1.6 ± 0.2	14.8 ± 0.8	1.6 ± 0.2
	RT + 4 days 50°C + RT	1.7 ± 0.1	17 ± 1	2.3 ± 0.2
	RT + 4 weeks 50°C	2.1 ± 0.2	24 ± 2	1.8 ± 0.2
B	RT	2.1 ± 0.2	25 ± 3	1.7 ± 0.2
	RT + 4 days 50°C +RT	2.3 ± 0.2	26 ± 5	1.7 ± 0.4
	RT + 4 weeks 50°C	2.8 ± 0.7	33 ± 9	1.7 ± 0.1
C	RT	2.2 ± 0.2	18 ± 4	1.4 ± 0.2
	RT + 4 days 50°C + RT	2.4 ± 0.4	18 ± 3	1.5 ± 0.4
	RT + 4 weeks 50°C	3.4 ± 0.4	23 ± 4	1.3 ± 0.3

7.9 Conclusions

Three epoxy-based coatings with applications in offshore wind turbine towers and transition pieces have been characterised through dynamic mechanical analysis. These tests have been formulated to mechanically characterise supported coatings and identify the different aspects affecting their mechanical properties, the development of internal stresses, and how these affect their performance in the field.

The adhesion test showed that the three coatings do satisfy the currently in-use standard NORSOK M-510 (2004) 'Surface preparation and protective coatings', and the minimum pull off stress of 5MPa is exceeded in every test, even at very high DFTs [54].

It is known that testing the mechanical properties of free films is complicated due to difficulties in production and handling. Very thin free films (DFT<200μm) do not self-support and the results by DMA are unreliable in modes such as 3-point bending and dual cantilever mode. On the other hand, very thick supported coatings (DFT>1200 μm) produce very high sample curvatures and tend to fail when clamped in dual cantilever mode in the DMA. Therefore, DFT is a decisive factor in determining the best test mode to use in dynamic mechanical analysis. As offshore wind turbine coatings are applied at DFTs from 60 to 350 μm, testing as supported coatings is more convenient than as free films. Further, studying the mechanical properties of coatings applied on substrates, rather than free films, takes into account coating/substrate interactions and its effect on the overall mechanical properties of the coating.

DMA is a relatively new and unexplored characterisation method. In this study, it has been found that a combination of testing modes may be used to provide a complete mechanical analysis of supported coatings in a wide range of DFTs (100-1200 μm). Short temperature scans below T_g in 3-point bending mode produce results for the composite modulus which are not affected by shearing stresses. These results may be used to determine the effective Young's modulus of the coatings by composite beam stress analysis and the residual stresses by beam theory. Followed by long temperature scans in dual cantilever mode to provide the temperature dependence of storage modulus and stiffness, and T_g.

It has been established by dynamic mechanical analysis on coatings A, B and C that the physical properties (glass transition temperature and coefficient of thermal expansion) and mechanical properties (elastic modulus, stiffness, and internal stresses) are dependent on coating thickness. Comparison of the experimental results obtained for the three different coatings indicates that:

- Coating A shows a noticeably lower T_g and higher CTE than coatings B and C. Further, coating A has a CTE that is highly dependent on DFT indicating that care must be taken when deciding the optimal DFT for a given application, and applying DFTs higher than specified may produce a considerable increase in CTE and consequential thermal strain in the coating/substrate system.

- Composite beam stress analysis has shown that coating A also has lower effective Young's modulus and tensile internal stresses than coating systems B and C.
- Coating C shows the higher tensile residual stress levels for DFT<500µm whilst coating B shows higher stress levels for DFT>500µm. DMA indicates that both coatings have high coating stiffness.
- Coatings B and C both have a high T_g and CTE. Overall coating C has the highest T_g and lowest CTE.

Ultimately, it has been established that an increase in coating stiffness, solvent retention, and pore density associated with an increase in coating thickness affects the glass transition temperature and effective Young's modulus of the coatings, and consequently the residual stress developed within the supported film. The decrease in T_g and increase in CTE associated with an increase in DFT is not desirable as it has been linked to a reduction in the thermo-resistance of the material. The glass transition temperature is also associated with stress relaxation, a coating with a lower T_g is more prone to experience stress relaxation.

The dynamic mechanical analyser allows determination of the temperature-dependent elastic modulus of protective coatings with the use of small amounts of materials and eliminates the need to conduct expensive tests in traditional testing machines at different temperatures. It was found that inevitable variations from sample to sample in the thickness of the coating and the substrate produce variations on the calculated elastic modulus. Finally, DMA results of supported and unsupported coatings indicate that similar behaviour and dependency with DFT is observed in both cases.

8 CONCLUSIONS AND FUTURE WORK

8.1 Conclusions

The need for improvement of protective coatings performance has motivated researchers to extensively investigate and characterise the physical, chemical, and mechanical properties of coatings. Most importantly, bi-layered systems constituted by a substrate and a coating. Experimental techniques were selected to characterise the physical and mechanical properties of protective coatings for marine applications, the results of which may facilitate the understanding of, and lead to an improvement in, the overall performance of coatings in the field. Three different coatings systems were characterised, and the analysis shows the effect of the film thickness on the properties of the coatings and the results obtained are consistent for all coating types. This suggests that the methodology presented in the analysis is reliable and repeatable.

It is known that the mechanical characterisation of protective coatings has faced many challenges in the past due to the brittle nature of organic protective coatings and the difficulties associated with the preparation of uniform and homogeneous test samples. In the present study it has been found that an increase in coating thickness affects the shape/morphology of the cross-sectional area of the samples and consequently, the stress distribution during mechanical testing. Additionally, the real cross-sectional area of the samples differs from the one assumed by the mathematical model for the determination of the elastic modulus and residual stresses of supported coatings, which may lead to an error in the results.

Due to the viscoelastic nature of coatings, dynamic mechanical analysis DMA has been found to be the preferred test method for the mechanical characterisation of convertible epoxy-based protective coatings. Dynamic mechanical analysis is a relatively-new and unexplored field, it has several advantages over static mechanical testing: the use of small samples, a temperature chamber, and software that records the change of mechanical behaviour of materials with changes in temperature.

Composite beam stress analysis provides a solution for the Young's modulus and residual stresses of supported coatings. Determination of the mechanical response of

the composite sample (coating/substrate) and of the unsupported substrate, and the geometrical parameters of the sample allows calculation of Young's modulus of the coatings. In the present study it has been shown that Benabdi and Roche's (1997) equation provides a viable solution for the residual stresses of thick and thin supported coatings of known mechanical properties.

Previous research had attributed the thickness-dependent physical and mechanical properties of coatings to the formation of an interphase between the epoxy-based coating and metallic substrate. It has been shown in this study, however, that this is not the case for the coating systems under study. Scanning electron microscopy (SEM) and electron dispersive spectroscopy (EDS) have shown that the coatings have a homogeneous composition. The coatings are composite materials composed of several types of pigments and fillers, of varying size and morphology, dispersed uniformly in an epoxy-based matrix. Analysis of the coating/substrate interface has shown that there is no formation of an interphase or significant orientation of pigments and fillers that may affect the mechanical properties of the coatings. Comparison of samples of different thicknesses has indicated that the heterogeneous nature of the coating is consistent. However, an increase in coating thickness does appear to be associated with an increase in pore density. It was found that the density of pores and defects in the materials is proportional to the reduction of the tensile strength and consequently, effective Young's modulus of the coatings.

From solvent loss studies and qualitative SEM analysis, it is proposed that solvent retention and pores density increases proportionally with coating thickness. Retained solvent acts as a plasticiser reducing the tensile strength and consequently the effective Young's modulus of the coatings. The solvent evaporation rate has a relevant effect on stress development. In solvent-borne convertible coatings, fast evaporating solvents are related to lower stress levels. The use of a post-cure schedule allows acceleration of the curing process (cross-linking) and solvent release.

In general, several observations were made regarding the relationship between the coatings physical and mechanical properties to possible coating performance in service. Coatings with lower Young's modulus and T_g experience lower residual stresses and higher coefficients of thermal expansion. Additionally, for all coatings studied, it has been established that an increase in coating thickness is associated with

an increase in coating stiffness, solvent retention, and pore density, which consequently leads to a reduction in the glass transition temperature, tensile strength, and effective Young's modulus of the coatings, and thus an increase in the tensile residual stresses within the supported film.

The progressive curing of the films and evolving coating properties determine stress development and affect the coating's performance in service. Additionally, the stress development in coatings depends on a balance between the curing stresses and stress relaxation. The interactions between the two must be acknowledged and are difficult to separate to quantify the effect of each of these in overall stress development.

Through comparative analyses, conclusions have also been drawn with respect to the coatings' relative properties. Coating A has been shown to have the lowest T_g and highest CTE by DMA compared to coatings B and C. Overall coating C has the highest T_g and lowest CTE, both calculated by DMA. As coating A's CTE is highly dependent on DFT, application of excessive DFT (or higher than specified) in service will result in a considerable increase in the thermal strain between coating and substrate. It will therefore have the highest thermal expansion mismatch with the substrate and lowest thermal resistance.

Coating A also shows lower effective Young's modulus and tensile internal stresses than coating systems B and C. Coating C shows the higher stress levels for DFT < 500µm whilst coating B shows higher stress levels for DFT>500µm. As offshore wind turbine tower coatings are applied to produce DFTs lower than 500µm, in service coating C will show the highest internal stresses. DMA indicates that coatings B and C have high coating stiffness.

As coating A develops lower tensile residual stresses, it may be considered as less likely to produce failure due to flaking or peeling. However, its low T_g and high CTE indicate that it would not perform well if placed in an area with exposure to moisture or water, which would reduce the T_g and tensile strength further.

Coatings B and C show very similar behaviours. Coating B has applications in immersion and splash zones and coating C in atmospheric zones. Due to the cumulative nature of residual stresses, high tensile internal stresses may be countered by compressive residual stresses. Coating B is more likely to relieve internal stresses

in service than coating C. It is suggested that coating B is less likely to fail due to excessive tensile stresses. Therefore, coating B is predicted to have the highest durability and reliability in service. This appears to be confirmed by actual performance in the field as reported by Hempel S/A.

The residual internal stresses in coatings B and C are roughly equal and higher than those in coating A. Despite this, coating B does not suffer from cracking and flaking found with coatings A and C. This suggests that residual stress is not the sole determining factor in causing cracking or flaking, and coating chemistry has a relevant effect on the mechanical behaviour of the coatings.

In general, deviations from the specified DFT may lead to an increase in tensile internal stresses and may affects the coatings performance in service as it reduces the capacity of the coating to accommodate additional tensile residual stresses during service.

In the offshore energy industry, prolonged coating reliability is required. In the present study, it has been found that it is possible to design more reliable and predictable coating systems by a judicious manipulation of the paint formulation and control of the DFT and post-cure schedule. Finally, as the coatings used in offshore wind turbines structures are adapted from the oil and gas industry any improvements in coating reliability would also be beneficial for the oil and gas industry.

8.2 Outline of future work

Future work has been categorised into four main areas which have been identified as relevant. Further research into these subjects will contribute to fill the current lacunae of knowledge in the field of mechanical characterisation of protective coatings. Sections 8.21, 8.22, and 8.23 will contribute to the characterisation of supported coatings and understanding of the relationships between protective coatings and substrate. Finally, the study of the performance of coatings under simulated marine environments, presented in section 8.2.4, will provide understanding regarding the effect of coating characteristics on the overall performance as barrier coatings for corrosion protection.

8.2.1 Evaluation of the residual stresses in a 3-layer system (2 coating layers and a substrate).

- Stress analysis for a composite beam composed of three different layers.
- Development of a mathematical model based on beam/plate theory for a three-layer system.
- Determination of residual stress in tri-layer systems compared to that in bi-layer systems
- Evaluation of the evolution of residual stresses with curing time and effect of cure schedule.
- Evaluation of the thermal expansion of the tri-layer system.
- Evaluation of residual stress variations with temperature and relative humidity changes.

8.2.2 Study of the interactions between residual stresses and stress relaxation processes in supported coatings

- Study the residual stresses of a bi-layered system consisting of a coating and a substrate.
- Development of a test method for the study of stress relaxation processes in supported coatings.
- Evaluation of the effect of coating characteristics in residual stresses and stress relaxation.
- Evaluation of the effect of cure schedule in residual stresses and stress relaxation.
- Evaluation of the effect of temperature and relative humidity changes in residual stresses and stress relaxation.

8.2.3 Study of the effect of substrate and coating characteristics in coating/substrate interactions.

- Study the effect of substrate characteristics in the coating/substrate interactions (type, thickness, surface treatment, mechanical properties).
- Study the effect of coating characteristics in the coating/substrate interactions (type, thickness, and mechanical properties).

- Determination of the mechanical response of supported coatings with different substrates.
- Determination of the residual stresses of supported coatings with different substrates.

8.2.4 Evaluate the performance of the supported coatings under simulated marine environments

- Exposure of supported coatings, with different compositions, to simulated marine conditions
- Determination of the residual stresses of aged supported coatings and evaluation of the effect of hygrothermal (thermal and hygroscopic) stresses on the final stress state.
- Development of a test methodology to assess the mechanical properties of aged supported coatings, including procedures such as dynamic mechanical analysis and slow-strain rate-tests in simulated seawater.
- Study the fracture surface of failed coatings due to exposure to harsh environments and relate the facture surface to the coating composition.

REFERENCES

1. Thick, J., *Offshore corrosion protection of wind farms* International Paint Ltd.

2. Momber A., P.P., Stenzel V., *Performance and integrity of protective coating systems for offshore wind power structures after three years under offshore site conditions.* Renewable Energy, 2015. **74**: p. 606-617.

3. BSI, *BS EN ISO 4618:2014 - Paints and varnishes. Terms and definition*. 2014.

4. Alam, M., Sherif, E., Al-Zahrami, S., *Fabrication of various epoxy coatings for offshore applications and evaluating their mechanical properties and corrosion behaviour.* Internal journal of electrochemical science, 2013. **8**: p. 3121-3131.

5. Sherif, E., Alam, M., Al-Zahrani, S, *Fabrication of different protective coatings and studying their mechanical properties and corrosion behaviour in sodium chloride solutions.* Internal journal of electrochemical science, 2015. **10**: p. 373-387.

6. Bierwagen, G., *Reflections on corrosion control by organic coatings.* Progress in organic coatings, 1996(28): p. 43-48.

7. Jeon, H., Park, J., Shon, M., *Corrosion protection by epoxy coating containing multi-walled carbon nanotubes.* Journal of industrail and engineering chemistry, 2013. **19**: p. 849-853.

8. Inone, P., Garcia, C., Ruvolo-Filho, A. , *Evaluationg barrier properties of organic coatings by water permeation and electrochemical methods* Journal of coating technology, 2003. **75**(939): p. 29-36.

9. Fredj, N., Cohendoz, S., Feagas, X., Touzain, S., *Some consequences of saline solution immersion on mechanical behaviour of two marine epoxy-based coatings.* Progress in Organic Coatings 2010. **69**: p. 82-91.

10. Lee, D., Kim, B., *Investigation of coating failure on the surface of a water ballast tank of an oil tanker* Journal of adhesion science and technology, 2012. **19**(10): p. 879-908.

11. Lambourne, R., *Paint composition and applications: a general introduction*, in *Paint and surface coatings*, S.T. Lambourne R. , Editor. 1999, Woodhead Publishing. p. 1-18.

12. Seymour, R., Mark, H., *Handbook of Organic Coatings*. 1990: Elsevier.

13. Turner, G.P.A., *Introduction to paint chemistry and principles of paint technology*. 3rd ed. 1988: Chapman and Hall.

14. Vicevic, M., *A comparison of fatigue properties of epoxy coatings in marine environments*, in *School of Chemical Engineering and Advanced Materials*. 2008, University of Newcastle Upon Tyne: Newcastle Upon Tyne. p. 266.

15. BSI, *BS EN ISO 12944-5 2007: Paint and varnishes - Corrosion protection of steel structures by protective paint systems -*, in *Part 5: Protective paint systems*. 2007.

16. Jeyranpour, F., Alahyarizadeh, G., Arab, B, *Comparative investigation of thermal and mechanical properties of cross-linked epoxy polymers with different curing agents by molecular dynamics simulation.* Journal of molecular graphics and modelling, 2015. **62**: p. 157-164.

17. Hobbiebrunken, T., Fiedler, B., Hojo, M., Ochiai, S., Schulte, K., *Microscopic yielding of CF/epoxy composites and the effect on the formation of thermal residual stresses.* composites science and technology, 2005. **65**: p. 1626-1635.

18. Osswald T., M.G., *Materials science of polymers for engineers*. 1996: Hanser. 475.

19. Bentley, J., *Organic film formers*, in *Paint and surface coatings* S.T. Lambourne R. , Editor. 1999, Woodhead Publishing. p. 19-90.

20. Parker, D., *Epoxy resins*, in *Principles of surface coating technology*, D. Parker, Editor. 1965, Interscience Publishers. p. 315-325.

21. McCrum, N., Buckley, C., Bucknall, C., *Principles of polymer engineering*. 1997: Oxford University Press

22. Kubisztal, M., Haneczok, G., Chrobak, G., Rams, B., Miara, D., Rasek, J., *Elastic properties of epoxy system coatings on aluminum substrate.* Surface & coating technology, 2009. **204**: p. 120-124.

23. Jiang, W., Jin, F., Park, S., *Thermo-mechanical behaviors of epoxy resins reinforced with nano-Al_2O_3 particles.* Journal of industrial engineering and chemistry, 2012. **18**: p. 594-596.

24. Barcia, F., Soares, B., Sampiao, E., *Adhesive properties of epoxy resin modified by end-funcionalized liquid polybutadiene.* Journal of applied polymer science, 2004. **93**: p. 2370-2378.

25. Ochi, M., Onishi, K., Ueda, S., *Internal stress and mechanical properties of epoxy resin coatings cured with acid catalyst in the presence of THF.* Polymer, 1991. **33**(21): p. 4550-4555.

26. Cowie, J., *Polymers: chemistry and physics of modern materials* 1991, Blackie and Son Ltd. .

27. Celinski, M., Sankowska, M., *Explosibility, flammability and the thermal decomposition of Bisphenol A, the main component of epoxy resin.* Journal of Loss Prevention in the Process Industries, 2016. **44**: p. 125-131.

28. Dorsey, J., Dorsey, G., Rutenberg, A., Green, L., *Determination of the epoxide equivalent weight of glycidyl ethers by proton magnetic resonance spectrometry.* Analytical chemistry 1977. **49**(8): p. 1144-1145.

29. Acebo, C., Ramis, X., Serra, A., *Improved epoxy thermosets by the use of poly(ethyleneimine) derivatives.* Physical Sciences Reviews, 2017. **2**(8): p. 20160128-1-20160128-34.

30. Guy, A., *Coatings components beyond binders*, in *The chemistry and physics of coatings*, A. Marrion, Editor. 2004, The royal society of chemistry. p. 267-316.

31. Croll, S., *Effect of solvent on residual strain in clear epoxy coatings.* Journal of oil and colour chemists' association, 1980. **63**: p. 230-236.

32. Brock, T., Groteklaes, M., Mischke, P., *European coatings handbook*, ed. U. Zorll. 2000: Vincentz.

33. Kalendova, A., Vesely, D., Kalendra, P., *A study of the effects of pigments and fillers on the properties of anticorrosive paints.* Pigments and resin technology, 2006. **35**(2): p. 83-94.

34. Parker, D., *Properties of raw materials*, in *Principles of surface coating technology*, D. Parker, Editor. 1965, Interscience publishers: Michigan. p. 8-25.

35. Sato, K., *The internal stress of coating films.* Progress in organic coatings, 1980(8): p. 143-160.

36. OCCA, *Surface coatings: paints and their applications*. Vol. 2. 1984: Chapman and Hall Ltd.

37. Smith, F., *White pigments*, in *Principles of surface coating technology*, D. Parker, Editor. 1965, Intescience publishers: Michigan. p. 70-87.

38. Karakas, F., Celik, M., *Effect of quantity and size distribution of calcite filler on the quality of water borne paints.* Progress in organic coatings, 2012. **74**(3): p. 555-563.

39. Yebra, D., Weinell, C., *Key issues on the formulations of marine antifouling paints*, in *Advances in marine antifouling coatings and technologies*, C. Hellio, Yebra, D., Editor. 2009, Woodhead publishing limited. p. 308-332.

40. Trinh, A., Nguyen,T., Thai, T., To, T., Nguyen, X., Nguyen, A., Aufray, Pébère, N., *Improvement of adherence and anticorrosion properties of an epoxy-polyamide coating on steel by incorporation of an indole-3 butric acid-modified nanomagnetite.* Journal of coating technology and research, 2016. **13**(3): p. 489-499.

41. Conradi, M., Kocijan, A., Kek-Merl, D., Zorko, M., Verpoest, I., *Mechanical and anticorrosion porperties of nanosilica-filled epoxy-resin composite coatings.* Applied surface science, 2014. **292**: p. 432-437.

42. Boxall, J., von Fraunhofer, J., *Concise paint technology* 1st ed. 1977: Paul Elek (Scientific Books) Ltd.

43. Port, A., *The physics of film formation* in *The chemistry and physics of coatings*, M. A, Editor. 1994, Royal society of chemistry.

44. Port, A., Cameron, C., *Film formation*, in *The chemistry and physics of coatings*, A. Marrion, Editor. 2004, The royal society of chemistry. p. 46-63.

45. Nawab, Y., Shahid, S., Boyard, N. , *Chemical shrinkage characterization techniques for thermoset resins and associated composites.* Journal of material science, 2013. **48**: p. 5387-5409.

46. Tawn, A., *The intrinsic properties of polymers*, in *Characterization of coatings: physical techniques*, R. Myers, Long, J., Editor. 1969, Marcek Dekker, Inc. p. 1-25.

47. ASTM, *D1640 - 03 Standard test methods for drying, curing, or film formation of organic coatings at room temperature*. 2009.

48. Escher, U., *Thermal expansion of epoxy resins with different cross-link densities at low temperatures.* Cryogenics, 1995. **35**: p. 775-778.

49. Glavchev, I., Petrova, K., Ivanova, M., *Determination of the coefficient of thermal expansion of epoxy composites.* Polymer testing, 2002. **21**: p. 177-179.

50. Jin, F., Park, S., *Thermal properties of epoxy resin/filler hybrid composites.* Polymer degradation and stability, 2012. **97**: p. 2148-2153.

51. Duda, J., Zielinski, J., *Free-volume theory*, in *Diffusion in polymers*, P. Neogi, Editor. 1996, Marcel Dekker, Inc.

52. Rodriguez M., G., J., Saura J., Suay J., *The influence of the critical pigment volume concentration (CPVC) on the properties of an epoxy coating Part II. Anticorrosion and economic properties* Progress in Organic Coatings, 2004. **50**: p. 68-74.

53. Muhlberg, K. *Corrosion protection of offshore wind turbines - A challenge for the steel builder and paint applicator*. Journal of protective coatings and linnings, 2010.

54. NORSOK, *M-501 Surface preparation and protective coating*. 2004: Norway.

55. ISO, *ISO 20340:2009 Paints and varnishes - Performance requirements for protective paint systems for offshore and related structures*. 2009.

56. WindEurope, *The European offshore wind industry - Key trends and statistics 2016*. 2017. p. 37.

57. Burton, T., Jenkins, N., Sharpe, D., Bossanyi, E., *Wind energy handbook*. 2nd ed. 2011: Wiley.

58. Lozano-Minguez E., K.A., Brennan F., *Multi-criteria assessment of offshore wind turbine support structures.* Renewable Energy, 2011. **36**: p. 2831-2837.

59. DNV-OS, *J101 Design of offshore wind turbine structures*. 2014.

60. Momber, D.A., *Corrosion and corrosion protection of offshore wind energy towers*. Muehlhan AG: Hamburg, Germany.

61. Armelin, E., Aleman, C., Irribarren, J., *Anticorrosion performances of epoxy coatings modified with polyaniline: A comparison between the emeraldine base and salt forms.* Progress in organic coatings, 2009. **65**: p. 88-93.

62. Wenliang Tian, L.L., Fandi Meng, Ying Liu, Yinh Li, Fuhui Wang, *The failure behaviour of an epoxy glass flake coating/steel system under marine alternating hydrostatic pressure.* Corrosion Science 2014. **86**: p. 81-92.

63. Perera, D., *Stress phenomena in organic coatings* in *MNL17-EB Paint and coating testing manual: 15th edition of the Gardner-Sward Handbook* 2012, ASTM International.

64. Hare, C., *The mechanical properties of coating films and their characterisation.* Journal of protective coatings and linnings, 1996: p. 77-95.

65. Hill, L.W., *Stress Analysis - A tool for understanding coatings performance* Progress in Organic Coatings, 1977. **5**: p. 277-294.

66. Wu, T., Irving, P., Ayre, D., Dell'Amo, D., Jackson, P., Zhao, F., *Fracture of epoxy-based marine coatings as free films and substrated coatings under static tension.* Engineering fracture mechanics, 2016. **159**: p. 1-15.

67. Dolgov, N., *Method for determining the modulus of elasticiy for gas thermal spray coatings.* Powder metallurgy and metal ceramics, 2004. **43**: p. 7-8.

68. Zosel, A., *Mechanical behaviour of coating films.* Progress in organic coatings, 1980(8): p. 47-49.

69. Strivens, T., *Mechanical properties of paints and coatings*, in *Paint and surface coatings*, S.T. Lambourne R. , Editor. 1999, Woodhead Publishing. p. 598-620.

70. ASTM, *D7028 - 07 Standard test method for glass transition temperature (DMA Tg) of polymer matrix composites by dynamic mechanical analysis (DMA).* 2015.

71. Bouchet, J., Roche , A., Jacquelin, E., *Determination of residual stresses in coated metallic substrates.* Journal of adhesion science and technology, 2001. **15**(3): p. 321-343.

72. Hare, C., *Internal Stress: Part I.* Journal of protective coatings and linnings, 1996: p. 65-75.

73. Negele, O., Funke, W., *Internal stress and wet adhesion of organic coatings.* Progress in organic coatings, 1996. **28**: p. 285-289.

74. Perera, D., *On adhesion and stress in organic coatings.* Progress in organic coatings, 1996. **28**: p. 21-23.

75. Evans, R., *The ultimate tensile properties of paint films*, in *Characterization of coatings: physical techniques*, R. Myers, Long, J., Editor. 1969, Marcel Dekker, Inc.

76. Lange, J., Toll, S., Månson, J-A., *Residual stress build-up in thermoset films cured above their ultimate glass transition temperature.* Polymer, 1995. **36**(16): p. 3135-3141.

77. Hare, C., *Internal Stress: Part II.* Journal of protective coatings and linnings, 1996: p. 101-115.

78. Yan, G., White, J., *Residual stresses in marine coatings under simulated service conditions.* Polymer engineering and science, 1999. **39**(10): p. 1866-1879.

79. Abdelkader A., W., J., *Influence of relative humdity on the development of internal stresses in epoxy resin based coatings.* Journal of materials science, 2002. **37**: p. 4769-4773.

80. Lambourne, R., *The paintins of ships*, in *Paint and surface coatings*, S.T. Lambourne R. , Editor. 1999, Woodhead Publishing.

81. Monsada, A., Haruyama, Yuasa, M., Sekine, I. *The relationship between the corrosion resistance and stresses of various organic coatings*. in *Proceedings of the symposium on advances in corrosion protection by organic coatings III*. 1998. The electrochemical society, Inc.

82. Perera, D., *Effect of thermal and hygroscopic history on physical ageing of organic coatings.* Progress in organic coatings, 2002. **44**: p. 55-62.

83. Olivier, M., Romano, A., Vandermiers, C., Mathieu, X., Poelman, M., *Influence of the stress generated during an ageing cycle on the barrier properties of cataphoretic coatings.* Progess in Organic Coatings, 2008. **63**: p. 323-329.

84. Nguyen, D., Peraudeau, B., Cohendoz, S., Mallarino, S., Feaugas, X., Touzain, S., *Effect of mechanical stresses on epoxy coating ageing approached by electrochemical impedance spectroscopy measurements* Electrochimica Acta, 2014. **124**: p. 80-89.

85. Perera, D., *Physical ageing of organic coatings.* Progress in organic coatings, 2003. **47**: p. 61-76.

86. Fredj, N., Cohendoz, S., Feagas, X., Touzain, S., *Effect of mechanical stress on kinetics of degradation of marine coatings.* Progress in Organic Coatings, 2008. **63**: p. 316-322.

87. Fredj, N., Cohendoz, S., Feagas, X., Touzain, S., *Ageing of marine coating in natural and artificial seawater under mechanical stresses.* Progess in Organic Coatings, 2012. **74**: p. 391-399.

88. Meiser, A., Possart, W. , *Epoxy-metal interphases: chemical and mechanical aging.* The journal of adhesion, 2011. **87**: p. 313-330.

89. Pierce, P., *Mechanical properties of coatings*, in *Characterization of coatings: physical techniques*, R. Myers, Long, J., Editor. 1969, Marcel Dekker, Inc.

90. Krstic, V., Erickson, W., *A model for the porosity dependence of Young's modulus in brittle solids based on crack opening displacement.* Journal of materials science, 1987. **22**: p. 2881-2886.

91. Phani, K., Niyogi, S., *Young's modulus of porous brittle solids.* Journal of materials science, 1987. **22**: p. 257-263.

92. Kovacik, J., *Correlation between Young's modulus and porosity in porous materials.* Journal of materials science letters, 1999. **18**: p. 1007-1010.

93. Wolock, I., Harris, B., *Porosity of paint films. Adsorption studies of unsupported linseed oil films.* Industrial and engineering chemistry, 1950. **42**(7): p. 1347-1349.

94. Eckhaus, S., Wolock, I., Harris, B., *Porosity of paint films. Water vapour adsorption and permeability.* Industrial and engineering chemistry, 1953. **45**(2): p. 426-428.

95. DIN, *EN ISO 178 Plastics - Determination of flexural properties* 2003.

96. Roche, A., Guillemenet, J., *Mechanical and chemical properties of organic coatings applied to metallic sheet substrates.* Thin solid films, 1999(342): p. 52-60.

97. Bouchet, J., Roche, A., Hamelin, P., *Internal stresses, Young's modulus and practical adhesion of organic coatings applied onto 5754 aluminium alloy.* Thin solid films, 1999. **355-356**: p. 270-276.

98. Bouchet, J., Roche, A., Jacquelin, E., *How do residual stresses and interphase mechanical properties affect practical adhesion of epoxy diamine/metallic substrate systems?* Journal of adhesion science and technology, 2002. **16**(12): p. 1603-1623.

99. Fawcett, N., *A novel method for the measurement of Young's modulus for thick-film resistor material by flexural testing of coated beams.* Measurement Science and Technology, 1998. **9**: p. 2023-2026.

100. Spinks, G., Liu, Z., Brown, H., Swain, M., See, H., Evans, E., *Paint layer thermomechanical properties determined by in situ dynamic mechanical analysis in 3-point bending.* Progress in Organic Coatings, 2004. **49**: p. 95-102.

101. Roche A., B., J., Bentadjine, S., *Formation of epoxy-diamine/metal interphases.* Internal journal of adhesion and adhesives, 2002. **22**: p. 431-441.

102. Aufray, M., Roche, A., *Residual stresses and practical adhesion: effect of organo-metallic complex formation and crystallization.* Journal of adhesion science and technology, 2006. **20**(16): p. 1889-1903.

103. Aufray, M., Roche, A., *Epoxy-amine/metal interphases: influences from sharp needle-like crystal formation.* Internal journal of adhesion and adhesives, 2007. **27**: p. 387-393.

104. Goyanes, S., Saavedra, F., Roncaglia, A., Rubiolo, G., *Variation in physical and mechanical properties with coating thickness in epoxy-diamine-aluminum system.* Journal of applied polymer science, 2005. **98**: p. 891-895.

105. Szauer, T., *Electrical and electrochemical resistance for the evaluation of protective nonmetallic coatings.* Progress in organic coatings, 1982. **10**: p. 157-170.

106. Benabdi, M., Roche, A., *Mechanical properties of thin and thick coatings applied to various substrates. Part II. Young's modulus determination of coating materials.* Journal of adhesion science and technology, 1997. **11**(3): p. 373-391.

107. Yan, G., White, J., *Residual stress development in a bi-layer coating.* Polymer engineering and science, 1999. **39**(10): p. 1856-1865.

108. Röll, K., *Analysis of stress and strain distribution in thin films and substrates.* Journal of applied physics, 1976. **47**(7): p. 3224-3229.

109. Stoney, G., *The tension of metallic films deposited by electrolisis.* Proceedings of the royal society A, 1909. **82**.

110. Hoffman, R., *Mechanical properties of thin condensed films*, in *Physics of thin films*, G. Hass, Thun, R., Editor. 1966, Academic Press.

111. Timoshenko, S., *Analysis of bi-metal thermostats.* Journal of the optical society of america, 1925. **11**(3): p. 233-255.

112. Zang, J., Feng, L., *Modified Timoshenko formula for bending of ultrathin strained bilayer films.* Applied Physics Letters, 2008. **92**(2).

113. Corcoran, E., *Determining stresses in organic coatings using plate beam deflection.* Journal of paint technology, 1969. **41**(538): p. 635-640.

114. ASTM, *D6991 - 05 Standard test method for measurements of internal stresses in organic coatings by cantilever (beam) method*. 2010.

115. Benabdi, M., Roche, A., *Mechanical properties of thin and thick coatings applied to various substrates. Part I. An elastic analysis of residual stresses within coating materials* Journal of adhesion science and technology, 1997. **11**(2): p. 281-299.

116. Ohtsuki, A., *An innovative method for measuring Young's modulus of multi-layered materials using postbucking behavior.* Engineering procedia, 2011. **10**: p. 1041-1046.

117. Raju, G., Green, D., Guillon, O, *Evaluation of drying stresses in coating using an optical method.* Measurement Science and Technology, 2012. **23**: p. 1-7.

118. Fu, Z., Eckstein, U., Dellert, A., Roosen, A., *In situ study of mass loss, shrinkage and stress development during drying of cast colloidal films.* Journal of the european ceramic society, 2015. **35**: p. 2883-2893.

119. Salencon, J., *Handbook of continuum mechanics*. Vol. 1. 2001: Springer.

120. Hibbeler, R., *Mechanics of materials*. 8th ed. 2011: Prentice Hall

121. Atkins, T., Escudier, M., *A dictionary of mechanical engineering*. 2014: Oxford universitity press.

122. Gere, J., *Mechanics of materials*. 5th ed. 2001: Nelson Thornes.

123. Shimbo, M., Ochi, M., Shigeta, Y., *Shrinkage and internal stress during curing of epoxide resins.* Journal of applied polymer science, 1981. **26**: p. 2265-2277.

124. Roche, A., Dumas, J., Quinson, J., Romand, M., *Determination of Young's modulus of materials by three-point flexure test. Applications to metallic and organic sheets, thin film coatings, and low density aerogels*, in *Mechanics and mechanisms of damage in composites and multi-materials*, D. Baptiste, Editor. 1991, ESIS Publication 11. p. 269-282.

125. Lambourne, R., Strivens, T., *Paint and surface coatings theory and practice*. 2nd ed. ed. 1999: William Andrew Pub.

126. ASTM, *D1005 - 95 Standard test method for measurement of dry-film thickness of organic coatings using micrometers*. 2013.

127. Leng, Y., *Materials Characterization: Introduction to Microscopic and Spectroscopic Methods*. 2013: Wiley.

128. Thornton, P., *Scanning Electron Microscopy*. 1968: Chapman and Hall Limited.

129. Henson, M., Jergovich, T., *Scanning electron microscopy and energy dispersive X-ray spectrometry (SEM/EDS) for the forensic examination of paint and coatings* in *Forensic examination of glass and paint*, B. Caddy, Editor. 2001, Hoboken Taylor and Francis. p. 243-272.

130. BSI, *BS ISO 22309:2006 Microbeam analysis - Quantitative analysis using energy-dispersive spectrosmetry (EDS)*. 2006.

131. Franquet, A., Conard, T., Gilbert, M., Hantschel, T., Vandervorst, W., *Thickness and composition measurements of nanoelectronics multilayer thin*

films by energy dispersive spectroscopy (EDS). Journal of physics: conference series, 2013(417).

132. BSI, *BS EN ISO 16276-1:2007 Corrosion protection of steel structures by protective pain systems - Assessment of, and acceptance criteria for, the adhesion/cohesion (fracture strength) of a coating* in *Part 1: Pull-off testing*. 2007.

133. Nelson, G., *Adhesion*, in *MNL17-EB Paint and coating testing manual: 15th edition of the Gardner-Sward Handbook*. 2012, ASTM International.

134. PerkinElmer. *DMA 8000*. 2015 [cited 2015 12th of May]; Available from: http://www.perkinelmer.co.uk/.

135. Deng, S., Hou, M., Ye, L., *Temperature-dependent elastic moduli of epoxies measured by DMA and their correlations to mechanical testing data.* Polymer testing, 2007. **26**: p. 803-813.

136. Menard K., N.D., *Use of DSC, DMA and TG-GC/MS in the study of epoxy materials* 2013, PerkinElmer, Inc.: Shelton, CT USA.

137. Lee-Sullivan, P., Dykerman, D., *Guidelines for performing storage modulus measurments using the TA Instruments DMA 2980 three-point bend mode I. Amplitude effects.* Polymer testing, 2000. **19**: p. 155-164.

138. Feng, J., Guo, Z., *Temperature-frequenty-dependent mechanical properties of epoxy resin and its composites.* Composites Part B, 2016. **85**: p. 161-169.

139. ASTM, *D5023-15 Standard test method for plastics: dynamic mechanical properties: in flexure (three-point bending)*. 2015.

140. Powell, P., Ingen, A., *Engineering with polymers*. 1998: Stanley Thornes Ltd.

141. BSI, *BS EN ISO 291:2008 Plastics - Standard atmosphere for conditioning and testing*. 2008.

142. Lossin, M., *Corrosion Protection for offshore wind turbines*. Germanischer Lloyd WindEnergie GmbH.

143. Totten, G., *Handbook on residual stress* in *SEM*. 2005, Bethel. p. 417.

144. Kvittem M., M.T., *The domian analysis procedures for fatigue assessment of a semi-submersible wind turbine.* Marine structures, 2015. **40**: p. 38-59.

145. BSI, *BS EB ISO 4287:1998 + A1:2009) Geometrical product specification (GPS) - Surface texture: Profile method - Terms, definitions and surface texture parameters.* 2009.

146. BSI, *BS EN ISO 4288:1998 Geometric product specifications (GPS) - Surface texture - Profile method: Rules and procedures for the assessment of surface texture*. 1998.

147. Roche, A., Aufray, M., Bouquet, J., *The role of the residual stresses of the epoxy-aluminium interphase on the interfacial fracture toughness* The journal of adhesion, 2006. **82**(9): p. 867-886.

148. BSI, *BS EN ISO 29601:2011 Paints and varnishes - Corrosion protection by protective paint systems - Assessment of porosity in a dry film*. 2011.

149. Murugan, E., Ramesh, R., Padmanabhan, K., *Investigation on static and dynamic mechanical properties of epoxy based woven fabri glass/carbon hydrid composite laminates.* Procedia engineering 2014. **97**: p. 459-468.

150. Wu, T., Foyet, A., Kodenstov, A., van der Ven, L., van Benthem, R, *Wet adhesion of epoxy-amine coatings on 2024-T3 aluminum alloy* Materials chemistry and physics, 2014. **145**: p. 342-349.

151. Rodriguez-Perez, M., Arcos y Rábagos, L., Gonzalez, A., de Saja, A., *Improvement of the measurement process used for the dynamic mechanical characterization of semicrystalline polymers in three-point bending.* Polymer testing, 2003. **22**: p. 63-67.

152. ASTM, *Standard practice for plastics: dynamic mechanical properties: determination and report of procedures*. 2012.

153. Michels, J., Widmann, R., Czarderski, C., Allahvirdizadeh, R., *Glass transition evaluation of commercially available epoxy resins used for civil engineering applications.* Composites Part B, 2015. **77**: p. 484-493.

154. Boerman, A., Perera, D., *Measurement of stress in multicoat systems.* Journal of coatings technology, 1998. **70**(881): p. 69-75.

155. Abdelkader A., W., J., *Comparison of internal stresses in coatings cured on rigid substrates and on unrestrained thin substrates.* Progress in organic coatings, 2002(44): p. 121-129.

156. Abdelkader A., W., J., *Curing characteristics and internal stresses in epoxy coatings: effect of crosslinking agent.* Journal of material science, 2005. **40**: p. 1843-1854.

157. Ueda, K., Kanai, H., Amari, T., *Viscoelastic properties of paint films and formability in deep drawing of pre-painted steel sheets.* Progress in organic coatings, 2002. **45**: p. 15-21.

158. Ochi, M., Yamazaki, K., Shimbo, M., *Internal stress of epoxide resin modified with spiro ortho-ester type resin. Part 2: relation between internal stress and phase structure.* Journal of materials science, 1989. **24**: p. 3189-3195.

159. Francis, L., McCormick, A., Vaessen, D. , *Development and measurement of stress in polymer coatings.* Journal of materials science, 2002. **37**: p. 4717-4731.

160. Xiaojing Sun, D.H., Guoqing Wu, *The current state of offshore wind energy technology development.* Energy, 2012(41): p. 298-312.

161. WindEurope, *The European offshore wind industry – Key trends and statistics 2015*. 2017.

162. Jamieson, P., *Offshore wind turbines*, in *Innovation in wind turbine design*. 2011, John Wiley & Sons, Ltd.

163. Koller, J., Koppel, J., Peters, W., *Conclusions and perspective*, in *Offshore wind energy: research on environmental impacts*, J. Koeller, Koeppel, J., Peters, W., Editor. 2006, Springer Verlag. p. 343-351.

164. Muhlberg, K., *Corrosion protection of windmills: onshore and offshore*. Hempel Ltd: Germany.

165. J.F. Manwell, C.N.E., A.L. Rogers, J.G. McGowan, *Review of design conditions applicable to offshore wind energy systems in the United States.* Renewable and sustainable energy reviews, 2007. **11**: p. 210-234.

166. Harrison R., H.E., Snel H., *Large wind turbines* 2000: John Wiley and Sons, Ltd. 185.

167. Arany, L., Bhattacharya, S., Macdonald, J., Hogan, S., *Design of monopiles for offshore wind turbines in 10 steps.* Soil dynamics and earthquake engineering, 2017. **92**(1): p. 126-152.

168. Jannie Jessen Nielsen, J.D.S., *On risk-based operation and maintenance of ohhshore wind turbine components.* Reliability Engineering and System Safety, 2011. **96**: p. 218-229.

169. McCafferty, E., *Introduction to corrosion science*. 2009: Springer.

170. El-Reedy, M., *Offshore Structures - Design, Construction and Maintenance*. 2012: Elsevier.

171. Jensen B.B., G.F., *Corrosion environment inside offshore monopile structures and challenges in monitoring*. DONG Energy, FORCE Technology: Denmark.

APPENDIX.

A. Corrosion protection of offshore wind turbines

A.1 Offshore wind turbines (OWTs)

The wind energy industry is increasingly moving to offshore areas. Excessive use of fossil fuels and the threat of climate change have encouraged stakeholders to concentrate on renewable energy sources. Increase in popularity and demand has produced a great growth and development of the wind power industry, both off and on shore. By the end of 2010 global wind power installations had reached 3,000MW, which represents 1.5% of the global energy supply [57, 160]. According to Wind Europe, the demand for global energy is expected to increase steadily at an annual growth rate of 21% until 2021. In Europe, by 2015 the cumulative total of power capacity increased to 11,027MW (3,320 turbines installed) [161]. **Figure A. 1** shows the cumulative and annual offshore wind installations from 2000 to 2016. The development of offshore wind energy in Europe has shown three stages of growth: initial research from 1980 to 1990; experimental tests and small projects from 1991 to 2000; and commercialization from 2001 to present day. Over 30 years of development have placed Europe in the lead in terms of offshore wind power [57, 160].

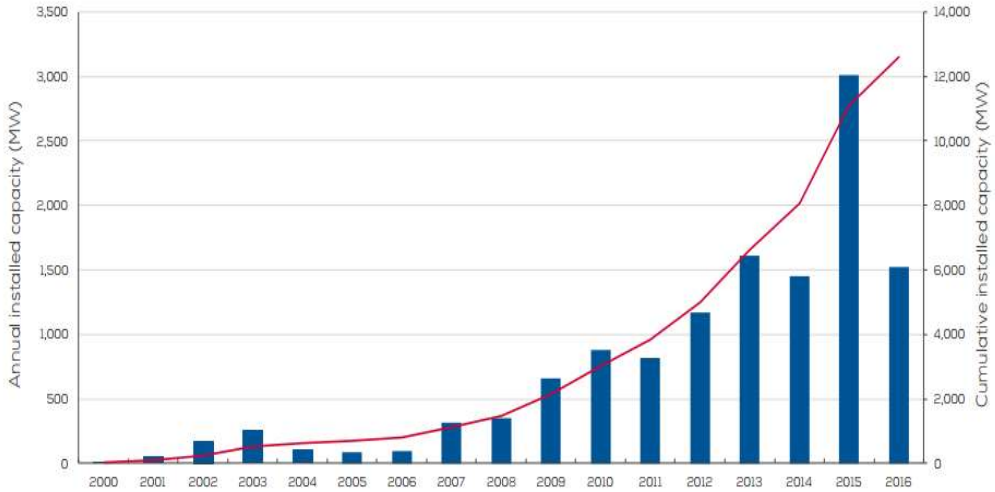

Figure A. 1 Cumulative and annual offshore wind installations 2000-2016 (1991-2012) [160].

By the end of 2016, Europe's net capacity increased to a total of 12,631MW with 3,589 grid-connected wind turbines in 10 counties. This represents a 48% decrease from 2015, where net capacity was 108% higher than in 2014. In terms of projects, 11 new projects reached final investment decision (FID) in 2016, which represents an increase of 39% compared to 2015. The completion of these 11 projects will rise the cumulative capacity in Europe to 17.4GW [56, 161].

The advantages of locating wind farms offshore are the larger unrestricted space; reduced environmental and social impact; higher mean wind speeds (and relatively low extreme winds); the wind turbulence is lower; and the landfalls of the cables and connection points are closer to load centres and cities. In general, an additional 50% of electricity can be generated offshore by a given wind turbine when compared to its onshore counterpart (size for size). Since these are unmanned structures with limited access, costs of repairs are significantly higher than for onshore repairs and the coatings are expected to show higher reliability and longer life. Therefore, research through Europe has directed interest towards developing materials capable of tolerating extreme marine climates with temperatures ranging from -25°C to 50°C [57, 58, 60, 162].

The offshore wind energy is a source of clean energy, which does not produce harmful gases, and reduces the demand on fossil fuels and energy imports. However, there are some possible environmental impacts which have not been fully explored. Due to gaps of knowledge and information, the issues of the possible effects on marine environments have been addressed only very generally. Research is being conducted on the effect of these structures on marine life due to the noises, electromagnetic fields around submerged cables, heating of the seabed by electric power transmission, and effects on marine life (mammals, birds, fish, and small organisms) and their activity [163].

A.2. Offshore wind turbine manufacturing

Offshore wind energy is still in its early stages and knowledge is being gained as wind farms move further from the shore and into more challenging environments [57]. In 2016, the average water depth was 29.2m and average distance from the shore was 43.5km. **Figure A. 2** shows the average water depth and size of wind farms under

construction during 2016. In terms of turbine size, the average size in 2016 was 4.8MW, an increase of 15% from 2015. The first 8MW turbines are being constructed in 2017 [56].

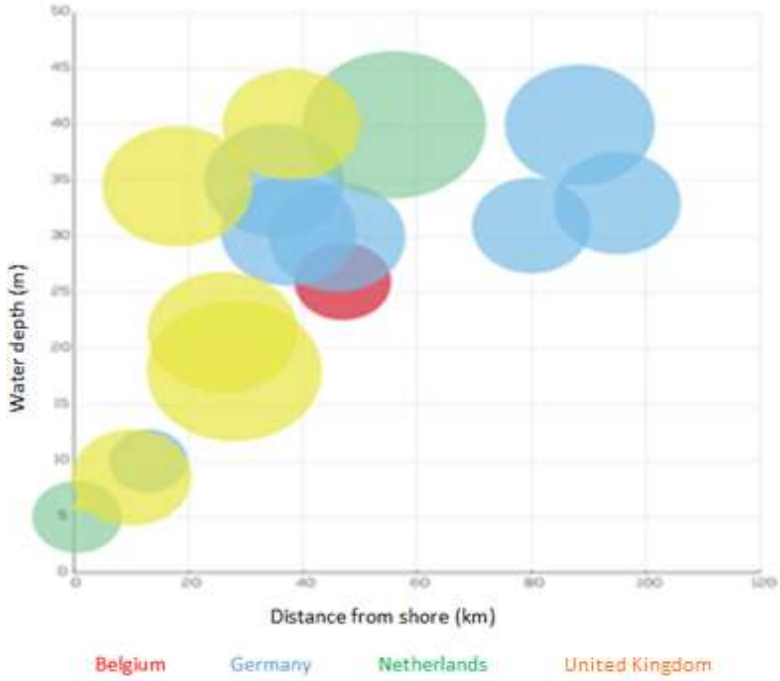

Figure A. 2 Average water depth, distance to shore and size of offshore wind farms under contruction during 2016 [160].

The move to more harsh environments requires the production of more robust structures. The corrosion protection of offshore wind turbines is especially important since these devices are expected to have a lifetime exceeding 25 years [164]. These are unmanned installations, so repair is both difficult and expensive. The most important design considerations for wind turbines are to cover both expected events during normal operations and extreme events, as well as fatigue. These considerations not only affect the steel structure but also the coating system. One of the main differences between onshore and offshore installations is the presence of waves and floating ice, which demands the design of a more robust foundation [165].

A.2.1 Support structures

In general, offshore wind turbines are inevitably bigger in diameter and height than onshore wind turbines because of the larger hub height relative to the foundation and the additional loading from waves. Accordingly, offshore towers have, proportionally,

a much higher installation cost, rendering economic design that much more important [57]. The support structure design depends on the wind and wave loading, vulnerability to sea ice, overall dynamic methods, the foundations design, and overall dynamic methods of support [166]. **Figure A. 3** presents a schematic representation of the different types of foundations depending on the depth of the water: these are gravity foundations, suction bucket, monopile, tripod, and jacket.

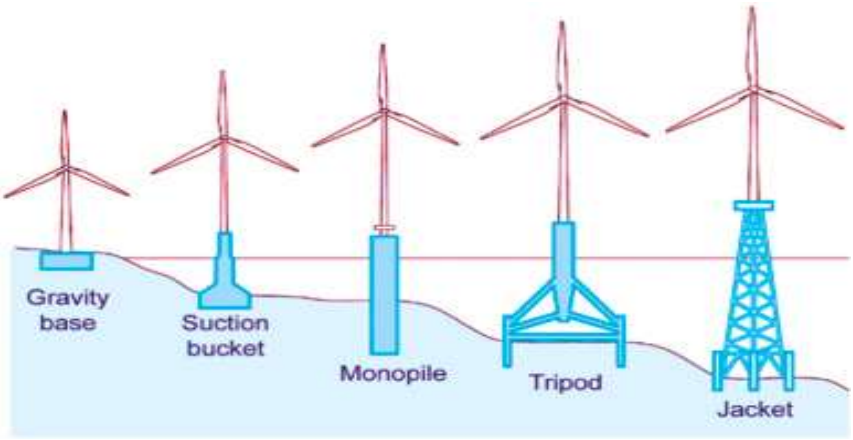

Figure A. 3 Fixed-bottom foundations commonly used in the offshore wind industry [166].

The selection of foundation type depends both on site characteristics, and maturity and track record of the different design types [167]. Floating platforms are often used for installations close to shore due to its potential for use in different areas independently of water depth and seabed conditions, relatively simple design, easy installation and decommissioning, and ease of retrieval for at-shore maintenance [162].

A.3 Corrosion protection of offshore wind turbines

Growth in the offshore wind energy industry has also resulted in an increase in the amount of corrosion due to the marine environment. Marine corrosion has been a problem for the oil and gas industry for decades, and it has been common practice to adapt corrosion protection methods originally developed for oil and gas structures to offshore wind devices. However, as unmanned structures, asset owners of OWTs need to plan inspections and repair of the protective systems due to premature failure and, consequent need for transport of personnel to the site, and challenging conditions for painting [1]. Operation and maintenance (O&M) constitutes 30% of the costs of energy from offshore wind turbines. The improved protection and inspection of wind turbines

should reduce the expected cost of O&M throughout the lifetime of the components [168].

The corrosion of steel structures is a widely observed phenomenon that involves its destructive attack due to reactions with the surrounding environments, which are bound to change with time and environmental factors. Moreover, the environment that actually attacks the metal is the micro-environment at its local surface [7, 169, 170]. Offshore wind turbines are exposed to harsh environments; and the complex stresses affecting OWTs include corrosive stress, biological stress and physical load-related stresses. These structures, during their lifetime, are exposed to both atmospheric air with high salt content and seawater; the exposure to an aqueous environment reduces the fatigue strength of steel components. Additionally, they are exposed to water condensation in internal spaces, and to soil on the foundation. It was originally assumed that the interior of foundations was airtight; this assumption is incorrect for several designs. Seawater and oxygen have access to the inside of the monopile, which can result in corrosion of the inside of the component. Consequently, the durability of the wind farm is compromised if the component is not protected from corrosion both inside and out [2, 60, 170, 171].

Research has focused on the study of corrosion processes on steel structures in seawater. Failure results in monetary losses due to the need to shut down and repair the asset. [170]. Offshore wind turbine support structures are exposed to different conditions along their height depending on their surrounding environment [2]. These zones are presented in **Table A. 1**. However, this information has to be used with caution since it's based on the corrosion of unprotected steel [60]. The corrosion rates of steel are highest in the splash zone of offshore constructions, and according to DNV-OS-J101 it requires extra plate thickness as corrosion allowance, in addition to the surface coating. Corrosion rates in the range of 0.5 to 0.5 mm a year are commonly assumed for structures installed in the North Sea [57, 59].

Table A. 1 Corrosion rates of steel in offshore service [3].

Environmental zone	Corrosion rate [mm/year]
Buried in soil	0.1
Underwater zone (UZ)	0.2
Intermediate zone (IZ)	0.25
Splash zone (SZ)	0.4

According to ISO 12944-5, corrosive environments are classified mainly into two categories, atmospheric environments and water and soil environments. Atmospheric corrosivity categories are presented in **Table A. 2** and water and soil categories are presented in **Table A. 3** [15]. In offshore wind turbine structures, protective systems should be able to stand C5-M and Im2 environments.

Table A. 2 Classification of atmospheric corrosivity [15].

Notation	Atmospheric corrosion categories
C1	Very low
C2	Low
C3	Medium
C4	High
C5-I	Very high (industrial)
C5-M	Very high (marine)

Table A. 3 Table 0.3 Classification for water soil [15]

Notation	Categories for water and soil
Im1	Immersion in fresh water
Im2	Immersion in sea or brackish water
Im3	Buried in soil

A.4 Corrosion

Corrosion of metals is an electrochemical process that occurs in the form of coupled electrochemical half-cell reactions. Four conditions are required in order for corrosion to initiate, and be maintained:

- an anodic reaction,
- a cathodic reaction;
- a metallic path of contact between the anodic and the cathodic sites; and
- the presence of an electrolyte medium.

In marine environments, the electrolyte is seawater, in which the surface of the metallic substrate develops localised anodes and cathodes at which the cathodic and anodic reactions take place [142, 169, 170]. The following examples illustrate cathodic and anodic reactions:

$$\text{At the local anodes: } Fe(s) \rightarrow Fe^{2+}(aq) + 2e^{-}$$

$$\text{At the local cathodes: } 2H^{+}(aq) + 2e^{-} \rightarrow H_2(g)$$

The overall reaction is the sum of the two half-cell reactions:

$$Fe(s) + 2H^{+}(aq) \rightarrow Fe^{2+}(aq) + H_2(g)$$

where (s), (aq), and (l) correspond to the solid, aqueous, and liquid phases, respectively. Cathodic reactions do not involve reduction of metal mass. Metal ions go into solution at anodic areas in an amount chemically equivalent to the reaction at cathodic areas, as shown in **Figure A. 4** [170].

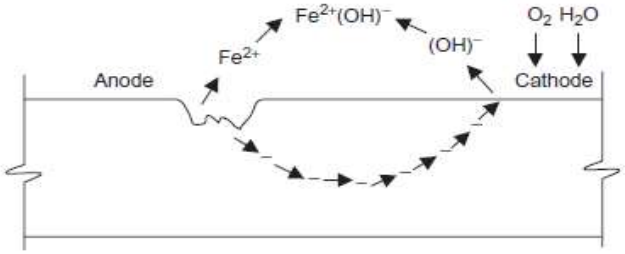

Figure A. 4 Corrosion process on the steel surface [169].

A.5.1 Cathodic protection

Inhibiting the cathodic reactions will also inhibit the development of the anodic reactions, which involves loss of metal. This is the principle behind cathodic protection. Cathodic protection (CP) or active corrosion protection is installed in the underwater zone and in the "buried in soil" zone. Generally, cathodic protection is achieved by the use of zinc-based or aluminium-based sacrificial anodes. For a tower of 5m diameter and in 20m depths, sacrificial anodes can weight around 5 tonnes. The use of protective coatings or passive corrosion protection is an effective method for the reduction in demand for cathodic protection. The active and passive corrosion protection systems must be compatible with each other and not produce impairment of functionality and quality of the coating system. Moreover, the CP potential should not produce hydrogen-induced damage to the steel structure [57, 59, 142, 170].

B. Details of publications

Mechanical characterization of protective coatings for offshore wind turbine towers and transition pieces

Abstract

Marine coatings develop residual stresses in all stages of their lifetime; excessive residual stresses affect adhesion and can compromise the integrity of both the coating system and substrate. The mechanical properties of three epoxy-based paint systems for offshore wind turbine towers and transition pieces were determined by dynamic mechanical analysis in 3-point bending mode. The coatings were airless sprayed onto steel substrates and cured. A mathematical model using composite beam stress analysis was developed to determine the Young's modulus of the coatings. The results show that the mechanical properties of the coatings depend on the film thickness. The composite modulus and Young's modulus of the coatings decrease when the coating thickness increases. Understanding the mechanical properties of marine coatings, and the factors which influence them, could lead to further improvements in the coating and corrosion protection of offshore structures in general.

Published in: International Conference for Students on Applied Engineering (ICSAE)
Date of Conference: 20-21 Oct. 2016
Date Added to IEEE *Xplore*: 09 January 2017
ISBN Information:
Electronic ISBN: 978-1-4673-9053-8
Print on Demand (PoD) ISBN: 978-1-4673-9028-6
INSPEC Accession Number: 16583870
DOI: 10.1109/ICSAE.2016.7810207
Publisher: IEEE
Conference Location: Newcastle upon Tyne, UK

Mechanical characterization of protective coatings for offshore wind turbine towers and transition pieces

Isbelis Lopez, P.S Leung, Fawad Inam
Department of mechanical and construction engineering
Northumbria University
Newcastle Upon Tyne, United Kingdom
isbelis.lopez@northumbria.ac.uk

Clare Till
Safinah Ltd
Gateshead, United Kingdom
clare.till@safinah.co.uk

Andreas Paulsen
R&D Group
Hempel A/S
Lyngby, Denmark
anpa@hempel.com

***Abstract*—Marine coatings develop residual stresses in all stages of their lifetime; excessive residual stresses affect adhesion and can compromise the integrity of both the coating system and substrate. The mechanical properties of three epoxy-based paint systems for offshore wind turbine towers and transition pieces were determined by dynamic mechanical analysis in 3-point bending mode. The coatings were airless sprayed onto steel substrates and cured. A mathematical model using composite beam stress analysis was developed to determine the Young's modulus of the coatings. The results show that the mechanical properties of the coatings depend on the film thickness. The composite modulus and Young's modulus of the coatings decrease when the coating thickness increases. Understanding the mechanical properties of marine coatings, and the factors which influence them, could lead to further improvements in the coating and corrosion protection of offshore structures in general.**

Keywords—DMA; 3-point bending; paint; wind turbines

I. INTRODUCTION

Epoxy-based marine coatings are widely used in the protection of metallic materials from corrosion; this is due to their high efficiency in seawater [1]. Epoxy coatings are thermoset polymers that can be cured at room temperature by amines, which react with the terminal epoxy groups. They generally outperform other resins in terms of mechanical properties and resistance to environment degradation. Epoxy resins possess a highly cross-linked structure which is responsible for their good mechanical properties. However, their structure is also responsible for their brittle behavior [2, 3]. They are film formers that consist of a linear chain molecule with a reactive epoxy group at each end. Different types of epoxies differ both in the length of the molecular chain between the epoxy groups and their detailed structure [4].

Epoxy paints cure by chemical reaction between components in the paint. To ensure that the ingredients in the paint won't react with each other, they are separated into two or more containers and mixed before application. These paint systems are denominated "two-pack systems" and the product is a cross-linked polymer [5].

Regardless of the mechanism of film formation, whether it's solvent evaporation, coalescence, chemical reaction, or a combination of these, coatings tend to contract. If the coating's contraction is prevented by the adhesion to the substrate and/or mobility of macromolecular segments is hindered, a tensile stress will develop within the coating [6].

The stress phenomenon in organic coatings and its effect on coating failure (delamination and/or cracking) has been the subject of numerous studies [7, 8]. Organic coatings experience stress due to some or all of the following causes: film formation, cyclic temperature and relative humidity changes, the stresses developed are identified as internal, thermal, and hygroscopic respectively. Whatever the nature of the cause, the stress developed will rise when the movements provoked by these processes are prevented by coating adhesion to the substrate and/or stiffness of the polymer segments [7].

During film formation, as the paint film gradually changes from liquid to solid and the solvent diffuses through the coating, the coating is mainly reduced in size parallel to the surface as a consequence of its adhesion to the substrate. Consequently, the internal stress developed is mainly in the

plane parallel to the substrate. The gradual molecular change in the coating over time, termed "aging" also contributes to the internal stresses in the film. Surface tension and internal stresses contribute to the formation of a flat and uniform film [2, 6, 9].

Coating films always have some degree of internal stresses, and they are almost always tensile in nature. Moreover, internal stresses always affect the mechanical properties of the coating, with the exception of high compressive internal stresses. It is important for the internal stresses to be small in comparison with the adhesive and cohesive forces that maintain the integrity of the coating. In general, internal stresses reduce the capacity of the coating to accommodate additional hygrothermal (thermal and hygroscopic) stresses, which are tensile in nature, during the component's lifetime. Failure due to internal stresses can be observed in the form of peeling or cracking. Peeling corresponds to the cases in where the internal stresses are greater than the film's adhesive strength. On the other hand, cracking is observed when the internal stresses are larger than the cohesive strength of the film. Hence, the nature of the failure will depend on the mechanical properties of the coating film. Generally, the tensile and compressive stresses affecting adhesion and cohesion will depend on film formation and service conditions, coating chemistry, composition, curing mechanism, age, thickness, among others [9, 10].

Paint systems applied on steel for protective and decorative purposes must be mechanically robust to maintain their integrity during the component's service life. The paint must be sufficiently ductile during application to coat complex profiles and resist cracking and delamination [11, 12].

Understanding of the mechanical properties and behavior of coatings is of paramount importance. However, there is very little information available on basic mechanical properties such as the Young's modulus of epoxy coatings, which is often assumed to be 3- 3.5GPa and constant regardless of coating thickness. Accurate knowledge of this property is crucial for the determination of the internal stresses affecting the coatings due to film formation. Properties such as the Young's modulus and residual stresses are essential for the appropriate modelling of the mechanical behavior of the multilayer system constituted by the substrate and paint scheme [11, 13, 14].

The increasing number of studies of the stress phenomena experienced by organic coating films resides in the strong evidence relating it to coating degradation. Modern coating systems such as thermosets are more susceptible to experiencing high stresses than traditional coatings such as alkyd paints [6]. Additionally, epoxy paints do not usually self-support to form uniform free films to determine the mechanical properties as neat films. The complications associated with the production of homogeneous free films for mechanical testing are considered to contribute to the lack of information regarding the mechanical properties of paint. Therefore it is convenient to apply them onto a flexible substrate to determine their mechanical properties as a system so then the properties of the neat coatings can be determined by the application of a mathematical model. Dynamic mechanical analysis (DMA) presents a means for calculating thermomechanical properties by studying the storage and loss modulus as a function of temperature, frequency or time. Graphical representation of moduli and tan δ (the ratio between storage and loss modulus) in terms of these variables can be used to determine functional properties, effectiveness of the curing processes and damping behavior under specific conditions [15].

II. EXPERIMENTAL

A. Materials

Three epoxy-based transition piece and tower coatings, presented in Table 1, were selected to perform a comparative study of their mechanical properties. The coatings were airless-sprayed onto steel substrates (50mm x 8.5mm x 0.23 mm) to produce bi-layer composite samples. The substrates were previously sanded and etched to promote adhesion to the coating. Additionally, thick films were airless-sprayed onto silicone coated paper to produce free films.

The samples were post-cured to establish a baseline that can be reproduced; the post cure temperature was chosen below the glass transition temperature (Tg) of the paints to avoid stress relaxation. The cure schedule consisted of 3 days at room temperature followed by 4 days at 50˚C.

B. Dynamic mechanical analysis

The dynamic mechanical analysis was performed in a DMA 8000 manufactured by PerkinElmer. The samples were mounted in the 3-point bending mode of the DMA presented in Fig 1. The tests were conducting with a static load of 1N, strain amplitude of 50µm, frequency oscillation of 1Hz and a temperature ramp from 25 to 45˚C at 2˚C/min.

C. Internal stresses

To determine the stress in a mono-layer coating system, Corcoran's equation was applied [6]. This equation considers that the stress (S) develops in two directions:

$$S = \frac{4dE_s t^3}{3l^2 t_c(t_s + t_c)(1 - \nu_s)} + \frac{4dE_c(t_s + t_c)}{l^2(1 - \nu_s)} \quad (1)$$

Where l is length of the sample [m], d is the deflection in the middle of the substrate [m], E_s is the elastic modulus of the substrate [Pa], E_c is the elastic modulus of the coating [Pa], ν_s is the Poisson's ratio of the substrate, t_s is the thickness of the substrate [m], and t_c is the thickness of the coating [m].

TABLE I. CHARACTERISTICS OF THE COATING SYSTEMS

Coating	Volume solids, VS [%]	Dry to touch [h, ˚C]
A	70±1	2 (20 ˚C)
B	79±1	8-10 (10 ˚C)
C	74±1	1.5 (20 ˚C)

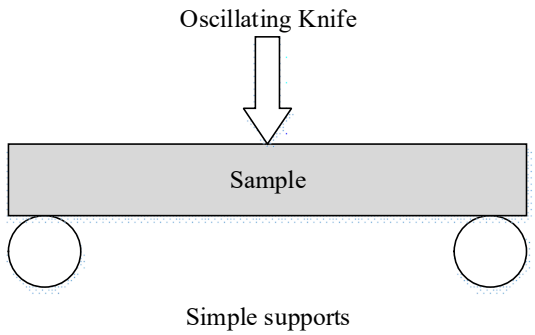

Fig. 1 Representation of the 3-point bending mode

III. YOUNG'S MODULUS: MATHEMATICAL MODEL

The mechanical response of the coated and uncoated substrates in 3-point bending and the geometrical parameters of the samples were analyzed using composite beam stress analysis. The model provided the Young's modulus of the coatings and was developed assuming that the materials in the coated system are elastic, homogeneous and isotropic. Moreover, it was assumed that the coating and the substrate have the same deformation [16]. Fig 2 shows the cross sectional area of the coated substrates. The location of the neutral axis (y) of a bi-layer beam is calculated by (2):

$$y = \frac{E_c t_c^2 + 2t_c t_s E_s + E_s t_s^2}{2E_c t_c + 2E_s t_s} \tag{2}$$

Assuming that the beams were subject to pure bending with no shear, the beams were simply supported and loaded with a concentrated load applied in the middle of the span. The bending stiffness of the bi-layer system can be determined by (3):

$$BS_{sample} = \frac{48}{L^3}(E_c I_c + E_s I_s) \tag{3}$$

where BSsample is the bending stiffness of the sample [kN/m], L is the span length [m], Ic is the moment of inertia of the coating [m4] and Is is the moment of inertia of the substrate [m4].

Substituting the moment of inertia of the coating and substrate into the equation for bending stiffness of the sample provides a quadratic equation for the determination of the Young's modulus of the coatings (Ec). The equation produces two roots; only one root is positive and has a physical meaning.

IV. RESULTS

In this section the mechanical properties of the coatings sprayed onto metallic substrates are discussed. This requires the measurement of the mechanical properties of the uncoated and coated substrates to determine the mechanical properties of the coatings through a mathematical model. The elastic modulus and the bending stiffness of the steel substrate were 196GPa and 1.89kN/m respectively. The theoretical value for the elastic modulus is 210GPa, which proves the dynamic mechanical analysis produces results close to those obtained by static mechanical instruments. Fig 3 shows the bending stiffness of the coated samples in terms of coating thickness. The bending stiffness is a geometry-dependent parameter and it increases with the increase of coating thickness. For epoxy coatings, the increase of stiffness also means an increase in the brittleness of the coating. The storage or elastic modulus determined by DMA is presented in Fig 4. The elastic modulus of the composite samples decreases with the increase of the coating thickness.

The mechanical response of the coated substrates in 3-point bending (at room temperature) and the geometrical parameters of the samples have been analyzed through the application of composite beam stress analysis. The mathematical expression developed provided the Young's modulus of the three coating systems and its variation with coating thickness, as presented in Fig 5. The Young's moduli of the free film are also shown in Fig 5, the free films present Young's moduli higher than the ones produced by coatings cured restrained on steel substrates.

With knowledge of the Young's modulus of the coatings, the internal stresses produced during film formation or curing are determined and presented in Fig 6.

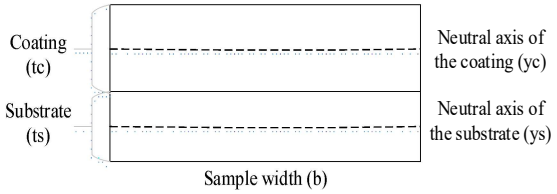

Fig 2. Cross section of the composite samples

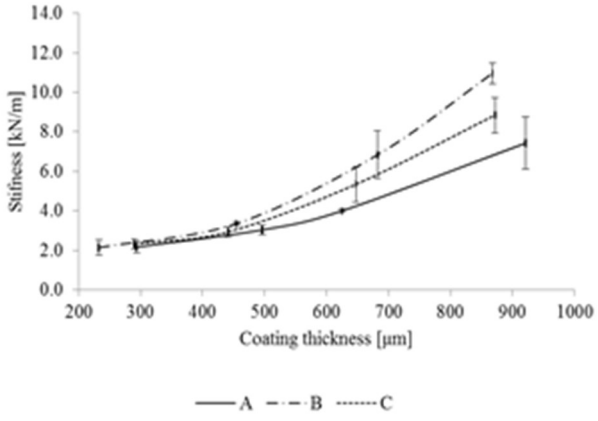

Fig 3. Variation of stiffness with coating thickness

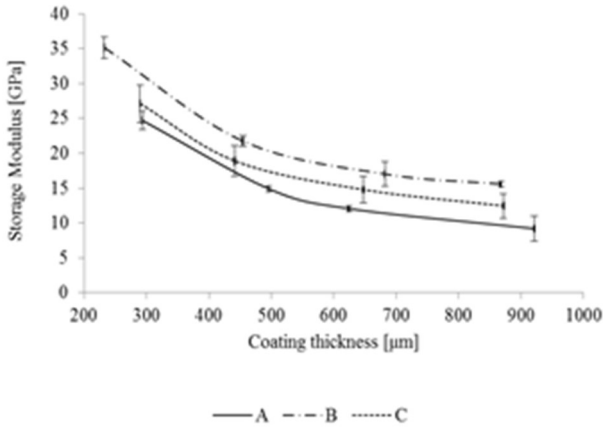

Fig 4. Variation of storage modulus with coating thickness

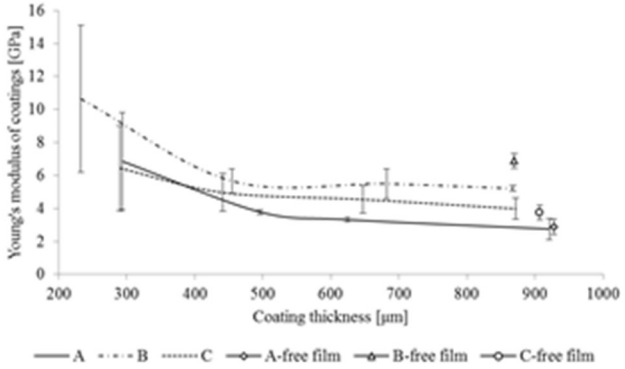

Fig 5. Variation of Young's modulus of the coatings with coating thickness

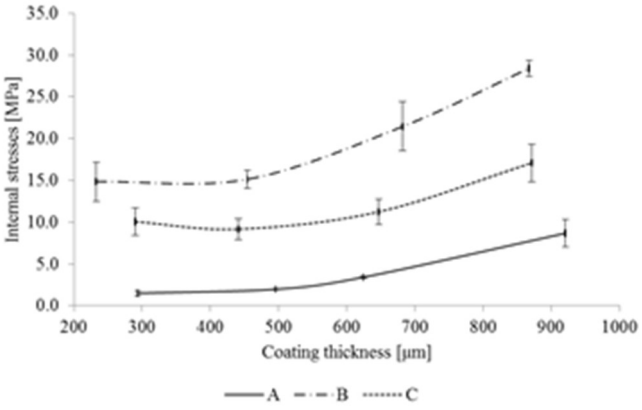

Fig 6. Variation of internal stresses with coating thickness

V. DISCUSSION

The Young's modulus of the coatings decreases with the increase of coating thickness. This behavior has also been observed by Roche and Bouchet in a series of studies on thin un-filled solvent-free epoxy coatings applied onto aluminum substrates and post-cured above Tg [14, 17]. The researchers state that this behavior is due to the formation of an interface between the substrate and the coating. The study proposes that the coating's Young's moduli reach the bulk value for coatings thicker than 200-250µm, suggesting that thickness as the interphase's thickness.

However, coatings A, B, and C are solvent-borne epoxy coatings, and post cured below the glass transition temperature. In coatings post-cured below Tg, a portion of the solvent is retained in the samples and the presence of trapped solvent plays an important role on the mechanical properties of the coatings. The retained solvent is not evenly distributed and a profile is formed within the coating with a minimal concentration in the air-coating interface. Overall, solvent retention increases with the increase of coating thickness.

Retained solvent acts as a plasticizer and reduces the crosslinking density of the coating. The solvent acts as a lubricant easing the movement of the polymer chains and increasing the flexibility of the polymers [18]. Thus, the presence of retained solvent lowers the Tg, tensile strength and elastic modulus of the coatings [18, 19]. Therefore, the increase in solvent retention associated with the increase of coating thickness also produces a reduction in the Young's modulus of the coating.

In the present study it has been stablished that for coatings A, B and C used in towers and transition pieces, the Young's moduli of the coatings decreases with the increase of film thickness and for coatings with thicknesses higher than 620 µm, the moduli reach a stable value. This value can be identified as the bulk value of the modulus for each coating. The thickness-dependent Young's modulus could also be attributed to structural changes of the cross-linked structure across the thickness of the coating.

The comparison between the Young's modulus of supported and unsupported coatings showed that when coatings are cured as free films, the Young's modulus produced is higher. This could be associated to a lower percentage of solvent retention on the free films. The presence of a steel substrate restrains the evaporation of the solvent to the air-coating interface.

DMA results are useful to perform comparative studies; it is known that there are small discrepancies between the temperature-dependent elastic moduli measured by DMA and the ones measured with a static mechanical testing machine. From all the test modes allowed by the DMA, 3-point bending mode is considered to be the most suitable for measuring the elastic modulus of materials. This bending mode eliminates the clamping effect, present on the single cantilever and dual cantilever mode, and serves as an analogous method to static mechanical test [20].

VI. CONCLUSIONS

A mathematical model which considers the 3-point bending results provides reasonable results for the Young's modulus of thick coatings with applications in offshore wind turbine towers and transition pieces. The Young's modulus of the coatings decreases with the increase of coating thickness due to the plasticizing effect of the solvent retained within the coating.

The dynamic mechanical analyzer allows the determination of the temperature-dependent elastic modulus of epoxy paints with the use of small amounts of materials and

eliminates the need to conduct expensive tests in traditional testing machines at different temperatures.

The present analysis was developed considering room temperature properties. However, depending on the application, the mechanical response of the material at any other temperature can be used to determine the Young's modulus of the material at the given temperature, given that the material is elastic at that temperature.

Nonetheless, the results obtained are dependent on a group of input parameters and small variations in these could introduce an error to the calculations [11]. Inevitable variations from sample to sample in the thickness of the coating and the substrate produce variations on the calculated Young's modulus, which is evident on the error bars shown in Fig 5.

In general, free films in the thickness range selected for the study are difficult to produce. When left to cure unsupported, epoxy coatings curl during curing and handling is difficult, by testing the material coated on steel substrates it can be ensured that the samples won't break while handling and meet the criteria of sufficient stiffness necessary to be tested in 3-point bending. Moreover, testing supported coatings allows accounting for the interaction between coating and substrate during mechanical testing.

REFERENCES

[1] Fredj, N., Cohendoz, S., Feagas, X., Touzain, S., Some consequences of saline solution immersion on mechanical behaviour of two marine epoxy-based coatings. Progress in Organic Coatings 2010. 69: p. 82-91.

[2] Seymour, R., Mark, H., Handbook of Organic Coatings. 1990: Elsevier.

[3] Hobbiebrunken, T., Fiedler, B., Hojo, M., Ochiai, S., Schulte, K., Microscopic yielding of CF/epoxy composites and the effect on the formation of thermal residual stresses. composites science and technology, 2005. 65: p. 1626-1635.

[4] Vicevic, M., A comparison of fatigue properties of epoxy coatings in marine environments, in School of Chemical Engineering and Advanced Materials. 2008, University of Newcastle Upon Tyne: Newcastle Upon Tyne. p. 266.

[5] Turner, G.P.A., Introduction to paint chemistry and principles of paint technology. 3rd ed. 1988: Chapman and Hall.

[6] Perera, D., Stress phenomena in organic coatings in MNL17-EB Paint and coating testing manual: 15th edition of the Gardner-Sward Handbook 2012, ASTM International.

[7] Perera, D., On adhesion and stress in organic coatings. Progress in organic coatings, 1996. 28: p. 21-23.

[8] Hare, C., The mechanical properties of coating films and their characterisation. Journal of protective coatings and linnings, 1996: p. 77-95.

[9] Hare, C., Internal Stress: Part I. Journal of protective coatings and linnings, 1996: p. 65-75.

[10] Sato, K., The internal stress of coating films. Progress in organic coatings, 1980(8): p. 143-160.

[11] Spinks, G., Liu, Z., Brown, H., Swain, M., See, H., Evans, E., Paint layer thermomechanical properties determined by in situ dynamic mechanical analysis in 3-point bending. Progress in Organic Coatings, 2004. 49: p. 95-102.

[12] Lambourne, R., Strivens, T., Paint and surface coatings theory and practice. 2nd ed. ed. 1999: William Andrew Pub.

[13] Benabdi, M., Roche, A., Mechanical properties of thin and thick coatings applied to various substrates. Part I. An elastic analysis of residual stresses within coating materials Journal of adhesion science and technology, 1997. 11(2): p. 281-299.

[14] Bouchet, J., Roche , A., Jacquelin, E., Determination of residual stresses in coated metallic substrates. Journal of adhesion science and technology, 2001. 15(3): p. 321-343.

[15] ASTM, Standard test method for plastics: dynamic mechanical properties: in flexure (three-point bending). 2015.

[16] Hibbeler, R., Mechanics of materials. 8th ed. 2011: Prentice Hall

[17] Bouchet, J., Roche, A., Hamelin, P., Internal stresses, Young's modulus and practical adhesion of organic coatings applied onto 5754 aluminium alloy. Thin solid films, 1999. 355-356: p. 270-276.

[18] Cowie, J., Polymers: chemistry and physics of modern materials 1991, Blackie and Son Ltd. .

[19] Boxall, J., von Fraunhofer, J., Concise paint technology 1st ed. 1977: Paul Elek (Scientific Books) Ltd.

[20] Deng, S., Hou, M., Ye, L., Temperature-dependent elastic moduli of epoxies measured by DMA and their correlations to mechanical testing data. Polymer testing, 2007. 26: p. 803-813.